Development of green CO2 capture technologies using immobilized carbonic anhydrase enzyme

Thèse

Hannaneh Rasouli Kenari

Doctorat en génie chimique
Philosophiæ doctor (Ph. D.)

Québec, Canada

Développement de technologies de captage du CO_2 vert utilisant l'enzyme anhydrase carbonique immobilisée

Thèse

Hannaneh Rasouli Kenari

Sous la direction de :

Maria C. Iliuta, directrice de recherche

Résumé

Les activités anthropiques ont considérablement augmenté la quantité de gaz à effet de serre (GES) dans l'atmosphère et sont un contributeur majeur au réchauffement climatique. Le dioxyde de carbone (CO_2) est considéré le principal gaz à effet de serre qui contribue largement aux changements climatiques. Diverses technologies sont explorées à travers le monde pour la capture et la séquestration du CO_2. Les solutions à base d'amines sont considérées des solvants efficaces, mais ils sont énergivores et ont des impacts négatifs sur l'environnement. L'absorption du CO_2 à l'aide de l'enzyme anhydrase carbonique (AC) comme catalyseur (libre en solution ou immobilisé) est une technologie prometteuse qui offre une sélectivité et une efficacité élevées pour la capture du CO_2, tout en utilisant des solvants non toxiques et moins énergivores. L'AC est un biocatalyseur bien connu, doté d'une aptitude extraordinaire à absorber les molécules de CO_2 (grâce à son énorme constante catalytique (*turnover number, TON*)), ce qui lui confère une très grande capacité à stimuler l'hydratation du CO_2. L'immobilisation de l'AC sur des surfaces solides améliore la stabilité et la réutilisation de l'enzyme, en permettant une séparation facile des produits de la réaction sans la contamination du biocatalyseur.

Dans ce contexte, cette thèse se concentre sur l'étude de l'absorption du CO_2 en utilisant l'AC immobilisée dans différents bioréacteurs. Plus précisément, les principaux objectifs sont: *i*) de développer un processus enzymatique amélioré en utilisant l'AC immobilisée dans une colonne à garnissage, *ii*) d'étudier l'absorption du CO_2 dans un contacteur à membrane avec l'enzyme immobilisée sur la surface de la membrane, et *iii*) de proposer un nouveau procédé enzymatique hybride dans un contacteur à membrane plane en intensifiant l'absorption du CO_2 par l'enzyme immobilisée autant sur la membrane que sur la surface de nanoparticules magnétiques (MNPs).

Une nouvelle technique d'immobilisation de l'AC a été développée en combinant (i) la co-déposition de Polydopamine (PDA)/Polyethyleneimine (PEI) contenant des groupes

fonctionnels aminés pour fonctionnaliser les surfaces et (ii) l'immobilisation covalente de l'enzyme sur les surfaces aminées en utilisant du glutaraldéhyde. L'approche proposée est intéressante en raison de sa simplicité, de l'abondance des fonctionnalités (amine) du PEI, et de la grande capacité d'adhésion du PDA pendant le processus de fonctionnalisation de la surface, ainsi que de la stabilité et de la réutilisation de l'enzyme immobilisée par liaison covalente.

Un procédé enzymatique hybride avec l'enzyme AC immobilisée sur la surface du garnissage et des MNPs dispersées dans l'absorbant liquide (eau) a été développé dans un bioréacteur constitué par une colonne gaz-liquide. L'enzyme a été immobilisée sur la surface fonctionnalisée des MNPs et du garnissage par liaisons covalentes. Même après 40 jours, l'enzyme immobilisée sur le garnissage et les MNPs a montré une remarquable stabilité, conservant, respectivement, 80 % et 84,7 % de son activité initiale. Étant donné que l'enzyme immobilisée sur les MNPs fonctionne comme une enzyme libre en solution, le processus d'hydratation du CO_2 s'est amélioré de manière significative, en particulier lorsqu'il y a une plus importante limitation de la diffusion lors du processus enzymatique avec l'enzyme immobilisée sur la surface du garnissage.

L'AC immobilisée sur la surface d'une membrane plane en polypropylène (PP) par codéposition de PDA/ PEI par liaison covalente a montré la plus grande activité et a conservé la plupart de son activité initiale après 40 jours (82.3%). Un flux d'absorption de CO_2 de $0{,}29\times10^{-3}$ mol/m^2s a été atteint en intégrant la membrane biocatalytique dans un contacteur à membrane plane (FSMC), en utilisant l'eau comme absorbant. Un taux stable d'absorption a été obtenu pendant l'opération à plus long terme (6 heures), illustrant le potentiel de cette technologie dans des applications industrielles. La résistance au transfert de masse dans les pores de la membrane partiellement remplis de liquide a été réduite par l'hydratation catalysée du CO_2 dans ces pores en présence de l'AC immobilisée.

L'absorption de CO_2 dans un contacteur à membrane plane avec de l'AC immobilisée sur la surface de la membrane a été intensifiée en incorporant également l'enzyme immobilisé sur la surface des MNPs dispersés dans la phase liquide. Le processus d'absorption du CO_2 a été amélioré grâce à la présence de MNPs biocatalytiques qui agissent comme une enzyme libre en phase liquide. L'AC a été immobilisée de manière covalente sur la surface des MNPs fonctionnalisées. L'absorption du CO_2 a été améliorée dans ce système hybride innovant de contacteur à membrane intensifié en maximisant l'utilisation du *TON* de cette enzyme, en particulier à des concentrations plus faibles d'enzyme sur la membrane biocatalytique. Autant la membrane que les MNPs avec l'AC immobilisée ont démontré leur réutilisabilité, en conservant leurs activités initiales même après 10 cycles d'absorption. Le contacteur à membrane intensifié a également montré un fonctionnement stable pendant plusieurs heures.

En conclusion, les résultats obtenus dans cette thèse illustrent le fait que la capture du CO_2 utilisant de l'anhydrase carbonique immobilisée peut offrir une stratégie rentable, verte et respectueuse de l'environnement, représentant une alternative attrayante aux technologies traditionnelles qui utilisent des absorbants à base d'amines. Avec la crise environnementale croissante, les technologies enzymatiques prennent de l'importance, ce qui suscite de plus en plus de tentatives pour les mettre en œuvre à l'échelle industrielle.

Abstract

Anthropogenic activities have significantly enhanced the amount of greenhouse gases (GHGs) in the atmosphere and are a major contributor to global warming. Carbon dioxide (CO_2) is a primary greenhouse gas that contributes to climate change. Various technologies are being explored across the world to tackle CO_2 capture and sequestration. Despite their efficiency, amine-based solutions have negative environmental impact and the process is energy intensive. CO_2 absorption using carbonic anhydrase (CA) enzyme as catalyst (free in solution or immobilized) is a promising technology which offers high selectivity and efficiency in CO_2 capture processes by using nontoxic and more energy efficient solvents. CA is a well-known biocatalyst endowed with an extraordinary turnover number (*TON*), which offers to it a very high capacity to boost CO_2 hydration. CA immobilization on solid surfaces enhances the enzyme stability, and reusability and provides the ability for easy separation of the reaction products without biocatalyst contamination.

In this context, the present thesis focuses on the investigation of CO_2 absorption process using immobilized CA in different bioreactors. More specifically, the main objectives are: *i*) developing an enhanced enzymatic process with immobilized CA enzyme in a packed-bed column bioreactor, *ii*) studying the CO_2 absorption in membrane contactor with immobilized CA enzyme on membrane surface, and *iii*) proposing a novel hybrid enzymatic process in an intensified flat sheet membrane contactor for improving CO_2 absorption via immobilized CA enzyme on both membrane and magnetic nanoparticles (MNPs).

An improved CA immobilization technique was developed in this work using two steps: (i) co-deposition of Polydopamine (PDA)/Polyethyleneimine (PEI) with amino functional groups for amine-functionalization of surfaces and (ii) covalent enzyme immobilization on the aminated surfaces using glutaraldehyde. The proposed approach is appealing because of its simplicity, abundant amine functionalities of PEI, and great adhesion capacity of PDA

during surface functionalization process, as well as the stability and reusability of immobilized enzyme via covalent bonding.

A hybrid enzymatic process with CA enzyme immobilized on packing surface and MNPs dispersed in the liquid absorbent (water) was developed in a gas-liquid packed-bed column bioreactor. CA was immobilized on amine functionalized surface of MNPs and packings via covalent attachments. Even after 40 days of storage in buffer solution, the immobilized CA on packing and MNPs showed remarkable stability, retaining 80% and 84.7% of its original activity, respectively. Since the enzyme immobilized on MNPs operates as a free solution-phase enzyme, the CO_2 hydration process improved significantly, specially when the diffusion limitation in the enzymatic process with immobilized CA enzyme on the packing surface was significant.

CA enzyme immobilized on polypropylene (PP) flat sheet membrane surface via co-deposition of PDA/PEI through covalent bonding method showed the highest activity and preserved most of its initial activity after 40 days (82.3%). A CO_2 absorption flux of 0.29×10^{-3} mol/m^{2}s was attained by integrating the biocatalytic membrane into a flat sheet membrane contactor (FSMC) using water as absorbent. Stable CO_2 absorption rate was obtained during a longer time operation (6 hours), illustrating its potential for industrial applications. Mass transfer resistance in partially liquid-filled membrane pores was shown to be reduced by the catalyzed CO_2 hydration in these pores in the presence of immobilized CA.

CO_2 absorption in flat sheet membrane contactor with immobilized CA on membrane surface was intensified by the incorporation of immobilized CA on the surface of MNPs dispersed in the liquid phase. CO_2 absorption process was improved due to the presence of biocatalytic MNPs, which act as a free solution-phase enzyme. CA was covalently immobilized on amine-functionalized MNPs surface. The proposed innovative hybrid enzymatic process in the intensified membrane contactor improved the CO_2 absorption by maximizing the utilization of CA's large *TON*, specially at lower CA loadings on the biocatalytic membrane. Immobilized membrane and MNPs demonstrated their reusability and retained their initial

activities even after 10 absorption cycles. The intensified membrane contactor also displayed a stable operation for several hours.

In conclusion, the results achieved in our work illustrate that CO_2 capture using immobilized CA can offer a cost-effective, green, and environmentally friendly strategy, representing an attracting alternative to customary technologies using amine-based absorbents. With the growing environmental crisis, enzymatic CO_2 capture technologies are becoming more important, prompting more attempts to implement them on industrial scales.

Table of Contents

Résumé ii
Abstract v
Table of Contents viii
List of Figures xiv
List of Tables xix
Nomenclature xx
Acknowledgment xxvii
Foreword xxix
Introduction 1
Chapter 1: Literature review 6
1.1. Carbonic anhydrase- CO_2 hydration biocatalyst for green CO_2 capture 6
1.2. Enzyme immobilization 9
1.2.1. Adsorption 15
1.2.2. Entrapment 16
1.2.3. Cross-linking 16
1.2.4. Covalent bonding 17
1.3. Support materials for CA immobilization 18
1.3.1. Inorganic oxide materials 24
1.3.2. Magnetic-based materials 25
1.3.3. Carbon-based materials 28
1.3.4. Polymeric membranes 28
1.3.5. Synthetic polymers 31
1.3.6. Biopolymers 33
1.3.7. MOFs 34
1.4. Enzymatic CO_2 capture technologies using CA 35
1.4.1. Absorption reactors 35
1.4.2. Selective membranes 39
1.4.3. Membrane contactors 41
1.5. Conclusion on literature and opportunities for research 44
1.6. Objective of the present research 46
1.6.1. General objective 47
1.6.2. Specific objectives 47
Chapter 2: Methodology 48

2.1. Materials and chemicals 48
2.2. Materials preparation 50
2.2.1. Biocatalytic membrane preparation 50
2.2.2. Enzyme immobilization on packing surface 50
2.2.3. Biocatalytic magnetic nanoparticles preparation 51
2.2.3.1. Magnetic nanoparticles synthesis 51
2.2.3.2. Enzyme immobilization on MNPs 51
2.3. Bradford test 52
2.4. Esterase activity test 52
2.5. k_{cat}/K_m evaluation for free and immobilized CA 53
2.6. Long-term stability 53
2.7. Materials characterization 53
2.7.1. Contact angle 53
2.7.2. Breakthrough pressure 54
2.7.3. Scanning Electron Microscope 54
2.7.4. Fourier transform infrared spectroscope 55
2.7.5. X-ray diffraction 55
2.7.6. Transmission Electron Microscopy 56
2.7.7. Nitrogen adsorption-desorption 56
2.8. CO_2 absorption tests 57
2.8.1. CO_2 absorption performance of biocatalytic membrane contactors 57
2.8.2. CO_2 absorption performance of packed-bed column bioreactor 57
2.8.3. CO_2 absorption rate calculation 58
2.9. Reusability of the immobilized enzyme in bioreactors 58
Chapter 3: Enhanced CO_2 capture in packed-bed column bioreactors with immobilized carbonic anhydrase 60
Résumé 60
Abstract 61
3.1. Introduction 62
3.2. Experimental 64
3.2.1. Materials and chemicals 64
3.2.2. Enzyme immobilization on packing surface 65

3.2.3. Biocatalytic magnetic nanoparticles preparation 65
3.2.3.1. Magnetic nanoparticles synthesis 65
3.2.3.2. Enzyme immobilization on MNPs 66
3.2.4. Bradford test 66
3.2.5. Esterase activity test 67
3.2.6. Characterization techniques 67
3.2.7. Long-term stability of immobilized CA 68
3.2.8. k_{cat}/K_m evaluation for free and immobilized CA 68
3.2.9. CO_2 absorption performance of packed-bed column bioreactor 68
3.2.10. Reusability of the enzyme in packed-bed column bioreactor 69
3.3. Mathematical model of the packed-bed column bioreactor 69
3.3.1. Hydrodynamic model 69
3.3.2. Mass transport/Reaction equations 72
3.3.3. Kinetics of CO_2 hydration 75
3.4. Results and discussion 76
3.4.1. Optimization of biocatalytic MNPs development 76
3.4.1.1. Effect of co-deposition time 76
3.4.1.2. Effect of glutaraldehyde concentration 80
3.4.1.3. Effect of enzyme immobilization time 80
3.4.1.4. Effect of enzyme solution pH during immobilization 81
3.4.2. Characterization of biocatalytic MNPs 81
3.4.3. Performance of the biocatalytic MNPs 83
3.4.4. Storage stability of immobilized CA on packing 85
3.4.5. CO_2 absorption performance of packed-bed column bioreactor 85
3.4.5.1. Impact of buffer type and concentration on the packed-bed column bioreactor performance 89
3.4.5.2. Impact of operational parameters on packed-bed column bioreactor performance 91
3.4.5.3. Reusability of the enzyme in packed-bed column bioreactor 96
3.5. Conclusion 97
Chapter 4: Enzyme-immobilized flat-sheet membrane contactor for green carbon capture 100

Résumé 100
Abstract 101
4.1. Introduction 102
4.2. Experimental 105
4.2.1.1. Materials and chemicals 105
4.2.1.2. Membrane surface modification 105
4.2.2. Enzyme immobilization 106
4.2.2.1. Bradford test 106
4.2.2.2. Esterase activity test 107
4.2.2.3. Membrane characterization 107
4.2.2.4. k_{cat}/K_m evaluation for free and immobilized CA 108
4.2.3. Long-term stability of immobilized CA 108
4.2.4. CO_2 absorption performance of biocatalytic membranes 108
4.3. Mathematical model of membrane contactor 109
4.3.1. Enzymatic CO_2 hydration mechanism and kinetics 110
4.3.2. Mechanism and kinetics of the uncatalyzed CO_2 hydration 111
4.3.3. Porous membrane scale model 111
4.3.4. Gas–liquid membrane contactor scale model 113
4.3.5. Model parameters 114
4.4. Results and discussion 115
4.4.1. Effect of different parameters on enzyme immobilization 115
4.4.1.1. PDA/PEI ratio 115
4.4.1.2. PDA/PEI co-deposition time 116
4.4.1.3. Glutaraldehyde concentration 120
4.4.1.4. CA concentration and immobilization time 121
4.4.1.5. Enzyme solution pH during immobilization 121
4.4.2. Characterisation of the biocatalytic membrane 122
4.4.3. Stability of immobilized CA 125
4.4.4. CO_2 absorption in membrane contactor 126
4.4.4.1. Impact of buffer type and concentration on the membrane bioreactor performance 127
4.4.4.2. Impact of liquid flow rate and orientation flow on the membrane bioreactor

performance 130
4.4.4.3. Impact of gas flow rate on the membrane bioreactor performance..... 132
4.4.4.4. Impact of liquid temperature on the membrane bioreactor performance.... 133
4.4.4.5. Stability test of membrane bioreactor 133
4.5. Conclusion 133
Chapter 5: Hybrid enzymatic CO_2 capture process in intensified flat sheet membrane contactors with immobilized carbonic anhydrase 137
Résumé 137
Abstract 138
5.1. Introduction 139
5.2. Experimental 142
5.2.1. Materials and chemicals 142
5.2.2. Biocatalytic membrane preparation 143
5.2.3. Biocatalytic MNPs preparation 143
5.2.4. Quantification of immobilized enzyme loading 144
5.2.5. Characterization tests 144
5.2.6. CO_2 absorption performance of the intensified membrane contactor 145
5.2.7. Reusability of the intensified membrane contactor 145
5.3. Mathematical model of the membrane contactor 146
5.3.1. Gas–liquid membrane contactor scale model 146
5.3.2. Porous membrane scale model 147
5.3.3. Kinetics of CO_2 hydration 150
5.4. Results and discussion 151
5.4.1. Characterisation tests of biocatalytic membranes and biocatalytic MNPs ... 151
5.4.2. CO_2 absorption performance of the intensified membrane contactor 153
5.4.2.1. Impact of buffer concentration and type on intensified membrane contactor performance 156
5.4.2.2. Impact of operational parameters on intensified membrane contactor performance 158
5.4.3. Stability and reusability of intensified membrane contactor 160
5.4.4. CO_2 absorption performance of intensified membrane contactor compared to

the performance of other membrane contactors 162
5.5. Conclusion 165
General conclusions and future outlook 168
1. General conclusions 168
2. Future outlooks 170
References 171

List of Figures

Figure I.1. Global energy-related CO_2 emissions, 1990-2021, and change in CO_2 emissions by fuel, 1990-2021 (Adapted from [2]). 2
Figure I.2. CO_2 capturing systems (Adapted from [9]). 3
Figure I.3. CO_2 capture technologies comparisons [10]. 3

Figure 1.1. Crystal structures of four CAs. (a) α-class CA, type II. (b) β-class CA. (c) γ-class CA. (d) ζ-class CA. Crystal structure of δ-class CA has not been reported [27]. 6
Figure 1.2. a) Structure of hCA II, b) View of hCA II active site [30]. 7
Figure 1.3. CO_2 hydration mechanism of CA (adapted from [34]). 9
Figure 1.4. Enzyme immobilization techniques. 14
Figure 1.5. Enzyme immobilization support features. 19
Figure 1.6. Schematic illustrations for the immobilization of CA in Mag-S-MCF via the approaches of enzyme adsorption (ADS), nanoscale enzyme reactor (NER), and NER with ammonium sulfate precipitation (p-NER) [93]. 27
Figure 1.7. Two possible reactions of PDA–PEI co-deposition coating [131]. 30
Figure 1.8. Schematic of contained liquid membrane (CLM) operation. 40
Figure 1.9. Principle of membrane contactor. 41
Figure 1.10. Enzyme immobilization by LBL technique on membrane (Adapted from [181]). 42
Figure 1.11. Schematic illustration of the biocatalytic composite hollow fiber membrane [97]. 43
Figure 1.12. Schematic of the gas-liquid hollow fiber membrane contactor [46]. 44

Figure 2.1. Scheme of MNPs synthesis. 51
Figure 2.2. Breakthrough pressure apparatus [177]. 54

Figure 3.1. Development of biocatalytic MNPs. 67
Figure 3.2. Packed-bed column bioreactor setup. 69
Figure 3.3. Effect of different parameters on biocatalytic MNPs performance: (a) co-deposition time (glutaraldehyde 2 (v/v)%, CA concentration 0.2 mg/ml, pH 7, immobilization time 24 h), (b) glutaraldehyde concentration (deposition time 5 h, CA concentration 0.2 mg/ml, pH 7, immobilization time 24 h), (c) CA immobilization time (deposition time 24 h, glutaraldehyde 2 (v/v)%, CA concentration 0.2 mg/ml, pH 7), and (d) enzyme solution pH (deposition time 24 h, glutaraldehyde 2 (v/v)%, CA concentration 0.2 mg/ml, immobilization time 24 h). 78
Figure 3.4. FTIR spectra of bare MNP and P-MNP with 12, 24 and 32 h co-deposition time. 79
Figure 3.5. TEM images with average particle size: (a) MNPs, (b) P-MNPs (12 h), (c) P-MNPs (24 h), and (d) P-MNPs (32 h). 79

Figure 3.6. XRD patterns of bare MNPs, P-MNPs and CA-P-MNPs. 81
Figure 3.7. FTIR spectra of bare MNPs, P-MNPs and CA-P-MNPs. 82
Figure 3.8. TEM image with average particle size: CA-P-MNPs. 83
Figure 3.9. Storage stability of free CA and immobilized on packing and MNPs. 84
Figure 3.10. Impact of enzyme concentration (provided by the immobilization of the enzyme on packing surface) on packed-bed column bioreactor performance (100 mM Tris buffer, inlet gas CO_2 percentage: 15%, liquid flow rate: 135 ml/min, gas flow rate: 500 ml/min, and counter-current flow): a) CO_2 absorption rate; b) CO_2 removal..... 87
Figure 3.11. Impact of enzyme concentration (provided by the immobilization of the enzyme on MNPs surface) on packed-bed column bioreactor performance (enzyme concentration immobilized on packing surface = 9.2 mg/$L_{reactor}$, 100 mM Tris buffer, inlet gas CO_2 percentage: 15%, liquid flow rate: 135 ml/min, gas flow rate: 500 ml/min, and counter-current flow): a) CO_2 absorption rate; b) CO_2 removal..... 88
Figure 3.12. Impact of buffer type on packed-bed column bioreactor performance (enzyme concentration immobilized on packing surface = 9.2 mg/$L_{reactor}$, enzyme concentration immobilized on MNPs surface = 1.4 mg/$L_{reactor}$, 100 mM buffer, inlet gas CO_2 percentage: 15%, liquid flow rate: 135 ml/min, gas flow rate: 500 ml/min, and counter-current flow): a) CO_2 absorption rate; b) CO_2 removal. 90
Figure 3.13. Impact of buffer concentration on packed-bed column bioreactor performance (enzyme concentration immobilized on packing surface = 9.2 mg/$L_{reactor}$, enzyme concentration immobilized on MNPs surface = 1.4 mg/$L_{reactor}$, Tris buffer, inlet gas CO_2 percentage: 15%, liquid flow rate: 135 ml/min, gas flow rate: 500 ml/min, and counter-current flow): a) CO_2 absorption rate; b) CO_2 removal..... 91
Figure 3.14. Impact of liquid flowrate on packed-bed column bioreactor performance (enzyme concentration immobilized on packing surface = 9.2 mg/$L_{reactor}$, enzyme concentration immobilized on MNPs surface = 1.4 mg/$L_{reactor}$, 100 mM Tris buffer, inlet gas CO_2 percentage: 15%, gas flow rate: 500 ml/min, and counter-current flow): a) CO_2 absorption rate; b) CO_2 removal..... 93
Figure 3.15. Impact of liquid/ gas ratio on packed-bed column bioreactor performance (enzyme concentration immobilized on packing surface = 9.2 mg/$L_{reactor}$, enzyme concentration immobilized on MNPs surface = 1.4 mg/$L_{reactor}$, 100 mM Tris buffer, inlet gas CO_2 percentage: 15%, gas flow rate: 500 ml/min, and counter-current flow): a) CO_2 absorption rate; b) CO_2 removal..... 94
Figure 3.16. Impact of gas flowrate on packed-bed column bioreactor performance (enzyme concentration immobilized on packing surface = 9.2 mg/$L_{reactor}$, enzyme concentration immobilized on MNPs surface = 1.4 mg/$L_{reactor}$, 100 mM Tris buffer, inlet gas CO_2 percentage: 15%, liquid flow rate: 135 ml/min, and counter-current flow): a) CO_2 absorption rate; b) CO_2 removal..... 95
Figure 3.17. Impact of inlet gas CO_2 concentration on packed-bed column bioreactor performance (enzyme concentration immobilized on packing surface = 9.2 mg/$L_{reactor}$, enzyme concentration immobilized on MNPs surface = 1.4 mg/$L_{reactor}$, 100 mM Tris buffer,

liquid flow rate: 135 ml/min, gas flow rate: 500 ml/min, and counter-current flow): a) CO_2 absorption rate; b) CO_2 removal. 96
Figure 3.18. Reusability of the enzyme in packed-bed column bioreactor (enzyme concentration immobilized on packing surface = 9.2 mg/$L_{reactor}$, enzyme concentration immobilized on MNPs surface = 1.4 mg/$L_{reactor}$, 100 mM Tris buffer, liquid flow rate: 135 ml/min, gas flow rate: 500 ml/min, inlet gas CO_2 percentage: 15%, and counter-current flow). 97

Figure 4.1. Illustration of the development of biocatalytic membranes. 106
Figure 4.2. FSMC setup. 109
Figure 4.3. Schematic diagram of CO_2 absorption in FSMC (immobilized enzyme on membrane surface and inside the pores) - membrane partially liquid-filled pores. 110
Figure 4.4. Effect of different parameters on enzyme immobilization: (a) PDA/PEI ratio, (b) co-deposition time, (c) glutaraldehyde concentration, (d) CA concentration, (e) CA immobilization time, and (f) enzyme solution pH. 117
Figure 4.5. FTIR spectra of outer surfaces of pristine PP and P-PP membranes with 3, 5 and 7 h deposition. 118
Figure 4.6. Effect of co-deposition time on membrane contact angle. 118
Figure 4.7. FTIR spectra of the outer surfaces of the pristine PP, P-PP and CA-P-PP membranes. 122
Figure 4.8. Surface SEM images of outer surface morphologies and cross section morphologies of (a1 and a2) the pristine PP and (b1 and b2) CA-P-PP membranes. 123
Figure 4.9. EDS analysis of inner surfaces of the (a) pristine PP, (b) CA-P-PP membrane and (c) EDS analysis of deposited layer on CA-P-PP membrane. 124
Figure 4.10. Storage stability of immobilized CA. 125
Figure 4.11. Effect of buffer concentration and type on the membrane bioreactor performance (liquid flow rate: 26 ml/min, gas flow rate: 100 ml/min, and counter-current flow): (a) Tris buffer; (b) N-methylimidazole buffer. 130
Figure 4.12. Effect of liquid flow rate and orientation flow on the membrane bioreactor performance (gas flow rate: 100 ml/min and 100 mM Tris in water): (a) counter-current flow; (b) co-current flow 131
Figure 4.13. Effect of gas flow rate on the membrane bioreactor performance (liquid flow rate: 26 ml/min, counter-current flow, and 100 mM Tris in water). 132
Figure 4.14. Stability test of membrane bioreactor (liquid flow rate: 10 ml/min, gas flow rate: 100 ml/min, counter-current flow, and 100 mM Tris in water). 134

Figure 5.1. Illustration of the biocatalytic membranes preparation. 143
Figure 5.2. Biocatalytic MNPs preparation. 144
Figure 5.3. FSMC setup. 145
Figure 5.4. Schematic diagram of CO_2 absorption in FSMC (immobilized enzyme on membrane surface and inside the pores) - membrane partially liquid-filled pores 148

Figure 5.5. SEM images of outer surface morphologies of (a) pristine PP membrane, and (b) biocatalytic membrane. 152
Figure 5.6. Contact angle display for: (a) the virgin membrane, and (b) the biocatalytic membrane. 152
Figure 5.7. TEM images of (a) MNPs and (b) biocatalytic MNPs, (PDI: Polydispersion index). 153
Figure 5.8. Impact of enzyme loading (provided by biocatalytic membranes) on FSMC performance (100 mM Tris buffer, inlet gas CO_2 concentration: 15%, liquid flow rate: 34 ml/min (Re_L = 31.6), gas flow rate: 100 ml/min (Re_G = 6), and counter-current flow). 155
Figure 5.9. Impact of enzyme loading (provided by biocatalytic MNPs) on intensified membrane contactor performance (enzyme loading immobilized on membrane surface = 6.49 mg/Lreactor (MNPs-biocatalytic membrane) or 0 mg/Lreactor (MNPs-bare membrane), 100 mM Tris buffer, inlet gas CO_2 concentration: 15%, liquid flow rate: 34 ml/min (ReL = 31.6), gas flow rate: 100 ml/min (ReG = 6), and counter-current flow). 155
Figure 5.10. Impact of buffer concentration on intensified membrane contactor performance (enzyme loading immobilized on membrane surface = 6.49 mg/$L_{reactor}$, enzyme loading immobilized on MNPs surface = 2.5 mg/$L_{reactor}$, Tris buffer, inlet gas CO_2 concentration: 15%, liquid flow rate: 34 ml/min (Re_L = 31.6), gas flow rate: 100 ml/min (Re_G = 6), and counter-current flow). 157
Figure 5.11. Impact of buffer type on intensified membrane contactor performance (enzyme loading immobilized on membrane surface = 6.49 mg/$L_{reactor}$, enzyme loading immobilized on MNPs surface = 2.5 mg/$L_{reactor}$, 100 mM buffer, inlet gas CO_2 concentration: 15%, liquid flow rate: 34 ml/min (Re_L = 31.6), gas flow rate: 100 ml/min (Re_G = 6), and counter-current flow). 157
Figure 5.12. Impact of liquid flow rate (Re_L = 13.9 to 31.6) on intensified membrane contactor performance (enzyme loading immobilized on membrane surface = 6.49 mg/$L_{reactor}$, enzyme loading immobilized on MNPs surface = 2.5 mg/$L_{reactor}$, 50 mM Tris buffer, inlet gas CO_2 concentration: 15%, gas flow rate: 100 ml/min (Re_G = 6), and counter-current flow). 159
Figure 5.13. Impact of gas flow rate (Re_G = 6 to 12) on intensified membrane contactor performance (enzyme loading immobilized on membrane surface = 6.49 mg/$L_{reactor}$, enzyme loading immobilized on MNPs surface = 2.5 mg/$L_{reactor}$, 100 mM Tris buffer, inlet gas CO_2 percentage: 15%, liquid flow rate: 34 ml/min (Re_L = 31.6), and counter-current flow). ... 159
Figure 5.14. Impact of inlet gas CO_2 concentration on intensified membrane contactor performance (enzyme loading immobilized on membrane surface = 6.49 mg/$L_{reactor}$, enzyme loading immobilized on MNPs surface = 2.5 mg/$L_{reactor}$, 100 mM Tris buffer, liquid flow rate: 34 ml/min (Re_L = 31.6), gas flow rate: 100 ml/min (Re_G = 6), and counter-current flow).161
Figure 5.15. Stability test of intensified membrane contactor (enzyme loading immobilized on membrane surface = 6.49 mg/$L_{reactor}$, enzyme loading immobilized on MNPs surface = 2.5 mg/$L_{reactor}$, 50 mM Tris buffer, inlet gas CO_2 percentage: 15%, liquid flow rate: 34 ml/min (Re_L = 31.6), gas flow rate: 100 ml/min (Re_G = 6), and counter-current flow). 161

Figure 5.16. Reusability of the enzyme in intensified membrane contactor (enzyme loading immobilized on membrane surface = 6.49 mg/$L_{reactor}$, enzyme loading immobilized on MNPs surface = 2.5 mg/$L_{reactor}$, 50 mM Tris buffer, inlet gas CO_2 percentage: 15%, liquid flow rate: 34 ml/min (Re_L = 31.6), gas flow rate: 100 ml/min (Re_G = 6), and counter-current flow).162

List of Tables

Table 1.1. Kinetic parameters of free and immobilized CA in literature (substrate: p-NPA). 13
Table 1.2. Properties of various immobilized CA. 20

Table 2.1. Flat sheet membrane and module specifications. 48
Table 2.2. Packings and packed-bed column specifications. 49
Table 2.3. Chemicals. 49

Table 3.1. Packings and packed-bed column specifications. 65
Table 3.2. BET surface area, mean BJH pore diameter and pore volume for bare MNPs and MNPs with 12, 24, and 32 h co-deposition times. 80
Table 3.3. Summary of CA immobilized on a variety of supports. 85

Table 4.1. Flat sheet membrane and module specifications. 105
Table 4.2. PDA/PEI loading and breakthrough pressure of the P-PP membrane for different deposition times. 119
Table 4.3. BET surface area, mean BJH pore diameter and pore volume for P-PP membrane at various deposition times. 120
Table 4.4. Performance of immobilized CA on different supports. 126
Table 4.5. Comparison of CO_2 absorption flux in different gas-liquid membrane contactors. 128

Table 5.1. Flat sheet membrane and module specifications. 143
Table 5.2. CO_2 absorption comparison in various membrane contactors. 164

Nomenclature

a gas-liquid interfacial area, m^2/m^3

$\bar{a}_s$ effective packing specific surface area, m^2/m^3

a_v specific area, m^2/m^3

B_1 coefficient in eq. (3.16), $B_1 = \dfrac{\left(1-\varepsilon^0\right)^{2/3}}{\eta^0} A_s^0 N_L^{1/8} N_R^{15/8}$

B_2 coefficient in eq. (3.16), $B_2 = 3.376\times10^{-3} \dfrac{\left(1-\varepsilon^0\right)^{2/3}}{\eta^0} A_s^0 N_G^{1.2} N_R^{-0.4}$

B_3 coefficient in eq. (3.16), $B_3 = \dfrac{4\sqrt[3]{A_s^0} N_{Pe}^{-2/3}}{\eta^0}$

c_{mp} micro-particles concentration, kg/m_r^3

C_{E0} loading of enzyme, $kmol/m_r^3$

$C_{E,mp}$ loading of enzyme immobilized on micro-particles, $kmol/m_l^3$

C_j concentration of species j, $kmol/m^3$

d_h hydraulic diameter, m

d_{mp} micro-particle diameter, m

d_p effective diameter, $d_p = \left(1-\varepsilon\right)/\bar{a}_s$, m

D column diameter, m

D_{ij} molecular diffusivity coefficient for binary gas systems, m^2/s

$D_{j,\alpha}$ molecular diffusivity coefficient of species j in α-phase ($\alpha = g, \ell$), m^2/s

$D_{j,\ell}$ molecular diffusivity coefficient of species j in liquid phase, m^2/s

$D_{j,\alpha}^{eff}$ effective diffusivity of species j inside membrane ($\alpha = g, \ell$), m^2/s

$D_{j,w}^{ef}$ effective diffusivity of species *j* inside washcoat, m^2/s

D_{kj} Knudsen diffusion coefficient of species *j*, m^2/s

$D_{\ell(g)}$ liquid and gas dispersion coefficients, m^2/s

D_{BM} Brownian diffusion coefficient, $D_{BM} = \frac{2k_B T}{6\pi\mu_\ell d_{mp}}$

D_x transverse dispersion coefficient, m^2/s

D_z axial dispersion coefficient, m^2/s

E_1, E_2 Ergun constants, –

f_e wetting efficiency, -

$F_{d\alpha}^m$ mechanical dispersion force, N/m^3

$F_{g\ell}$ gas-liquid drag force, N/m^3

F_{gs} gas-solid drag force, N/m^3

$F_{\ell s}$ liquid-solid drag force, N/m^3

g gravitational acceleration, m/s^2

H reactor height, m

${}_H E$ enzyme isomerized form

Ha Hamaker constant, J

$j_{rz(r,\theta)}$ dispersion drift velocity, $j_{rz(r,\theta)} = u_{gz(r,\theta)} - \frac{\varepsilon - \varepsilon_\ell / f_e}{\varepsilon_g} u_{\ell z(r,\theta)}$, m/s

$k_\ell a$ volumetric liquid-phase mass transfer coefficient, 1/s

$k_{\ell s}$ liquid-solid mass transfer coefficient, m/s

k_B Boltzmann's constant, J/K

k_g gas-phase mass transfer coefficient, m/s

$K_{g\ell}$ gas-liquid interaction force coefficient,

$$K_{g\ell} \cong \left\{ \frac{E_1}{36} \frac{\overline{a}_s^2 \mu_g \varepsilon_g}{\left(\varepsilon - \varepsilon_\ell / f_e\right)^2} + \frac{E_2}{6} \overline{a}_s \rho_g \frac{\varepsilon_g^2}{\left(\varepsilon - \varepsilon_\ell / f_e\right)^2} \sqrt{j_{rz}^2 + j_{rr}^2 + j_{r\theta}^2} \right\}$$

K_{gs} gas-solid interaction force coefficient,

$$K_{gs} = \left\{ \frac{E_1}{36} \frac{\overline{a}_s^2 \mu_g \varepsilon_g}{\varepsilon^3} + \frac{E_2}{6} \overline{a}_s \left(\frac{\varepsilon_g}{\varepsilon} \right)^3 \rho_g \sqrt{u_{gz}^2 + u_{gr}^2 + u_{g\theta}^2} \right\}$$

$K_{\ell s}$ liquid-solid interaction force coefficient,

$$K_{\ell s} = \left\{ \frac{E_1}{36} \frac{\overline{a}_s^2 \mu_\ell f_e}{\varepsilon_\ell} + \frac{E_2}{6} \overline{a}_s \rho_\ell \sqrt{u_{\ell z}^2 + u_{\ell r}^2 + u_{\ell \theta}^2} \right\}$$

L membrane length, m

m distribution coefficient

m_{CO_2} distribution coefficient

M_j molecular mass of species j, kg/kmol

N_G gravitational dimensionless group, $N_G = \dfrac{\left(\rho_{mp} - \rho_\ell\right) d_{mp}^2 g}{18 \pi \mu_\ell v_{s\ell}}$

N_L London-van der Waals dimensionless group, $N_L = \dfrac{4Ha}{9\pi \mu_\ell d_{mp}^2 v_{s\ell}}$

N_{mp} deposition rate of micro-particles, kg/m^{3}s

N_{Pe} Brownian diffusion group, $N_{Pe} = \dfrac{d_p(t)v_{s\ell}}{D_{BM}}$

P pressure, bar

P_j partial pressure of species j, Pa

P_c capillary pressure, Pa

r radial coordinate, m

R ideal-gas constant

$R^{c}_{CO_2,m}$ enzymatic CO_2 hydration reaction rate, kmol/m^3_ms

$R^{cat}_{CO_2}$ enzymatic CO_2 hydration reaction rate, kmol/m$^3_{reactor}$s

$R^{cat}_{CO_2,\ell f}$ enzymatic CO_2 hydration reaction rate in liquid film, kmol/m^3_ls

$R^{cat}_{CO_2,w}$ enzymatic CO_2 hydration reaction rate in washcoat, kmol/m^3_ws

$R^{mp}_{CO_2}$ enzymatic CO_2 hydration reaction rate on the surface of micro-particles, kmol/m^3_ls

$R^{uc}_{CO_2}$ uncatalyzed CO_2 hydration reaction rate, kmol/m^3_ls

$R^{uncat}_{CO_2}$ uncatalyzed CO_2 hydration reaction rate, $R^{uncat}_{CO_2} = R^{uncat}_{CO_2}\big|_{\ell}\,\varepsilon_{\ell}$, kmol/m$^3_{reactor}$s

$R^{uncat}_{CO_2,\ell f}$ uncatalyzed CO_2 hydration reaction rate in liquid film, kmol/m^3_ls

$R^{uncat}_{CO_2,w}$ uncatalyzed CO_2 hydration reaction rate in washcoat, kmol/m^3_ws

R^{c}_{j} enzymatic reaction rate of component j, kmol/m^3_rs

Re Reynolds number

S axial spreading factor, m

Sc Schmidt number

Sh Sherwood number

t time, s

T temperature, K

TON turnover number

$u_{\square}$ interstitial α-phase velocity, m/s

$u_{d\alpha}$ drift velocity, $u_{d\alpha,z(r,\theta)} = -\frac{S\left|u_{\ell,\alpha}\right|}{\varepsilon_\alpha}\frac{\partial \varepsilon_\alpha}{\partial z(r,\theta)}$, m/s

$v_{\square}$ superficial α-phase velocity, m/s

$v_{s\alpha}$ α-phase superficial velocity, m/s

x transverse coordinate within porous membrane and membrane contactor, m

z axial coordinate of the membrane contactor, m

w liquid (gas) side depth, m

Greek Letters

α α-phase, $\alpha = g, \ell$

δ_ℓ liquid film thickness, m

δ_m membrane thickness, m

$\delta_m^{g\ell}$ position of gas-liquid interface in membrane, m

δ_w washcoat thickness, m

ε packed bed porosity, -

ε_α α-phase holdup, -

ε_d porosity of solid deposit, -

ε_m membrane porosity

ε_w washcoat porosity, -

η collector efficiency, -

η_{cat} effectiveness factor for the enzymatic CO_2 hydration reaction, -

λ filter coefficient, m^{-1}

λ^0 clean filter coefficient, m^{-1}

μ_α dynamic viscosity of α-phase, kg/m s

μ_α^{ef} α-phase effective viscosity (combination of bulk and shear terms), kg/m s

σ_{ij} characteristic length, Å

θ circumferential coordinate, m

τ tortuosity factor

ρ_α α-phase density, kg/m^3

σ specific deposit (reactor volume basis), $\sigma = \left(\varepsilon^0 - \varepsilon\right)\left(1-\varepsilon_d\right)$, -

σ_{cr} critical specific deposit, $\sigma_{cr} = \left[\left(\frac{d_p^0 + 2d_{mp}}{d_p^0}\right)^3 - 1\right]\left(1-\varepsilon_d\right)\left(1-\varepsilon^0\right)$

σ_ℓ surface tension, N/m

υ_j stoichiometric coefficient, ($\upsilon_{CO_2(B)} = -1$, $\upsilon_{HCO_3^-(BH^+)} = 1$)

ξ washcoat radial coordinate, m

ζ liquid film coordinate, m

Ω_{ij} diffusion collision integral

Subscripts/Superscripts

0	clean packed bed state
c	catalyzed
cat	catalyzed
fe	free (solution-phase) enzyme
g	gas phase
i	gas-liquid interface
ie	immobilized enzyme
in	inlet, inside
ℓ	liquid phase
ℓf	liquid film
m	membrane
mp	micro-particle
r	reactor
s	solid phase
z	axial direction
uncat	uncatalyzed
w	washcoat

Abbreviations

B	buffer
BH^+	protonated buffer

Acknowledgment

I would like to express my eternal gratitude to Prof. Maria-Cornelia Iliuta, my Ph.D. supervisor, for her full support during my Ph.D. studies and providing an opportunity for me to study at Université Laval in Canada. Her scientific knowledge and enthusiasm guided me throughout every step of my research project. I would also like to express my sincere gratitude to Dr. Ion Iliuta for his endless advisement and mentorship through my Ph.D. research project. Many of the challenges in this path would not be solved without their creative ideas and supports. In addition, I would like to thank my co-supervisors, Profs. Francis Bougie and Alain Garnier for useful comments and assistance with enzyme production and characterization.

This thesis could not be accomplished without financial supports of Fonds de recherche du Québec - Nature et technologies (FRQNT) and the Natural Sciences and Engineering Research Council of Canada (NSERC).

I would like to acknowledge all Chemical Engineering Department staffs, who considerably helped me through my study at Université Laval, especially Jean-Nicolas Ouellet and Jérôme Noël. I really appreciated the help of Dr. Thierry Vincent and Barbara Valeria Mejia Bohorquez for the enzyme production and characterization.

I am very grateful to all my friends and colleagues in Prof. Iliuta's research group, whose motivations and supports assisted me through tough times during this period. I particularly thank Ommolbanin Ali Zadeh Sahraei, Kang Gao, Alex Desgagnés, Alexandre Babin, and Thi Ngoc Mai Dang. I wish them the best of luck in their future career.

Last, but by far the most, I would like to thank my parents and brothers for their unconditional love and supports during this period of my life, without whom I undoubtedly could not accomplish this doctorate.

I cannot express in words my deep sense of gratitude to my beloved husband and best friend, Saeed, with his undying love, tremendous understandings and supports.

Finally, I thank my lovely daughter, Arshida, for giving me hope and encouragement to be able to complete this project successfully.

Foreword

This dissertation comprises 5 chapters, which come after an introduction regarding CO_2 emissions and CO_2 capture technologies. Chapter 1 provides a comprehensive literature review on carbonic anhydrase enzyme, recent advancements in carbonic anhydrase enzyme immobilization and its implementation in various CO_2 capture technologies. Chapter 2 describes the chemicals and materials used in our work, the methodology of biocatalytic materials preparation and characterization, measurements of biocatalytic materials activity, enzyme loading and kinetic constants, and CO_2 capture experiments. Chapters 3-5 represent the main part of this thesis (results and discussions), which consists of the research findings and their analysis. Finally, the general conclusions and suggestions for future work are given.

This thesis was prepared based on the following published articles:

1. **Rasouli, H.,** Nguyen, K., Iliuta, M.C. Recent advancements in carbonic anhydrase immobilization and its implementation in CO_2 capture technologies: A review. *Separation and Purification Technology* 2022, *in press*. IF 7.3 (Chapter 1)
2. **Rasouli, H.**, Iliuta, I., Bougie, F., Garnier, A., Iliuta, M.C. Enhanced CO_2 capture in packed-bed column bioreactors with immobilized carbonic anhydrase. *Chemical Engineering Journal* 2022, 432, 134029. IF 13.3 (Chapter 3)
3. **Rasouli, H.**, Iliuta, I., Bougie, F., Garnier, A., Iliuta, M.C. Enzyme-immobilized flat-sheet membrane contactor for green carbon capture. *Chemical Engineering Journal* 2021, 421, 129587. IF 13.3 (Chapter 4)
4. **Rasouli, H.**, Iliuta, I., Bougie, F., Garnier, A., Iliuta, M.C. Hybrid enzymatic CO_2 capture process in intensified flat sheet membrane contactors with immobilized carbonic anhydrase. *Separation and Purification Technology* 2022, 287, 120505. IF 7.3 (Chapter5)

The candidate performed all the experimental work presented in the current thesis and prepared the manuscripts by considering the supervisor/coauthors comments. The modeling parts were performed by Dr. Ion Iliuta.

Introduction

According to the World Energy Outlook 2016, global energy consumption is continuously increasing, with a predicted 30% growth by 2040 [1]. World economy is dependent on fossil fuels for energy generation and carbon dioxide (CO_2) is one of the principal greenhouse gases produced by excessive reliance on fossil energy, which contributes to global warming. There is growing political and public awareness, that rising global emissions will soon increase atmospheric CO_2 concentrations to never-before-seen levels, posing a growing risk of rapid climate change. **Figure I.1** represents global energy-related CO_2 emissions, 1990-2021, and change in CO_2 emissions by fuel, 1990-2021, reported by International Energy Agency [2].

In this context, carbon capture and storage (CCS) is a recent technology to capture the CO_2 from main sources, which will give the opportunity to use the existing fossil fuels while stabilizing the CO_2 concentrations in the atmosphere [3]. Also, the concentrated stream of the captured CO_2 will be ready for sequestration or further use (like conversion into valuable products). Post-combustion, oxycombusion and pre-combustion are the three technological concepts of CO_2 capture (**Figure I.2**)[4]. These technologies can be installed in new plants or adapted to existing ones.

CO_2 capture can be implemented based on a variety of physicochemical methods of separation, like absorption in liquids (solvents), adsorption on solids, membrane technologies, and cryogenic distillation [5]. Their main advantages and disadvantages are summarized in **Figure I-3**.

Absorption using amine-based absorbents is the most prevalent method in CO_2 capture due to its high efficiency. Nevertheless, there is interest in using benign solvents (such as water and potassium carbonate) in CO_2 capture processes, due of the negative features of amine-based absorbents such as substantial energy and electricity consumption especially for absorbent regeneration, toxicity, degradation, and corrosivity [6]. Benign solvents are, however, slow in CO_2 absorption. Thus, in the last decades, to increase the CO_2 absorption rate in benign solvents such as water, enzymatic capture using *carbonic anhydrase* (CA) has been developed to promote the absorption rate [7, 8].

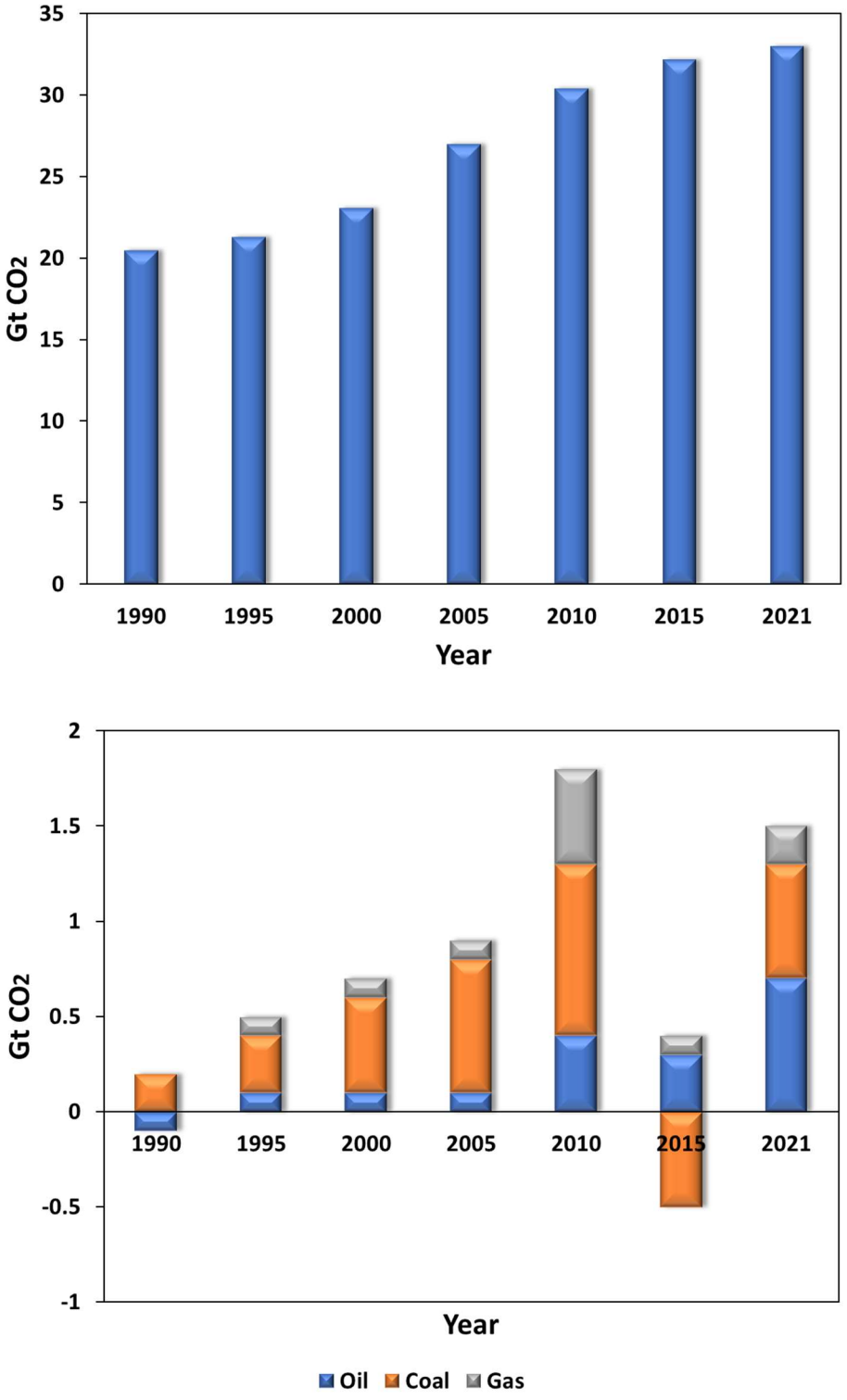

Figure I.1. Global energy-related CO_2 emissions, 1990-2021, and change in CO_2 emissions by fuel, 1990-2021 (Adapted from [2]).

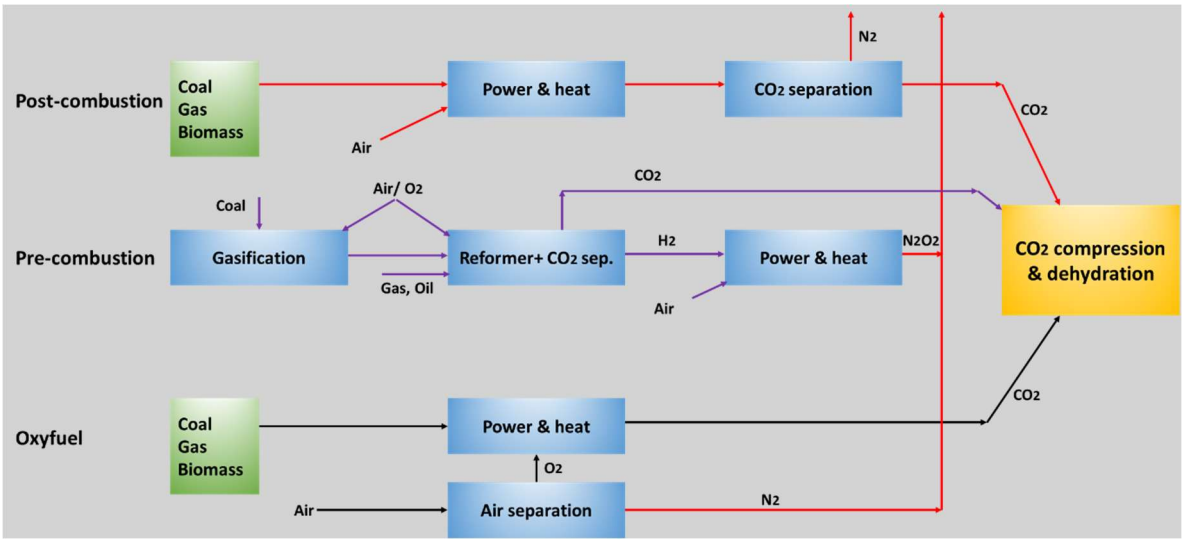

Figure I.2. CO_2 capturing systems (Adapted from [9]).

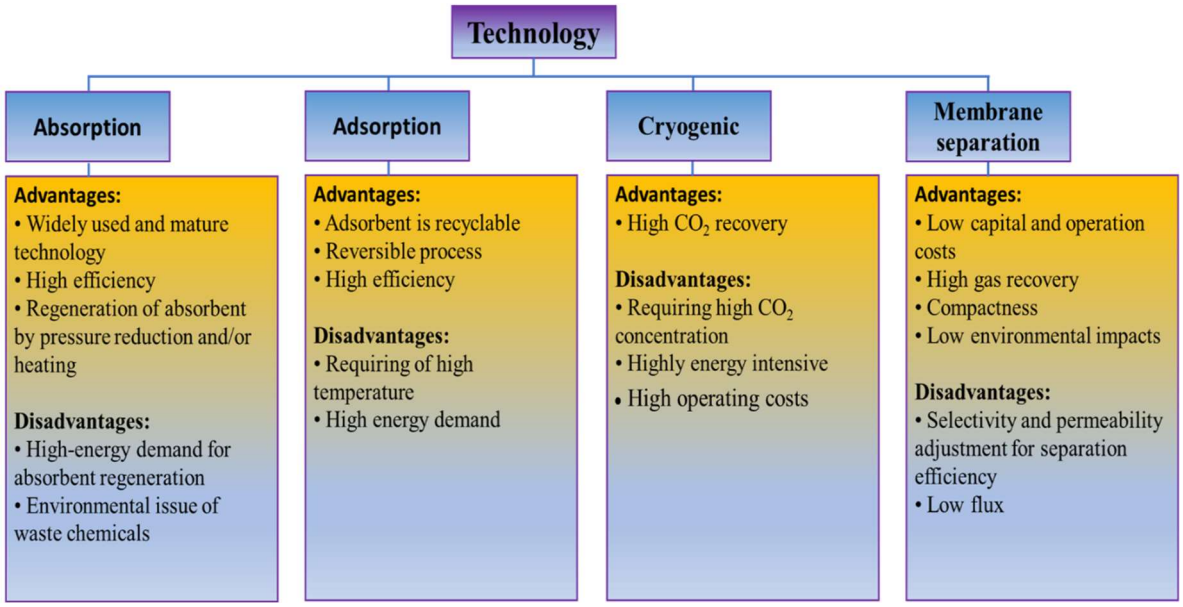

Figure I.3. CO_2 capture technologies comparisons [10].

CA, a naturally occurring enzyme, is recognized to catalyze the CO_2 conversion to bicarbonate. Due to its extremely high turnover rates, CA shows a great potential to promote the absorption rates of CO_2 in the CO_2 capture technologies working with benign solvents, catalyzing the CO_2 hydration step, which is the rate limiting step in the CO_2 absorption process. CA can be employed in two forms: free (in solution) or immobilized (on solid

surfaces). Working with free enzyme, on the other hand, has a number of difficulties that have been extensively reported in the literature. Consequently, immobilization of enzyme to solid surfaces is a focus of research since it improves enzyme recovery and reusability. Immobilization also improves enzyme stability and prolongs its lifespan.

In this context, the present thesis focusses on *enzymatic CO_2 capture*, as *green alternative* to customary technologies.

Various enzymatic CO_2 capture reactors utilising CA, such as random packed-bed column [11, 12], structured packed-bed column [13], bubble column [14], spray tower [15], trickle-bed reactor [16], Integrated Vacuum Carbonate Absorption Process (IVCAP) reactor [17], selective membrane [18], and membrane contactor [19], have been developed over the last years. The most reported technology in literature for CO_2 capture concerns the gas-liquid packed-bed columns due to the process maturity, high efficiency, high surface area, low pressure drop, and high mechanical stability [11]. Investigations on CO_2 capture in packed-bed column with immobilized CA are, however, very scarce in the open literature. On the other hand, gas-liquid membrane contactors represent a forefront technology offering several advantages over traditional packed columns. Membrane contactors combine the membrane technologies and absorption system, offering the advantages of both technologies: high selectivity, compactness, simple operation, operating and capital costs reduction and modularity [6, 8, 20-23]. Gas-liquid membrane contactors involve the mass transfer of CO_2 from gas phase through the membrane pores and then its absorption in the liquid phase flowing on the opposite side of the membrane [6, 23, 24]. However, very few efforts have been made to develop enzymatic process in membrane contactors for capturing CO_2.

In this context, this thesis concentrates on *the performance of CO_2 absorption using immobilized CA in two different technologies: packed-bed column and membrane contactor bioreactors*.

Chapter 1 will therefore mainly focus on important features of CA immobilization with a discussion on kinetic parameters of free and immobilized CA enzyme and outline various techniques and support materials for immobilizing CA, paying particular attention to enzyme

activity, stability, reusability, and enzyme loading parameters. Diverse CO_2 capture technologies assisted by immobilized CA enzyme, including recent advances, will be critically highlighted, focusing not only on the separation processes, but also on possible problems associated with the developed systems.

Chapter 1: Literature review

1.1. Carbonic anhydrase- CO_2 hydration biocatalyst for green CO_2 capture

CA is a metalloenzyme catalyst which usually exists in nature (mammals, plants, algaes and bacteria) and converts CO_2 into bicarbonate ion and a proton [25]. It adjusts biological processes in human and other living organisms and according to the Enzyme Commission (EC), it is defined by EC 4.2.1.1 [7]. k_{cat} is the turnover number and changes between 10^4 and 10^6 molecules of CO_2 per molecule of CA per second based on CA origin. This makes CA a powerful enzyme in CO_2 capture and sequestration [19, 25]. In addition, non-toxicity, biodegradability, and operating in moderate conditions are other advantages of CA [7]. There are five distinct classes (α, β, γ, δ and ζ) of CA based on their structure and origin. α-CA is the most common enzyme that lives in mammals in the forms of monomer. Its activity corresponds to the cofactor Zn^{2+} ion placed at the bottom of the active site and connected to three histidine residues in a cone shaped cavity. The first β-CAs were recognized in spinach and pea chloroplasts [26] and they live more in plants and algae and sometimes in Bacteria and Archaea, existing as a dimer, tetramer, or hexamer. The cofactor in this case (Zn^{2+} ion) connects to two cysteine residues and one histidine. γ-CA is mostly present in Archaea in the form of trimer and its active site corresponds to three histidine residues and metal-bound water. Zinc is the cofactor, but iron and cobalt can also be substituted as active metal in this type. δ-CA active metal is zinc which bounds two cysteines and one histidine. ζ-CA has Cd^{2+} as active ion and connects to two cysteines and one histidine. The last two classes are found in diatoms [27, 28]. Crystal structures of four classes of CA are shown in **Figure 1.1**.

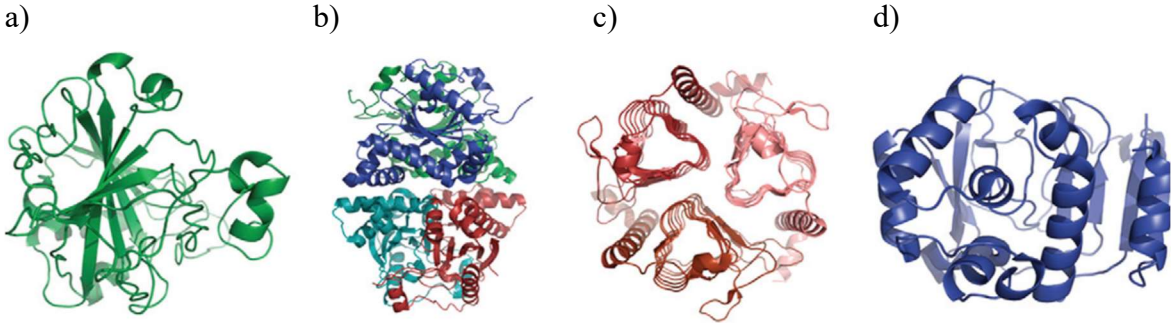

Figure 1.1. Crystal structures of four CAs. (a) α-class CA, type II. (b) β-class CA. (c) γ-class CA. (d) ζ-class CA. Crystal structure of δ-class CA has not been reported [27].

Isozymes of α-CA exist in seven categories in human body (I, II, III, IV, V, VI and VII) [26]. Human carbonic anhydrase (hCA, or CA for simplicity) I is found in tissues and CA III is found in some muscles. CA III has a low hydration rate among the seven isoenzymes. CA IV is present on the plasma surface of endothelial cells and CA V could be found in mitochondria of certain tissues. CA VI and VII are expressed in salivary glands [26]. CA II is widespread in the human body and its k_{cat} is ~ 10^6 s^{-1}, the highest k_{cat} among the other types. The interest of using CA II in CO_2 capture is because of its high hydration rate [26, 27]. **Figure 1.2** shows more information about the CA II structure. The zinc ion (Zn^{2+}) is located at the bottom of the cavity and is linked to three nitrogen atoms of His-94, His-96 and His-119 in tetrahedral coordination geometry. Also, it is linked to H_2O or OH^-. These ligands are connected to other groups in protein with hydrogen bonds. His-64, is located at the mouth of active site cavity and has an appropriate pKa value (acid dissociation constant, pKa: 6.1) for the dual function as proton acceptor and donor [26, 29].

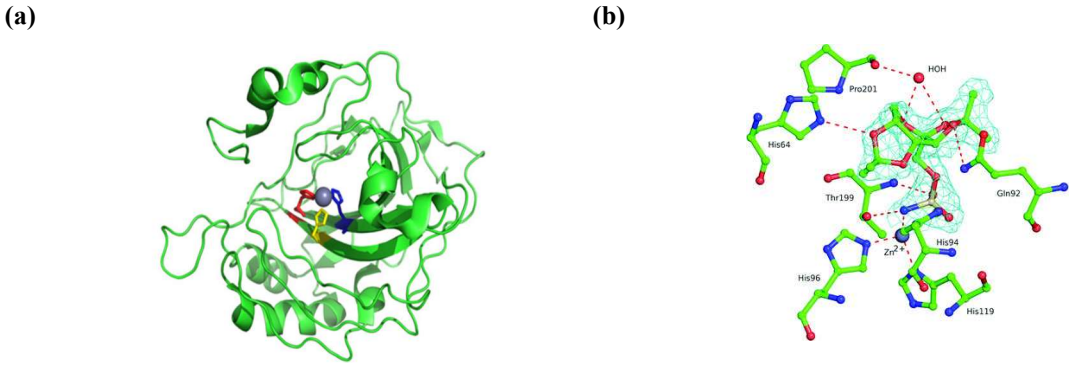

Figure 1.2. a) Structure of CA II, b) View of CA II active site [30].

The CO_2 hydration mechanism is given by:

$$CO_2 + H_2O \rightleftharpoons H^+ + HCO_3^- \quad (1.1)$$

In presence of CA, this reaction mechanism is modified as follows:

$$Zn^{2+}\text{-}OH^- + CO_2 \rightleftharpoons Zn^{2+} + HCO_3^- \quad (1.2)$$

$$Zn^{2+} + H_2O \rightleftharpoons H^+ + Zn^{2+}\text{-}OH^- \quad (1.3)$$

Figure 1.3 illustrates the CO_2 hydration mechanism of CA. Zinc's role (+2 charge) in CA is attracting the water's oxygen, converting water to hydroxide ion by deprotonation of water that would be better nucleophile. pKa decreases due to the binding of water to zinc and with the lower pKa, water molecules are easily able to turn into a hydroxide ion [26]. In detail, there are five steps in this mechanism [26, 31]:

- In the first step, CO_2 molecule is linked to the enzyme through replacing the water molecule. It means CO_2 makes a bound with NH peptide group of Thr-199.

- In the second step, bicarbonate ion is formed through the nucleophilic attack of hydroxyl ion of zinc ion to CO_2 molecule. Bicarbonate ion connects with three bonds to the enzyme (hydrogen bond to peptide NH group of Thr-199, hydrogen bond to hydroxyl group of Thr-199 and oxygen bond to zinc ion).

- The third step is the release of the bicarbonate ion which is replaced with two molecules of water. One water molecule binds to zinc ion to obtain the tetrahedral shape again and another one binds to the peptide NH group of Thr-199 amino acid.

- The fourth step is the isomerization step or intramolecular transfer step. In this step, His-64 of enzyme picks up proton of water molecule which linked to zinc ion. It acts as proton shuttle and its role is removing hydrogen from the water molecule and transferring the proton to enzyme's edge that should be easily removed by buffer [26, 29].

- The fifth step is intermolecular transfer step. In this step, the proton bound to His-64 is transferred to an unprotonated buffer. Therefore, the enzyme will return to its initial form.

The proton transport from the active site is a rate-limiting step for the enzyme. Buffers are the proton-transfer agents in the CA II catalytic hydration mechanism and the unprotonated buffer concentration determines that either intramolecular proton-transfer controls the catalytic reaction or intermolecular proton-transfer. A low unprotonated buffer concentration leads to a rate limiting intermolecular step and then small CO_2 hydration rate. On the contrary, the CO_2 hydration rate is large in sufficiently high unprotonated buffer concentration [32]. Also, in the reaction between CO_2 and water, the liquid is acidified. Using buffer prevents acidity problems and regulates specific pH for enzyme [33].

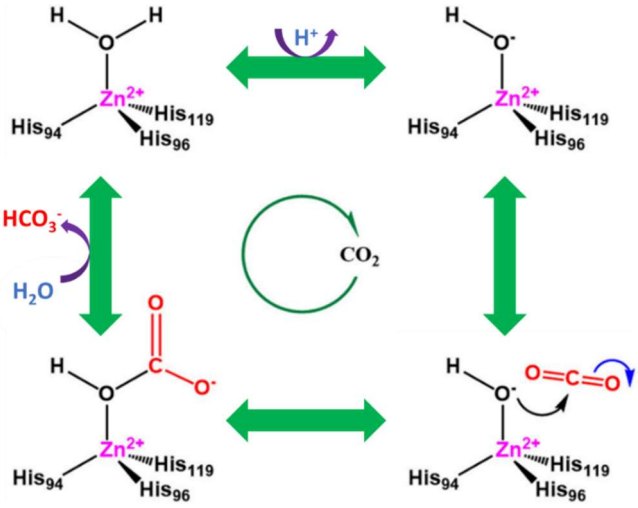

Figure 1.3. CO_2 hydration mechanism of CA (adapted from [34]).

CA enzyme enhances the CO_2 absorption rates when benign solvents are used, accelerating the CO_2 hydration rate which is known as rate limiting step in the CO_2 absorption process. There are two approaches to utilize the CA enzyme in the liquid phase of CO_2 capture technologies which are free enzyme in solution and immobilized form on solid surfaces. Due to the advantages of enzyme immobilization (more detail in next section), the thesis will focus on development of green CO_2 capture technologies using immobilized CA enzyme.

1.2. Enzyme immobilization

CA enzymes are fragile molecules with a limited range of working conditions (temperature: 20-40 ºC, pH: 6-8) and their use in its free form is not recommended because it cannot be extracted from the reaction environment [35], which severely limits its large-scale industrial applications. Also, the use of free enzyme dissolved in the solution phase is not favorable due to the considerable required amount of enzyme in enzymatic process. Enzyme denaturation is another challenge which causes the loss of the enzyme's CO_2 hydration activity over time. To address these issues, immobilization was used to overcome the challenges. The confinement or attachment of enzyme molecules within a matrix is referred to immobilization [36]. Enzyme immobilization provides flexibility in reactor design and prevents from biocatalyst contamination during separation process [7, 11, 25, 37]. Furthermore, the immobilization increases enzyme recovery and reusability, lowering the overall cost of the enzyme [19, 38, 39]. It can also make the enzymes more stable by

shielding them from the medium or consolidating their structure, since there is significant evidence of the beneficial effect of immobilization on biocatalyst stability under harsh operating conditions. CA immobilized on nanofibers retained approximately 95% of its initial activity during 60 days at 4 °C and also maintained about 60% activity after 40 reuses, whereas free enzyme showed only 40% activity after 60 days at 4 °C [40]. Immobilized enzyme on mesoporous silica also retained about 85% of activity at pH more than 10, while free enzyme lost almost 90% of its activity [41]. Regarding to enzyme resistance to chemical impurities, the immobilized CA on controlled pore glass (CPG) maintained total of their initial activity in presence of 0.4 M SO_4^{2-}, 0.05 M NO_3^- and 0.3 M Cl^- anions after 20 days, while free enzyme showed only 37% of its initial activity in the same conditions [17]. Concerning the thermal stability of CA enzyme, the immobilized enzymes on glass beads can retain 60% of their initial activities after three months at 50 °C compared to their free counterparts at the same temperature, which display 30% of initial activity only [17]. CA sourced from thermophilic organisms are stable at higher temperatures ranging from 70 °C to 90 °C [16]. A γ-class CA from *Methanosarcina thermophila* (CAM) and a β-class CA from *Methanobacterium thermoautotrophicum* (CAB) can operate optimally in a temperature range of 55-70°C [27]. An alternative approach is to engineer or evolve a CA and construct an artificial enzyme mimic. Zinc cyclen perchlorate, which consists of a zinc atom coordinated to a cyclic amine ligand, has been used as a CA mimic. The artificial enzyme mimic was shown to be stable at higher temperatures (75-100 °C) [42]. However, they exhibit five-fold lower activity compared to the original one [42].

It is worth noting that enzyme immobilization is a complicated topic. The immobilization process may reduce the enzyme activity for a variety of reasons: mass transfer limitations, conformational change of enzyme, enzyme turnover reduction or partitioning of substrate and products in the support [43, 44]. Diffusional effects are more significant with immobilized enzyme, resulting in a lower CO_2 conversion [38]. Via simulation, Iliuta et al. [38] focused on a study of catalyzed or uncatalyzed CO_2 hydration in a isothermal microreactor with CA II in solution phase or immobilized on the inner surface of the reactor. Under similar conditions, CO_2 conversion with immobilized CA was found to be 47% compared to 76% for free enzyme. Diffusional limitation was considerable in the system with immobilized CA, restricting a suitable exploitation of the high hydration turnover of CA

enzyme, while diffusion was not a constraint in the system with free enzyme in solution [38]. Additionally, immobilization makes the enzyme to behave differently, since the immobilized enzyme faces different environment and may obtain different conformation compared to the enzyme in solution phase [45, 46].

The immobilization also affects intrinsic enzyme kinetics, which can be evaluated by hydrolysing p-nitrophenyl acetate (p-NPA) in the presence of CA to produce p-Nitrophenol (p-NP). The catalytic activity of free and immobilized CA is then measured at different concentrations of p-NPA [47, 48] and the kinetic parameters (Michaelis constant (K_m) and kinetic constant (k_{cat}/K_m)) are obtained using the Michaelis–Menten equation **(equation 1.4)** and the Lineweaver– Burk equation **(equation 1.5)**, as shown in **Table 1** for different kind of supports. The maximum rate achieved by the system is represented via V_{max}, which occurs at maximum substrate concentration for a given enzyme concentration. K_m is the substrate concentration when the reaction rate is half of V_{max}.

$$V = \frac{k_{cat}[E][S]}{K_m + [S]} \quad (1.4)$$

$$\frac{1}{V} = \frac{K_m}{V_{max}}\frac{1}{[S]} + \frac{1}{V_{max}} \quad (1.5)$$

Where:

V: Formation rate of p-Nitrophenol (p-NP), $M^{-1}.s^{-1}$;

k_{cat}: Catalytic rate constant, s^{-1};

K_m: Michaelis constant (the affinity of the enzyme for the substrate), M^{-1};

V_{max}: Maximum rate, $M^{-1}.s^{-1}$;

[E]: Concentration of enzyme (CA), M^{-1};

[S]: Concentration of substrate (p-NPA), M^{-1}.

As seen in **Table 1.1**, the k_{cat}/K_m of CA enzyme generally decreases, while K_m increases after immobilization. Structural changes of CA in the process of immobilization, a lower accessibility to the active site, a decreased affinity for the substrate, the mass transfer resistance of the substrate onto the immobilized enzyme, as well as the steric hindrance effect after immobilization, are possible reasons of the k_{cat}/K_m reduction [49, 50]. For example,

k_{cat}/K_m of CA enzyme decreased from 488 $M^{-1}s^{-1}$ to 206 and 117 $M^{-1}s^{-1}$ after immobilization on PVDF membrane modified by amine and epoxy functionalities via 3-aminopropyl triethoxy silane (KH550) and γ -(2,3-epoxypropoxy) propyl trimethoxy silane (KH560), respectively [51]. The lower k_{cat}/K_m obtained from immobilized CA via KH560 may be attributed to a conformational change of CA in the alkaline environment during immobilization. Also, in the same conditions, immobilized CA on PE depicted higher k_{cat}/K_m over PVDF due to the higher activity recovery (about 53% and 76% for PVDF-attached CA and PE-attached CA, respectively) because the former has a wider pore structure and improved hydrophilicity, resulting in a higher loading quantity and enhanced enzyme affinity [52]. According to **Table 1.1**, the K_m value of CA immobilized within polyurethane foam reduced from 12.2 to 9.6 mM [53], which might be ascribed to surface charge variation. However, little information was provided in this study on the subject. CA-conjugated liposomes (CALs) was synthesized with the formation of amide bonds between the main amines of CA molecules and the carboxyl group-bearing liposomes modified by the 3-(3 dimethylaminopropyl) N′-ethylcarbodiimide (EDC)/sulfo-N-hydroxysuccinamide (NHS) reagents [54]. CALs generated a K_m value that was equivalent to free CA. k_{cat} value of free CA, on the other hand, was 3.3 times more than the value of CALs. The results showed that the affinity of liposome-conjugated CA for p-NA was equal to that of free CA, despite the fact that the enzyme was partially deactivated on the liposome surface. Active CA molecules filled around 10% of the surface of liposomes. The orientation of CA molecules generated by the local charge of the enzyme was proposed to impact the enzyme activity. CA attached in silica monoliths using the sol-gel technique maintained its overall conformation [55]. Although the K_m was nearly identical with free enzyme, the turnover number and specific activity of the encapsulated enzyme were only 1-2% of those of the enzyme in solution. Because the substrate diffused slowly through silica pores, the enzymes attached at the surface of silica monolith were responsible for the majority of the catalytic effect. Also, Vinoba et al. [56] immobilized CA on gold nanoparticles assembled over mesoporous silica (SBA-15) and the kinetic parameters (k_{cat}/K_m and k_{cat}) were almost similar to those of free CA, illustrating that the thermodynamics equilibrium is not affected by the immobilization. However, the kinetics could be negatively affected depending on the geometrical aspect of the system.

As support, microspheres or nanoparticles outperform a polymer membrane in terms of affinity or catalytic effectiveness, due to the former's greater mobility. Compared to K_m value of the free enzyme, the K_m values of immobilized CA on PVDF-KH550 [51], PVDF-KH560 [51], and TiO_2 coated membrane [48] increased by 1.6, 2.0, and 4.0 times, respectively, and this increase is significantly superior than the increase in the case of immobilized CA on some of the nanoparticles (see **Table 1.1**). It is clearly indicated that there is a higher mass transfer resistance in coated membranes in comparison with the biocatalytic nanoparticles and free CA [44, 57]. This finding suggests that CA enzyme immobilized on nanoparticles generates a high level of enzyme activity, successfully preserving the CA-p-NPA affinity after immobilization [58]. Besides, CA immobilized on membranes activated by polyethyleneimine (PEI)-polydopamine (PDA) displayed less enhancement of K_m rather than CA immobilized on the membranes functionalized by KH550, KH560 and TiO_2, highlighting the higher affinity of CA enzyme to the PEI and PDA and less conformation change of enzyme after immobilization [48, 52].

Table 1.1. Kinetic parameters of free and immobilized CA in literature (substrate: p-NPA).

Support type	**Free enzyme**		**Immobilized enzyme**		**Ref.**
	K_m (mM)	**k_{cat}/K_m ($M^{-1}.s^{-1}$)**	**K_m (mM)**	**k_{cat}/K_m ($M^{-1}.s^{-1}$)**	
PVDF-KH550	6.18	488	9.97	206	[**51**]
PVDF-KH560	6.18	488	12.5	117	[**51**]
PVDF modified by PEI/PDA	6.18	488	10.62	132.2	[**52**]
PE modified by PEI/PDA	6.18	488	8.65	312.9	[**52**]
TiO_2 coated membrane	10.8	-	42.3	-	[**48**]
TiO_2 nanoparticles	10.8	-	13.7	-	[**48**]
Magnetic nanoparticles	0.48	1917	1.02	59	[**59**]
Chitosan stabilized iron nanoparticles	1.594	-	1.727	-	[**60**]
Gold nanoparticles	13.07	1663.35	27.75	1612.25	[**56**]
SBA-15	56.67	873.76	65.2	740	[**45**]
SBA-15	27.29	7768	26.59	7569	[**61**]
Amine-functionalized SBA-15	2.4	896.4	3.0	728.2	[**41**]
Epoxy-functionalized SBA-15	2.4	896.4	3.1	757.4	[**41**]
Silica monoliths	14	-	16	-	[**55**]

Epoxy-functionalized magnetic polymer microspheres	6.091	372.68	8.077	82.95	[**58**]
Liposomal NG-POPE	9.7	505	9.4	159.58	[**54**]
Chitosan beads	0.87	-	2.36	-	[**49**]
Nanosilver	-	1660	-	1640	[**62**]
Polyurethane foam	12.2	166.4	9.6	-	[**53**]
Chitosan-alginate polyelectrolyte complex	18.26	-	19.12	-	[**50**]

Selection of the appropriate immobilization technique and support material are very crucial parts of the immobilization process as they play significant roles in determining the enzyme activity and stability [39].

There are different procedures of immobilization, each with its own set of strengths and weaknesses [63]. Generally, the strategies for enzyme immobilization are divided into: (1) adsorption, (2) covalent coupling, (3) entrapment, and (4) cross-linked enzyme aggregates (CLEA) [64-66]. The first three techniques are all based on specific interactions between enzyme molecules and support materials. The last technique does not need to use support materials [35, 67]. Schematics of these immobilization techniques are shown in **Figure 1.4**.

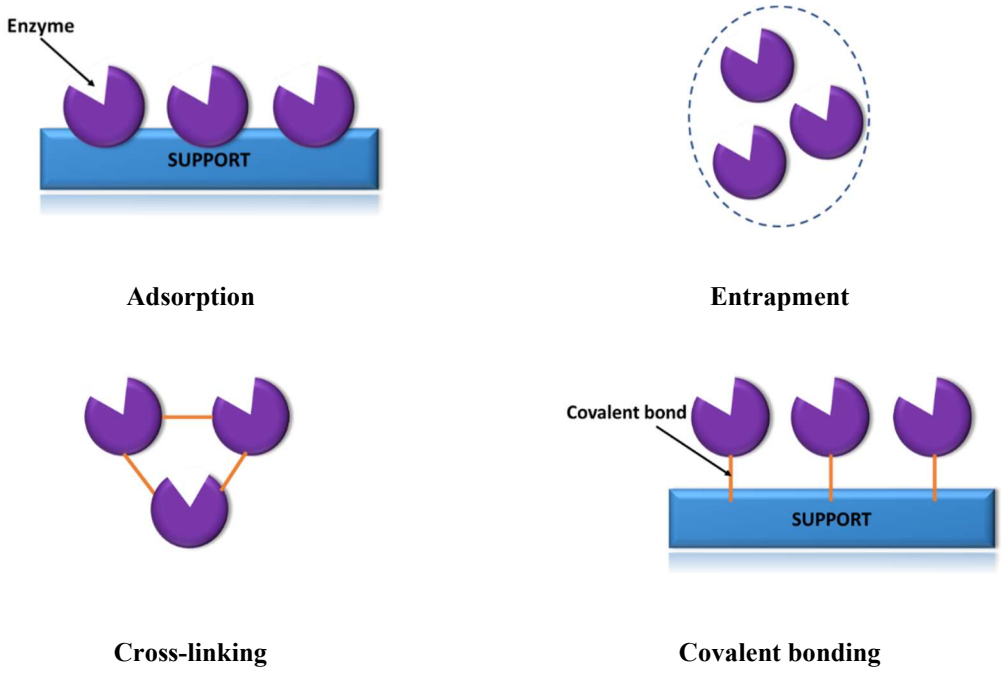

Figure 1.4. Enzyme immobilization techniques.

1.2.1. Adsorption

Adsorption includes physical adsorption and electrostatic binding. The physical adsorption method is the most common method of immobilization whereby the enzymes are physically attached to the support material [68].The enzyme is dissolved in a solution, and then the support is put in solution for a defined time and appropriate conditions [69]. In this method, the enzymes are adsorbed to the support via hydrogen bonding forces, van der Waals forces, or hydrophobic interactions [39]. This method is simple and cost-effective, chemical free and there is no need for modification of support surface. The immobilization by adsorption is generally non-destructive with respect to the enzyme and thus preserves the initial enzyme catalytic activity as much as possible [70]. But adsorption is somewhat a reversible method so that the enzymes could easily detach from the support due to the weak forces [71]. The immobilized CA on mesoporous silica SBA-15 using adsorption method lost its initial activity 10% more than with the covalent bonding method after 30 days due to the weak forces between enzyme and support. Also, the immobilized CA via the adsorption method lost its initial activity 20% more than with the covalent bonding method after 40 cycles of catalysis, again due to the weak forces [45]. Similar trend of losing activity (about 10%) was achieved for immobilized CA on TiO_2 nanoparticles after 20 days [48].

In the electrostatic binding method, the electrostatic forces interfere in enzyme immobilization. Enzyme molecules surface may carry positive or negative charges due to the isoelectric point of the enzyme and solution pH. So the enzyme is immobilized on opposite charged surface via ionic and strongly polar interactions [72]. The two conventional electrostatic adsorption immobilization techniques are the layer-by-layer (LBL) deposition and the electrochemical doping. In the LBL deposition method, the opposite charged layers and the enzyme all overlap on the support. This process involves the immersion of a cationic/anionic charged support in anionic/cationic polyelectrolyte solutions and then in a cationic/anionic enzyme solution [73]. A polyelectrolyte is categorized either cationic (polycations) or anionic (polyanions). poly(allylamine) (PAA), poly(l-lysine) (PLL), poly(ethyleneimine) (PEI), poly(dimethyldiallylammonium chloride) (PDDA), poly(allylamine hydrochloride) (PAH) and chitosan (CHIT) belong to polycations and poly(stryrenesulfonate) (PSS), poly(vinylsulfonate) (PVS), poly(anilinepropanesulfonic acid) (PAPSA), poly(acrylic acid)(PAA) and poly(methacylic acid) (PMA) belong to

polyanions [74]. Yong et al. [70, 73] immobilized CA on porous PP membrane surfaces via LBL (PEI/PSS/PAH) electrostatic adsorption technique, although stability of immobilized enzyme was not reported. In the electrochemical doping method, enzymes are immobilized into the conductive polymer film during the oxidation or reduction process of the polymer in which the polymer becomes positively/negatively charged. Therefore, the charged enzymes are attached into that conductive polymer, respectively [71, 75].

1.2.2. Entrapment

In the entrapment method, the enzymes are blocked in a polymeric network and are not attached to the support. The network allows only passing of substrate and products but retains the enzyme. Firstly, enzyme is mixed into a monomer solution and secondly the monomer solution is polymerized [68]. In this method, the enzyme is physically confined within a polymer network and does not chemically interact with the network, retaining most of the enzyme activity. This method helps prevent enzymes aggregation, protecting the enzyme activities [39]. For biomimetic CO_2 sequestration, the CA was immobilized in polyurethane (PU) foam, and the immobilized enzyme retained 100% of its activity [53]. However, the enzyme reusability is an important parameter because it affects the total cost of the immobilization process. The immobilized enzyme in chitosan-alginate polyelectrolyte complex using the entrapment technique retained only 53% activity after 8 cycle and 25-30% after 10 cycle [50]. The poor reusability of the enzyme using the entrapment method is related to the enzyme leakage from the matrices due to the large pore size of the support and also to the loss of enzyme during rinsing process [76-79].

1.2.3. Cross-linking

Cross-linking is formed by intermolecular reactions and covalent bonds between enzyme molecules by means of functional reagents and is an irreversible method [80]. Because it is affordable and widely accessible, glutaraldehyde is a common functional reagent [72]. It is possible to decrease the enzyme activity in this method due to the use of glutaraldehyde as this could possibly cause the conformational changes of enzyme [68]. In the cross-linking enzyme crystal (CLEC) method, after crystallization, glutaraldehyde is used to cross-link enzyme crystals [78]. In cross-linked enzyme aggregate (CLEA) method, the enzyme aggregation is induced by precipitants (salts, organic solvents or non-ionic polymers) and in

the second step; bifunctional reagent is used for cross-linking [72]. CLEA has the advantage of working in aqueous solutions while CLEC needs the formation of crystals. Peirce et al. [81, 82] reported the utilization of bovine CA (bCA) immobilized via CLEA to ameliorate the biocatalyst stability at the typical operating conditions of CCS processes. A magnetic CLEA (m-CLEA) was also prepared by crosslinking the precipitated bCA/nanoparticles (NPs) aggregates with glutaraldehyde. Enzyme concentration, precipitating agent, concentration of glutaraldehyde, crosslinking operating conditions, and concentration of MNPs were optimized to improve the immobilization procedure. CA was immobilized over SBA-15 [45] and on polystyrene/poly(styrene-co-maleic anhydride) (PS/PSMA) nanofibers [40] using cross-linking method. Immobilized CA on mesoporous silica SBA-15 with cross-linking method illustrated a higher enzyme loading than the adsorption and covalent bonding methods, exhibiting a 20% larger kinetic constant [45]. In addition, a higher amount (5-10%) of precipitated $CaCO_3$ (using calcium solution) was obtained in the case of CA immobilization via cross-linking approach compared to other methods.

1.2.4. Covalent bonding

The covalent bonding is a chemical reaction between the support and the enzyme molecule and is an irreversible method. In this method, the supports require functional groups such as amine, epoxy, hydroxyl, carboxyl, etc. which could be either activated or added to the surface and react with functional groups on the enzyme through covalent bonding. Carbodiimides and glutaraldehyde are widely used as an activating reagent and then the enzymes are linked to the support by covalent bonding [71]. Carbodiimides are used for bonding between an amine functionalized support and a carboxyl functionalized enzyme or a carboxyl functionalized support and an amine functionalized enzyme. Through carbodiimide activation of the enzyme, the CA was immobilized by covalent bonding to the nanoparticles of paramagnetic Fe_3O_4. In the alkaline carbonate solution used as a solvent for CO_2 absorption experiments, the efficient covalent attachment of enzyme and the support was confirmed [83]. Glutaraldehyde coupling is extensively used for immobilization via the reaction of the aldehyde group of glutaraldehyde molecule with the amino group of enzyme and also the reaction of another aldehyde group of the glutaraldehyde molecule with the amino group of support [84]. Because of the chemical reactions, it is possible that the active site of the enzyme has a lower activity or not at all due to denaturation. Also, more care,

complexity and long-time are the other disadvantages [39]. The direction of binding is very important; it is reported that the maximum enzyme activity could be obtained when the amino groups at the center of the enzyme are not included in the binding [39]. The covalent bonding is a strong binding between the enzymes and functional groups of the support, so the possibility of leakage is low and the enzyme achieves high stability [71]. CA immobilized on epoxy-functionalized magnetic polymer microspheres [58], amine-functionalized magnetic nanoparticles [59] and amine-functionalized SBA-15 [41] by covalent bonding method has excellent storage stability and reusability. Due to the high stability and reusability of immobilized enzyme by covalent bonding method, this technique is one of the most widely used methods in literature.

1.3. Support materials for CA immobilization

Various efforts have been made to immobilize CA on/in various materials to reuse the enzyme efficiently and decrease the ultimate cost of the CO_2 capture process to make the process economically feasible. The choice of the support material is an important factor which must be considered, as it has an important effect on the performance of biocatalytic system [48]. Some features should be considered for support material selection such as availability, low cost, functional group availability, mechanical stability, rigidity, non-toxicity and biodegradability (see **Figure 1.5**) [85]. Recently, a broad range of inorganic, organic, and hybrid compounds have been investigated as carrier materials for CA immobilization with the aim of increasing the stability of CA enzyme under hazardous conditions, its efficiency and enzyme recovery. **Table 1.2** presents a detailed comparison in terms of enzyme loading, storage stability and reusability of different immobilized CA enzyme using various support materials and immobilization methods.

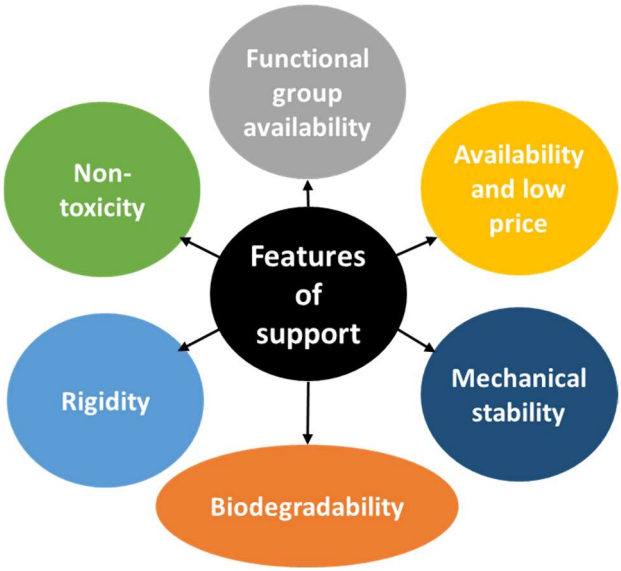

Figure 1.5. Enzyme immobilization support features.

Table 1.2. Properties of various immobilized CA.

Support type	Support material	Functional reagents	Immobilization technique	Enzyme loading	Storage stability	Reusability	Ref.
Inorganic oxide materials	SBA-15	-	adsorption	-	98% after 6 days, 40 ºC	-	[**86**]
	SBA-15	gold nanoparticles/3-amino-propyltriethoxysilane (APTES)	covalent bonding	207.93 mg/g silica	92% after 20 days	90% after 20 cycles	[**56**]
		gold nanoparticles/3-mercaptopropyltriethoxy silane (MPTES)		289.13 mg/g silica	100% after 20 days	95% after 20 cycles	
	SBA-15	Ag/ octa(aminophenyl)silsesquioxane (OAPS)	covalent bonding	307 mg/g support	87% after 30 days	83% after 30 cycles	[**62**]
	synthesized SiO_2-ZrO_2 composite nanoparticles	γ-aminopropyl triethoxysilane and glutaraldehyde (GA)	covalent bonding	50.2 mg/g support	90% after 60 days, 50 ºC	-	[**87**]
	spherical SBA-15	APTES/GA	CLEA	0.193 mg/g silica	94% after 30 days	100% after 10 cycles	[**88**]
	silica nanoparticles	γ-aminopropyl triethoxysilane/GA	covalent bonding	55 mg/g support	40% after 30 days, 50 ºC	-	[**89**]
	titania naoparticles	APTES/GA	covalent bonding	163 mg/g support	70% after 20 days	90% after 20 cycles	[**48**]
	aluminum oxide carrier	organosilane	covalent bonding	-	85% after 40 days, 40 ºC	-	[**90**]
Magnetic particles	magnetic nanoparticles	tetraethyl orthosilicate (TEOS)/3-chloropropyltrimethoxysilane (CPTMS)/ OAPS/GA	covalent bonding	-	75% after 30 days	80% after 30 cycles	[**91**]

	chitosan-stabilized iron nanoparticles (CSIN)	-	ionic bonding	-	50% after 30 days	0 after 6 cycles	[**60**]
	magnetic composite material	chitosan/GA	covalent bonding	-	100% after 80 days	80% after 40 cycles	[**92**]
	magnetically mesocellular silica foam	GA	CLEA	32.9% (w/w)	90% after 160 days	84% after 10 cycles	[**93**]
	Fe_3O_4 nanoparticles	EDC/carbodiimide	covalent bonding	40 mg/g solids	95% after 30 days	-	[**83**]
	magnetic iron oxide nanoparticles	APTES/EDC-NHS	covalent bonding	5.7 mg	100% after 30 days	50% after 25 cycles	[**94**]
	MNPs	TEOS/APTES/GA	covalent bonding	-	85% after 40 days	61% after 13 cycles	[**59**]
	magnetic nanogel	APTES/N-acryloylsuccinimide (NAS)/GA	encapsulation	-	100% after 80 min at 60 ºC	-	[**95**]
	magnetic polymer microspheres	Glycidyl methacrylate (GMA)- divinyl benzene (DVB)	covalent bonding	-	90% after 30 days	50% after 6 cycles	[**58**]
Carbon-based material	macroporous carbon foam	poly(aminopropyl)pyrrole film	electropolymerization	1.25 mg/cm^3	40% after 42 days at 70 °C	-	[**96**]
Polymeric membrane	Nylon 6.6	GA/chitosan	covalent bonding	0.019 µg/ mm^2 membrane	-	-	[**7**]
	PVDF flat sheet	plasma modification, silane coupling agents: KH550 and GA	covalent bonding	-	50% after 50 days	85% after 10 cycles	[**51**]
		plasma modification, silane coupling agents: KH560	covalent bonding		50% after 37 days	72% after 10 cycles	

	PVDF	TiO_2 coating, APTES, GA	covalent bonding	150 μg/cm^2	60% after 20 days	40% after 20 cycles	[**48**]
	PVDF	PDA-PEI/GA	cross linking	-	73% after 40 days	-	[**97**]
	PVDF	PDA-PEI/GA	covalent bonding	-	65% after 30 days	80% after 10 cycles	[**52**]
	PE	PDA-PEI/GA	covalent bonding		75% after 30 days		
Synthetic polymers	PU foam	-	entrapment	-	100% after 45 days	-	[**98**]
	PU foam	-	entrapment	4 mg/g support	100% after 45 days	100% after 7 cycles	[**53**]
	nanocomposite hydrogel	NHS- N, N'-dicyclohexylcarbodiimide (DCC)	covalent bonding	4.6 mg/g support	-	-	[**99**]
	electrospun polymer nanofibers (EPC)	-	covalent attachment, precipitation, and cross-linking	916 μg/ mg nanofibers	65.3% after 868 days	-	[**100**]
Biopolymers	surfactant-modified silylated chitosan (SMSC)	GA	covalent bonding	-	30% after 30 days	-	[**101**]
	alginate	-	entrapment	1.16 g/g beads	60% after 20 days	67% after 6 cycles	[**76**]
MOFs	microporous zeolite imidazolate framework, ZIF-8	-	encapsulation	100 ± 1.2 mg/g	80% after 25 days	85% after 12 cycles	[**102**]
	ZIF-8	-	adsorption	-	-	90% after 9 cycles	[**103**]
	ZIF-8 and poly(vinyl alcohol)	-	co-precipitation/ encapsulation	-	-	50% after 11 cycles	[**104**]

	(PVA)–chitosan (CS)						
	ZIF-L	-	Co-precipitation	67 mg/g	100% after 20 days at 40 °C	134% after 6 cycles	[**105**]
	Ni-BTC	-	adsorption	-	40% after 10 days	65% after 8 cycles	[**106**]

1.3.1. Inorganic oxide materials

For immobilization of enzymes, silica is one of the most utilized inorganic support materials. Silica-based material can be used in many different forms such as sol-gel silica, fumed silica, silica nanoparticles and silica gel [89, 107]. Also, its significant resistance to heat and chemicals, as well as its good mechanical characteristics, make it a promising support for a wide range of applications. It provides a high surface area and possesses a porous structure which make it efficient in enzyme binding while reducing diffusional constraints [108]. In the literature, porous silica materials have been well investigated for CA immobilization. Shao et al. [86] proposed mesoporous molecular sieves with different dimensions and pore sizes as immobilization support of CA enzyme. KIT-6, SBA-15, and MCM-41 which the same chemical composition but a different physical structure was utilized. Compared to the free enzyme, CA/KIT-6, CA/SBA-15, and CA/MCM-41 achieved an improvement of 3.0, 2.8, and 2.0 times of their half-life ($t_{1/2}$: duration of one-half its initial activity loss). SBA-15 showed a higher CA enzyme loading due to a two-dimensional structure and large pore size of the carrier and retained 96% initial activity after 6 days at 40 °C, making the CA/SBA-15 more interesting for CO_2 capture than CA/MCM-41 and CA/KIT-6. The presence of numerous hydroxyl groups on the surface of silica facilitates enzyme attachment and surface functionalization [109]. Crumbliss et al. [110] immobilized CA on porous silica beads using glutaraldehyde as a linker and enzyme activity was maintained up to 97% and 70% after 50 and 500 days storage, respectively. To enhance the enzyme's temperature and pH stability, bioconjugates with CA immobilized on gold nanoparticles assembled over amine/thiol-functionalized mesoporous SBA-15 (Au/APTES/SBA-15 and Au/MPTES/SBA-15) were synthesized [56]. Thiol-functionalized bioconjugates were found to be very stable due to the electronegativity of Au/MPTES/SBA-15, which interacted significantly with CA. Further, Vinoba et al. [62] developed a biocatalyst with CA on silver nanoparticles confined on amine-functionalized mesoporous SBA-15 to retain significantly biocatalytic activity. From the amount of $CaCO_3$ precipitated over free and immobilized CA, the activity of silver conjugated CA was 25 times that of free CA. Badjić and Kostić [55] utilized sol−gel method for the encapsulation of CA in silica monoliths and immobilized CA preserved its overall activity. In theory, $CaCO_3$ is produced in an alkaline environment, where a high pH destroys the structure of silica, resulting in enzyme leakage. However, CA immobilized on

synthesized SiO_2-ZrO_2 composite nanoparticles showed a higher stability of the immobilized CA enzyme than pure silica nanoparticle or other silica composites in an alkaline solution [87]. The higher the concentration of zirconia in the nanoparticles, the less silica was dissolved, demonstrating that zirconia doping prevented the silica-based nanoparticles from dissolving in the alkaline solution. Vinoba et al. [88] believed that main requirements for successful immobilization of biomolecules are that the pores should not leach out the enzyme or limit the diffusivity of biomolecules inside the pores. They have successfully attached CA to spherical SBA-15 via CLEA approach and CA-CLEA was found to be thermally stable, reusable, stable upon storage, and not suffering from leaching problems. Wanjari et al. [111] displayed, using adsorption method for immobilization of CA on mesoporous aluminosilicates (AlKIT-5), increased half life period (HLP) of immobilized CA up to 67% after 25 days of storage compared to its free CA counterpart.

The oxides of titanium, aluminum and zirconium have also been used for the immobilization of CA enzymes [112]. The excellent mechanical resistance and stability, as well as sorption capacity of these supports are well-known. These materials are extremely hydrophilic due to the presence of numerous hydroxyl groups on their surface, which facilitates the immobilization of enzymes and the modification of the surface. The titania nanoparticles was used by Hou et al. [48] for CA immobilization using glutaraldehyde as a functional reagent, maintaining an activity recovery grater than 80% and 70% of initial activity after 20 days, reaching a CA loading of 160 mg enzyme per gram of support. The CO_2 hydration effectiveness of this biocatalytic nanoparticles was investigated, illustrating a slight reduction of catalytic efficiency compared to the free CA counterpart, showing that these biocatalytic nanoparticles have a high potential for CO_2 conversion. Also, an aluminum oxide support was selected as the immobilization support and was coated with silane coupling agents to immobilize the CA. The immobilization efficiency reached over 99%, and even after 40 times reusing, the immobilized CA activity became over 80% [90].

1.3.2. Magnetic-based materials

When using immobilized enzymes, one of the most difficult challenges is to separate the biocatalysts from the reaction mixture after the catalytic process. The attachment of enzymatic molecules to the magnetic particles and the easy separation of the biocatalytic system using an external magnetic field is a proposed solution [113]. Metal oxide

nanoparticles with large surface area, high biocompatibility and coordination ability with amine/carboxyl groups have been intensively investigated for the immobilization of CA. Meanwhile, the magnetically catalyzed nanoparticles cluster could be easily isolated from the solid products due to the magnetic response. Peirce et al. [81, 82] used magnetic CLEA approach to separate effectively the biocatalyst from the reaction mixture while avoiding the problems that centrifugation and filtration cause with CLEA aggregation and compaction. Vinoba et al. [91] explored the immobilization of bovine CA on a matrix of encapsulated magnetic nanoparticles using glutaraldehyde as a spacer. Fe_3O_4 nanoparticles were coated with SiO_2 and OAPS (octa(aminophenyl)silsesquioxane). The immobilized CA showed excellent reusability after 30 cycles and retained 82% of original activity after 30 days, indicating its potential for CO_2 sequestration. Yadav et al. [60] used chitosan as a stabilizer (coating agent) for iron oxide nanoparticles to improve the biocompatibility of nanoparticles. To effectively prevent the enzyme leaching, Woo et al. [92] examined a kind of composite materials. They immobilized CA into magnetically-separable spherical mesocellular siliceous foam (Mag-S-MCF) by adsorption (ADS-CA/Mag-S-MCF) and then chitosan was adsorbed onto the surface of ADS-CA/Mag-S-MCF, and further crosslinked via glutaraldehyde. The resulting composite materials showed no decrease of enzyme activity under shaking (200 rpm) for 85 days and maintained initial performance even after 30 times of recycled uses through magnet separation and rigorous washings. Kim et al. [93] proposed a "precipitation-based nanoscale enzyme reactor (p-NER)" approach, as depicted in **Figure 1.6**, to prevent the losing of CA enzyme activities in CO_2 conversion processes. They used a two-step enzymatic adsorption method in magnetic mesoporous silica and simultaneous enzymatic precipitation/cross-linking to improve the loading of CA. The enzyme loading was improved from 20.1% (w/w) to 32.9% (w/w) with ammonium sulfate precipitation (p-NER reactor) contribution. Vinogradov et al. [114] presented a methodology with only two biocompatible components: an enzyme and magnetite nanoparticles. Magnetic biocomposites were successfully generated by the direct entrapment of CA within a sol–gel magnetite matrix under neutral pH and they observed a remarkable thermal stabilization even at temperature of 90 °C.

Due to features such as minimal cytotoxicity and stability under acidic conditions, as well as fulfilling the responsiveness and inertness to redox processes, silanization of iron magnetic

nanoparticles (MNPs) is becoming the most frequently utilized method for adding functional groups to the surface of magnetic nanoparticles [115]. Furthermore, without the need for expensive equipment, the surface modification can be performed simply in aqueous or organic fluids at moderate temperatures, making it a suitable approach for preserving the inner magnetic core. Magnetic iron oxide nanoparticles were silanized using 3-(aminopropyl) triethoxysilane (APTES) [94]. In another work, MNPs were coated with tetraethyl orthosilicate (TEOS) and then amine-functionalized by using 3-aminopropyltriethoxysilane (APTES), namely ASMNPs. After activation with glutaraldehyde, CA II was immobilized on ASMNPs. After 40 days of incubation at 4ºC and 25°C, the immobilized CA II maintained 89% and 85% of its activity, respectively [59]. To improve the thermostability at elevated temperatures, CA was encapsulated with magnetic nanogel (MNPs-CA nanogel). First, amino and vinyl groups were grafted onto the surface of MNPs using 3-aminopropyltriethoxysilane (APTES) and *N*-acryloylsuccinimide (NAS), followed by CA attachment with glutaraldehyde and in situ polymerization with acrylamide. Due to multiple linkage, the thermostability of immobilized CA ameliorated, preserving the original performance at 60°C for 80 min [95]. Jing et al. [58] suggested epoxy functionalization for immobilization of CA on magnetic polymer microspheres. Their findings illustrated a stable and efficient catalytic ability of CO_2 hydration of immobilized CA, making this immobilization approach a promising candidate for CO_2 capture.

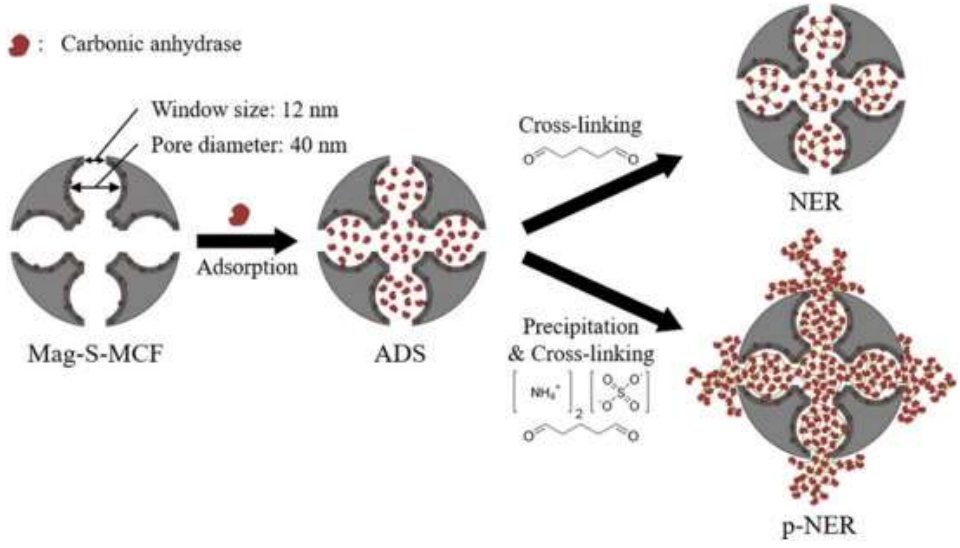

Figure 1.6. Schematic illustrations for the immobilization of CA in Mag-S-MCF via the approaches of enzyme adsorption (ADS), nanoscale enzyme reactor (NER), and NER with ammonium sulfate precipitation (p-NER) [93].

1.3.3. Carbon-based materials

Carbon-based materials (like activated carbons and charcoals) have proven to be valuable support materials for enzyme immobilization. These materials have a well-developed porous structure, with pores of varying sizes and volumes, as well as a large surface area (up to 1000 m^2/g), which means they have multiple contact sites on their surface for enzyme immobilization [116]. Merle et al. [96] utilized a macroporous carbon foam for CA immobilization to improve the stability of CA in the tertiary amine solvent. The enzyme was chemically grafted onto an electropolymerized poly(aminopropyl)pyrrole film on a highly porous carbon support. After 42 days at 70 °C in an amine solvent, these enzymatic supports retained 40% of their original activity, but the free enzyme showed no activity after 1 h under the same circumstances. Recently, a bioactive protein with high binding sites was developed with functionalization of CA via the protein fusion with a single-walled carbon nanotube (SWNTs)-binding peptide [117]. A 51% surface coverage of CA to SWNTs was achieved, maintaining the enzyme catalytic activity. In addition, Crumbliss et al. [110] used graphite rods as immobilization support for CA using glutaraldehyde as a linker.

1.3.4. Polymeric membranes

Polymeric membranes are increasingly being used as immobilization supports because of their good mechanical stability, availability, and relatively low cost [85]. They are appealing alternative supports especially in membrane-based technologies. In addition, the membranes have a large surface area and propose good porosity and hence, efficient immobilization not only on the surface but also inside the pores [118]. Hanna et al. [7] immobilized CA on nylon 6.6 using the covalent bonding method via chitosan and glutaraldehyde. The enzyme loading was 0.089 μg enzyme/mm^2 nylon and 0.019 μg enzyme/mm^2 operated actively. This difference was due to steric hindrance and wrong orientation of enzyme located on the immobilization support surface [7]. Hydrophobic polymeric membranes such as polytetrafluoroethylene (PTFE), polypropylene (PP), polyethylene (PE) and PVDF have an inert surface and do not have a tendency to react and therefore, some surface modifications are necessary to change these polymer properties to achieve the appropriate characteristics for specific application [119]. Plasmas are the most widely used methods for surface modification of polymers [120]. Depending on the type of plasma method used; different functionalized surfaces are obtained (amine, hydroxyl or plasma polymer films (PPF) on

surfaces) [119, 121, 122]. CA was covalently immobilized on the surface of PP hollow fiber membranes to accelerate the removal of CO_2 from the blood in the artificial lungs and the respiratory assist devices [121]. In this research, PP membranes were aminated after plasma modification, and then amine groups of chitosan were connected to amine groups of fibers with the assisting of glutaraldehyde. It was assumed that chitosan as a polymer rich in amino groups increased the bonding of CA on the hollow fiber membrane surface and so enhanced the CO_2 removal. Further in the same research group, Arazawa et al. [123] used 1.0 M cyanogen bromide and 1.5 M triethylamine (TEA) as an activator to immobilize CA onto the surface of PMP hollow fiber membranes after plasma modification. Also, Sun et al. [51] immobilized CA on PVDF flat sheet membranes treated via water plasma and silane coupling agents (KH550 and KH560) to bring amine or epoxy functionalities on support surface. In term of biocatalytic membrane reusability, PVDF-KH550 and PVDF-KH560 retained 85% and 72% of their initial activity after undergoing 10 cycles, respectively. However, plasma treatment is an expensive and difficult process and requires equipment which is not easily accessible. Considering a different approach for modification of membrane surface, Hou et al. [48] developed a TiO_2-coated PVDF membrane as a support for CA immobilization. Sequential immobilization was used for TiO_2-coated PVDF membranes, so that APTES was used for amine functionalization of the membrane. CA was then covalently immobilized on membrane surface by glutaraldehyde. Reusability tests have shown that after 20 cycles of hydration, the biocatalytic membrane achieved 40% of its initial activity. During the initial 5 cycles, a high reduction of enzyme activity was observed probably because of the detachment of CA which was linked on the support by physical attachment (Hou et al. [48]).

The deposition or coating of polyelectrolyte layers on the surface of polymer is an interesting method for the functionalization of the surface, because the simplicity, the low cost and the variability of the applicable materials are the advantages of this technique [124]. Dopamine (DA) is a powerful molecule for spontaneous deposition on inorganic or organic materials with a great adaptation capacity. Dopamine structure resembles to mussel adhesive protein [125] and is known as a famous “bio-glue” due to its strong adhesion ability. First, Lee et al. [126] reported that dopamine could form a strong adhesive PDA layer with auto-oxidative self-polymerization on various surfaces which has outstanding adherence to organic and

inorganic surfaces (including PTFE, which is usually an adhesion-resistant surface) under aerobic and weak alkaline solution conditions (pH~ 8.5) [127-132]. Polymers with abundant amine groups such as chitosan and PEI could simply connect to PDA based on Michael-type addition and Schiff base reactions [133, 134]. Hu et al. [125] modified the PP surface with dopamine and chitosan, by simply dipping the PP surface into a dopamine solution and then in the solution of chitosan. Also, PEI is a cationic polyelectrolyte that is rich in primary, secondary and tertiary amine groups due to the three-dimensional PEI polymer's abundant binding sites. There is improvement in enzyme loading as reported by Cao et al. [135] whose enzyme loading on PDA/PEI coated membrane was two times higher than the enzyme loading on single PDA coated membrane. But pure PDA coating takes too much time and is heterogeneous. Using PEI in the co-deposition method (DA and PEI together) prevents the self-aggregation of PDA and ruins the non-covalent interactions in PDA, thus allowing homogeneous polymerization and deposition of dopamine on the support surface [136]. PEI can easily react through the Michael addition reaction and/or Schiff base reaction with PDA according to **Figure 1.7** [132, 137].

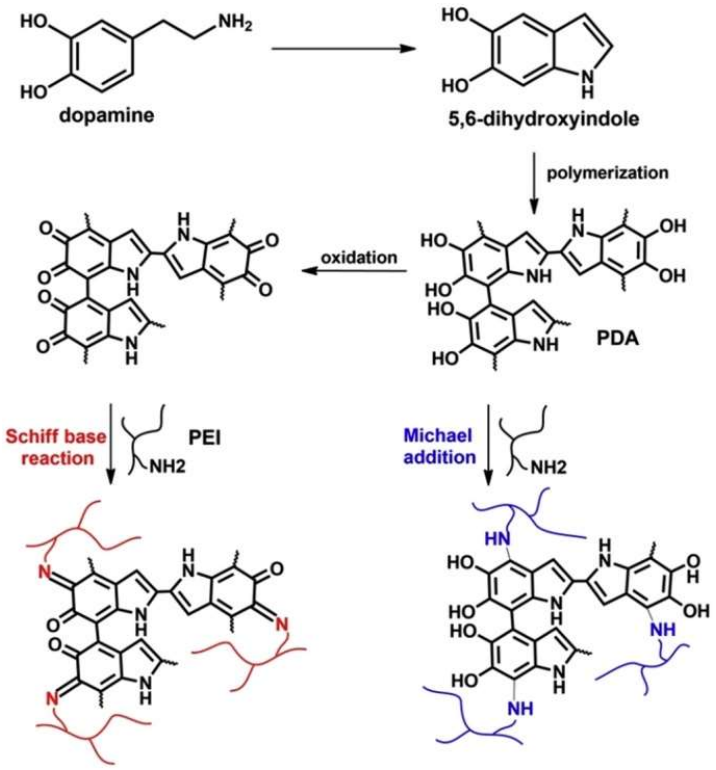

Figure 1.7. Two possible reactions of PDA–PEI co-deposition coating [132].

Chew et al. [137] noticed that the PDA/PEI coated PVDF membrane had a much narrower pore size distribution with an smaller average pore size of 0.017 μm compared to a pristine membrane with a well-defined distribution and an average pore size of 0.027 μm. The co-deposition of PDA/PEI covered the outer surface of membrane and consequently, there was a reduction in its pore size. The developed membrane was therefore less vulnerable to pore wetting [137]. Moreover, Li et al. [138] showed that surface modification using PDA and PEI reduced the pores of polymeric membranes and altered the surface morphology as membrane permeability to water dropped. Concerning the hydrophobicity of surfaces, after the PDA coating, the contact angle of polymeric membranes (initial values for pristine supports were 75-85°) decreased insignificantly, but after the PEI grafting, the hydrophobicity increased and the contact angle of these surfaces reached 80–90°. After enzyme immobilization, the contact angle reduced slightly again as the enzyme filled the valleys. Lv et al. [129] fabricated a polyacrylonitrile (PAN) nanofiltration membrane via co-deposition of PDA and PEI and they concluded that because PEI is more hydrophilic than PDA, thus the surface hydrophilicity increased via the reduction of dopamine/PEI ratio (from 2:0 to 2:2) on support surface. On the other hand, a small value of this ratio decreased the density of the surface amine group because the dopamine concentration was too low to be polymerized into PDA and the PEI was not able to adhere to the polymer surface. The optimized ratio of 2:2 was used in this work [129]. In addition, the deposition time of the PDA/PEI co-deposition is also an important parameter which controls the hydrophobicity of the surface. Expanding the deposition time brought more amine group on the surface and consequently, the contact angle reduced due to the improved hydrophilic properties of the surface [129]. The co-deposition of PDA/PEI offers numerous amine functionalities on the polymeric surface, as well as the strong adhesion capability of PDA to prevent leaching and reversing of the deposited layer on the surface. Then CA gets the opportunity to immobilize covalently on the amine functionalized surface via glutaraldehyde [52, 97].

1.3.5. Synthetic polymers

The most significant benefit of using synthetic polymers as support materials is that the monomers in the polymeric chain may be chosen to meet the needs of the enzyme and immobilization process. A very wide range of chemical functional groups can be observed in

the structure of polymers such as carbonyl, carboxyl, hydroxyl, epoxy, amine and diol groups, as well as strongly hydrophobic alkyl groups and trialkyl ammine moieties [139]. These groups contribute to efficient enzyme binding as well as to the functionalization of the polymer surface. It should be emphasized, however, that the synthesis of a polymer with the necessary characteristics and functional groups is typically a time-consuming and expensive procedure. For enzyme immobilization, different synthetic polymers with various functional groups have been employed. CA was covalently attached to polyurethane (PU) foam by crosslinking to improve thermal stability of CA and it was 98% stable below 50 °C [98]. In another work, CA was immobilized within PU foam for biomimetic CO_2 sequestration [53]. Because of its high hydrophilic and porous polymeric properties, PU foam was proven to be a useful support material for the CA immobilization. The enzyme immobilized within this material could retain its total activity over 45 days (room temperature), this period being the limiting time for free enzyme to retain its activity even at 4 °C.

Porous superabsorbent hydrogels are ideal as immobilization supports because they provide enough sites for attachment, consequently there is a growing interest in the development of hydrogels for the enzyme immobilization. Nanocomposite hydrogels were used as support for CA immobilization via covalent bonding as immobilization technique [99]. CA was immobilized on a hybrid poly (acrylic acid-co-acrylamide)/hydrotalcite nanocomposite activated by NHS and DCC. The porous embedding and the multi-point covalent connection between the enzyme and the hydrogels improved the enzyme stability in the presence of organic solvents and at high temperatures. PVA/CS@CANF hydrogel membrane was developed by embedding the synthesised bimetallic hybrid nanoflowers (CANF) into PVA-chitosan (CS) hydrogel networks. PVA/CS@CANF hydrogel membrane was mechanically strong, possessed high catalytic activity, and was simple to flow out without centrifugation or filtering. At the same time, the PVA/CS@CANF outperformed free CA and CANF in terms of thermostability, storage stability, and pH stability, as well as reusability and CO_2 capture capacity [140]. Jun et al. [100] reported highly loaded and stabilized immobilized CA onto electrospun polymer nanofibers (EPC). Even after 868 days of incubation in aqueous solution at ambient temperature with 200 rpm shaking, the EPC procedure of enzyme maintained 65.3 % of original activity.

1.3.6. Biopolymers

Biopolymers, or polymers of natural origin, can be used as an alternative to synthetic polymers for the enzymatic support. Materials such as chitin, chitosan and alginate are examples of biopolymers used for immobilization [141]. Biopolymers have a unique combination of characteristics, ranging from biodegradability to non-toxic compounds, biocompatibility, and non-toxicity, to an exceptional affinity for proteins, making them ideal enzyme supports. Because of their natural origin and biocompatibility, they have a small detrimental influence on enzyme structure and characteristics, allowing immobilized proteins to retain high catalytic activity. In addition, the presence of reactive functional groups in their structure—primarily hydroxyl but also amine and carbonyl moieties—allows direct interaction between enzyme and matrix, as well as surface modification. Importantly, these materials are renewable and simple to acquire; in many situations, they are by-products of numerous industries, making them affordable and lowering the cost of the immobilization process [142].

According to the literature, chitosan is the biopolymer most often used for the immobilization of enzymes, (chitosan beads [49] and surfactant-modified silylated chitosan (SMSC) [101]). Chitosan-NH_4OH beads, multilayered beads, and alginate beads are among the materials that demonstrated a strong affinity for enzyme. The presence of a hydroxyl group on the surface of the chitosan-NH_4OH beads resulted in the 42 U/ml_{enzyme} immobilization activity (esterase activity test conditions: 100 mM phosphate buffer, room temperature, pH 7 and 3 mM p-NPA), which allowed considerably enzyme adsorption [143]. Alginate is a cheap and hence economic alternative for entrapment of enzymes. Yadav et al. [76] investigated the immobilization of CA in alginate, evaluating its optimum pH and temperature. Even after six cycles, the immobilized beads demonstrated superior operational stability, keeping approximately 67% of their original activity. For the first time, CA was immobilized in the chitosan-alginate system by Simsek-Ege et al. [144]. The enzyme was used in a new biomimetic CO_2 sequestration system using chitosan-coated alginate beads, which are biodegradable and ecologically friendly.

1.3.7. MOFs

Metal Organic Frameworks (MOFs) are unique high-surface porous crystalline materials formed by the arranged assembly of metal ions and organic ligands [145]. MOFs show potential advantages in enzyme activity retention after immobilization [146]. Liang and Ge [147] first presented the idea of embedding a protein in-situ within a MOF. For the first time, CA was encapsulated into the microporous zeolite imidazolate framework, ZIF-8, proposed by Asadi et al. [102]. ZIF-8 was utilized for CA in-situ encapsulation due to their low cytotoxicity and high biocompatibility. The produced biocatalyst preserved 30-120% of its activity throughout a wide pH (6.0-10.0) and 60-120% of its activity throughout a temperature range (25-65 ºC), as well as long-term storage stability up to 37 days. Because of the structural stiffness and confinement of the ZIF-8 scaffolds, the thermal stability and reusability of immobilized CA improved substantially. In another work, by adsorbing CA onto ZIF-8, a combined immobilization system of CA and ZIF-8 with a cross flower-like shape (CA@ZIF-8 composites) was developed for the first time [103]. The immobilization effectiveness was more than 95%, and the highest activity recovery was 75%, showing that the immobilization procedure was extremely efficient. When compared to free CA, the CA@ZIF-8 composites demonstrated superior thermostability, denaturant tolerance, and reusability. Ren et al. [104] co-precipitated CA into ZIF-8 to form CA@ZIF-8 nanocomposites, which were then encapsulated in PVA–CS hydrogel networks to form CA@ZIF-8–PVA–CS composite hydrogels (PVA/CS/CA@ZIF-8), resulting in 70% immobilization efficiency. PVA/CS/CA@ZIF-8 preserved 72% of its initial activity under acidic conditions and 50% of its initial activity after 11 cycles. An immobilization efficiency of more than 70% was obtained, indicating a good immobilization effectiveness. PVA/CS/CA@ZIF-8 hydrogel membranes produced 20 and 1.63 times more calcium carbonate than free CA and CA@ZIF-8 composites, respectively, confirming the great ability of PVA/CS/CA@ZIF-8 hydrogel membranes for CO_2 capture. Furthermore, Zhang et al. [148] embedded CA into ZIF-8. Biocatalytic composite membranes were developed by growing ZIF-8@CA nanocrystal seeds in-situ on a halloysite nanotube layer attached to a porous polyacrylonitrile (PAN) substrate. Importantly, the biocatalytic composite membranes were stable and they were easily scalable, allowing them to be applied in industrial applications. A novel CA/ZIF-L-1 composite with inserting CA enzymes into ZIF-L

nanoparticles was established to increase the thermal stability and reusability of CA enzyme [105]. Due to the structural stiffness and confinement of ZIF-L scaffolds, the CA/ZIF-L-1 had a good thermal stability and reusability. Regarding the Ni-based MOFs, CA II was efficiently immobilized via adsorption on Ni-BTC under optimal conditions by a simple mixing step due to the specific binding abilities of Ni-BTC. As a result, the immobilized CA restored 99% of its activity and the immobilized CA retained 40% activity after 10 days of storage, while the free enzyme lost 91% of its original activity [106].

1.4. Enzymatic CO_2 capture technologies using CA

1.4.1. Absorption reactors

Gas-liquid packed-bed columns are the most documented technology for CO_2 capture and the packing materials offer high surface area to ensure good contact between the gas and liquid phases [11]. Their significant drawbacks are foaming, flooding and channeling [149]. In case of enzymatic CO_2 capture, the column packing (made of ceramic, silica, polymer, or nylon) can be utilized as immobilization support. Blais and Rogers [12] proposed a counter-current packed tower bioreactor with CA immobilized covalently on the packing surface. Packings could have different forms (Raschig rings. Berl saddles, Intalox metal, Intalox saddles, Pall rings, etc.) and sizes and made of different materials: polymer, ceramic, metal, etc. The bicarbonate-rich solution was delivered to an ion exchange system, where the bicarbonate was exchanged for hydroxyl ions. Bhattacharya et al. [150, 151] immobilized the CA onto a silica-coated steel matrix or an iron filing matrix. The water was sprayed very tiny at the top of the column and the gas was fed radially at the top of the column (reactor volume: 0.059 m^3). The optimal CO_2 reduction was attained at an inlet CO_2 concentration of 70%, a gas flow rate of 5-7 l/min, an enzyme loading of 2 mg/ml and a spraying water flow of rate 8 ml/min [151]. However, the utilization of this system on an industrial scale seems unlikely due to the very low superficial gas velocities of around 1 mm/s and significant pressure drop because of the sub-millimeter packing size. They reported that a large enhancement in CO_2 conversion (from 22% to 80%) was achieved with an increase of the enzyme loading in the reactor from 0.25 to 4 mg/mL, until a plateau is reached [150]. Using 112 mg/L immobilized CA on Nylon-6,6 Raschig rings (6.25 mm), Larachi et al. [152] investigated the catalytic CO_2 hydration in a counter-current packed scrubber (reactor

volume: 0.0078 m^3) and 40% CO_2 conversion was achieved (80 mM 2-amino-2-hydroxymethyl-1,3-propanediol (AHPD) buffer concentration, 18% feed CO_2 percentage, liquid velocity: 3 mm/s and gas velocity: 17 mm/s). Two techniques for reducing the accumulation of bicarbonate were introduced via its continuous in-situ removal from the liquid phase. The objective was to increase the CO_2 hydration intrinsic kinetics by avoiding the dehydration reaction. In the first strategy, the precipitation of calcium carbonate via $CaCl_2$-$2H_2O$ was used allowing the bicarbonate to be consumed on the place. In the second strategy, spherical ion exchange resins (37–74 μm or 200–400 mesh) were used to adsorb the bicarbonate. The second one improved the conversion of CO_2 by a factor of two [152]. However, the authors concluded that due to the fine resin particles capture within the bed, implementing this strategy in large scale packed-bed scrubbers with random packing would be complicated. A newer approach for the counter-current packed bed column reactor was proposed by Iliuta and Iliuta [11] with the CA II enzyme immobilized on fourth generation random packing with a high surface area, enhancing the mass transfer. The authors concluded that to increase even more the performance of the proposed counter-current packed bed column, the in-situ removal of bicarbonate by ion exchange would be promising because the capture of fine resin particles inside the bed can be avoided due to the large and uniform open area of fourth generation random packing in every ring orientation [11]. Besides, this aspect has been investigated theoretically by Iliuta and Larachi [32] for the catalytic CO_2 hydration in a three-phase (gas-liquid-solid) monolith slurry reactor with immobilized (washcoat) CA II and in-situ bicarbonate removal by ion exchange. The slurry ion exchange resin (a strong base anion exchange resin; amberlite IRN-150) which was regularly regenerated, reduced the bicarbonate inhibition effect by attracting negative charge ion. CO_2 conversion reached a plateau at resin concentration of 10 kg/m^3, more than that the resin became inefficient. With an increase of CA loading from 2 to 12 mg/l, the conversion of CO_2 augmented by 30%, however, at more than 10 mg/L CA concentration, the hydration of CO_2 was limited by mass transfer.

A recent research studied a counter-current packed-bed column (reactor volume: 0.0015 m^3; diameter: 5 cm, height: 75 cm, packing height: 3 cm) with immobilized CA on the polyester polyurethane prepolymer 80 [153]. CO_2 absorption efficiency dropped from 63 to 42.7% with

an increase in the inlet CO_2 concentration from 9 to 15.4%, because with the increase of CO_2 concentrations the resistance to liquid and gas phase mass transfer increases, resulting in lower CO_2 conversion. Furthermore, a bioreactor containing SspCA (A type of CA with different source and high tolerant to high temperatures) trapping within a polyurethane (PU) foam (three-phase trickle-bed reactor, reactor volume: 0.00075 m^3) was utilized to evaluate the CO_2 capture capabilities in circumstances similar to those of a power plant application [16]. Overall, the results demonstrated that regulating the reactor liquid flow rate (higher than 75 ml/min) improved the CO_2 capture performance of the immobilized CA and a CO_2 conversion of 30% obtained with 75 ml/min water flow rate, 0.5 l/min gas flow rate, 25 g catalyst, and 20% inlet CO_2 percentage. Below 75 ml/min liquid flowrate, mass transfer resistance within the liquid phase made it unable to fully exploit the CA catalytic activity.

Before advancing to the commercial scale, pilot demonstrations are compulsory. Bucholz et al. [154] and Leimbrink et al. [155] studied the absorption of CO_2 in a pilot scale packed-bed column. Bucholz et al. [154] operated the column for more than 5 months at 40 ºC using potassium carbonate and the mass transfer coefficient only dropped by around 20%. They predicted a reduction in performance by half after 1.5 years. Leimbrink et al. [155] also examined the absorption of CO_2 in a packed-bed column (reactor volume: 0.0057 m^3) with immobilized CA in 30 wt% MDEA, obtaining an absorption efficiency 70% lower than that of dissolved CA, which could be due to various factors, including: (1) differences in the interfacial area during experiments, differences in the amount of enzyme in the column and also additional resistance to mass transfer when using the immobilized enzyme. Madore et al. [156] proposed an activity replenishment system in a packed-bed reactor. The packed-bed reactor included a reaction chamber containing packing and immobilized enzymes where the gas containing CO_2 contacted the liquid solution. The enzyme activity was monitored and at low enzyme activity over time, the operation of the packed-bed reactor was stopped, and the enzymatic activity was reconstituted by providing an enzyme replenishing solution into the packed-bed reactor.

Although traditional packed-bed columns with CA immobilized on the packing surface ameliorate CO_2 conversion, they exhibit insufficient mass transfer coefficients to totally utilize the high turnover of CA enzyme. The immobilized CA on packing is not close enough

to the gas-liquid interface and the absorbent film increases the resistance to mass transfer. The solution is the use of free CA in solution phase or immobilized CA on micro/nanoparticles surface, placing the enzyme nearer the gas-liquid interface [15, 46, 157, 158]. One of the recent works of our group proposed a novel hybrid enzymatic process in a packed-bed column reactor including an enzyme immobilized both on the surface of packing and suspended micro/nanoparticles dispersed in the liquid phase [159]. Incorporation of the biocatalytic micro/nanoparticles considerably amended the CO_2 removal process since in this way, immobilized CA works as a free solution-phase enzyme in the reactive liquid film and in the bulk liquid, enhancing the catalysis of CO_2 hydration reaction. This enhancement was more important under the operating conditions with enlarged mass transfer resistance. Leimbrink et al. [160] implemented successfully a biocatalyst delivery system (BDS, suspended microparticles with immobilized CA (1.5 wt%) in 30 wt% MDEA solution) for CO_2 absorption: a uniform slurry mixture was provided to pass through the column packing (reactor volume: 0.0013 m^3). Although, the CO_2 absorption performance was lower to that of the system with dissolved CA in 30 wt% MDEA, the authors estimated that due to the easy separation of BDS from MDEA, the overall efficiency of BDS as a CO_2 absorption catalyst would be higher than that of dissolved CA.

Besides packed-bed columns, there are several static configurations that have not received many interests. The spraying tower proposed by Fradette [15] was a counter-current absorption tower in which the liquid containing a free biocatalyst or immobilized on fine particles was sprayed into the reaction chamber. The bicarbonate was removed by membrane separation systems (UF and NF), ion exchange or an adsorption column. A bubble column with enzyme (free or immobilized on solid support) suspended in the liquid phase was proposed by Parent and Dutil [14]. This bioreactor was operated at high pressure and ultrafiltration or nanofiltration membranes or cartridge filters with preferably pores with smaller diameters than biocatalyst diameters were used to make it possible to recover a maximum amount of biocatalyst. However, ultra and nanofiltration membranes are subject to clogging [161]. In another work, Russo et al. [162] theoretically investigated a counter-current staged bubble column (SBC) for the absorption of CO_2 in 20 %wt K_2CO_3 solution containing immobilized CA on fine particles. Three case studies were considered: 1) CO_2 absorption in the pure solvent (20 %wt K_2CO_3 solution); II) CO_2 absorption in K_2CO_3

solution with dissolved CA III) CO_2 absorption in K_2CO_3 solution with CA immobilized on suspended fine particles. The results showed that CO_2 absorption rate in the presence of CA immobilized on fine particles increased by about three times rather than using pure alkaline solvent as liquid phase.

1.4.2. Selective membranes

Selective membranes are used in gas permeation to remove CO_2 from a gas mixture. Membrane permeators present the advantages of high surface area, easier scale-up and not being limited by gravity. However, lower efficiency compared to traditional chemical absorption columns, high pressure differences through the fibers, liquid loss and surface fouling are their most important drawbacks [21, 22]. A contained liquid membrane (CLM, **Figure 1.8**) system for CO_2 capture using CA as promoter was developed by Trachtenberg et al. [163] to study the separation performance (CO_2 permeance and selectivity of CO_2 versus N_2 and O_2). The CLM system (effective area of 380 mm^2) was constructed by sandwiching a CA (as free catalyst) containing phosphate buffer solution between two PP membranes. The CO_2 in the flue gas diffuses through the first membrane and is absorbed into the solvent where it is converted by CA to bicarbonate. The bicarbonate then must cross the liquid membrane and is converted to CO_2 with help of CA. CO_2 is released to the sweep gas on the other side of the second membrane [163]. According to some researchers, the CA must be entrapped between porous membranes [33, 164]. A further approach was the hollow fiber contained CA dissolved liquid membrane (HFCLM), consisting of two hollow fiber membranes. Flue gas containing CO_2 passes through the inside of one membrane and sweep gas passes through the inside of the other membrane with solvent encapsulated in the space within these two membranes [33]. Further, Trachtenberg et al. [165] proposed to immobilize the CA on the hollow fiber membrane's external wall to ensure the contact of CA and CO_2 at gas-liquid interface. To avoid decreasing of water extent in the CLM, a hollow fiber contained hydrogel–CA membrane contactor (CA immobilized within a poly(acrylic acid-co-acrylamide) hydrogel) was proposed by Cheng et al. [166], holding the water molecules within the network of hydrogel. The highly water-swollen membrane (hydrogel membrane), with its network configuration, achieved a high permeation rate due to the large gas passage through the membrane, preventing membrane liquid loss to preserve the liquid within the hydrogel network, and considerably improving gas permeability and mechanical properties.

Also, the hydrophilic hydrogels inhibited the leaching of the enzyme. To immobilize more CA solution within the hydrogels, Zhang et al. [167] suggested using hydrogels with high salt-absorbency. They immobilized CA within the poly(acrylic acid-co-acrylamide)/hydrotalcite (PAA-AAm/HT) nanocomposite hydrogel, while keeping in the interstitial space between two microporous PVDF hollow fibers. However, the full utilization of the immobilized enzymes due to the high mass transfer resistance of hydrogel was limited.

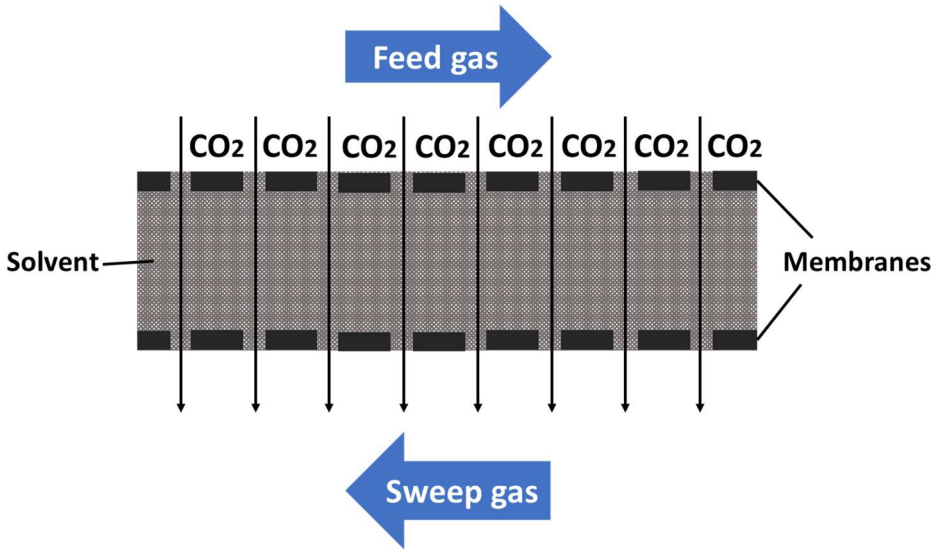

Figure 1.8. Schematic of contained liquid membrane (CLM) operation.

In a supported liquid membrane (SLM), the liquid phase is held by capillary forces into the pores of a microporous membrane. The immobilized liquid is a microporous film serves as a support for the membrane. A known disadvantage of SLM systems is instability due to the liquid evaporation. Fu et al. [168] recently presented an ultra-thin biomimetic membrane with immobilized CA within the nanopore contained ultra-thin water film.. Average loading of CA was two CA enzymes per nanopore, increasing the possible CA concentration in solution by a factor of ten. The liquid membrane was significantly more stable due to nanoconfinement. Hydrophilic holes of membrane stabilized water by capillary condensation and perfectly accommodated the CA. Supported ionic liquid membranes (SILM) have been the focus of other efforts to prevent liquid membrane evaporation with non-volatile ionic liquids (or solvents) [169]. A SILM system using ionic liquid ([C4MIM][Tf2N]) and PEG containing CA enzyme were therefore reported by Neves et al. [22]. The liquid phases were immobilized into the pores of a hydrophobic polymeric support (PVDF). Recently, Bednar et al. [170]

developed an enzymatically-boosted supported ionic liquid membrane (EB-SILM) for CO_2 separation from gaseous effluents. In this work, the mixture of CA and [bmim][Tf_2N] ionic liquid was loaded by a syringe to the surface of PVDF membrane and then was dispersed. It was discovered that this specific ionic liquid resulted in a quick and severe loss of initial biocatalyst activity, putting the membrane process design at risk [171]. All these supported ionic liquid membranes exhibited some degree of improvement in preventing liquid evaporation.

1.4.3. Membrane contactors

Gas-liquid membrane contactors involve mass transfer of CO_2 from the gas phase through the membrane pores and then its absorption by the liquid phase; the gas and liquid phases flow on the opposite sides of the membrane [24]. As shown in **Figure 1.9**, in the absorption process into a membrane contactor, the pores should be filled with gas and the mass transfer happens by diffusion towards gas-liquid interface [24, 148, 172-178]. Among all the technologies for CO_2 capture, membrane contactors are the attracting alternative technology that offer several advantages over conventional contacting devices such as high contact area, flexible operations, independent control of liquid and gas, size reduction, a recognized gas–liquid interfacial area, being easy for scaling-up and modularity [179-181].

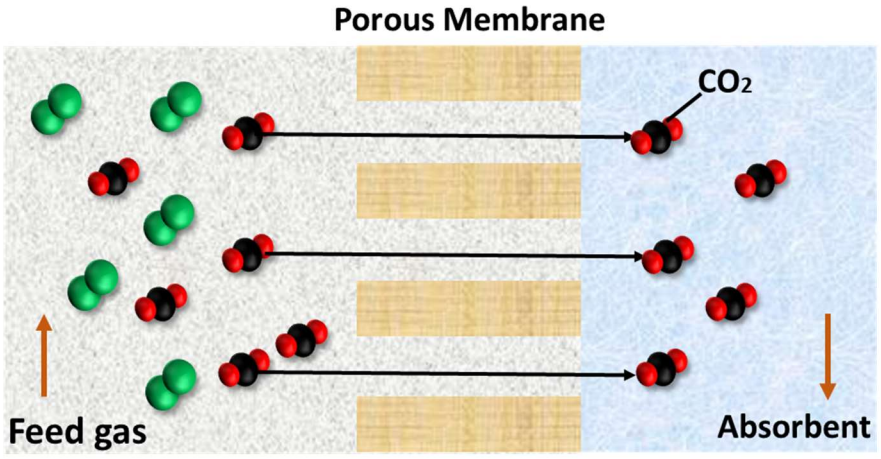

Figure 1.9. Principle of membrane contactor.

There are a few studies investigating the performance of CO_2 absorption in membrane contactors with immobilized CA enzymes. Using a layer-by-layer electrostatic adsorption method, Yong et al. [70, 73, 182] immobilized CA on the surface of flat sheet or hollow fibre

polymer membrane. For the hollow fiber membrane, CA was immobilized on the shell side via a LBL electrostatic adsorption method, as displayed in **Figure 1.10** [70]. Membrane modules were coated with a polyelectrolyte solution through pumping and circulating the solutions for a definite time [182]. Coating with the polyelectrolyte film reduced the pore wetting from 4% to 0.5-2.3% (depending on the numbers of polyelectrolyte layers on the surface), due to the pore obstruction and pore size reduction. However, the adsorption techniques are still unreliable due to leaching and process reversibility. Stability and reusability of the immobilized enzyme on the PP membrane using the proposed method have not been reported. A biocatalytic PVDF composite membrane was also developed for CO_2 conversion and capture in the gas-liquid hollow fibre membrane contactor (HFMC), and CO_2 absorption flux was increased when compared to a non-biocatalytic PVDF membrane, as shown in **Figure 1.11** [97].

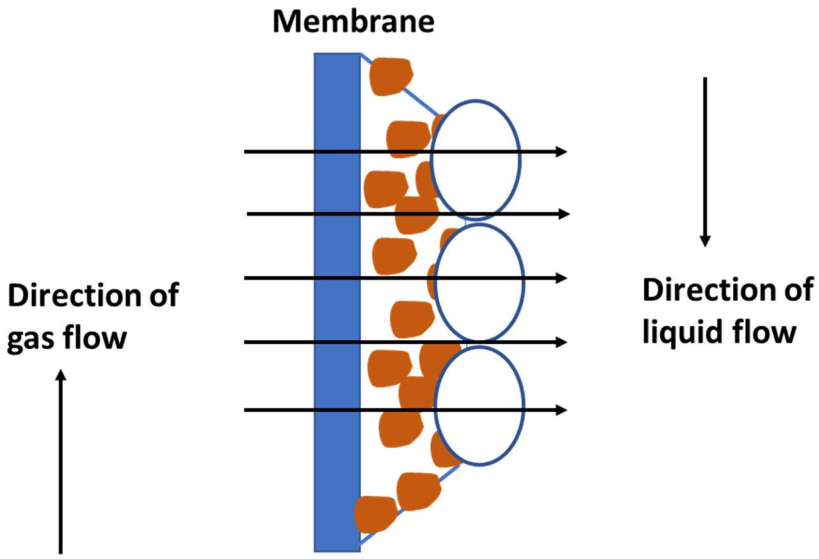

Figure 1.10. Enzyme immobilization by LBL technique on membrane (Adapted from [182]).

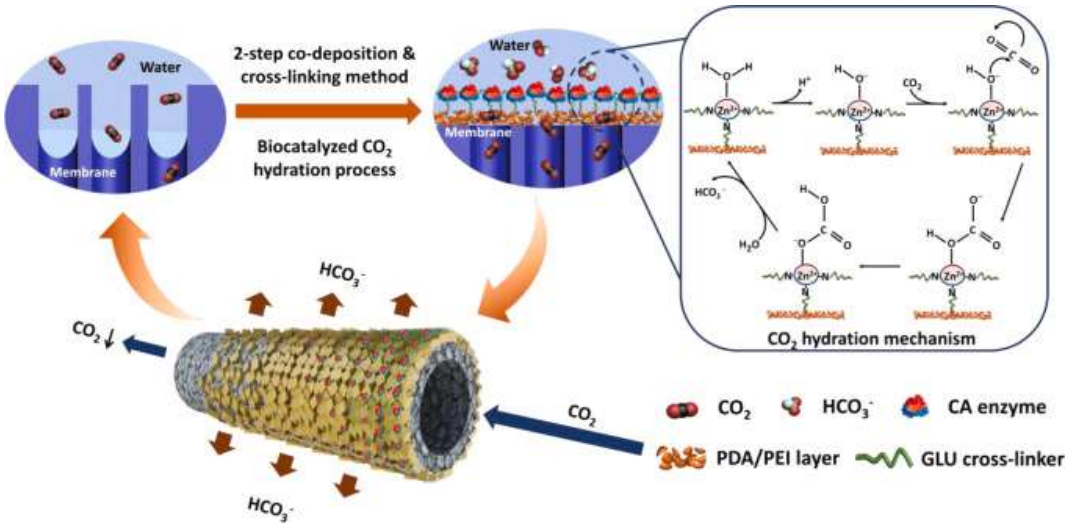

Figure 1.11. Schematic illustration of the biocatalytic composite hollow fiber membrane [97].

To facilitate the mass transfer, Hou et al. [158] proposed a Janus membrane, as depicted in **Figure 10**, which provided a hydrophilic layer (enzyme immobilization) and a hydrophobic layer (wetting limitation). The fabrication of these kind of membranes is however complex, limiting their wide application [183]. Later, Hou et al. [46] investigated a biocatalytic gas-liquid membrane contactor for CO_2 capture using an aqueous solution (benign solvent) with 0.1 M sodium phosphate (buffer) containing suspended biocatalytic TiO_2 nanoparticles with covalently immobilized CA (see **Figure 1.12**). According to this work [46], Wilson plot showed that the most important parameter in membrane contactor was membrane resistance, which was accounted for around 82% of the total mass transfer resistance, indicating the occurrence of membrane wetting. Moreover, a rapid loss of CO_2 hydration rate was observed within the first 5 minutes because of the partial pore wettings in membrane contactor. The PP membrane used in this work had a large pore opening (approximately 30 μm) causing a membrane sensitive to wetting [178]. Recently, a novel approach for enzymatic CO_2 capture in hollow fiber membrane contactors with immobilizing CA on the membrane surface and inside the membrane pores was proposed [19]. The model considered (i) the uncatalyzed CO_2 hydration in the wetted membrane surface pores when the CA was immobilized only on the membrane and (ii) the uncatalyzed and catalyzed CO_2 hydration in the wetted membrane surface pores when the CA is immobilized both on the membrane and inside the pores. The biocatalytic membrane contactor highlighted a competitive efficiency of immobilized CA

enzyme. Mass transfer resistance in membrane liquid-filled pores was shown to be reduced by the catalyzed CO_2 hydration in the wetted membrane pores with attached CA.

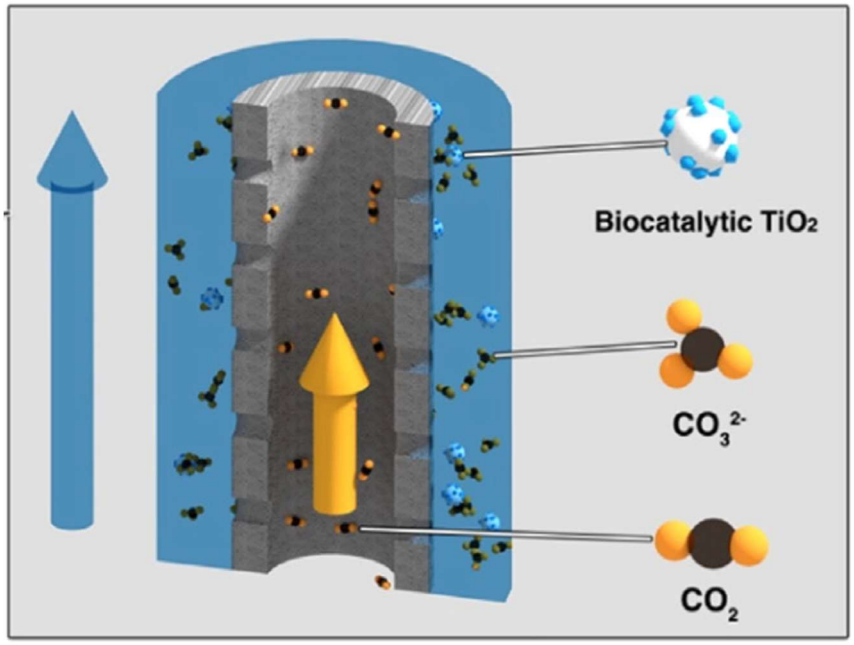

Figure 1.12. Schematic of the gas-liquid hollow fiber membrane contactor [46].

1.5. Conclusion on literature and opportunities for research

A cost-effective and environmentally viable methodology of CA-mediated CO_2 capture could be an attractive approach in the area of global warming research. This literature overview clearly revealed that there is a growing interest in enzymatic CO_2 capture technologies using CA and has inspired several patents and scientific investigations. The use of CA as catalyst, free (in solution) or immobilized, allows to take advantage of nontoxic and energy efficient benign solvents in CO_2 capture processes. The immobilization overcomes the challenges ascribed to the use of free enzyme, providing repetitive use and superior stability of enzyme, as well as easy separation of the reaction products without enzyme contamination. Many of the studies have been surveyed different CA immobilization techniques and immobilization support materials. Although the results presented in different investigations highlight several significant trends in CA immobilization, making meaningful comparisons on immobilization strategies and carrier materials is difficult. In addition, the integration of biocatalytic

materials in industrial and commercial configurations with maximizing the exploitation of CA as biocatalyst and obtaining an acceptable CO_2 removal is another challenging concept in biomimetic capture of CO_2. It is crucial to have good knowledge of how the enzymatic capture of CO_2 is influenced by operating parameters, which can be achieved by combining experimental work and mathematical models.

Current bioreactors exhibit insufficient mass transfer coefficients to maximize the utilization of the enzyme's exceptional turnover number due to the limitation of CO_2 hydration process in the gas-liquid mass transfer. Therefore, there are rooms for various innovative ideas to improve the enzymatic processes in gas-liquid bioreactors with promoted mass transfer. Thorough research is therefore required on CO_2 capture performance using immobilized CA enzyme in packed-bed columns, as most prevalent technologies for CO_2 capture, and in membrane contactors, as a very promising technology. This kind of studies are very scarce in the literature.

Packed-bed columns with immobilized CA enzyme on packing surface do not generate sufficient mass transfer because the enzyme is located several millimeters away from the gas-liquid interface and the reactive liquid film. In the gas-liquid reactor, it is preferable to have the enzyme nearer the gas-liquid interface to attain the most benefit from the enzyme, obtaining a maximum impact on the CO_2 hydration kinetics. We consider that additional CA enzyme immobilized on nanoparticles dispersed in liquid phase will locate the enzyme in the nearest position to gas-liquid interface in packed-bed columns. No research work has examined the performance of CO_2 hydration process in packed-bed columns with enzyme immobilized on both packing and nanoparticles surfaces, even if these immobilized enzyme systems could be a very attractive alternative for CO_2 capture.

CO_2 capture in gas–liquid membrane contactors offer several advantages such as high selectivity, modularity, and compactness. Despite significant advancements in the design of CO_2 absorption processes in membrane contactors, there are very few studies on CO_2 absorption in membrane contactors with immobilized enzymes. Due to the good mechanical stability, availability, and relatively low cost of polymeric membranes, there is an interest to further investigate and optimize the CO_2 absorption performance in a flat sheet membrane contactor with immobilized CA on the membrane surface and partially within the membrane

pores as immobilization support. Also, there is no experimental study on enzymatic CO_2 hydration process in partially wetted membrane porous structure.

Even though membrane contactors with biocatalytic membrane are the alluring approach for CO_2 capture, the insufficient gas-liquid-solid mass transfer and the additional mass transfer resistance in the coating structure of biocatalytic membranes are the main restrictions. Because the enzymatic process is severely limited by internal/external diffusion and does not fully take advantage of the high hydration turnover of CA enzyme, we consider that incorporating additional CA immobilized on nanoparticles dispersed in liquid phase could be an innovative solution to intensify the CO_2 capture process.

1.6. Objective of the present research

Implementation of immobilized CA enzyme in CO_2 capture technologies offers the opportunity for low-cost and environmentally friendly process. Bioreactors with immobilized CA could be a very attractive alternative to traditional CO_2 capture technologies because of the non-toxicity and biodegradability of enzyme, long-term cyclic operation of immobilized enzyme, and no need for expensive and energy consuming solvent regeneration. The key factors that strongly affect the success of this process include the development of: (i) stable and efficient enzyme immobilization techniques and (ii) systems able to locate the enzyme in a nearest position to the gas-liquid interface to maximize the utilization of the high hydration turnover of CA. To increase the industrial implementation opportunities, this area of research requires further extensive investigations to maximize process efficiency. The present research makes an attempt to explore the performance of CO_2 absorption process via novel enzymatic approaches. First, a novel hybrid CO_2 absorption enzymatic process will be studied in a gas-liquid packed-bed column bioreactor to enhance the CO_2 capture. Then, the use of flat membranes as CA immobilization support and their application in a flat sheet membrane contactor for enzymatic CO_2 capture will be investigated. Finally, a hybrid CO_2 absorption enzymatic process in an intensified flat sheet membrane contactor will be developed.

The following objectives were defined:

1.6.1. General objective

The main objective of the current PhD thesis is to investigate the performance of the CO_2 absorption process in bioreactors (packed-bed column and flat sheet membrane contactor) with immobilized CA enzymes.

To achieve this goal, the following specific goals were defined:

1.6.2. Specific objectives

- Developing an improved immobilization technique to attach CA on membrane, packing, and magnetic nanoparticles (MNPs) surfaces, to offer high stability, activity, and reusability of immobilized CA.
- Studying the influence of immobilization parameters such as co-deposition time, polydopamine (PDA)/ poly(ethyleneimine) (PEI) ratio, glutaraldehyde concentration, CA enzyme concentration, immobilization time, and pH, on the performance of immobilized CA.
- Investigating the CO_2 absorption performance in the bioreactors.
- Evaluating the effect of buffer concentration and type, flow (G/L) orientation, gas flowrate, liquid flowrate, and CO_2 inlet concentration on CO_2 absorption performance in the bioreactors.
- Analyzing the stability of the CO_2 absorption and reusability of the immobilized CA in bioreactors.

Chapter 2: Methodology

This chapter describes the methodology employed in this study. It provides an overview of materials preparation and performance evaluation of immobilized CA in flat sheet membrane contactor and packed-bed column bioreactors for CO_2 capture purposes. In addition, different measurements related to the CA enzyme and characterization techniques, providing several information to rationalize the performance of developed materials, are explained in detail.

2.1. Materials and chemicals

Polypropylene (PP) flat sheet membranes (chapters 4 and 5) were provided by Membrana (North Carolina, USA) and membrane/module characteristics are reported in **Table 2.1**. Packings and packed-bed column (chapter 3) characteristics are reported in **Table 2.2**.

CA II enzyme (molecular weight of approximately 29 200 Da) was produced and purified in our biotechnology laboratory. Over-expression of CAs was performed by transforming the recombinant plasmid into the E. coli BL21 expression strain and an affinity chromatography column was used in the purification step. The specifications of all chemicals used in the current work such as supplier and purity are listed in **Table 2.3**.

Table 2.1. Flat sheet membrane and module specifications.

Parameters	**PP membrane**	**Module/1 membrane**
Thickness (µm)	100	-
Pore diameter (µm)	0.1	-
Porosity	0.8	-
Length (m)	-	0.059
Width (m)	-	0.070
Gas-liquid contact area (m^2)	-	0.0041

Table 2.2. Packings and packed-bed column specifications.

Parameters	**Packings**	**Packed-bed column**
Type	Raschig rings	-
Material	Nylon 6.6	-
Size (mm)	ID: 6 × OD: 8 × L: 8	-
Column internal diameter (m)	-	0.05
Bed height (m)	-	0.25
Bed porosity	-	0.71

Table 2.3. Chemicals.

Chemical	**Supplier**	**Purity**
Dopamine hydrochloride	Sigma-Aldrich	≥ 98%
P-nitrophenyl acetate (p-NPA)	Sigma-Aldrich	≥ 98%
Glutaraldehyde	Thermo Fischer Scientific	25 wt% solution in water
Polyethyleneimine (PEI, MW = 600 Da)	Thermo Fischer Scientific	≥ 99%
Ferric chloride hexahydrate ($FeCl_3 \cdot 6H_2O$)	MP Biomedicals LLC	99.4%
Ferrous chloride tetrahydrate ($FeCl_2 \cdot 4H_2O$)	Avantor Performance Materials Inc.	99.0%−103.0%
Ammonium hydroxide (NH_4OH)	Sigma-Aldrich	28%−30%
N-methylimidazole	Alfa Aesar	≥ 99%

Tris base	Fischer Bio Reagents	
2-amino-2-methyl-1,3-propanediol (AMPD)	Laboratoire MAT	≥ 99%
Bradford Protein Assay Kit	Bio Basic Inc.	
Commercial grade CO_2 gas	Praxair	99.9%
Commercial grade N_2 gas	Praxair	99.9%

2.2. Materials preparation

2.2.1. Biocatalytic membrane preparation

Membrane surface was functionalized by amine using co-deposition of polydopamine (PDA)/polyethyleneimine (PEI). The dopamine hydrochloride and PEI (in different PDA/PEI ratios: 0/2, 1/2, 2/2, 2/1 and 2/0 $mg.ml^{-1}$/ $mg.ml^{-1}$) were dissolved in a Tris/HCl solution (pH = 8.5, 50 mM) and then PP membranes were soaked in the PDA/PEI solution at room temperature. They were under shaking for 3, 5, 7, 9, and 11 h. Subsequently, the membranes were rinsed with DI water and dried for 24 h at room temperature.

The amine-functionalized PDA/PEI membranes were immersed in CA solution with different CA enzyme concentrations: 0.1, 0.2, 0.6, 0.8, 1.0 and 1.2 mg/ml for enzyme immobilization. Glutaraldehyde was dissolved in this solution to obtain a concentration of 0.1, 1.0, 2.0 or 4.0 %(v/v). Then, the final solution was shaken at room temperature for a period of time. The membranes were washed with DI water and dried at room temperature for 24 hours after immobilization. The schematic illustrations of the biocatalytic membranes preparation are shown in chapters 4 and 5.

2.2.2. Enzyme immobilization on packing surface

CA immobilization on the Raschig ring surface followed the same approach as stated in section 2.2.1 for biocatalytic membranes. In summary, the packing surface was modified via amine-functionalization through co-deposition of PDA/PEI method (PDA/PEI: 2/2 $mg.ml^{-1}$/$mg.ml^{-1}$ and co-deposition time: 7 h) and CA enzyme was then covalently immobilized on

the packing surface via glutaraldehyde. The conditions for enzyme immobilization included: glutaraldehyde concentration: 1% (v/v), immobilization time: 32 h and CA concentration: 0.06-0.1 mg/ml.

2.2.3. Biocatalytic magnetic nanoparticles preparation

2.2.3.1. Magnetic nanoparticles synthesis

Synthesis of MNPs (Fe_3O_4 nanoparticles) were carried out by coprecipitation method in basic solution (equation 2.1). First, $FeCl_3 \cdot 6H_2O$ (1 g) and $FeCl_2 \cdot 4H_2O$ (0.35 g) were dissolved in 150 mL of distillated water using nitrogen protection and the mixture was stirred for 30 min. Then, the mixture solution was heated to 80 °C. Aqueous ammonia (28 wt%, 10 mL) was injected slowly to the mixture solution, while stirring at 80 °C for another 30 min. Afterwards, the solution was cooled to room temperature and the resultant MNPs were separated with a magnet and were washed completely with distillated water until a neutral pH was attained [184]. **Figure 2.1** illustrates the scheme of MNPs synthesis.

$$2Fe^{3+} + Fe^{2+} + 8OH^- \rightarrow Fe_3O_4 + 4H_2O \quad (2.1)$$

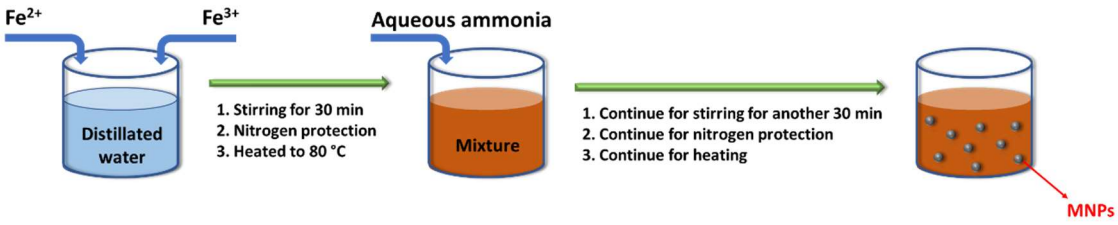

Figure 2.1. Scheme of MNPs synthesis.

2.2.3.2. Enzyme immobilization on MNPs

MNPs surface was amine-functionalized via co-deposition of PDA/PEI. First, MNPs (200 mg) were dispersed under ultrasonic conditions in Tris/HCl buffer solution (50 mM, pH: 8.5, 200 mL). Second, dopamine (2 mg/ml) and PEI (2 mg/ml) were added to the mixture solution of MNPs and Tris/HCl buffer and was stirred for a period of time (3, 5, 7, 12, 24 or 32 h) at room temperature. Amine-functionalized MNPs were separated and collected with a magnet and then washed with distillated water several times [185]. Amine-functionalized MNPs were suspended in a mixture solution of CA and glutaraldehyde. Condition of this mixture solution included: buffer solution: 50 mM NaH_2PO_4 and 500 mM NaCl, pH: 7.4, CA

concentration: 0.045-0.17 mg/ml, glutaraldehyde concentration: 0.5, 1.0, 2.0 or 4.0 % (v/v). Subsequently, the final solution was shaken for a specific time (2, 4, 7, 12, 24 or 32 h) at room temperature. Biocatalytic MNPs were collected with a magnet and afterwards, were rinsed with distillated water several times. The schematic illustration of biocatalytic MNPs preparation is shown in chapter 3 and 5.

2.3. Bradford test

By using an indirect protein test, the immobilized enzymes were quantified. The enzyme concentration in the residual solution after immobilization and the enzyme concentration in the washing water was deducted from the starting enzyme concentration. Using Coomassie blue dye, the enzyme content was determined using a colorimetric approach (Bradford test). The quantity of protein in the solution was determined by measuring the absorbance of the solution at 595 nm. A small amount of sample was mixed with the assay Bradford reagent and incubated briefly before measuring the absorbance at 595 nm. The absorbance of standard protein dilutions was used to calculate the protein concentration (analyzed together with the unknown samples). The standard was bovine serum albumin (BSA) [7]. The results of this test determined the amount of immobilized enzyme loading on support surface.

The enzyme loading efficiency was evaluated with following equation:

$$enzyme\ loading\ efficiency\ (\%) = \frac{loaded\ enzyme\ on\ surface(\mu g)}{total\ amount\ of\ enzyme(\mu g)} \times 100 \qquad (2.2)$$

2.4. Esterase activity test

The rate of hydrolysis of p-NPA in the presence of CA was examined to quantify the CA activity as a function of the Zn^{2+} ion's capability for p-NPA hydrolysis. At room temperature, at a wavelength of 400 nm, esterase activity was measured spectrophotometrically. For both free and immobilized CA, the catalytic activity was assessed.

For the free CA activity test, 3.5 ml Tris/HCl buffer solution (50 mM, pH = 8), 0.4 ml acetonitrile containing p-NPA (3 mM), and 0.1 ml free CA solution were mixed in an agitated

beaker. To eliminate the influence of p-NPA self-hydrolysis, a blank experiment was carried out in the absence of CA.

The activity test for immobilized CA enzyme on a known surface of membrane (3 cm^2) was conducted under a magnetically agitated beaker with 3.6 ml Tris/HCl buffer solution (50 mM, pH: 8) and 0.4 ml acetonitrile containing p-NPA (3 mM) at room temperature. The absorbance rate (abs/min) was determined by taking 1 ml of reaction liquid every minute. The sample was returned to the cell after each measurement [7].

For the immobilized CA enzyme on MNPs, the activity test was performed in a magnetically agitated beaker with 3.6 ml Tris/HCl buffer solution (50 mM, pH: 8), 0.4 ml acetonitrile containing p-NPA (3 mM) and 5 mg MNPs with immobilized enzyme at room temperature [48].

The enzyme activity efficiency was calculated with following equation:

$$enzyme\ activity\ efficiency\ (\%) = \frac{immobilized\ enzyme\ activity\ on\ surface}{initial\ \ free\ enzyme\ activity\ in\ solution} \times 100 \qquad (2.3)$$

2.5. k_{cat}/K_m evaluation for free and immobilized CA

The k_{cat}/K_m values of free and immobilized CA were measured by determining the CA activity at different substrate concentrations (p-NPA as the substrate). k_{cat}/K_m values were then calculated using the Michaelis–Menten and Lineweaver–Burk equations.

2.6. Long-term stability

Free enzyme and immobilized enzyme stability were investigated for 40 days. They were added to a Tris buffer solution (pH: 7) at 25 °C and their relative activities were monitored on a regular basis using the esterase activity assay [48, 51].

2.7. Materials characterization

2.7.1. Contact angle

The optical contact angle analyzer (OCA 15 Plus) was used to measure the contact angle of the biocatalytic membranes and water based on the sessile drop method. In this approach, a tiny droplet of solvent was dropped on the membrane surface, and the contact angle was

calculated via software with images taken by camera of analyzer. The average values from one sample's measurement was indicated [178]. Results of this test shows the hydrophobicity of the membrane surface which has significant importance in wetting prevention in the membrane contactor to have reasonable efficiency.

2.7.2. Breakthrough pressure

For determining the breakthrough pressure, the setup presented in **Figure 2.2** was used. Water was pressurized with nitrogen at ambient temperature. One screen mesh was considered on above of the membrane to keep away the membrane against of deforming due to the high pressure. Pressure was increased slowly until one small droplet of liquid was observed.

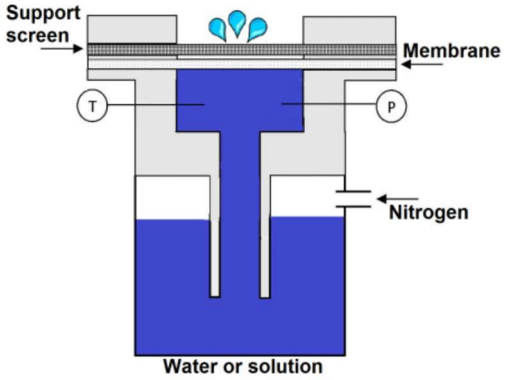

Figure 2.2. Breakthrough pressure apparatus [178].

2.7.3. Scanning Electron Microscope

The most popular form of electron microscope, scanning electron microscopy (SEM), analyses the sample's surface topography and composition. The material surface is scanned with a focussed electron beam, and secondary and backscattered electrons are measured at the same time. The backscattered electrons are responsible for providing information on the sample's elemental composition contrast, while the secondary electrons are used to obtain topographic contrast. Because of the varying distances between the surface topology and the beam detector, the equipped detectors are utilized to catch these signals discharged from a

scanning region of the sample surface, and a three-dimensional picture is formed that illustrates spatial changes in these attributes. Because of the distance between the surface topology and the beam detector, the sample portion closest to the beam detector seems brighter, while the sample section further away appears darker. As a result, SEM [186] can provide three-dimensional pictures. Furthermore, a SEM equipped with energy-dispersive X-ray spectroscopy (EDX) is commonly used to obtain and assess chemical elemental maps distributions or spot chemical composition studies.

SEM analysis was carried out on an Inspect F50 from FEI (accelerating voltage: 15 kV). An Energy Dispersive Spectrometer (EDS; Octane Super-A from Edax Ametek) was employed to characterize the elemental composition of the membrane. To make the surface electron conductive, samples should be coated with a thin coating of gold and palladium prior to doing the SEM test. This stage was completed with a Technic Hummer 2 machine.

2.7.4. Fourier transform infrared spectroscope

FTIR (Fourier Transform Infrared Spectroscopy) was used for measuring the chemical functional groups of membrane surfaces. According to this technique, the absorption of infrared radiation versus wavelength for the sample is determined. The infrared absorption bands identify molecular components and structures. It is a measurement including 64 scans with a resolution of 4 cm^{-1}. The absorption peaks at different wavenumbers (cm^{-1}) represent the functional groups on the support surface [51].

The surface functional groups were analyzed by a FTIR (MB3000 from ABB) over a scan range of 400–4000 cm^{-1}. For each sample, transmittance (absorbance) versus the wavelength is plotted and the peaks presenting different bonds are identified.

2.7.5. X-ray diffraction

The most extensively used technique for material characterisation, X-ray powder diffraction (XRD), is used to identify the phases of crystalline materials. It also gives useful information, such as polymorphs and crystal sizes. A beam of X-rays is directed to the sample in this procedure, and crystallographic planes scatter the rays into specified directions. Strong X-ray diffraction are produced in specific directions as a result, and the distribution and strength of these diffraction lines are linked to the crystal structure. The intensity signal of the

reflected X-rays is registered and processed into a chemical fingerprint while the sample and detector are rotated. The crystalline phase is recognized by comparing this diffraction pattern to the database. Bragg's law can be used to identify the crystal structure of a material by measuring the angle and intensity of diffracted rays [186].

XRD patterns for samples were obtained using an AERIS X-ray diffractometer with a Ni-filtered Cu-Kα radiation (λ = 1.5418 Å, generated at 40 kV and 8 mA). Bragg angles from 5° to 85° were scanned with a step size of 0.04° and a counting time of 0.6 s per step. By comparing peak positions to references in the literature and software database, the crystalline phase and its polymorphs are determined.

2.7.6. Transmission Electron Microscopy

Transmission electron microscopy (TEM) generates pictures with a significantly greater resolution of up to 0.3 nm by using electromagnetic lenses and electron beams. It can only create two-dimensional projected pictures due to its principle and structure, which are frequently used to investigate the structure and morphology of nanoparticles. The sample should be disseminated in a solvent using an ultrasonic processer to eliminate overlapping nanoparticles and get excellent two-dimensional pictures. Ethanol or toluene are used to disperse nanoparticles depending on their nature (hydrophilic or hydrophobic). Take one drop of the prepared mixture and gently lay it on a carbon grid. Following the adsorption of surplus solvent from the grid, it should be dried overnight at room temperature. The TEM equipment is then used to get the pictures when this stage is done [186].

TEM analysis was performed on a JEOL JEM 1230 electron microscope (accelerating voltage: 80 kV). To provide high quality photos, a Gatan dual-view multi-scan camera was used. ImageJ analysis software was used to assess the average size of nanoparticles from TEM pictures. Particle average size for each sample was acquired by measuring the diameter of a certain count of particles.

2.7.7. Nitrogen adsorption-desorption

The specific surface area and pore size distribution of porous materials may be determined using N_2 adsorption-desorption isotherms. On the basis of intermolecular forces, it is a well-established exact approach for defining the physical texture of materials. At constant

temperature, these isotherms are produced based on the quantity of adsorbed gas on the solid surface versus the equilibrium relative pressure (P/P_0).

Nitrogen adsorption-desorption isotherms of samples were obtained by a Micromeritics Gemini VII analyzer at −196 °C (77 K). Specific surface areas were calculated by the Brunauer-Emmett-Teller (BET) method in the relative pressure range of 0.05-0.3. Prior to measurements, all samples were degassed under vacuum for 10 min at room temperature and 4-6 h at 100 °C.

2.8. CO_2 absorption tests

2.8.1. CO_2 absorption performance of biocatalytic membrane contactors

The schematic experimental setup for CO_2 absorption in FSMC is illustrated in chapters 4 and 5. Per flat sheet membrane, the gas-liquid contact area is roughly 0.0041 m^2. Mass flow controllers were used to regulate the gas streams (flow and composition). An IR CO_2 analyzer was used to monitor the CO_2 concentration in the exit gas flow. The flow rate of the liquid (water in the presence of a buffer (Tris; 100 mM, pK_{a2} = 8.07 [7, 19])) was controlled and measured using a gear pump and a rotameter. A needle valve was used to keep the liquid outlet pressure slightly higher than the gas pressure. Fluids (gas and liquid) were flowing counter-currently or concurrently during the tests. The liquid and gas flow rates were 26 ml/min and 100 ml/min, respectively, with a volumetric percentage of 15% CO_2 in the intake gas (unless otherwise indicated).

Intensified FSMC was operated counter-currently and the absorbent was distillated water in presence of 100 mM Tris buffer with or without dispersed biocatalytic MNPs. All experiments in intensified FSMC were carried out at 298 K with one, two or three membranes.

2.8.2. CO_2 absorption performance of packed-bed column bioreactor

There is an illustration of the setup for the CO_2 absorption performance with Raschig ring packings in a counter-current packed-bed column in chapter 3. To vary the flow rate and composition of gas streams, mass flow controllers were installed at the inlet, and a bubble flowmeter was utilized to monitor the gas flow rate at the outlet. The gas mixture entered the bottom of the packed-bed column and the liquid was introduced by a distributor on the top

(controlled by a pump and a flowmeter). Inlet and output pressures were measured using pressure transducers. An IR CO_2 analyzer was used to measure the CO_2 composition. The operation in packed-bed column was counter-currently and the absorbent was distillated water in presence of Tris buffer with or without dispersed biocatalytic MNPs.

2.8.3. CO_2 absorption rate calculation

The CO_2 absorption rate (mol/min) in the flat sheet membrane contactor and packed-bed column was calculated with the following equation:

$$\mathrm{CO_2\ absorption\ rate} = \mathrm{Q_{inlet} y_{CO_2,inlet} - Q_{outlet} y_{CO_2,outlet}} \quad (2.4)$$

where Q_{inlet}, Q_{outlet}, $y_{CO_2,inlet}$ and $y_{CO_2,outlet}$ are the inlet gas molar flow rate (mol/min), outlet gas molar flow rate (mol/min), CO_2 mole fraction at the gas inlet and CO_2 mole fraction at the gas outlet, respectively.

2.9. Reusability of the immobilized enzyme in bioreactors

The reusability of immobilized CA on membrane, packing and MNPs in bioreactors were determined by monitoring the CO_2 absorption rate for 10 absorption cycles. Upon the completion of each cycle, the biocatalytic membranes and packings were washed with distillated water, and then reused for the next cycle. Also, the biocatalytic MNPs were collected with a magnet, washed with distillated water, and then re-suspended in a fresh liquid absorbent for the next cycle.

According to the literature, packed-bed column reactors, as extensive CO_2 capture technologies, with immobilized CA enzyme on the packing surfaces exhibited a low mass transfer due to the diffusional limitations.

In the first part or our work, CO_2 capture performance in packed-bed column bioreactor with immobilized CA enzyme on packing with additional biocatalytic MNPs dispersed in liquid phase is studied. To develop the biocatalytic MNPs, a comprehensive work is performed in this chapter. Based on the literature review, this is the first experimental and theoretical work to discuss the performance of packed-bed column reactors with immobilized CA enzyme on the packing, combined by CA enzyme attached on nanoparticles surface, elaborated by detailed experiments of influences of effective factors on CO_2 absorption performance in bioreactor.

Chapter 3: Enhanced CO_2 capture in packed-bed column bioreactors with immobilized carbonic anhydrase

Résumé

Un nouveau procédé enzymatique hybride utilisant l'enzyme Carbonic Anhydrase II humaine (hCA II) immobilisée sur la surface du garnissage et des nanoparticules magnétiques (MNPs) dispersées dans l'absorbant liquide dans un bioréacteur à colonne à garnissage gaz-liquide a été proposé. Les surfaces du garnissage et des MNPs ont été fonctionnalisées par co-déposition de polydopamine (PDA)/polyéthylèneimine (PEI) et l'hCA II a été immobilisé sur la surface modifiée via le glutaraldéhyde. hCA II immobilisée sur le garnissage et les MNPs a montré une grande stabilité (même après 40 jours), en conservant 80 % et 84,7 % de l'activité initiale, respectivement. Le processus d'hydratation du CO_2 a été significativement amélioré grâce à l'enzyme hCA II additionnelle immobilisée sur la surface des MNPs qui agissent comme une enzyme libre en solution, en particulier lorsque la limitation de diffusion du processus enzymatique avec l'enzyme hCA II immobilisée sur la surface du garnissage était très importante. Les performances d'absorption du CO_2 ont été évaluées expérimentalement et théoriquement dans différentes conditions (type et concentration du composant tampon et paramètres opératoires). Un modèle 3D décrivant l'hydrodynamique, le transport de masse/la réaction dans les phases liquide/gaz, l'accumulation de MNPs biocatalytiques dans le garnissage, la réaction et la diffusion dans la couche d'enzyme/film liquide a été développé pour étudier le comportement du bioréacteur. Dans l'ensemble, les résultats obtenus dans ce travail ont illustré que le bioréacteur à colonne à garnissage avec l'enzyme CA immobilisée sur le garnissage et la surface des MNPs est une conception encourageante de technologie verte de capture du CO_2, qui améliore l'utilisation du *TON* de l'enzyme.

Abstract

A novel hybrid enzymatic process with human Carbonic Anhydrase II (hCA II) enzyme immobilized on packing surface and magnetic nanoparticles (MNPs) dispersed in liquid absorbent in a gas-liquid packed-bed column bioreactor was proposed. Packing and MNPs surface were amine-functionalized by co-deposition of polydopamine (PDA)/polyethyleneimine (PEI) and hCA II was immobilized on the modified surface via glutaraldehyde. Immobilized hCA II on packing and MNPs displayed a high storage stability even after 40 days, preserving 80% and 84.7% of their initial activities, respectively. CO_2 hydration process achieved significant improvements due to the additional hCA II enzyme immobilized on the MNPs surface, functioning as a free solution-phase enzyme, especially when the diffusion limitation of the enzymatic process with immobilized hCA II enzyme on the packing surface was very significant. CO_2 absorption performance has been evaluated experimentally and theoretically under different conditions, including buffer type, buffer concentration, and operational parameters. A 3-D model describing the hydrodynamics, mass transport/reaction in liquid/gas phases, accumulation of biocatalytic MNPs in packed bed, reaction and diffusion in enzyme washcoat/liquid film was used to investigate the behavior of the packed-bed column bioreactor. Overall, the results achieved in this work illustrated that packed-bed column bioreactor with immobilized CA enzyme on the packing and MNPs surface is an encouraging green CO_2 capture technology design, which improve the utilization of CA enzyme large turnover number.

3.1. Introduction

One of the most crucial environmental problems confronting the world today is global warming. The ever-increasing level of CO_2 concentration in the atmosphere, main responsible for global warming and climate change problems, is receiving more attention. Post-combustion CO_2 capture, specially CO_2 removal via absorption system in packed-bed column using chemical solvents, is the most widely used method for capture of CO_2 due to its maturity and high efficiency [187]. However, they can be energy intensive, especially for amine-based absorption [188]. While CO_2 absorption in monoethanolamine and diethanolamine solutions is fast [189], the energy required for regeneration accounts for approximately 70%–80% of the overall operating cost of a CO_2 capture process, which has posed a significant challenge in this field for many years [6, 190, 191]. Additional drawbacks of the amine-based processes include equilibrium limits, amine degradation, production of oxidative degradation materials, and equipment corrosion [192]. Due to these negative features of amine-based solvents, the use of benign solvents is gaining popularity. In recent decades, biological catalysts used to accelerate the CO_2 hydration process is particularly attractive for CO_2 capture process [59] to increase the absorption rate of benign absorbents such as water.

Human Carbonic Anhydrase II (hCA II or CA for simplicity) is a natural enzyme catalyst whose hydration turnover is very high (between 10^4 and 10^6 molecules of CO_2 per molecule of CA per second), making it an effective enzyme in CO_2 capture [25, 27, 64, 193]. Enzyme immobilization is an appealing alteration that improves enzyme stability and its life span while also allowing the enzyme to be reused in a variety of cyclic operations [7, 11, 25, 37, 160]. The enzyme-based method opens up new avenues for developing cost-effective CO_2 capture methods, as well as a broader CO_2 emission reduction and climate change mitigation technologies [194].

There have been published researches on enzyme-based CO_2 removal in gas-liquid reactors using immobilized CA: hollow-fiber membrane contactor [19], random packed-bed columns with fourth generation random packings [11], structured packed-bed columns [13], bubble column [14], trickle-bed reactor [16] and spray column [15]. Gas-liquid packed-bed columns offer high efficiency, high surface area, low pressure drop and high mechanical stability and

are widely used for CO_2 capture [11]. Studies on CO_2 capture with packed-bed column in which CA was immobilized on the packing surface are very rare in the open literature. Bhattacharya et al. [150, 151] immobilized CA onto silica-coated steel matrix or iron filing matrix and sprayed a very tiny water flow rate from the top of the column. Larachi et al. [152] studied catalytic CO_2 hydration in a counter-current packed scrubber using immobilized CA on Nylon-6,6 Raschig rings (6.25 mm). In a more recent research, the CO_2 absorption in water was assessed in a counter-current packed-bed column using CA immobilized on polyester polyurethane prepolymer 80 [153]. Packed-bed column bioreactors with immobilized enzyme on packing surface [152, 153] showed some degree of improvement in CO_2 abatement, but exhibited insufficient mass transfer to fully utilize the enzyme's high turnover rate. The CO_2 hydration mechanism is constrained by the gas-liquid mass transfer since the enzyme immobilized on the packing surface is several millimeters away from the gas-liquid interface and the absorbent film.

To obtain most profit from the enzyme in a gas-liquid reactor, it should be placed nearer the gas-liquid interface (dissolved free enzyme or dispersed immobilized enzyme on the surface of micro/nanoparticles [15, 157]) to minimize the mass transfer resistance [46, 158]. Iliuta and Iliuta [159] studied through simulation an innovative hybrid enzymatic process in a packed-bed column reactor with enzyme immobilized both on the packing surface and suspended micro-particles dispersed in the liquid phase. The results indicated that the CO_2 absorption improved by the incorporation of additional immobilized CA enzyme on the micro-particles surface. In the literature, there is an increasing attention to employ nanoparticles such as TiO_2 [48], gold [195], SBA-15 [41], silica [89], and SiO_2–ZrO_2 [87] as support for enzyme immobilization. Magnetic nanoparticles (MNPs) also attracted more and more attention owing to properties such as high specific surface area, effective enzyme loading, low toxicity, and facile separation from the reaction medium by applying an external magnetic field [83, 196, 197]. As there is a weak interaction between Fe-OH functional groups of bare MNPs and enzymes, functionalized MNPs modified by adding reactive functional groups such as amine, hydroxyl, carboxyl and epoxy are utilized as support for covalent enzyme immobilization [54, 58, 71, 84, 96, 184, 196]. In the literature, CA was covalently immobilized on MNPs functionalized by amine [59, 83, 91, 198] and carboxyl groups [199]. Co-deposition of polyethyleneimine (PEI) and polydopamine (PDA) has

received much interest recently as a facile strategy to activate a support surface with abundant amine functional groups for subsequent enzyme immobilization through Schiff base and/or Michael addition reactions between amine groups of the enzyme and amine groups of the activated support surface [124, 126-128, 130-133, 200-202].

According to the promising results of the previous work in our group [159], we developed an enhanced enzymatic process with hCA II enzyme immobilized on packing surface and magnetic nanoparticles dispersed in the liquid phase in a packed-bed column bioreactor. In the present work, nylon packing and MNPs were modified via co-deposition of PDA/PEI and subsequently, CA enzyme was immobilized covalently via glutaraldehyde on the modified surfaces. Optimum conditions for biocatalytic MNPs preparation were revealed, and the storage stability of the immobilized CA on MNPs and packing was determined. Also, the ability for reusing the immobilized CA in enhanced packed-bed column bioreactor was demonstrated for several cycles. The impact of the additional hCA II enzyme immobilized on the MNPs surface, on the performance of CO_2 hydration process in the packed-bed column bioreactor was investigated. CO_2 absorption performance has been evaluated experimentally and theoretically under different conditions, including buffer type, buffer concentration, and operational parameters. A 3-D model describing the hydrodynamics, mass transport/reaction in liquid/gas phases, accumulation of biocatalytic MNPs in packed bed, reaction and diffusion in enzyme washcoat/liquid film was used to investigate the behavior of the packed-bed column bioreactor. For the best of our knowledge, this is the first experimental and theoretical work to discuss the performance of packed-bed column reactors with immobilized CA enzyme on the packing, combined by additional CA enzyme attached on nanoparticles surface. This study focuses to demonstrate that this innovative enhanced CO_2 absorption process in packed-bed column bioreactors, a green and environmentally friendly technology, could be a promising alternative to the traditional packed-bed column.

3.2. Experimental

3.2.1. Materials and chemicals

Packings and packed-bed column characteristics are reported in **Table 3.1**. Ferric chloride hexahydrate ($FeCl_3 \cdot 6H_2O$, 99.4%, MP Biomedicals LLC), ferrous chloride tetrahydrate ($FeCl_2 \cdot 4H_2O$, 99.0%−103.0%, Avantor Performance Materials, Inc.), and ammonium

hydroxide (NH_4OH, 28%−30%) were used for MNPs synthesis. HCA II enzyme with molecular weight of 29200 Da was produced and purified in our biotechnology laboratory. Over-expression of CAs was performed by transforming the recombinant plasmid into the E. coli BL21 expression strain and an affinity chromatography column was used in the purification step. Dopamine hydrochloride (≥ 98%, CAS no. 62-31-7) and p-nitrophenyl acetate (p-NPA; ≥ 98%, CAS no. 830-03-5) were obtained from Sigma-Aldrich. Glutaraldehyde (25 wt% solution in water) and PEI (MW = 600 Da; ≥ 99%) were purchased from Thermo Fischer Scientific. Tris Base, 2-amino-2-methyl-1,3-propanediol (AMPD; ≥ 99%) and N-methylimidazole (≥ 99%) were supplied from Bio Basic, Laboratoire MAT, and Alfa Aesar, respectively. Bradford Protein Assay Kit containing Bradford reagent and bovine serum albumin (BSA) standard protein was supplied by Bio Basic Inc. The commercial grade CO_2 and N_2 gases (minimum purity of 99.9%) were purchased from Praxair, Canada.

Table 3.1. Packings and packed-bed column specifications.

Parameters	Packings	Packed-bed column
Type	Raschig rings	-
Material	Nylon 6.6	-
Size (mm)	ID: 6 × OD: 8 × L: 8	-
Column internal diameter (m)	-	0.05
Bed height (m)	-	0.25
Bed porosity	-	0.71

3.2.2. Enzyme immobilization on packing surface

CA immobilization on the Raschig ring surface followed the immobilization procedure described in chapter 2. Briefly, the packing surface was amine-functionalized by co-deposition of PDA/PEI (PDA/PEI: 2/2 $mg.ml^{-1}/mg.ml^{-1}$ and co-deposition time: 7 h) and then the CA enzyme was immobilized on the packing surface via glutaraldehyde through covalent bonding (glutaraldehyde concentration: 1% (v/v), immobilization time: 32 h and CA concentration: 0.06- 0.1 mg/ml).

3.2.3. Biocatalytic magnetic nanoparticles preparation

3.2.3.1. Magnetic nanoparticles synthesis

MNPs (Fe_3O_4 nanoparticles) were synthesized by coprecipitation in basic solution. In the preparation process, $FeCl_3 \cdot 6H_2O$ (1 g) and $FeCl_2 \cdot 4H_2O$ (0.35 g) were dissolved in 150 mL

of distillated water with nitrogen protection under stirring for 30 min. The mixture solution was heated to 80 °C and then aqueous ammonia (28 wt%, 10 mL) was injected slowly. The reaction was maintained while stirring at 80 °C for another 30 min. After cooling the mixture to room temperature, the resultant MNPs were separated with the aid of a magnet and were washed thoroughly with distillated water for further modification until a neutral pH was attained [184].

3.2.3.2. Enzyme immobilization on MNPs

Functionalization and enzyme immobilization on MNPs were performed using the procedure described in chapter 2. MNPs surface was modified using co-deposition of PDA/PEI for amine functionalization. MNPs (200 mg) were first dispersed in Tris/HCl buffer (50 mM, pH: 8.5, 200 mL) under ultrasonic conditions. Then, dopamine (2 mg/ml) and PEI (2 mg/ml) were simultaneously added to the mixture solution of MNPs and Tris/HCl buffer. Then, the mixture was allowed to proceed for a certain time (3, 5, 7, 12, 24 or 32 h) under stirring at room temperature. Resultant products, namely P-MNPs, were separated and collected with a magnet and subsequently washed with distillated water several times [185]. The P-MNPs were suspended in a mixture of CA solution (buffer solution: 50 mM NaH_2PO_4 and 500 mM NaCl, pH: 7.4, CA concentration: 0.045-0.17 mg/ml) and glutaraldehyde (glutaraldehyde concentration: 0.5, 1.0, 2.0 or 4.0 % (v/v)) for covalent enzyme immobilization and then, the solution was shaken for a specific time (2, 4, 7, 12, 24 or 32 h) at room temperature. The P-MNPs with immobilized CA were referred as CA-P-MNPs. CA-P-MNPs were collected with a magnet and subsequently, were rinsed with distillated water several times. The schematic illustration of biocatalytic MNPs preparation is shown in **Figure 3.1**.

3.2.4. Bradford test

The protein amount in initial and final enzyme solution and in the washing solution were measured by the Bradford method. For this purpose, the amount of immobilized CA was determined by subtracting the protein amount of final enzyme solution and washing solution from the initial protein amount . Enzyme loading efficiency was calculated from the following equation:

$$\text{enzyme loading efficiency } (\%) = \frac{\text{loaded enzyme on surface } (\mu g)}{\text{total amount of enzyme } (\mu g)} \times 100 \qquad (3.1)$$

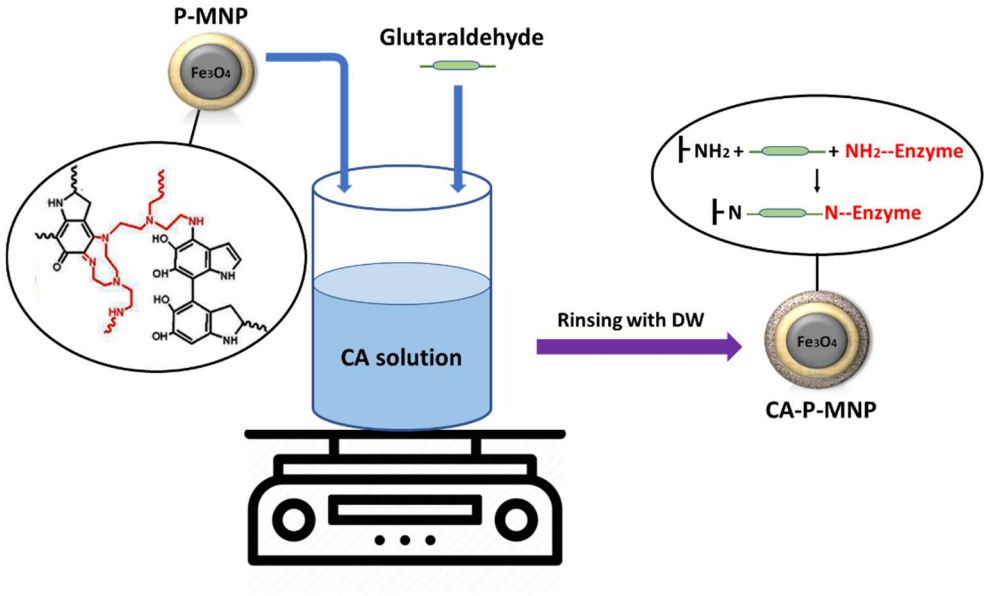

Figure 3.1. Development of biocatalytic MNPs.

3.2.5. Esterase activity test

Free and immobilized CA activity was determined by using p-NPA as a substrate, according to a described method in chapter 2. For the immobilized CA enzyme, the activity test was performed in a magnetically agitated beaker with 3.6 ml Tris/HCl buffer solution (50 mM, pH: 8), 0.4 ml acetonitrile containing p-NPA (3 mM) and 5 mg MNPs with immobilized enzyme at room temperature [48]. Enzyme activity efficiency was calculated by following equation:

$$\text{enzyme activity efficiency } (\%) = \frac{\text{immobilized enzyme activity on surface}}{\text{initial free enzyme activity in solution}} \times 100 \quad (3.2)$$

3.2.6. Characterization techniques

X-ray diffraction (XRD) patterns for MNP samples were obtained using an AERIS X-ray diffractometer with a Ni-filtered Cu-Kα radiation (λ = 1.5418 Å, generated at 40 kV and 8 mA) at 2θ range of 5°−85°. Fourier transform infrared (FTIR) spectra were recorded in the range 400–4000 cm^{-1} using FTIR spectrometer (Manufacturer: ABB; Model: MB3000). The morphologies of MNP samples were studied by Transmission Electron Microscopy (TEM) (JEOL JEM 1230 electron microscope with an accelerating voltage of 80 kV). Nitrogen

adsorption-desorption isotherms of MNP samples were obtained by a Micromeritics Gemini VII analyzer at −196 °C (77 K). Before each measurement, the samples were degassed under vacuum for 10 min at room temperature and 4 h at 100 °C.

3.2.7. Long-term stability of immobilized CA

Free enzyme and immobilized CA were analyzed for their storage stability for 40 days. The immobilized and the free CA were stored in Tris buffer solution (pH=7) at 25 °C and their residual activities were measured via an esterase activity test [48, 51].

3.2.8. k_{cat}/K_m evaluation for free and immobilized CA

Free and immobilized CA activities were measured as described in the section 2.5 at various substrate (p-NPA) concentrations (0.4, 1.0, 1.5, 2.0, and 3.0 mM). CA enzyme concentration was kept constant (0.195 mg/ml) and accordingly, k_{cat}/K_m values of free and immobilized CA were calculated via the Michaelis–Menten and Lineweaver–Burk equations.

3.2.9. CO_2 absorption performance of packed-bed column bioreactor

Figure 3.2 illustrates the setup for the CO_2 absorption performance with Raschig ring packings in a counter-current packed-bed column. Mass flow controllers were placed at the inlet of gas streams to adjust the flow rate and composition and a bubble flowmeter was used to measure the gas flow rate at the outlet. The gas mixture entered from the bottom of the packed-bed column and liquid passed through a liquid distributor at the top of packed-bed column, purchased from McMaster-Carr, to ensure uniform liquid distribution. The liquid flow rate was controlled using a pump and a flowmeter. Pressure transducers determined the inlet and outlet pressures of gas and liquid streams. An IR CO_2 analyzer was present at the gas effluent to measure the CO_2 percentage and the data were recorded with a LabVIEW program in real time. The packed-bed column was operated counter-currently and the absorbent was distillated water in presence of Tris buffer with or without dispersed CA-P-MNPs (condition respectively named CA-packing system and CA-packing/CA-MNPs system). The experimental tests in the bioreactor were assured to be conducted far from the flooding point (which corresponds to the accumulation of the liquid at the top of the column).

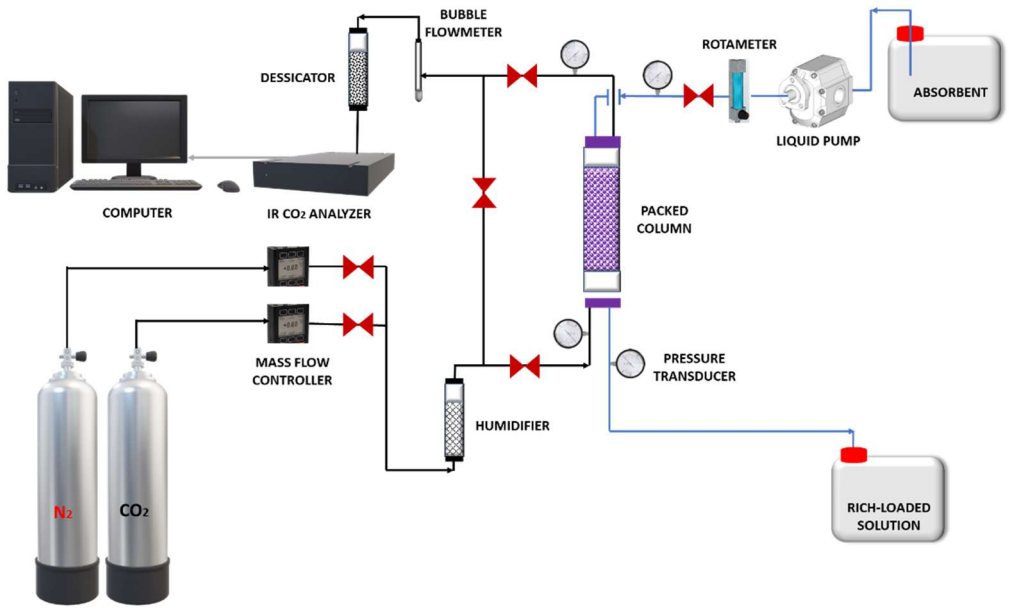

Figure 3.2. Packed-bed column bioreactor setup.

The CO_2 absorption rate (mol/min) in the packed-bed column was calculated with the following equation:

$$CO_2 \text{ absorption rate} = Q_{inlet} y_{CO_2,inlet} - Q_{outlet} y_{CO_2,outlet} \quad (3.3)$$

where Q_{inlet}, Q_{outlet}, $y_{CO_2,inlet}$ and $y_{CO_2,outlet}$ are the inlet gas molar flow rate (mol/min), outlet gas molar flow rate (mol/min), CO_2 mole fraction at the gas inlet and CO_2 mole fraction at the gas outlet, respectively.

3.2.10. Reusability of the enzyme in packed-bed column bioreactor

The reusability of the immobilized CA was investigated by monitoring the CO_2 hydration for 10 absorption cycles. Upon the completion of each cycle, the biocatalytic MNPs were collected by a magnet, washed with distillated water and then, were re-suspended in a fresh liquid absorbent for the next cycle.

3.3. Mathematical model of the packed-bed column bioreactor

3.3.1. Hydrodynamic model

The hydrodynamic model was presented somewhere else [159] and is only briefly described. The macro-scale hydrodynamics was modeled via a two-fluid Eulerian-Eulerian 3D model.

The fluids system is isothermal, incompressible, Newtonian and the countercurrent gas-liquid flow matches the pre-loading zone with the packing partially wetted by the liquid. The multiphase system was considered to have three interpenetrating continua: (i) the gas phase, (ii) the pseudo-homogeneous suspension phase with the biocatalytic MNPs dispersed in the liquid phase and (iii) the packing with the immobilized enzyme. Euler-Euler 3D model integrates the macro-scale continuity and momentum (with interphase interaction forces approximated via the double-slit model [203]) conservation equations with the dispersion mechanisms. In addition, the model incorporates the species balance equation for biocatalytic MNPs and the filtration equation referring to the accumulation of micro-particles in the bed. 3D continuity and momentum transport equations, species balance and filtration equations for the micro-particles are:

- Continuity and momentum balance equations

$$\frac{\partial}{\partial t}\left(\rho_\alpha \varepsilon_\alpha\right)+\frac{\partial}{\partial z}\left(\rho_\alpha \varepsilon_\alpha u_{\alpha z}\right)+\frac{1}{r}\frac{\partial}{\partial r}\left(r\rho_\alpha \varepsilon_\alpha u_{\alpha r}\right)+\frac{1}{r}\frac{\partial}{\partial \theta}\left(\rho_\alpha \varepsilon_\alpha u_{\alpha \theta}\right)=0\left(-N_{mp}\rho_{mp}\ \ for\ \ \alpha=\ell\right) \tag{3.4}$$

$$\begin{aligned}&\frac{\partial}{\partial t}\left(\rho_\alpha \varepsilon_\alpha u_{\alpha z}\right)+u_{\alpha r}\frac{\partial}{\partial r}\left(\rho_\alpha \varepsilon_\alpha u_{\alpha z}\right)+\frac{u_{\alpha\theta}}{r}\frac{\partial}{\partial \theta}\left(\rho_\alpha \varepsilon_\alpha u_{\alpha z}\right)+u_{\alpha z}\frac{\partial}{\partial z}\left(\rho_\alpha \varepsilon_\alpha u_{\alpha z}\right)=-\varepsilon_\alpha\frac{\partial P_\alpha}{\partial z}\\&+\mu_\alpha^{ef}\left[\frac{1}{r}\frac{\partial}{\partial r}\left(r\frac{\partial\left(\varepsilon_\alpha u_{\alpha z}\right)}{\partial r}\right)+\frac{1}{r^2}\frac{\partial^2\left(\varepsilon_\alpha u_{\alpha z}\right)}{\partial \theta^2}+\frac{\partial^2(\varepsilon_\alpha u_{\alpha z})}{\partial z^2}\right]+\varepsilon_\alpha\rho_\alpha g+f_{\text{int},\alpha,z}+F_{d,\alpha,z}^m\end{aligned} \tag{3.5}$$

$$\begin{aligned}&\frac{\partial}{\partial t}\left(\rho_\alpha \varepsilon_\alpha u_{\alpha r}\right)+u_{\alpha r}\frac{\partial}{\partial r}\left(\rho_\alpha \varepsilon_\alpha u_{\alpha r}\right)+\frac{u_{\alpha\theta}}{r}\frac{\partial}{\partial \theta}\left(\rho_\alpha \varepsilon_\alpha u_{\alpha r}\right)-\rho_\alpha\frac{u_{\alpha\theta}^2\varepsilon_\alpha}{r}+u_{\alpha z}\frac{\partial}{\partial z}\left(\rho_\alpha \varepsilon_\alpha u_{\alpha r}\right)=-\varepsilon_\alpha\frac{\partial P_\alpha}{\partial r}\\&+\mu_\alpha^{ef}\left[\frac{\partial}{\partial r}\left(\frac{1}{r}\frac{\partial\left(r\varepsilon_\alpha u_{\alpha r}\right)}{\partial r}\right)+\frac{1}{r^2}\frac{\partial^2\left(\varepsilon_\alpha u_{\alpha r}\right)}{\partial \theta^2}+\frac{\partial^2(\varepsilon_\alpha u_{\alpha r})}{\partial z^2}-\frac{2}{r^2}\frac{\partial\left(\varepsilon_\alpha u_{\alpha\theta}\right)}{\partial \theta}\right]+f_{\text{int},\alpha,r}+F_{d,\alpha,r}^m\end{aligned} \tag{3.6}$$

$$\begin{aligned}&\frac{\partial}{\partial t}\left(\rho_\alpha \varepsilon_\alpha u_{\alpha\theta}\right)+u_{\alpha r}\frac{\partial}{\partial r}\left(\rho_\alpha \varepsilon_\alpha u_{\alpha\theta}\right)+\frac{u_{\alpha\theta}}{r}\frac{\partial}{\partial \theta}\left(\rho_\alpha \varepsilon_\alpha u_{\alpha\theta}\right)+\rho_\alpha\frac{u_{\alpha\theta}u_{\alpha r}\varepsilon_\alpha}{r}+u_{\alpha z}\frac{\partial}{\partial z}\left(\rho_\alpha \varepsilon_\alpha u_{\alpha\theta}\right)=-\frac{\varepsilon_\alpha}{r}\frac{\partial P_\alpha}{\partial \theta}\\&+\mu_\alpha^{ef}\left[\frac{\partial}{\partial r}\left(\frac{1}{r}\frac{\partial\left(r\varepsilon_\alpha u_{\alpha\theta}\right)}{\partial r}\right)+\frac{1}{r^2}\frac{\partial^2\left(\varepsilon_\alpha u_{\alpha\theta}\right)}{\partial \theta^2}+\frac{\partial^2(\varepsilon_\alpha u_{\alpha\theta})}{\partial z^2}+\frac{2}{r^2}\frac{\partial\left(\varepsilon_\alpha u_{\alpha r}\right)}{\partial \theta}\right]+f_{\text{int},\alpha,\theta}+F_{d,\alpha,\theta}^m\end{aligned} \tag{3.7}$$

- Local volume conservation

$$\varepsilon_\ell+\varepsilon_g=\varepsilon \tag{3.8}$$

- Momentum balance at the gas-liquid interface [204]

$$P_g - P_\ell = 2\sigma_\ell \left(\frac{1-\varepsilon}{1-\varepsilon_g}\right)^{0.33} \left(\frac{1}{d_p} + \frac{1}{d_{\min}}\right) \tag{3.9}$$

- Species balance equation for biocatalytic micro-particles

$$\begin{aligned} &\frac{\partial}{\partial t}\left(\varepsilon_\ell c_{mp}\right) + u_{\ell r}\frac{\partial}{\partial r}\left(\varepsilon_\ell c_{mp}\right) + \frac{u_{\ell\theta}}{r}\frac{\partial}{\partial \theta}\left(\varepsilon_\ell c_{mp}\right) + u_{\ell z}\frac{\partial}{\partial z}\left(\varepsilon_\ell c_{mp}\right) = \\ &\frac{D_{\ell r}}{r}\frac{\partial}{\partial r}\left(r\varepsilon_\ell \frac{\partial c_{mp}}{\partial r}\right) + \frac{D_{\ell\theta}}{r^2}\frac{\partial^2}{\partial \theta^2}\left(\varepsilon_\ell c_{mp}\right) + D_{\ell z}\frac{\partial^2}{\partial z^2}\left(\varepsilon_\ell c_{mp}\right) - N_{mp}\left(c_{mp}\right) \end{aligned} \tag{3.10}$$

- Accumulation of micro-particles in packed bed

$$\frac{d\sigma}{dt} = N_{mp}\frac{1}{\rho_{mp}} \tag{3.11}$$

The micro-particles deposition rate (N_{mp}) was stated as a function of micro-particles concentration and liquid velocity via deep-bed filtration mechanisms:

$$N_{mp} = \lambda c_{mp}\varepsilon_\ell \sqrt{u_{\ell z}^2 + u_{\ell r}^2 + u_{\ell\theta}^2} \tag{3.12}$$

The filter coefficients for mono-layer ($\sigma \le \sigma_{cr}$) and multi-layer deposition ($\sigma > \sigma_{cr}$) were approximated via the correlations developed by Rajagopalan and Tien [205] (Eq. 3.13) and Tien et al. [206] (Eq. 3.16):

$$\lambda = \lambda^0 = \frac{3}{2}\left(1-\varepsilon^0\right)^{1/3}\frac{\eta^0}{d_p^0} \tag{3.13}$$

where:

$$\eta^0 = A_s^0\left(1-\varepsilon^0\right)^{\frac{2}{3}} N_R^{\frac{15}{8}} N_L^{\frac{1}{8}} + 0.00338 A_s^0\left(1-\varepsilon^0\right)^{\frac{2}{3}} N_G^{\frac{6}{5}} N_R^{-\frac{2}{5}} + 4\left(A_s^0\right)^{\frac{1}{3}}\left(1-\varepsilon^0\right)^{\frac{2}{3}} N_{Pe}^{-\frac{2}{3}} \tag{3.14}$$

$$A_s^0 = \frac{2\left(1-p^5\right)}{w},\quad p = \left(1-\varepsilon^0\right)^{\frac{1}{3}},\quad w = 2 - 3p + 3p^5 - 2p^6 \tag{3.15}$$

$$\frac{\lambda}{\lambda^0} = B_1\frac{A_s}{A_s^0}\left[1 + \frac{\sigma}{\left(1-\varepsilon^0\right)\left(1-\varepsilon_d\right)}\right]^{\frac{17}{24}} + B_2\frac{A_s}{A_s^0}\left[1 + \frac{\sigma}{\left(1-\varepsilon^0\right)\left(1-\varepsilon_d\right)}\right]^{\frac{4.4}{3}} + B_3\left(\frac{A_s}{A_s^0}\right)^{\frac{1}{3}}\left[1 + \frac{\sigma}{\left(1-\varepsilon^0\right)\left(1-\varepsilon_d\right)}\right]^{\frac{4}{9}} \tag{3.16}$$

where:

$$\frac{A_s}{A_s^0} = \left[\frac{1-\left(1-\varepsilon\right)^{\frac{5}{3}}}{1-\left(1-\varepsilon^0\right)^{\frac{5}{3}}}\right]\left[\frac{2-3\left(1-\varepsilon^0\right)^{\frac{1}{3}}+3\left(1-\varepsilon^0\right)^{\frac{5}{3}}-2\left(1-\varepsilon^0\right)^2}{2-3\left(1-\varepsilon\right)^{\frac{1}{3}}+3\left(1-\varepsilon\right)^{\frac{5}{3}}-2\left(1-\varepsilon\right)^2}\right] \tag{3.17}$$

The boundary conditions (Dirichlet-type boundary conditions at *z=0*; open boundary conditions at *z=H*, no-slip conditions at packed-bed column wall) for continuity and momentum balance equations and for species balance equation of biocatalytic micro-particles are given in Iliuta and Iliuta [11, 159]. The centerline gas/liquid velocities were approximated via the diametrical average approach using the nearby gas-liquid flow field and the extra midline flow variables were calculated via the free-slip condition.

The volume-averaged interphase interaction forces under partially wetted packing conditions and the related drag forces, approximated via the double-slit model [203], are:

$$f_{\text{int},g,z(r,\theta)} = f_e F_{g\ell,z(r,\theta)} + \left(1-f_e\right) F_{gs,z(r,\theta)} \tag{3.18}$$

$$f_{\text{int},\ell,z(r,\theta)} = -\frac{\varepsilon f_e - \varepsilon_\ell}{\varepsilon_g}\left[f_e F_{g\ell,z(r,\theta)} + \left(1-f_e\right) F_{gs,z(r,\theta)} \right] - f_e F_{\ell s,z(r,\theta)} \tag{3.19}$$

$$F_{\ell s,z(r,\theta)} = \left\{ \frac{E_1}{36}\frac{\overline{a}_s^2 \mu_\ell f_e}{\varepsilon_\ell^2} + \frac{E_2}{6}\frac{\overline{a}_s}{\varepsilon_\ell}\rho_\ell \sqrt{u_{\ell z}^2 + u_{\ell r}^2 + u_{\ell\theta}^2} \right\} u_{\ell z(r,\theta)} \varepsilon_\ell \tag{3.20}$$

$$F_{gs,z(r,\theta)} = \left\{ \frac{E_1}{36}\frac{\overline{a}_s^2 \mu_g \varepsilon_g}{\varepsilon^3} + \frac{E_2}{6}\overline{a}_s \frac{\varepsilon_g^2}{\varepsilon^3}\rho_g \sqrt{u_{gz}^2 + u_{gr}^2 + u_{g\theta}^2} \right\} u_{gz(r,\theta)} \varepsilon \tag{3.21}$$

$$F_{g\ell,z(r,\theta)} = \left\{ \frac{E_1}{36}\frac{\overline{a}_s^2 \mu_g}{\left(\varepsilon - \frac{\varepsilon_\ell}{f_e}\right)^2} + \frac{E_2}{6}\overline{a}_s \frac{\varepsilon_g}{\left(\varepsilon - \frac{\varepsilon_\ell}{f_e}\right)^2}\rho_g \sqrt{j_{rz}^2 + j_{rr}^2 + j_{r\theta}^2} \right\} j_{rz(r,\theta)} \varepsilon_g \tag{3.22}$$

Mechanical dispersion forces were quantified with the model by Lappalainen et al. [207] via the momentum exchange coefficients and axial drift velocities:

$$F_{d,\ell,z(r,\theta)}^m = f_e K_{\ell s} u_{d\ell,z(r,\theta)} - \varepsilon f_e K_{g\ell}\left(u_{dg,z(r,\theta)} - u_{d\ell,z(r,\theta)}\right) \tag{3.23}$$

$$F_{d,g,z(r,\theta)}^m = \left(1-f_e\right) K_{gs} u_{dg,z(r,\theta)} + \varepsilon f_e K_{g\ell}\left(u_{dg,z(r,\theta)} - u_{d\ell,z(r,\theta)}\right) \tag{3.24}$$

3.3.2. Mass transport/Reaction equations

3D hydrodynamic model is associated with species balance equations in the liquid/gas phases, simultaneous diffusion and chemical reaction in the liquid film neighboring the gas-liquid interface (reaction catalyzed by the immobilized enzyme on moving micro-particles)

and simultaneous diffusion and chemical reaction in enzyme washcoat (reaction catalyzed by the immobilized enzyme on packing surface).

- 3D species balance equations in liquid phase

$$\frac{\partial}{\partial t}\left(\varepsilon_\ell C_{j,\ell}\right)+u_{\ell r}\frac{\partial}{\partial r}\left(\varepsilon_\ell C_{j,\ell}\right)+\frac{u_{\ell\theta}}{r}\frac{\partial}{\partial\theta}\left(\varepsilon_\ell C_{j,\ell}\right)+u_{\ell z}\frac{\partial}{\partial z}\left(\varepsilon_\ell C_{j,\ell}\right)=$$
$$\frac{D_{\ell r}}{r}\frac{\partial}{\partial r}\left(r\varepsilon_\ell\frac{\partial C_{j,\ell}}{\partial r}\right)+\frac{D_{\ell\theta}}{r^2}\frac{\partial^2}{\partial\theta^2}\left(\varepsilon_\ell C_{j,\ell}\right)+D_{\ell z}\frac{\partial^2}{\partial z^2}\left(\varepsilon_\ell C_{j,\ell}\right)$$
$$+\upsilon_j R_{CO_2}^{cat,ie}\left(C_{j,\ell}\right)\eta_{cat}+\upsilon_j R_{CO_2}^{cat,fe}\left(C_{j,\ell}\right)+\upsilon_j R_{CO_2}^{uncat}\left(C_{j,\ell}\right)$$
$$-D_{j,\ell}\left.\frac{\partial C_{j,\ell f}}{\partial\zeta}\right|_{\zeta=\delta_\ell}a-\left[D_{CO_2,\ell}\left.\frac{\partial C_{CO_2,\ell f}}{\partial\zeta}\right|_{\zeta=0}a\right]_{only\ for\ CO_2}$$

where j=CO_2, HCO_3^- (3.25)

$$\frac{\partial}{\partial t}\left(\varepsilon_\ell C_{j,\ell}\right)+u_{\ell r}\frac{\partial}{\partial r}\left(\varepsilon_\ell C_{j,\ell}\right)+\frac{u_{\ell\theta}}{r}\frac{\partial}{\partial\theta}\left(\varepsilon_\ell C_{j,\ell}\right)+u_{\ell z}\frac{\partial}{\partial z}\left(\varepsilon_\ell C_{j,\ell}\right)=$$
$$\frac{D_{\ell r}}{r}\frac{\partial}{\partial r}\left(r\varepsilon_\ell\frac{\partial C_{j,\ell}}{\partial r}\right)+\frac{D_{\ell\theta}}{r^2}\frac{\partial^2}{\partial\theta^2}\left(\varepsilon_\ell C_{j,\ell}\right)+D_{\ell z}\frac{\partial^2}{\partial z^2}\left(\varepsilon_\ell C_{j,\ell}\right)$$
$$+\upsilon_j R_{CO_2}^{cat,ie}\left(C_{j,\ell}\right)\eta_{cat}+\upsilon_j R_{CO_2}^{cat,fe}\left(C_{j,\ell}\right)-D_{j,\ell}\left.\frac{\partial C_{j,\ell f}}{\partial\zeta}\right|_{\zeta=\delta_\ell}a$$

where j=*B*, BH^+ (3.26)

The kinetic model of Larachi [208] for the hydration of CO_2 with solution-phase enzyme was used to describe the hydration of CO_2 in the presence of the enzyme immobilized on the surface of moving micro-particles (these very small bioparticles act as free enzymes). CO_2 hydration reaction catalyzed by the moving bioparticles occurs in the liquid film and bulk liquid. The effectiveness factor of CO_2 hydration reaction in enzyme washcoat (η_{cat}) was approximated as the product of the effectiveness factor for a fully wetted washcoat and wetting efficiency:

$$\eta_{cat}=\frac{\int_V R_{CO_2,w}^{cat}\left(C_{j,w}\right)dV}{R_{CO_2,w}^{cat}\left(C_{j,\ell}\right)}f_e \qquad (3.27)$$

- 3D species balance equation in gas phase

$$\frac{\partial}{\partial t}\left(\varepsilon_g P_{CO_2,g}\right)+u_{gr}\frac{\partial}{\partial r}\left(\varepsilon_g P_{CO_2,g}\right)+\frac{u_{g\theta}}{r}\frac{\partial}{\partial \theta}\left(\varepsilon_g P_{CO_2,g}\right)+u_{gz}\frac{\partial}{\partial z}\left(\varepsilon_g P_{CO_2,g}\right)=D_{gz}\frac{\partial^2}{\partial z^2}\left(\varepsilon_g P_{CO_2,g}\right)$$
$$+D_{CO_2,\ell}\left.\frac{\partial C_{CO_2,\ell f}}{\partial \zeta}\right|_{\zeta=0} aRT \qquad (3.28)$$

The related boundary conditions for eqs. (3.25, 3.26, 3.27 and 3.28) are provided in Iliuta and Iliuta [11].

- Mass balance equations in enzyme washcoat

The diffusion and reaction equations in the enzyme washcoat (reaction catalyzed by the immobilized enzyme on packing surface) are:

$$\varepsilon_w\frac{\partial C_{j,w}}{\partial t}=D_{j,w}^{ef}\left(\frac{\partial^2 C_{j,w}}{\partial \xi^2}+\frac{1}{\xi}\frac{\partial C_{j,w}}{\partial \xi}\right)+\upsilon_j R_{CO_2,w}^{cat,ie}\left(C_{j,w}\right)+\upsilon_j R_{CO_2,w}^{uncat}\left(C_{j,w}\right) \qquad \text{j=CO}_2, \text{HCO}_3^- \qquad (3.29)$$

$$\varepsilon_w\frac{\partial C_{j,w}}{\partial t}=D_{j,w}^{ef}\left(\frac{\partial^2 C_{j,w}}{\partial \xi^2}+\frac{1}{\xi}\frac{\partial C_{j,w}}{\partial \xi}\right)+\upsilon_j R_{CO_2,w}^{cat,ie}\left(C_{j,w}\right) \qquad \text{j=}B, \text{BH}^+ \qquad (3.30)$$

The kinetic model of Hanna et al. [7] for the hydration of CO_2 by immobilized enzyme was used to describe the hydration of CO_2 in the enzyme washcoat. The related boundary conditions are:

$$t>0,\ \xi=\delta_w \qquad D_{j,w}^{ef}\left.\frac{\partial C_{j,w}}{\partial \xi}\right|_{\xi=\delta_w}=k_{\ell s,j}\left(C_{j,\ell}-C_{j,w}^{\delta_w}\right) \qquad (3.31)$$

$$t>0,\ \xi=0 \qquad \left.\frac{\partial C_{j,w}}{\partial \xi}\right|_{\xi=0}=0 \qquad (3.32)$$

- Mass balance equations inside the liquid film

The species molar fluxes at $\zeta=0$ (gas-liquid interface) and $\zeta=\delta_\ell$ were calculated by the integration of diffusion and reaction equations within the liquid film bordering the gas-liquid interface (reaction catalyzed by the immobilized enzyme on moving micro-particles):

$$\frac{\partial C_{j,\ell f}}{\partial t} = D_{j,\ell}\frac{\partial C_{j,\ell f}}{\partial \zeta} + \upsilon_j R^{cat,fe}_{CO_2,\ell f}\left(C_{j,\ell f}\right) + \upsilon_j R^{uncat}_{CO_2,\ell f}\left(C_{j,\ell f}\right) \qquad \text{j=CO}_2\text{, HCO}_3^- \quad (3.33)$$

$$\frac{\partial C_{j,\ell f}}{\partial t} = D_{j,\ell}\frac{\partial C_{j,\ell f}}{\partial \zeta} + \upsilon_j R^{cat,fe}_{CO_2,\ell f}\left(C_{j,\ell f}\right) \qquad \text{j=}B\text{, BH}^+ \quad (3.34)$$

$$t>0,\ \zeta=0 \qquad C_{CO_2,\ell f}\Big|_{\zeta=0} = C^i_{CO_2,\ell} \qquad \left.\frac{\partial C_{j,\ell f}}{\partial \zeta}\right|_{\zeta=0} = 0 \quad (3.35)$$

$$t>0,\ \zeta=\delta_\ell \qquad -D_{CO_2,\ell}\left.\frac{\partial C_{CO_2,\ell f}}{\partial \zeta}\right|_{\zeta=\delta_\ell} a = \left[R^{cat,fe}_{CO_2}\left(C_{j,\ell}\right) + R^{uncat}_{CO_2}\left(C_{j,\ell}\right)\right]\left(\varepsilon_\ell - \delta_\ell a\right) \quad (3.36)$$

$$C_{j,\ell f}\Big|_{\zeta=\delta_\ell} = C_{j,\ell} \qquad \text{where} \quad \text{j=}B\text{, BH}^+\text{, HCO}_3^- \quad (3.37)$$

3.3.3. Kinetics of CO_2 hydration

The catalyzed CO_2 hydration by human carbonic anhydrase II was described via Quad Quad Iso Ping Pong mechanism with a transitory complex, rapid solvation in the enzyme binding cavity and competitive inter-molecular proton transfer with respect to buffer (B) [208]:

$$CO_2 + ZnOH^-(E) \underset{k_{-1}}{\overset{k_1}{\rightleftarrows}} ZnHCO_3^-(ES) \quad (3.38)$$

$$H_2O + ZnHCO_3^-(ES) \underset{k_{-2}}{\overset{k_2}{\rightleftarrows}} HCO_3^- + ZnH_2O(E_W) \quad (3.39)$$

$$E_W \underset{k_{-3}}{\overset{k_3}{\rightleftarrows}} {}_H E \quad \text{(enzyme isomerization)} \quad (3.40)$$

$$B + ZnH_2O({}_H E) \underset{k_{-4}}{\overset{k_4}{\rightleftarrows}} BH^+ + ZnOH^-(E) \quad (3.41)$$

$$HCO_3^- + ZnH_2O({}_H E) \underset{k_{-5}}{\overset{k_5}{\rightleftarrows}} CO_2 + H_2O + ZnOH^-(E) \quad (3.42)$$

The enzymatic reaction rate for CO_2 hydration with solution-phase hCA II enzyme is [208]:

$$R^{cat}_{CO_2} = \frac{k_h\left(C_{CO_2}C_B - \frac{K_{a2}}{K_{a1}}C_{HCO_3^-}C_{BH^+}\right)\left(1+\frac{C_{HCO_3^-}}{K_{iHCO_3^-,3}}\right)C_{E0}}{\left[\begin{array}{l} K_B C_{CO_2} + K_{CO_2}C_B + \frac{K_B}{2}\frac{K_E}{K_{a1}}C_{HCO_3^-} + 2K_{CO_2}\frac{K_{a2}}{K_E}C_{BH^+} + C_{CO_2}C_B + 2\frac{K_{CO_2}}{K_{HCO_3^-}}\frac{K_{a2}}{K_E}C_{HCO_3^-}C_{BH^+} + \frac{K_B}{K_{iHCO_3^-,1}}C_{CO_2}C_{HCO_3^-} \\ + \frac{K_{CO_2}}{K_{iHCO_3^-,2}}C_B C_{HCO_3^-} + \frac{1}{2}\frac{K_B}{K_{iHCO_3^-,3}}\frac{K_E}{K_{a1}}\left(C_{HCO_3^-}\right)^2 + \frac{K_B}{K_{iHCO_3^-,1}K_{iHCO_3^-,4}}C_{CO_2}\left(C_{HCO_3^-}\right)^2 + \frac{1}{K_{iHCO_3^-,5}}C_{CO_2}C_B C_{HCO_3^-} \end{array}\right]} \quad (3.43)$$

The kinetic parameters were revised by Hanna et al. [7] in the case of CO_2 hydration with immobilized hCA II enzyme. Hydration/dehydration rate constants (k_h and k_d), apparent bicarbonate inhibition constants ($K_{iHCO_3^-,j}$) and apparent binding constants (K_B, K_{CO_2} and $K_{HCO_3^-}$) are given in Larachi [208] and Hanna et al. [7].

Uncatalyzed CO_2 hydration was described via Ho and Sturtevant [209] mechanism:

$$H_2O + CO_2 \underset{k_{13}}{\overset{k_{31}}{\rightleftarrows}} H^+ + HCO_3^- \quad (3.44)$$

$$H^+ + HCO_3^- \underset{k_{21}}{\overset{k_{12}}{\rightleftarrows}} H_2CO_3 \quad (3.45)$$

$$H_2O + CO_2 \underset{k_{23}}{\overset{k_{32}}{\rightleftarrows}} H_2CO_3 \quad (3.46)$$

The uncatalyzed CO_2 hydration reaction rate is:

$$R_{CO_2}^{uncat}\Big|_{\ell} = k_{31}^{'} C_{CO_2} - k_{13}^{'} C_{H^+} C_{HCO_3^-} \quad \text{where } k_{31}^{'} = k_{31} + k_{32};\ k_{13}^{'} = k_{13} + k_{23} / K_{H_2CO_3} \quad (3.47)$$

The rate constants are (25°C): $k_{31}^{'} = 0.037 \text{s}^{-1}$; $k_{13}^{'} = 5.5 \times 10^4 \text{ m}^3 / kmol_l\, s$ [209].

3.4. Results and discussion

3.4.1. Optimization of biocatalytic MNPs development

3.4.1.1. Effect of co-deposition time

The synthesized MNPs with the co-precipitation method were dispersed in the PDA/PEI solution for 3, 5, 7, 12, 24 or 32 h, all followed by a 24 h CA enzyme immobilization time. As shown in **Figure 3.3a**, the increase of the PDA/PEI co-deposition time from 3 h to 24 h, significantly improved the enzyme activity efficiency and enzyme loading efficiency due to the proliferation of amine functionalities on MNPs as support. However, the activity efficiency decreased with further extension of the PDA/PEI co-deposition time to 32 h because extensive amounts of PDA/PEI increased steric hindrance between the enzyme and the support and enwrapped the enzyme, thus reducing the enzyme activity efficiency [138]. This observation confirmed that PDA/PEI deposition layer covered thoroughly the MNPs surface with 24 h co-deposition time and thus, this time was selected for the subsequent support functionalization due to higher enzyme activity efficiency. Moreover, FTIR was used to analyze the chemical structure of bare MNPs and P-MNPs with co-deposition times of 12,

24, and 32 h as shown in **Figure 3.4.** The characteristic absorption band of the Fe-O bond was observed at 501 and 547 cm^{-1} from FTIR spectra of bare MNPs and P-MNPs [210, 211]. Two main absorption peaks at 1507-1681 cm^{-1} and 3000-3500 cm^{-1} appeared after co-deposition of PDA/PEI on MNPs surface, which were related to the amide II band (N-H bond (primary amine groups) and C=N stretching [129, 137]) and N-H (secondary amine groups) with O-H stretching vibrations of PDA and PEI, respectively. With the increase of co-deposition time from 12 to 32 h, the representative peaks of amine functional groups became broader due to the PDA/PEI deposition enhancement on the MNPs surface [51, 136].

To further study the co-deposition time effect on amine-functionalization of MNPs surface, TEM and nanostructure architecture analyses were utilized. **Figure 3.5** illustrates the TEM images of MNPs, P-MNPs (12 h), P-MNPs (24 h), and P-MNPs (32 h). As shown in **Figure 3.5**a, bare MNPs have an average particle size of 9.2 nm. By prolonging the co-deposition time from 12 to 32 h, more PDA/PEI deposited on the MNPs substrate and the average particle size enhanced from 14.2 to 20.2 nm showing an increase of the coating layer thickness. The particle size is an important parameter for support materials since smaller particles possess higher surface area, resulting in more enzyme immobilization on support surface and less restriction for substrates and products diffusion[185]. BET surface area, BJH pore diameter, and BJH pore volume for bare MNPs, P-MNPs (12 h), P-MNPs (24 h), and P-MNPs (32 h) are presented in **Table 3.2**. BET surface area of P-MNPs (24 h) only decreased to 70.9 m^2/g compared to the one of P-MNPs (12 h) with 76.4 m^2/g. However BET surface area of P-MNPs (32 h) was much lower (55.5 m^2/g) than the one for P-MNPs (24 h) (70.9 m^2/g). Therefore, P-MNPs (24 h) were considered as the optimal support for enzyme immobilization. According to **Table 3.2**, mean BJH pore diameter boosted from 13.2 to 29.3 nm with raising co-deposition time from 12 to 32 h. A greater BJH pore diameter reduces mass transfer resistance while also preventing unintended intermolecular interactions between the enzymes. In addition, the PDA/PEI deposition layer creates more nanostructures on the surface of the MNPs, resulting in a larger pore volume [212, 213].

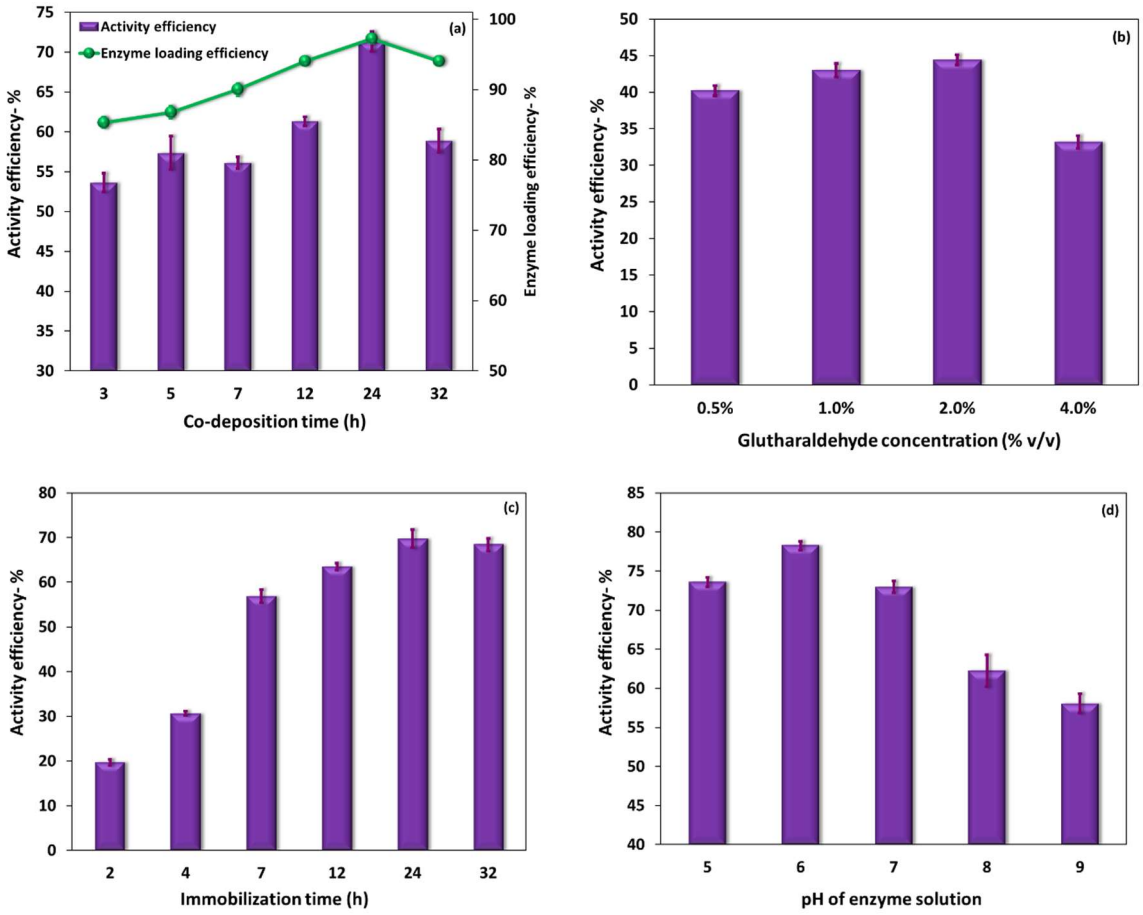

Figure 3.3. Effect of different parameters on biocatalytic MNPs performance: (a) co-deposition time (glutaraldehyde 2 (v/v)%, CA concentration 0.2 mg/ml, pH 7, immobilization time 24 h), (b) glutaraldehyde concentration (deposition time 5 h, CA concentration 0.2 mg/ml, pH 7, immobilization time 24 h), (c) CA immobilization time (deposition time 24 h, glutaraldehyde 2 (v/v)%, CA concentration 0.2 mg/ml, pH 7), and (d) enzyme solution pH (deposition time 24 h, glutaraldehyde 2 (v/v)%, CA concentration 0.2 mg/ml, immobilization time 24 h).

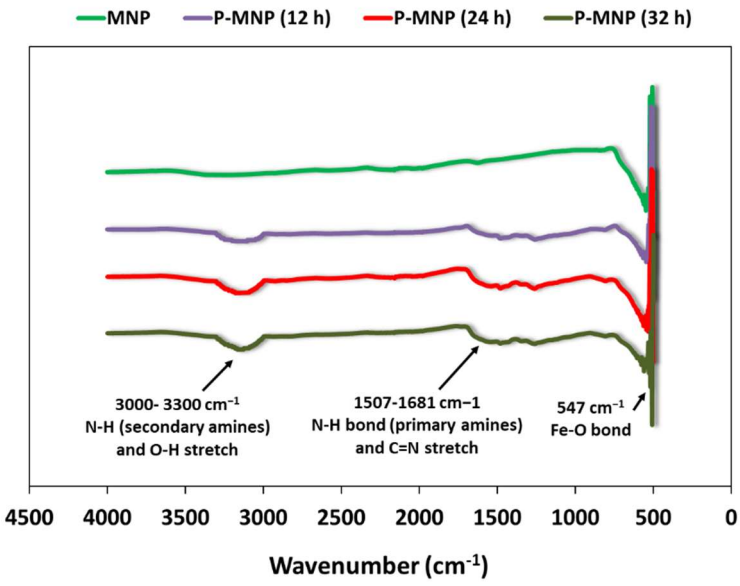

Figure 3.4. FTIR spectra of bare MNPs and P-MNPs with 12, 24 and 32 h co-deposition time.

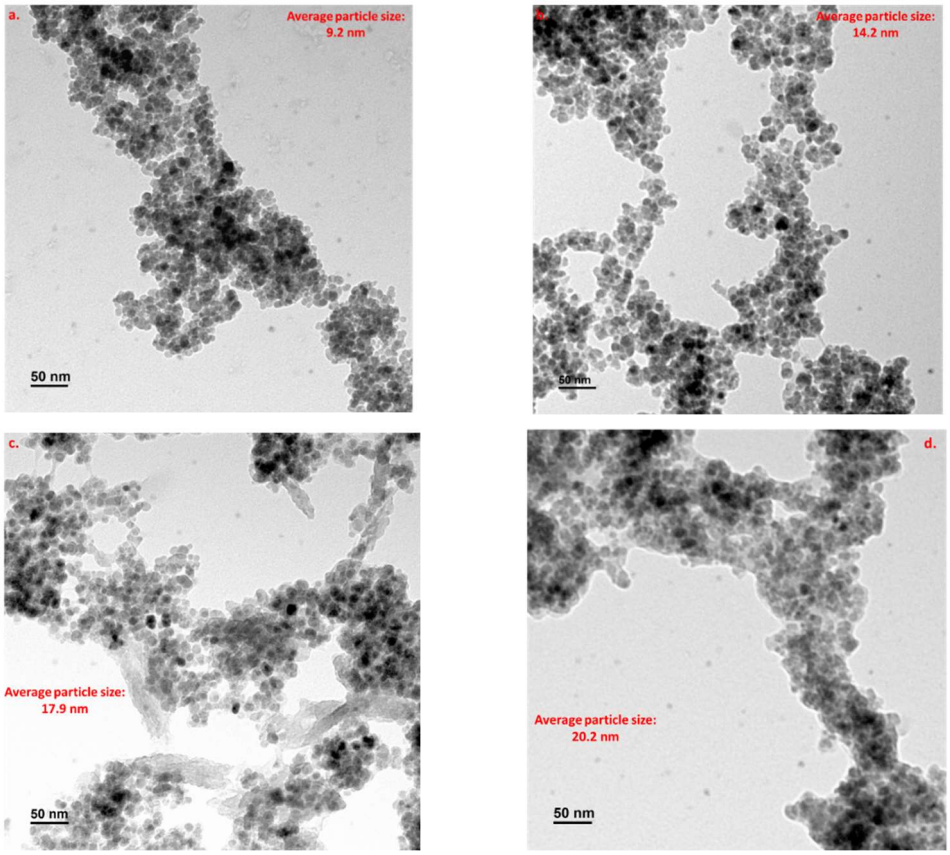

Figure 3.5. TEM images with average particle size: (a) MNPs, (b) P-MNPs (12 h), (c) P-MNPs (24 h), and (d) P-MNPs (32 h).

Table 3.2. BET surface area, mean BJH pore diameter and pore volume for bare MNPs and MNPs with 12, 24, and 32 h co-deposition times.

Sample	BET surface area (m^2/g)	Mean BJH pore diameter (nm)	BJH pore volume (cm^3/g)
MNPs	101.4	8.8	0.28
P-MNPs (12 h)	76.4	13.2	0.30
P-MNPs (24 h)	70.9	24.1	0.49
P-MNPs (32 h)	55.5	29.3	0.47

3.4.1.2. Effect of glutaraldehyde concentration

Addition of glutaraldehyde augments the enzyme rigidity and provides more reactive end groups for enzyme immobilization on the support, but an extra amount of glutaraldehyde may greatly alter the enzyme catalytic properties [214]. Therefore, the effect of glutaraldehyde concentration on enzyme immobilization was investigated (deposition time 5 h, CA 0.2 mg/ml, pH 7, immobilization time 24 h). As shown in **Figure 3.3**b, the enzyme activity efficiency amended when the glutaraldehyde concentration raised in the range of 0.5− 2.0 (v/v)% due to the higher number of reactive end groups of glutaraldehyde on the support, and then, the enzyme activity efficiency decreased as the glutaraldehyde concentration exceeded 2.0 (v/v)%. An extensive amount of glutaraldehyde reactive end groups reacted with the enzyme, altering the enzyme conformation and leading to a decrease of the enzyme activity efficiency [59, 214, 215]. Consequently, the optimum glutaraldehyde concentration was 2.0 (v/v)%, insuring greater enzyme activity for biocatalytic MNPs.

3.4.1.3. Effect of enzyme immobilization time

Figure 3.3c illustrates the impact of immobilization time (2-32 h) on the enzyme activity efficiency on CA-P-MNPs. Specifically, the activity efficiency of immobilized CA enhanced up to 24 h and then declined at 32 h. This could be explained that with lengthening the immobilization process, enzyme activity mitigated due to the extensive cross-linking of enzyme by glutaraldehyde, changing the enzyme conformation. Furthermore, excessive enzyme immobilization on the support with extending immobilization time leaded to

substrate diffusion limitations and enzyme mobility reduction by crashing the chain of surrounding enzyme molecules, resulting in enzyme activity diminishment [59].

3.4.1.4. Effect of enzyme solution pH during immobilization

The optimal CA solution pH to achieve the best activity of the biocatalytic MNPs was examined by dispersing the P-MNPs in the CA solution mixed with 2.0 (v/v)% glutaraldehyde and by adjusting the pH from 5.0 to 9.0, (**Figure 3.3**d). Enzyme structure is maintained while working with enzyme solution pH near to the enzyme isoelectric point (IEP) [48]. CA posses an IEP of approximately 6.0 and consequently, the highest CA enzyme activity efficiency should be obtained at pH 6.0 [48, 138, 216].

3.4.2. Characterization of biocatalytic MNPs

The crystal structure of the synthesized MNPs, P-MNPs and CA-P-MNPs was characterized by XRD. As displayed in **Figure 3.6**, the characteristic peaks occurred in the spectrum of MNPs at 2θ = 18.3°, 30.1°, 35.0°, 43.1°, 53.4°, 57.3°and 62.6°, which were consistent with the peaks of bare Fe_3O_4: (220), (220), (311), (400), (422), (511), and (440), respectively [59, 185]. XRD patterns of P-MNPs and CA-P-MNPs also owned similar peaks compared to the spectrum of MNPs, indicating that the crystalline structure of the modified MNPs was not modified during the deposition and immobilization processes [58, 185].

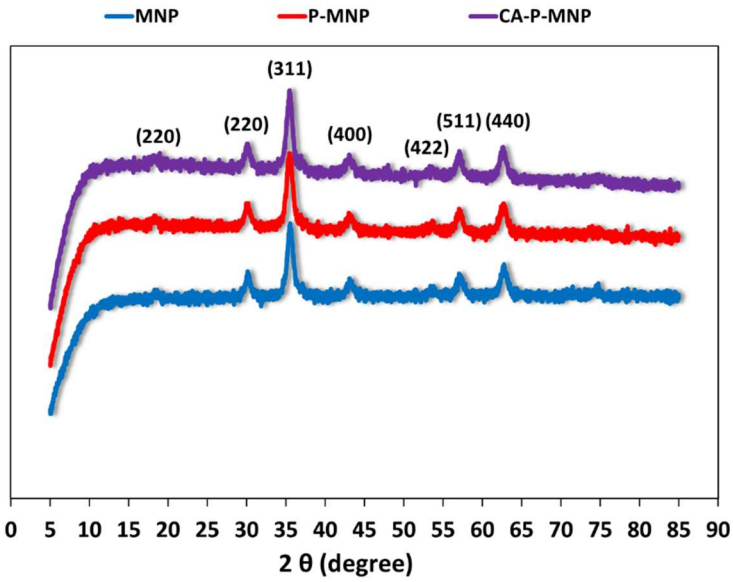

Figure 3.6. XRD patterns of bare MNPs, P-MNPs and CA-P-MNPs.

FTIR spectra of the MNPs, P-MNPs, and CA-P-MNPs (**Figure 3.7**) displayed strong peaks at 501 and 547 cm^{-1} which was assigned to the stretching vibration of the Fe-O bond [210, 211]. After coating of MNPs by PDA/PEI layer (P-MNPs), peaks around 1507-1681 cm^{-1} and 3000-3500 cm^{-1} were revealed owing to the introduction of amine groups of PDA/PEI deposition on the surface of MNPs [217]. CA-P-MNPs depicted a FTIR spectrum with weaker peaks at 1507-1681 cm^{-1} and stronger peaks at 3000-3500 cm^{-1} rather than the ones for P-MNPs. Enzyme immobilization through covalent bonding consumed primary amine groups, resulting to the less primary amine groups and more secondary amine groups on the MNPs surface [185, 218].

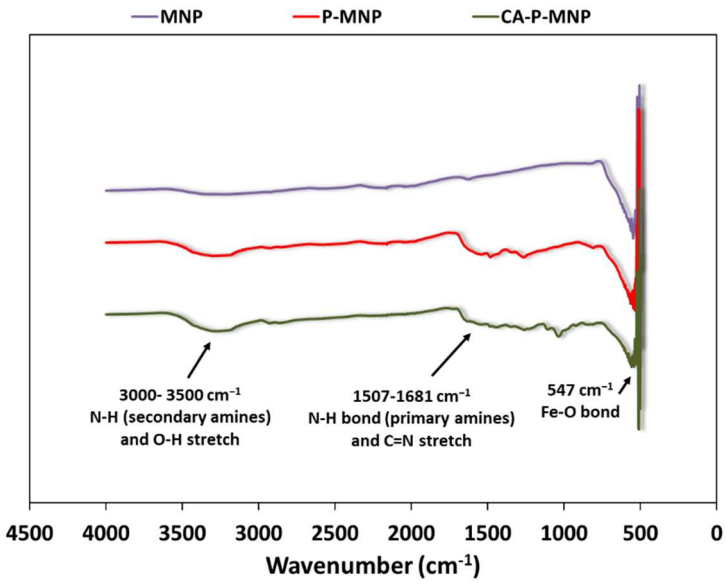

Figure 3.7. FTIR spectra of bare MNPs, P-MNPs and CA-P-MNPs.

The morphologies of the MNPs, P-MNPs (see **Figure 3.5**), and CA-P-MNPs (**Figure 3.8**) were characterized by TEM analysis. Particle size of MNPs increased from 9.2 to 17.9 nm with co-deposition of PDA/PEI layer and then to 25.6 nm with CA immobilization. It can be seen that P-MNPs and CA-P-MNPs cores are encased in an obvious irregular grey layer, indicating that the deposition/CA enzyme layers were successfully coated/ immobilized on the surface of these MNPs [58]. In addition, the mean BJH pore diameter (37.7 nm) and BJH pore volume (0.51 cm^3/g) for CA-P-MNPs are much higher than the values for P-MNPs corresponding to the addition of an immobilized layer on P-MNPs surface. CA-P-MNPs displayed a lower BET specific area (43.1 m^2/g) after the enzyme immobilization compared

to the values of bare MNPs and P-MNPs. Such a decrease in the BET specific area for the CA-P-MNPs was due to either the pore filling of MNPs surface by enzyme or particle size growth after enzyme immobilization [41].

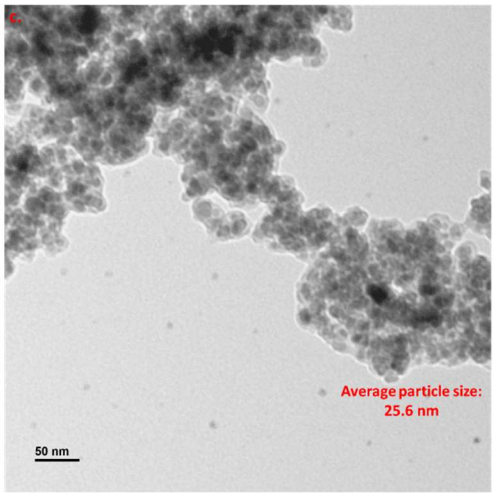

Figure 3.8. TEM image with average particle size: CA-P-MNPs.

3.4.3. Performance of the biocatalytic MNPs

The biocatalytic MNPs were fabricated according to optimum parameters found in section 3.4.1: co-deposition time of 24 h, glutaraldehyde concentration of 2.0% (v/v), enzyme immobilization time of 24 h, and enzyme solution pH of 6.0. For free CA, the calculated value of k_{cat}/K_m was 1468.1 M^{-1} s^{-1}. However, k_{cat}/K_m of immobilized CA on MNPs surface decreased about 20% (1134.4 M^{-1} s^{-1}) due to the possible change of CA enzyme structure after immobilization on MNPs. This decrease was much lower than the one found for the biocatalytic membranes (about 56%) developed in chapter 4. The high surface area for enzyme immobilization on MNPs and greater mobility of CA enzyme after immobilization on MNPs helped to preserve a higher enzyme activity on this support in comparison with the CA immobilized on membranes [44, 57]. This result indicates that CA enzyme immobilized on MNPs achieved a high retention of enzyme activity and MNPs could effectively preserves the affinity between CA and p-NPA after immobilization [58].

Furthermore, the long-term storage stability of free and immobilized CA was investigated for 40 days as shown in **Figure 3.9**. Immobilized CA on MNPs preserved 84.7% of its initial activity after 40 days, but the free CA activity declined continuously and after 40 days, the

free CA only maintained 43% of its initial activity. Better storage stability was observed with the biocatalytic MNPs compared with free CA, indicating the effectiveness of the immobilization in maintaining the enzyme activity over time. This could be ascribed that the enzyme unfolding and denaturation were avoided due to the intense and multiple covalent bonds between the enzyme and amine-functionalized MNPs surface, resulting in the stability growth of CA [97]. Compared with the values in the literature (**Table 3.3**), the biocatalytic MNPs prepared in this work have an excellent storage stability. Also, the highest value of enzyme activity efficiency achieved in the literature was 87.6% with TiO_2 nanoparticles [48] which was approximately on a level with the activity efficiency results in this work (up to 78.3%). Additionally, the enzyme loading of the biocatalytic MNPs (up to 28.5 mg/g support) with 0.2 mg/ml initial CA enzyme concentration at the beginning of immobilization process was comparable with the other data in literature (**Table 3.3**), considering the initial CA enzyme concentration utilized. Only the SBA-15 support attained significantly higher amounts of CA loading due to its large surface area (213 m^2/g) but there was a possible aggregation of the particles that constrained the approachability of CA to SBA-15 support [218]. Finally, these results validated the appealing features of the proposed biocatalytic MNPs for CO_2 absorption in a packed-bed column application.

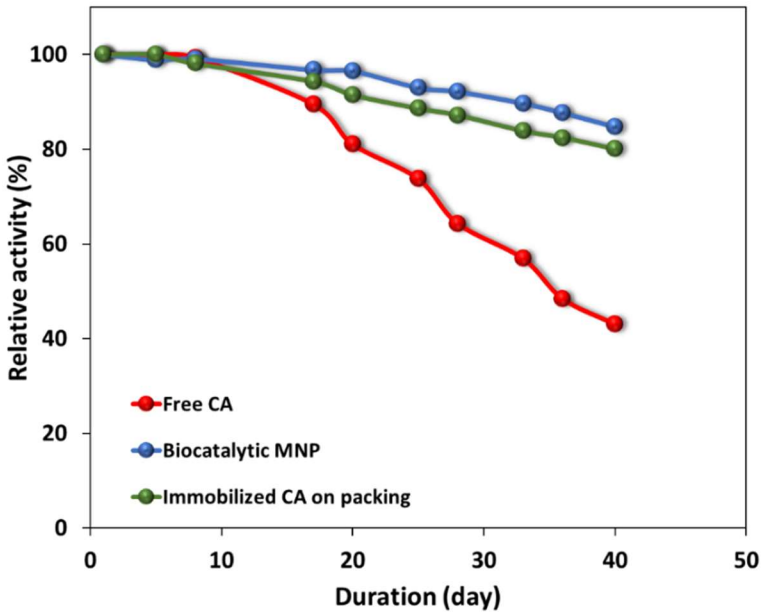

Figure 3.9. Storage stability of free CA and immobilized on packing and MNPs.

Table 3.3. Summary of CA immobilized on a variety of supports.

Support	Functional reagents	Initial CA conc. (mg/ml)	Enzyme loading	Activity efficiency (%)	Relative activity after 20 days (%)	Ref.
MNPs	PDA/PEI and glutaraldehyde	0.2	28.5 mg/g support	78.3	96.5	Current work
TiO_2 coated nanoparticles	3-aminopropyl triethoxy silane (KH550) and glutaraldehyde	0.1	27.4 mg/g support	87.6	72	[**48**]
Porous glass	KH550 and glutaraldehyde	0.4	32.6 mg/g support	35	85 (at 50 °C)	[**17**]
SBA-15	KH550 and glutaraldehyde	3.0	209 mg/g support	-	95	[**218**]
Silica nanoparticles	KH550 and glutaraldehyde	0.8	65 mg/g support	45	55 (at 50 °C)	[**89**]
SiO_2–ZrO_2 nanoparticles	KH550 and glutaraldehyde	0.5	69.2 mg/g support	32.5	95 (at 50 °C)	[**87**]
SBA-15	3-glycidyloxypropyltrimethoxysilane (GPTMS) and glutaraldehyde	2.0	222 mg/g support	-	95	[**41**]
MNPs	Glycidyl methacrylate (GMA), divinyl benzene (DVB), 3-(trimethoxysilyl) propylmethacrylate (MPS)	0.02	-	-	75	[**58**]
MNPs	tetraethyl orthosilicate (TEOS), KH550 and glutaraldehyde	-	-	-	85	[**59**]

3.4.4. Storage stability of immobilized CA on packing

The storage stability of immobilized CA on packing surface was also investigated and it revealed that the immobilized CA retained 80% of its initial activity after 40 days. Compared to the storage stability of free CA (**Figure 3.9**), there is a significant improvement of the storage stability of CA after immobilization.

3.4.5. CO_2 absorption performance of packed-bed column bioreactor

Figure 3.10 illustrates the impact of CA enzyme loading (CA enzyme immobilized on packing surface) on packed-bed column bioreactor performance. The ability of the model to capture the influence of the enzyme loading on the packed-bed column bioreactor performance is also shown. As shown in this figure, in counter-current packed-bed column with CA enzyme immobilized on packing surface (enzyme concentration in bioreactor: 9.2 $mg/L_{reactor}$), an experimental CO_2 absorption rate of $9.1 \pm 0.32 \times 10^{-4}$ mol/min was attained

with 135 ml/min liquid flow rate, 500 ml/min gas flow rate, 100 mM Tris buffer, and 15% inlet gas CO_2 percentage. This amount of enzyme (9.20 mg/$L_{reactor}$) respected the optimum enzyme amount on packing surface of the previous work in our group (9.45 mg/$L_{reactor}$) [159], which matched the conditions of a diffusional limited CO_2 hydration process. A 2.1 times raise of the enzyme concentration in the bioreactor (19.1 mg/$L_{reactor}$) generated only a 4.9% increase of the CO_2 absorption rate ($9.51 \pm 0.30 \times 10^{-4}$ mol/min). These results confirm that internal/external diffusion limits CO_2 hydration process at higher CA enzyme loading, resulting in a limitation of the utilization of the large turnover number of the CA enzyme. Similar observations can be found in other publications [152, 153, 159]. Contradictorily, as shown in **Figure 3.11**a, CO_2 absorption rate significantly enhances by 21 and 25% when adding 0.69 and 1.4 mg/$L_{reactor}$ CA enzyme loading in packed-bed column bioreactor via biocatalytic MNPs (the extra amounts of CA loading represent an 8 and 15% increase in total CA enzyme loading in packed-bed column bioreactor, considering 9.2 mg/$L_{reactor}$ enzyme loading on packing surface). Immobilization of CA enzyme on MNPs surface locates the enzyme closer to the gas-liquid interface [160, 184] and catalyzes the CO_2 hydration reaction as a free solution-phase CA enzyme in the liquid bulk. Consequently, CO_2 absorption rate and CO_2 removal in packed-bed column bioreactor is significantly increased by the employment of extra immobilized CA on the biocatalytic MNPs dispersed in the liquid phase. Also, **Figure 3.11** reveals that the packed-bed column reactor with bare packing and biocatalytic MNPs operates efficiently even with a small amount of enzyme immobilized on MNPs. In addition, Figures 3.10 and 3.11 illustrate that this immobilized enzyme system permits to obtain a reasonable CO_2 conversion, even when a component of the enzymatic system (CA-packing system or CA-MNPs system) does not work at optimal parameters and avoids the decline of the CO_2 absorption because of the contraction of enzyme activity in time.

There are very few experimental research works introducing enzyme in a packed-bed column system in the literature. In a spray column, Bhattacharya et al. [150] immobilized a high amount of CA enzyme on packing surface (250 mg/L) and only 22% CO_2 conversion was attained. In a packed-bed column (15.2 cm ID column and 43 cm bed height) by Larachi et al. [152], 112 mg/L CA enzyme immobilized on packing surface and 40% CO_2 conversion was obtained (80 mM 2-amino-2-hydroxymethyl-1,3-propanediol (AHPD) buffer

concentration, 18% feed CO_2 percentage, liquid velocity: 3 mm/s and gas velocity: 17 mm/s). Compared with other works using traditional packed-bed columns with immobilized CA on packing surface, the packed-bed column bioreactor proposed in this work exhibits strongly competitive CO_2 absorption performance; 71% CO_2 removal with 10.6 mg/$L_{reactor}$ overall CA enzyme immobilized on both packing and MNPs surfaces (100 mM Tris buffer concentration in water, 15% feed CO_2 percentage, liquid velocity: 4.1 mm/s and gas velocity: 4.2 mm/s); according to **Figure 3.14**b. These results highlight a competitive efficiency of our proposed system in CO_2 absorption process compared to conventional enzymatic processes with immobilized CA enzyme on the packing surface.

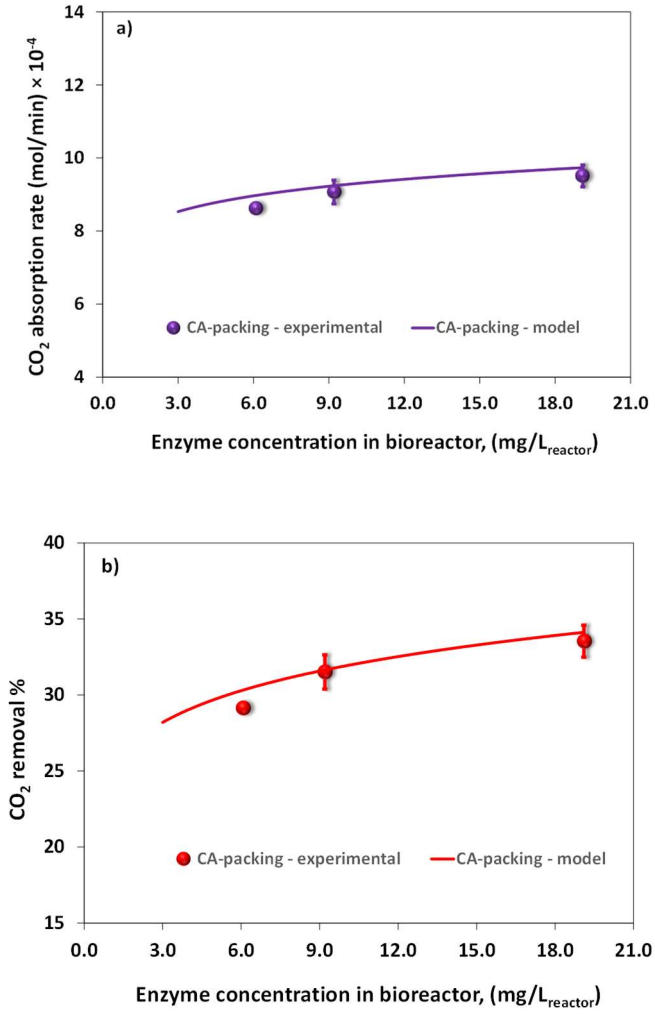

Figure 3.10. Impact of enzyme concentration (provided by the immobilization of the enzyme on packing surface) on packed-bed column bioreactor performance (100 mM Tris buffer, inlet gas CO_2 percentage: 15%, liquid flow rate: 135 ml/min, gas flow rate: 500 ml/min, and counter-current flow): a) CO_2 absorption rate; b) CO_2 removal.

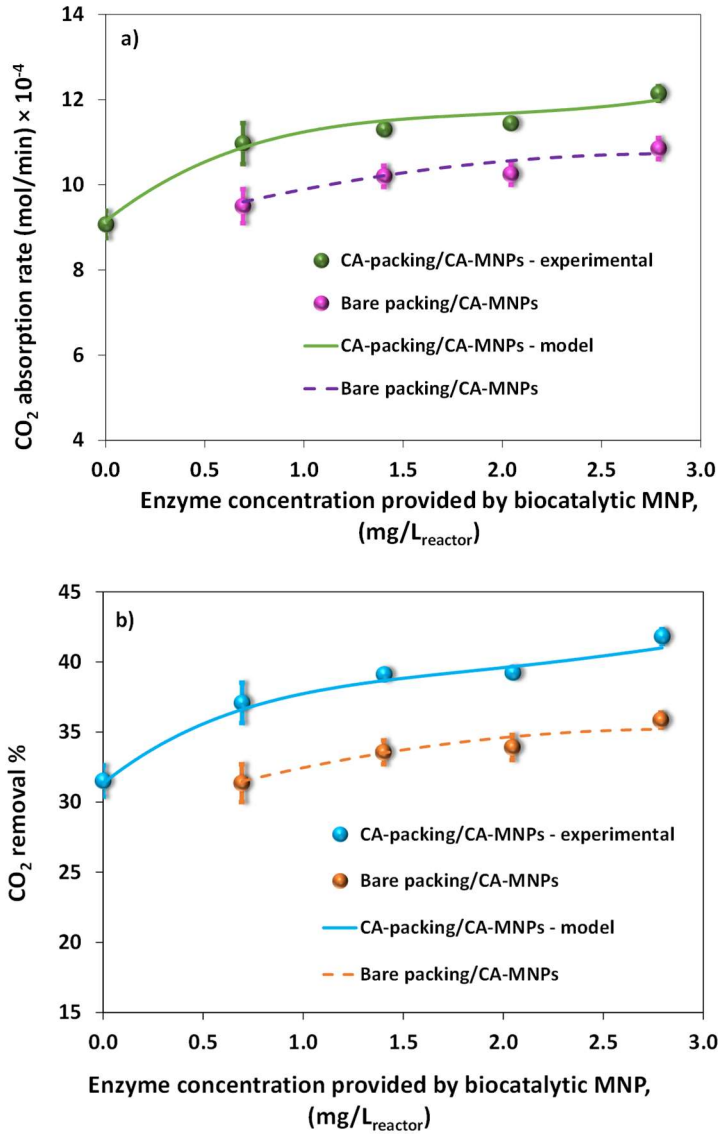

Figure 3.11. Impact of enzyme concentration (provided by the immobilization of the enzyme on MNPs surface) on packed-bed column bioreactor performance (enzyme concentration immobilized on packing surface = 9.2 mg/$L_{reactor}$, 100 mM Tris buffer, inlet gas CO_2 percentage: 15%, liquid flow rate: 135 ml/min, gas flow rate: 500 ml/min, and counter-current flow): a) CO_2 absorption rate; b) CO_2 removal.

In the next sections, the CO_2 hydration process performance of packed-bed column bioreactor with CA-packing/CA-MNPs systems will be compared with the conventional packed-bed column bioreactor (CA-packing system) in different operating conditions.

3.4.5.1. Impact of buffer type and concentration on the packed-bed column bioreactor performance

Figure 3.12 shows the performance of CO_2 hydration process in a counter-current packed-bed column bioreactor (CA-packing system and CA-packing/CA-MNPs system) using various buffers with different pK_{a2} constants (N-methylimidazole, Tris and AMPD, which possess pK_{a2} constants of 7.19, 8.07, 8.83). Buffer operates as a proton-transfer agent in the enzymatic CO_2 hydration process and is able to significantly improve the CO_2 hydration kinetics. Higher CO_2 absorption rate and CO_2 removal for both immobilized CA enzymatic systems (CA-packing system and CA-packing/CA-MNPs system) were achieved when working with buffer having larger pK_{a2} constant [11], specially when working with the CA-packing/CA-MNPs system. One possible reason would be that higher buffer pK_{a2} constant create greater driving force of the CO_2 hydration process [11, 196].

As revealed in **Figure 3.13**, CO_2 absorption rate and CO_2 removal increased sigificantly with the buffer concentration amplification (25-100 mM) for the both systems (CA-packing and CA-packing/CA-MNPs system). At larger buffer concentration, the inter-molecular proton transfer step improved which consequently intensified the CO_2 hydration process and CO_2 absorption rate [11, 19, 152]. Packed-bed column bioreactor performance was amended significantly (up to 25%) with CA enzyme immobilized on packing and MNPs surface (CA-packing/CA-MNPs system), especially at larger feed buffer concentrations. The figure shows the ability of the model to estimate the packed-bed performance at different values of buffer concentration.

Packed-bed column bioreactor with the CA enzyme on the packing and MNPs surface improves significantly the CO_2 hydration process, particularly at lower buffer pK_{a2} constant and at higher buffer concentrations.

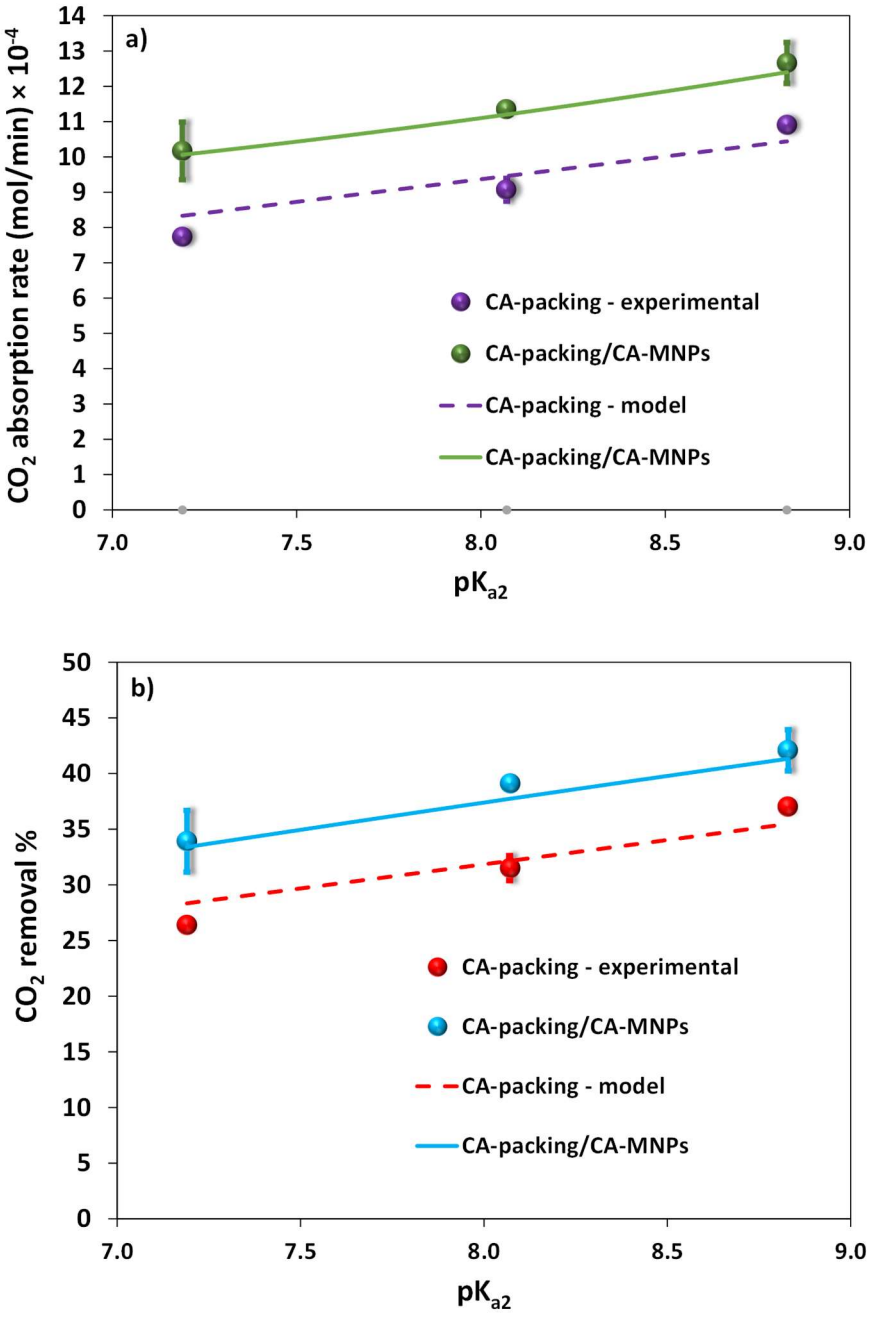

Figure 3.12. Impact of buffer type on packed-bed column bioreactor performance (enzyme concentration immobilized on packing surface = 9.2 mg/$L_{reactor}$, enzyme concentration immobilized on MNPs surface = 1.4 mg/$L_{reactor}$, 100 mM buffer, inlet gas CO_2 percentage: 15%, liquid flow rate: 135 ml/min, gas flow rate: 500 ml/min, and counter-current flow): a) CO_2 absorption rate; b) CO_2 removal.

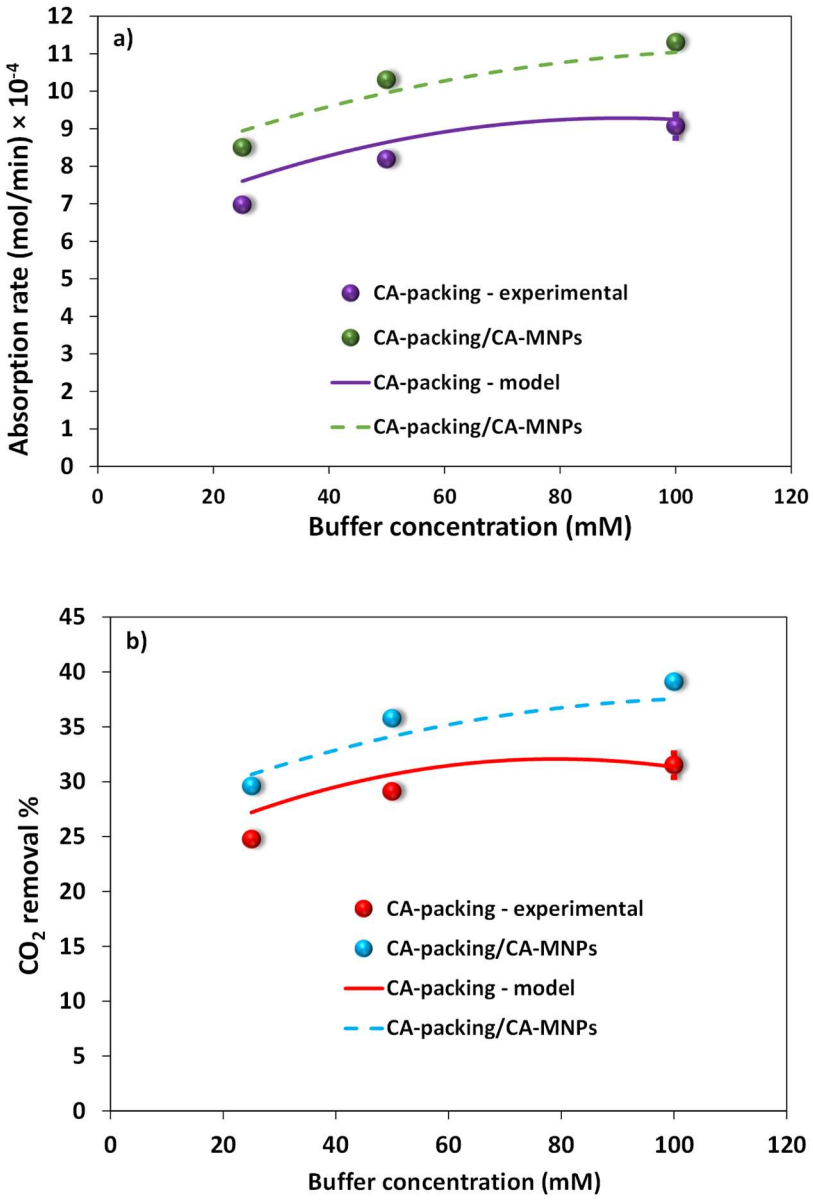

Figure 3.13. Impact of buffer concentration on packed-bed column bioreactor performance (enzyme concentration immobilized on packing surface = 9.2 mg/$L_{reactor}$, enzyme concentration immobilized on MNPs surface = 1.4 mg/$L_{reactor}$, Tris buffer, inlet gas CO_2 percentage: 15%, liquid flow rate: 135 ml/min, gas flow rate: 500 ml/min, and counter-current flow): a) CO_2 absorption rate; b) CO_2 removal.

3.4.5.2. Impact of operational parameters on packed-bed column bioreactor performance

Figure 3.14 depicts the impact of liquid flow rate (120-485 mL/min) on CO_2 absorption rate and CO_2 removal performance in a counter-current packed-bed column bioreactor with

immobilized CA enzyme on packing and MNPs surface. Larger liquid flow rate results in the growth of the CO_2 absorption rate and CO_2 removal for both systems (CA-packing system and CA-packing/CA-MNPs system), but particularly for the packed-bed column with immobilized CA enzyme on the packing and MNPs surface. CO_2 absorption rate and CO_2 removal approximately doubled with the increase of the liquid flow rate from 120 to 485 ml/min. The liquid film surrounding the enzyme diminishes at higher liquid flow rate, consequently the mass transfer resistance decreases, boosting the CO_2 absorption rate and CO_2 removal [219]. Moreover, more buffer is transferred at higher liquid flow rate, improving the inter-molecular transfer step of enzymatic CO_2 hydration, then recuperating of the CO_2 hydration performance [11].

The variation of CO_2 absorption rate and CO_2 removal is also illustrated in terms of liquid-to-gas flow ratio (L/G) in the packed-bed column bioreactor for both systems (CA-packing system and CA-packing/CA-MNPs system) (**Figure 3.15**), to help in any scale-up procedure in future works. Because of the higher gas-liquid interface area and liquid mass transfer coefficient, as well as the additional buffer solution provided per unit of gas, CO_2 absorption rate and CO_2 removal rise significantly with increasing L/G ratio for both enzymatic systems. All of these factors are more conducive to the overall capture efficiency [153, 220].
CO_2 hydration process performance (experimental and modeling) in the counter-current packed-bed column bioreactor with immobilized CA enzyme (CA-packing system and CA-packing/CA-MNPs system) as a function of the gas flow rate (370, 420 and 500 ml/min) is displayed in **Figure 3.16**. For both immobilized enzyme systems, the amplification of gas flow rate generates a larger gas-liquid mass transfer and, consequently, a slightly increase in the CO_2 absorption rate. This observation is in good agreement with other researcher's works [221-223]. Furthermore, CO_2 removal decayes significantly with the higher gas flow rate as a result of the gas residence time reduction, and therefore, shortening the gas−liquid contact time and the catalytic absorption time with immobilized CA [153].

The impact of inlet CO_2 concentration (10, 15 and 20%) on CO_2 absorption rate and CO_2 removal of the counter-current packed-bed column bioreactor with immobilized CA enzyme on packing surface and on both packing and MNPs surface is depicted in **Figure 3.17**. CO_2 absorption rate enhances with the amplification of inlet CO_2 concentration due to the higher

driving force in the gas phase. CO_2 uptake faces greater resistance to liquid and gas phase mass transfer as CO_2 concentrations increase, resulting in decreased CO_2 conversion [153].

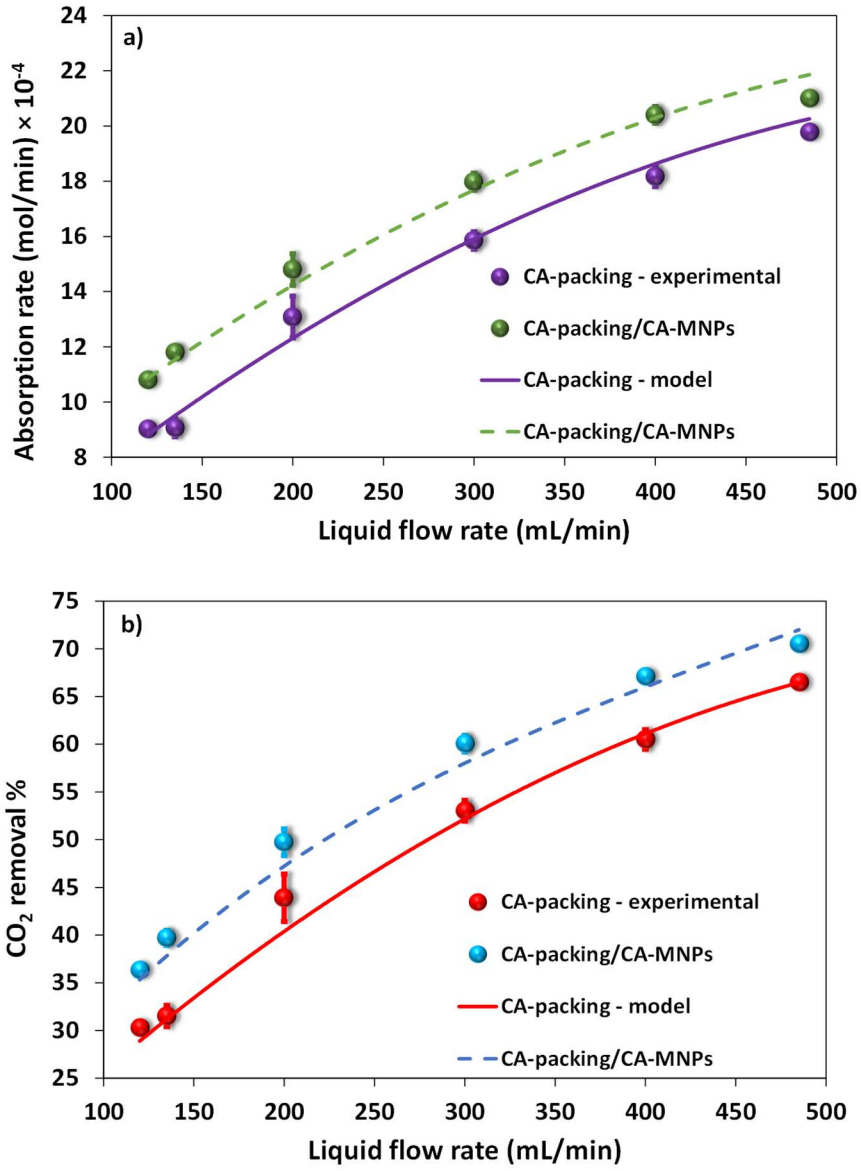

Figure 3.14. Impact of liquid flowrate on packed-bed column bioreactor performance (enzyme concentration immobilized on packing surface = 9.2 mg/$L_{reactor}$, enzyme concentration immobilized on MNPs surface = 1.4 mg/$L_{reactor}$, 100 mM Tris buffer, inlet gas CO_2 percentage: 15%, gas flow rate: 500 ml/min, and counter-current flow): a) CO_2 absorption rate; b) CO_2 removal.

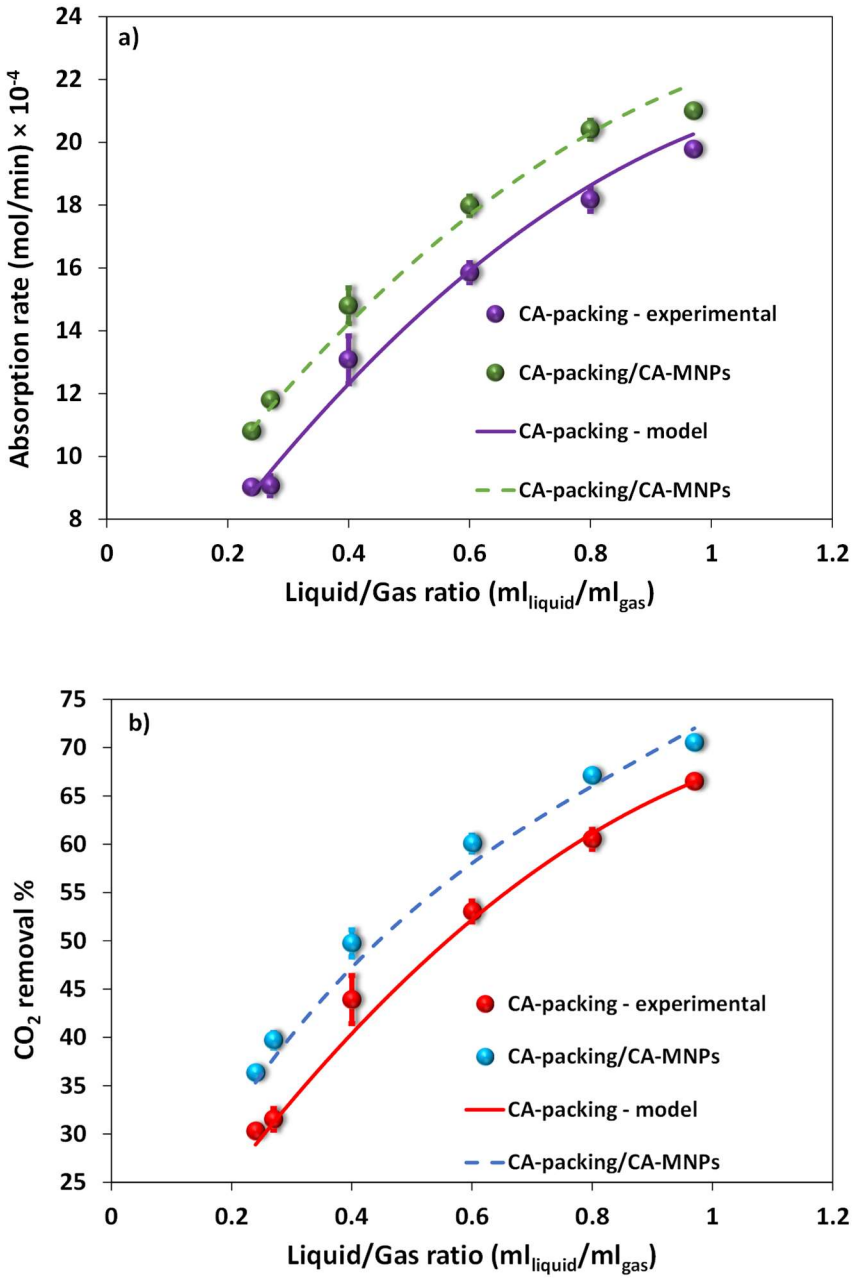

Figure 3.15. Impact of liquid/ gas ratio on packed-bed column bioreactor performance (enzyme concentration immobilized on packing surface = 9.2 mg/$L_{reactor}$, enzyme concentration immobilized on MNPs surface = 1.4 mg/$L_{reactor}$, 100 mM Tris buffer, inlet gas CO_2 percentage: 15%, gas flow rate: 500 ml/min, and counter-current flow): a) CO_2 absorption rate; b) CO_2 removal.

For the entire range of liquid flow rate, gas flow rate and inlet CO_2 concentration employed in our experiments, CO_2 absorption process was improved notably in packed-bed column

bioreactor with enzyme immobilized on packing and MNPs surface compared to the conventional packed-bed column bioreactor with enzyme immobilized on packing surface only, confirming the attracting features of the proposed hybrid system for green CO_2 capture.

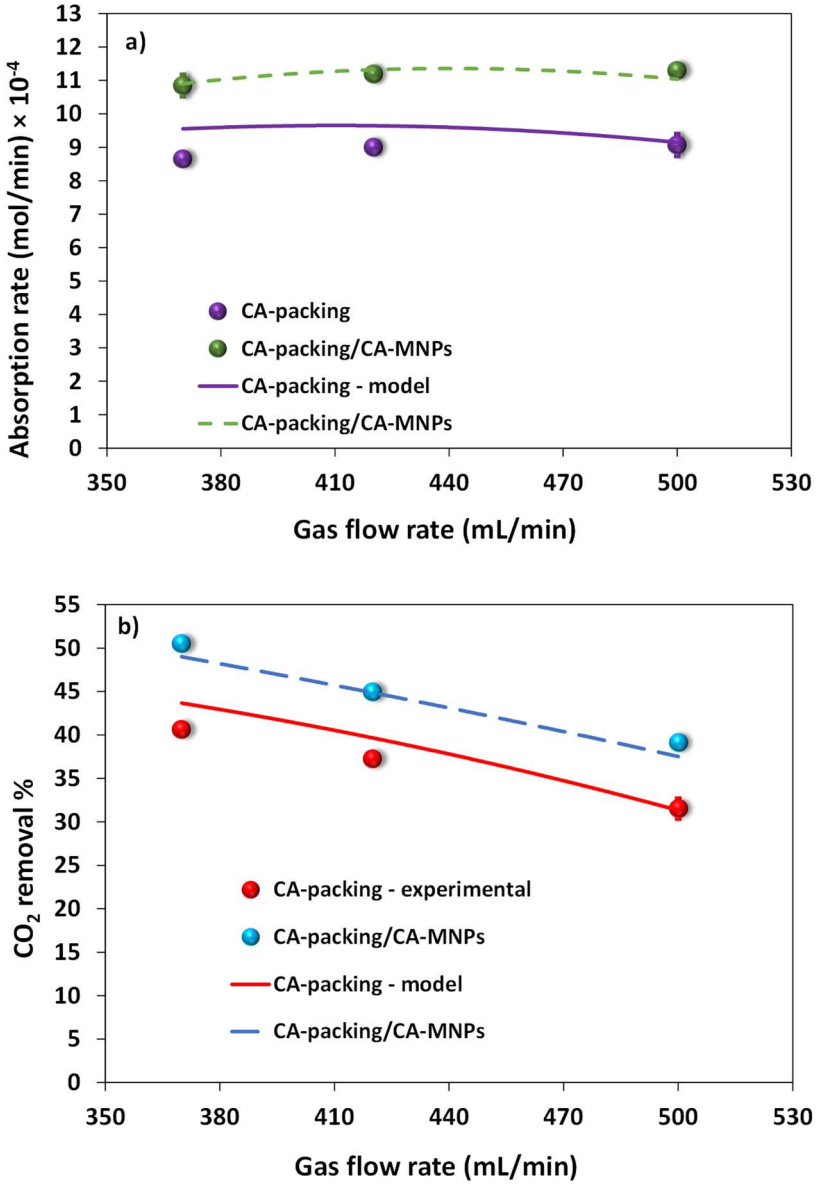

Figure 3.16. Impact of gas flowrate on packed-bed column bioreactor performance (enzyme concentration immobilized on packing surface = 9.2 mg/$L_{reactor}$, enzyme concentration immobilized on MNPs surface = 1.4 mg/$L_{reactor}$, 100 mM Tris buffer, inlet gas CO_2 percentage: 15%, liquid flow rate: 135 ml/min, and counter-current flow): a) CO_2 absorption rate; b) CO_2 removal.

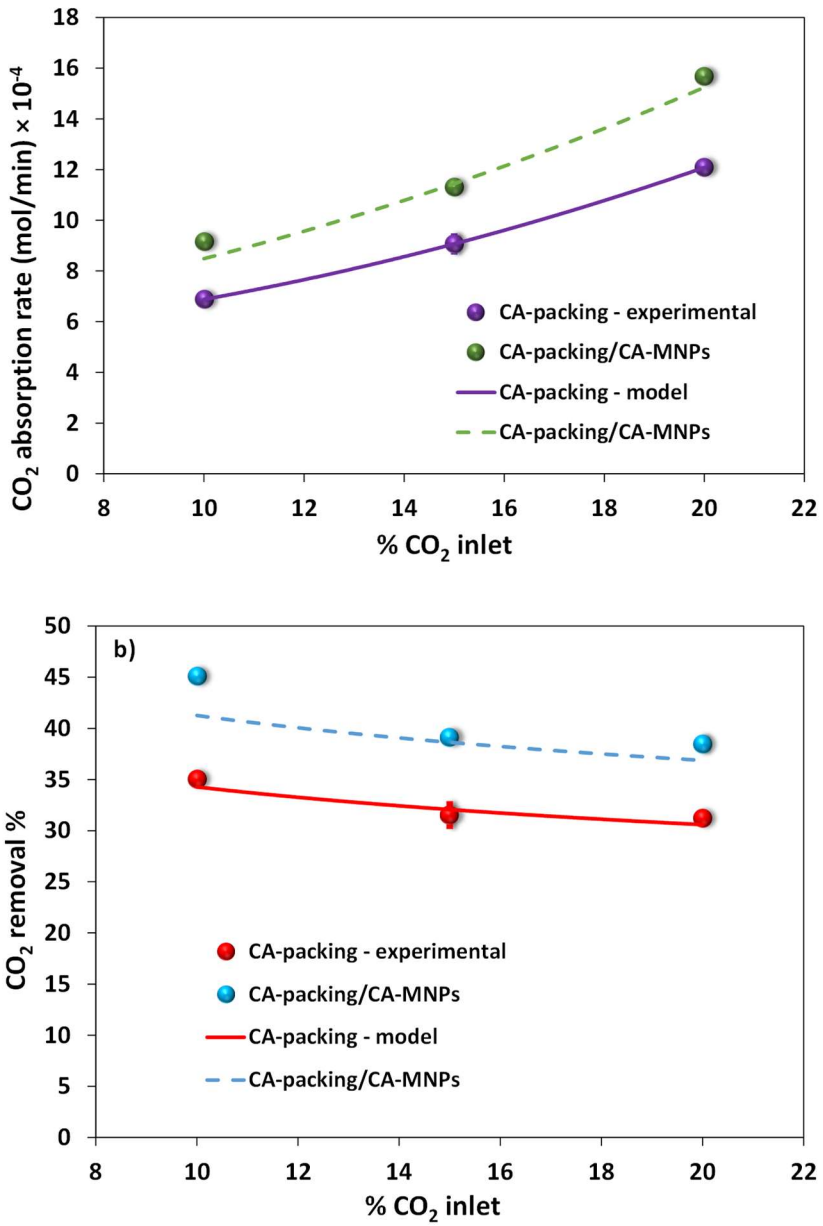

Figure 3.17. Impact of inlet gas CO_2 concentration on packed-bed column bioreactor performance (enzyme concentration immobilized on packing surface = 9.2 mg/$L_{reactor}$, enzyme concentration immobilized on MNPs surface = 1.4 mg/$L_{reactor}$, 100 mM Tris buffer, liquid flow rate: 135 ml/min, gas flow rate: 500 ml/min, and counter-current flow): a) CO_2 absorption rate; b) CO_2 removal.

3.4.5.3. Reusability of the enzyme in packed-bed column bioreactor

Operational cost is the key for the biocatalytic reactor, and in order to estimate them and reduce them to a minimum in industrial operation, it is necessary to evaluate the reusability

of the enzyme. The immobilization process potentially ameliorates the reusability of the enzyme and, for the first time, the reusability of immobilized CA for CO_2 hydration tests within a gas-liquid packed-bed column bioreactor has been studied. 10 cycles of CO_2 hydration test with the immobilized CA enzyme on packing and MNPs surface were conducted. **Figure 3.18** shows that CO_2 absorption rate in packed-bed column bioreactor is very stable, revealing a very good reusability of the enzyme which preserve its original CO_2 hydration performance. The results are in agreement with another research which studied the reusability of immobilized CA on nanoparticles in a hollow fiber membrane contactor [46].

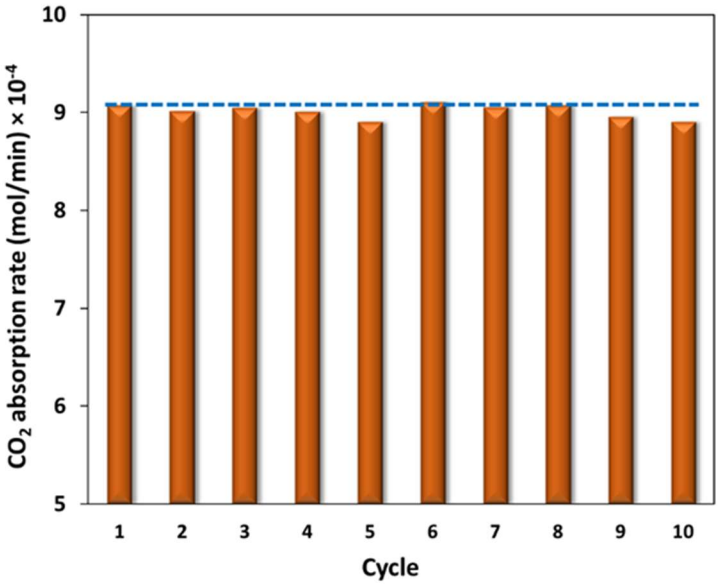

Figure 3.18. Reusability of the enzyme in packed-bed column bioreactor (enzyme concentration immobilized on packing surface = 9.2 mg/$L_{reactor}$, enzyme concentration immobilized on MNPs surface = 1.4 mg/$L_{reactor}$, 100 mM Tris buffer, liquid flow rate: 135 ml/min, gas flow rate: 500 ml/min, inlet gas CO_2 percentage: 15%, and counter-current flow).

3.5. Conclusion

Packed-bed column reactors with hCA II enzyme immobilized on the packing surface do not generate enough mass transfer to completely utilize the enzyme's high hydration turnover. To promote the mass transfer, an innovative enzymatic CO_2 hydration process was proposed here and consist of hCA II enzyme attached on the packing surface accompanied by hCA II enzyme immobilized on MNPs dispersed in the liquid phase. This work is the first

experimental study to highlight the influence of employment of additional immobilized CA enzyme on MNPs surface on the CO_2 hydration process in a packed-bed bioreactor. A 3-D model describing the hydrodynamics, mass transport/reaction in liquid/gas phases, accumulation of biocatalytic MNPs in packed bed, reaction and diffusion in enzyme washcoat/liquid film was used to investigate the behavior of the packed-bed column bioreactor.

Packing and MNPs surface were amine-functionalized by co-deposition of PDA/PEI and hCA II was immobilized on the modified surface via glutaraldehyde. Biocatalytic MNPs were developed through an optimized process involving various co-deposition and enzyme immobilization conditions. Immobilized CA on packing and MNPs demonstrated strong storage stability after 40 days of storage. Packed-bed column bioreactor with enzyme immobilized on packing and MNPs surface outperformed the packed-bed column bioreactor with enzyme immobilized only on packing surface since the additional amount of CA enzyme on MNPs behaves as a free solution-phase enzyme in the absorbent, augmenting the CO_2 absorption by catalysing the CO_2 hydration reaction instantly. CO_2 absorption process was considerably improved when hCA II loading on biocatalytic MNPs gradually increases. The impact of additional enzyme immobilized on the MNPs surface was more important at larger buffer concentration and lower buffer pK_{a2} constant. CO_2 absorption performance in packed-bed column bioreactor improved as liquid flow rate, liquid-to-gas (L/G) ratio, gas flow rate and CO_2 inlet composition were increased.

Thus, according to the results of this work, packed-bed column bioreactor with immobilized CA enzyme on the packing and MNPs surface is an encouraging green CO_2 capture technology design, which improve the utilization of CA enzyme large turnover number. This immobilized enzyme system provides a reasonable CO_2 conversion, even when a component of the enzymatic system (CA-packing system or CA-MNPs system) does not work at optimal parameters and avoids the decline of the CO_2 absorption because of the contraction of enzyme activity in time.

Based on the literature review, there are very few studies on CO_2 absorption with immobilized CA enzymes. Membrane contactors, on the other hand, have received little attention in the literature despite the fact that they are promising technology with several advantages. The next chapter concerns the first study on the integration of biocatalytic membrane in a flat-sheet membrane contactor to evaluate the CO_2 absorption performance. Comprehensive studies are conducted to develop an efficient biocatalytic membrane and then the impact of different parameters on CO_2 absorption rate is evaluated.

Chapter 4: Enzyme-immobilized flat-sheet membrane contactor for green carbon capture

Résumé

Les contacteurs à membrane (MC) représentent un système attrayant pour la capture du CO_2 en raison de l'amélioration du transfert de masse et des interfaces gaz-liquide, de leur modularité et de leur compacité. Un nouveau MC gaz-liquide à membrane plane biocatalytique a été développé. La membrane biocatalytique a été préparée par codépôt de polydopamine (PDA)/polyéthylèneimine (PEI) et liaison covalente de l'anhydrase carbonique (AC) sur une membrane plane en polypropylène (PP), en utilisant différentes conditions d'immobilisation. L'activité la plus élevée a été obtenue pour les conditions suivantes du processus d'immobilisation : temps de dépôt de 7 h, rapport PDA/PEI = 2/2, 1,0 (v/v)% de glutaraldéhyde, 0,8 mg/ml de solution d'enzyme, temps d'immobilisation de 32 h et un pH de 6,0. La membrane biocatalytique a montré une bonne stabilité de stockage après 40 jours. Les performances de la MC ont été étudiées dans diverses conditions, notamment le type/concentration de tampon, le débit du liquide, la température et les conditions de fonctionnement à contre-courant/co-courant. Un flux d'absorption de CO_2 de $0{,}29\times10^{-3}$ mol/m^2s a été obtenu lorsque la membrane biocatalytique a été intégrée dans un MC à membrane plane, en utilisant de l'eau en présence de 100 mM de Tris. L'absorption dans le MC a également été examinée pendant plusieurs heures afin de vérifier le potentiel du nouveau bioréacteur pour les applications industrielles. Un modèle multi-échelle (considérant la structure poreuse de la membrane remplie de gaz ou partiellement remplie de liquide et l'enzyme immobilisée à la surface de la membrane et à l'intérieur des pores) a été développé pour étudier le comportement du MC. Dans l'ensemble, l'utilisation d'une membrane biocatalytique dans le MC à membrane plane est une approche nouvelle, verte et respectueuse de l'environnement permettant la capture du CO_2 dans l'eau (en présence d'un tampon) comme absorbant.

Abstract

Membrane contactors (MC) represent an attracting system for CO_2 capture due to the enhanced mass transfer and gas–liquid interfaces, modularity, and compactness. A novel gas-liquid MC with biocatalytic flat sheet membrane was developed. The biocatalytic membrane was prepared via co-deposition of polydopamine (PDA)/ polyethyleneimine (PEI) and covalent bonding of carbonic anhydrase (CA) on polypropylene (PP) flat sheet membrane, using different deposition and enzyme immobilization conditions. The highest CA activity was achieved for 7 h deposition time, PDA/PEI ratio = 2/2, 1.0 (v/v)% glutaraldehyde, 0.8 mg/ml CA solution, 32 h immobilization time, and pH 6.0 in the immobilization process. The biocatalytic membrane showed good storage stability after 40-day. The MC performance was investigated under various conditions, including buffer type/concentration, liquid flow rate, temperature, and counter-current/co-current operating conditions. A CO_2 absorption flux of 0.29×10^{-3} mol/m^{2}s was obtained when the biocatalytic membrane was integrated into a flat sheet MC and 100 mM Tris in water was used in the absorption process. The absorption rate stability of the biocatalytic MC was also examined for several hours to verify the potential of the new flat sheet bioreactor in industrial applications. A multiscale model (with gas-filled or partially liquid-filled membrane porous structure and enzyme attached on the surface of the membrane and inside the pores) was developed to investigate the behaviour of the MC. Overall, the employment of biocatalytic membrane in flat sheet MC is a novel, green, and environmentally friendly approach allowing CO_2 capture with water (in presence of buffer) as absorbent.

4.1. Introduction

Carbon capture and storage (CCS) is a recent technology enabling CO_2 (major greenhouse gas) to be captured, transported and stored by geological storage or under the ocean [3]. While the CO_2 capture with amine-based absorbents is still considered the most prevalent method, due to negative features of amine-based solvents like substantial energy and electricity consumption, toxicity, degradation products and corrosivity, there is a growing interest in using benign absorbents. Enzymatic capture using carbonic anhydrase (CA) has been introduced in the last decades to promote the absorption rate of benign solvents such as water [7, 8, 25]. This natural enzyme catalyst converts CO_2 into bicarbonate with a high turnover rate (k_{cat}) which varies between 10^4 and 10^6 $molecule_{CO_2} / (molecule_{CA} \cdot s)$ and a specificity constant (k_{cat}/K_m) of about 10^8 M^{-1} s^{-1} [19, 25]. In addition, non-toxicity, biodegradability, and the ability to operate in moderate conditions are other advantages of CA [35].

Different enzymatic CO_2 capture reactors using CA have been developed over the last years such as packed columns [12], bubble columns [14], spray towers [15], integrated vacuum carbonate absorption process (IVCAP) reactors [17] and membrane-based reactors [18]. Although conventional packed-bed columns are mature and efficient for carbon capture, they still face some major drawbacks such as large footprint, low operational flexibility and high operating and energy costs [179]. Membrane technology is a promising technique that offers a reduction in size, while being easy in operation and modularity [6, 20]. Combination of an absorption system with the membrane technology via the membrane contactor (MC) allows to get the benefits of both systems: high selectivity of the absorption process and operational flexibility, small footprint, facility in scaling up and operating and capital costs reduction of membrane technology [8, 23]. Enzymatic CO_2 capture in MC using CA is an appealing combination for capturing CO_2 from stationary emission sources: it merges the utilization of water (in presence of a buffer) as a green and environmentally friendly absorbent, with CA as a non-toxic, biodegradable and an efficient catalyst in CO_2 hydration [19].

Utilization of free enzyme in solution is not favorable because of the significant amount of enzyme required in the process and enzyme denaturation which causes the decrease of CO_2 hydration activities over time. Enzyme immobilization on solid surface is an attractive

modification which increases the enzyme stability and life span and provides the ability to reuse the enzyme in various cyclic operations [19, 38, 39]. The immobilization also provides flexibility in the reactor design and prevent the biocatalyst contamination during the CO_2 separation [11, 25, 37, 44, 45, 51]. Immobilization by covalent bonding provides a strong binding between the enzyme and functional groups of the support; the possibility of leakage is small, and the enzyme achieves high stability [58, 71, 96]. Because polymeric membranes (as immobilization support) offer good mechanical stability, availability, and relatively low cost [85], most MC use hydrophobic materials like polytetrafluoroethylene (PTFE), polypropylene (PP), and polyvinylidene fluoride (PVDF). However, their inert surface requires a functionalization to bring the reactive functional groups on the polymer surface for the covalent enzyme immobilization [119]. Although the plasma treatment is a widely used method for surface modification of polymers, the process requires complex equipment [120]. Deposition or coating of polyelectrolyte layers on polymer surface is a simple and low-cost method of functionalization [124]. As a powerful molecule for spontaneous deposition on organic and inorganic materials, dopamine (DA) can form a strong adhesive polydopamine (PDA) layer with auto-oxidative self-polymerization on various surfaces in aerobic and weak alkaline solution conditions (pH~ 8.5) [126-128, 130]. PDA possesses abundant functional groups such as catechol, amine, and imine groups that can be used for further chemical bonding and the cross-linked structure of PDA provides the adhesion property [131, 132, 224]. Using polyethyleneimine (PEI) in the co-deposition method (combination of DA and PEI) could prevent the self-aggregation of PDA and non-covalent interactions in PDA, thus providing a homogeneous polymerization and deposition of dopamine [133, 134, 136]. Moreover, the three-dimensional PEI polymer's abundant binding sites offer an improvement in the enzyme loading [135]. Because the co-deposition of PDA/PEI provides abundant amine functionalities on the polymeric surface, CA can further be immobilized covalently on the amine functionalized surface with glutaraldehyde as cross-linker.

There are very few studies on CO_2 absorption in membrane contactors with immobilized enzymes (all the works were almost published at the same time). Hou et al. [46] used a benign solvent (pure water with 0.1 M sodium phosphate buffer solution) and TiO_2 nanoparticles with covalently immobilized CA suspended in the solvent. To facilitate the mass transfer and

locate the immobilized enzyme near the gas-liquid interface, Janus membrane was developed with special layers: a hydrophilic layer providing enzyme immobilization and a hydrophobic layer protecting membrane from wetting [183]. However, Janus membranes have an intricate fabrication process which limit wider application. Yong et al. [70] proposed the immobilization of CA on the shell side of porous PP hollow fiber membrane surface through the layer by layer (LBL) electrostatic adsorption method. Experimental results showed that CO_2 absorption rate into the 30 wt% K_2CO_3 tripled when CA was immobilized on the PP membrane surface compared to unmodified membrane. However, there is always unreliability about adsorption processes due to its reversibility and leaching. The stability and reusability of immobilized enzyme on the PP membranes have not been reported. Iliuta and Iliuta [19] proposed the utilization of membranes as immobilization supports of CA and investigated the CO_2 absorption performance in a gas-liquid hollow fiber MC (HFMC) via simulation using immobilized CA enzyme on the lumen side of membranes. According to this research, the hollow fiber membrane bioreactor is a promising candidate for the CO_2 capture process. Indeed, the mass transfer resistance in the wetted membrane pores can be reduced via CO_2 hydration catalyzed by the CA immobilized inside the pores.

Taking into account our previous promising results [19], a novel gas-liquid MC with biocatalytic flat sheet membrane for CO_2 capture was developed in the present work. Flat sheet membrane contactors (FSMC) are a potential alternative in CO_2 separation because of the simplicity in (i) membrane fabrication and characterization, (ii) module assembly, and (iii) scale-up, as well as the higher absorption flux for comparable gas–liquid contact area [225-227]. PP was considered the appropriate material for the membrane with water as absorbent solution [24, 172] because water has high surface tension and high compatibility with polymeric membranes and there is no need to employ materials with high resistance against chemicals and wetting [25, 178]. PP flat sheet membranes were modified via co-deposition of PDA/PEI and subsequently, CA covalently immobilized on the membrane surface using glutaraldehyde. Comprehensive investigations were carried out to discern the optimum conditions for biocatalytic membrane preparation and to study the stability of the immobilized enzyme. CO_2 absorption performance in the biocatalytic FSMC under several conditions and the impact of buffer type and concentration, liquid flow rate, liquid temperature and flow orientation were investigated. Also, the absorption rate stability was

examined for several hours to verify the potential of this bioreactor in industrial applications. A multiscale model, with gas-filled or partially liquid-filled membrane porous structure and enzyme immobilized on the membrane surface and within the membrane pores, was developed to investigate the behaviour of the membrane bioreactor. This study aims to demonstrate that the FSMC with biocatalytic membranes could be an appealing alternative to the traditional membrane contactors with amine-based absorbents.

4.2. Experimental

4.2.1.1. Materials and chemicals

PP flat sheet membranes were provided by Membrana (North Carolina, USA). Membrane characteristics are reported in **Table 4.1**. hCA II enzyme (molecular weight of approximately 29 200 Da) was produced and purified in our biotechnology laboratory. Dopamine hydrochloride (≥ 98%, CAS no. 62-31-7) and p-nitrophenyl acetate (p-NPA; ≥ 98%, CAS no. 830-03-5) were purchased from Sigma-Aldrich. Glutaraldehyde (25 wt% solution in water) and PEI (MW = 600 Da; ≥ 99%) were supplied from Thermo Fischer Scientific and Tris Base was acquired from Fischer Bio Reagents. Bradford Protein Assay Kit containing Bradford reagent and bovine serum albumin (BSA) standard protein was purchased from Bio Basic Inc. N-methylimidazole (≥ 99%) was supplied by Alfa Aesar. The gases (CO_2 and N_2) were of commercial grade with a minimum purity of 99.9% (Praxair, Canada).

Table 4.1. Flat sheet membrane and module specifications.

Parameters	PP membrane	Module/1 membrane
Thickness (µm)	100	-
Pore diameter (µm)	0.1	-
Porosity	0.8	-
Length (m)	-	0.059
Width (m)	-	0.070
Gas-liquid contact area (m^2)	-	0.0041

4.2.1.2. Membrane surface modification

For amine-functionalization, the membrane surface was modified using co-deposition of PDA as cross-linked component due to its excellent adhesive characteristic to attach PEI to

the polymeric surface. The dopamine hydrochloride and PEI (in different PDA/PEI ratios: 0/2, 1/2, 2/2, 2/1 and 2/0 $mg.ml^{-1}$/ $mg.ml^{-1}$) were dissolved in a Tris/HCl solution (pH = 8.5, 50 mM). The PP membranes were soaked in the PDA/PEI solution at room temperature (under shaking for 3, 5, 7, 9, and 11 h). Thereafter, the membranes were rinsed with DI water and dried for 24 h at room temperature. This surface modification provided the amine functionalities on the membrane surface required in the subsequent steps. The PDA/PEI coated PP membrane will be referred to as P-PP.

4.2.2. Enzyme immobilization

The schematic illustration of the biocatalytic membranes preparation is shown in **Figure 4.1**.

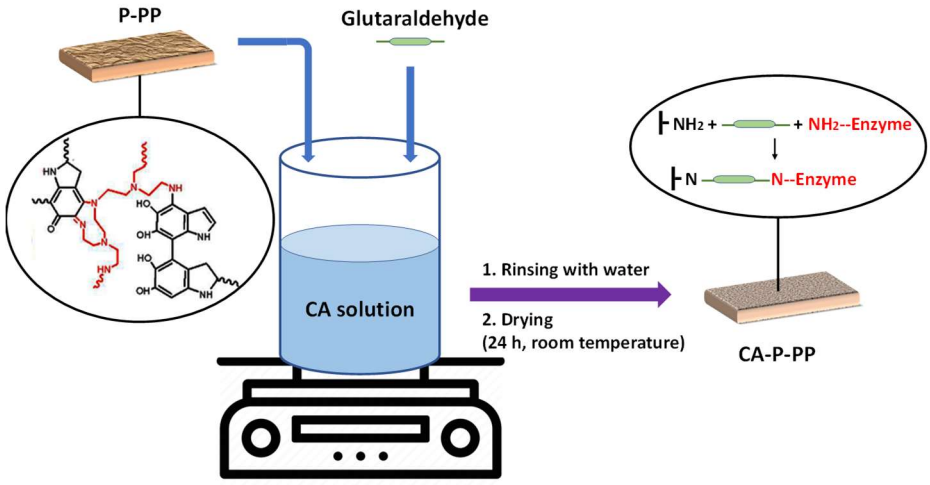

Figure 4.1. Illustration of the development of biocatalytic membranes.

The amine-functionalized PDA/PEI membranes (P-PP) (section S1) were immersed in CA solution (with various enzyme concentrations: 0.1, 0.2, 0.6, 0.8, 1.0 and 1.2 mg/ml) for enzyme immobilization via glutaraldehyde. Glutaraldehyde was dissolved in this solution to reach a concentration of 0.1, 1.0, 2.0 or 4.0 %(v/v) and the mixture was then shaken for a certain time at room temperature. After immobilization, the membranes were rinsed with DI water and dried for 24 h at room temperature. The membrane with immobilized CA will be referred to as CA-P-PP.

4.2.2.1. Bradford test

The immobilized enzymes were quantified by indirect protein assay (the enzyme

concentration in the residual solution after immobilization and the enzyme concentration in the washing water were subtracted from the initial enzyme concentration). The enzyme concentration was measured via colorimetric method (Bradford test) using Coomassie blue dye. Determination of the absorbance of the solution at 595 nm defined the amount of protein existing in the solution. A small amount of sample was mixed with the assay Bradford reagent and incubated briefly before measuring the absorbance at 595 nm. The protein concentration was determined by reference to the absorbance of standard protein dilutions (analyzed together with the unknown samples). Bovine serum albumin (BSA) was used as standard [7]. The results of this test determined the amount of immobilized enzyme loading on membrane surface. The enzyme loading efficiency was evaluated with Equation (4.1):

$$enzyme\ loading\ efficiency\ (\%) = \frac{loaded\ enzyme\ on\ surface\ (\mu g)}{total\ amount\ of\ enzyme\ (\mu g)} \times 100 \qquad (4.1)$$

4.2.2.2. Esterase activity test

To quantify the CA activity as a function of the capability of Zn^{2+} ion for the hydrolysis of p-NPA, the rate of hydrolysis was measured in the presence of CA. Esterase activity was performed spectrophotometrically at room temperature at a wavelength of 400 nm. The catalytic activity was measured for both free and immobilized CA.

For free CA, the activity test was performed in an agitated cell with 3.5 ml Tris/HCl buffer solution (50 mM, pH = 8), 0.4 ml acetonitrile containing p-NPA (3 mM), and 0.1 ml free CA solution. A blank experiment was also done in the absence of CA (which was replaced with pure water), to eliminate the effect of p-NPA self-hydrolysis. For immobilized CA enzyme, the activity test was performed for a membrane with immobilized enzyme on a known surface under the same experimental conditions. 1 ml of reaction mixture was taken every minute to determine the absorbance rate (abs/min). After each measurement, the sample was returned to the cell [7]. The enzyme activity efficiency was calculated with Equation (4.2):

$$enzyme\ activity\ efficiency\ (\%) = \frac{immobilized\ enzyme\ activity\ on\ surface}{initial\ \ free\ enzyme\ activity\ in\ solution} \times 100 \qquad (4.2)$$

4.2.2.3. Membrane characterization

The optical contact angle analyzer (OCA 15 Plus) was used to measure the contact angle of the biocatalytic membranes based on the sessile drop method. The breakthrough pressure was

measured based on the Laplace-Young equation [178]. The specific surface area was measured using the Micromeritics Gemini VII Analyzer.

The surface morphology was evaluated with a Scanning Electron Microscope (SEM; Inspect F50 from FEI). An Energy Dispersive Spectrometer (EDS; Octane Super-A from Edax Ametek) was employed to characterize the elemental composition of the membrane. The surface functional groups were analyzed by a Fourier transform infrared spectroscope (FTIR; MB3000 from ABB) over a scan range of 600–4000 cm^{-1}.

4.2.2.4. k_{cat}/K_m evaluation for free and immobilized CA

The k_{cat}/K_m values of free and immobilized CA were determined by measuring the CA activity at different substrate concentrations (p-NPA as the substrate). k_{cat}/K_m values were then calculated using the Michaelis–Menten and Lineweaver–Burk equations.

4.2.3. Long-term stability of immobilized CA

The stability of free enzyme and biocatalytic membrane (immobilized enzyme) was tested for 40 days. For this purpose, they were added in Tris buffer solution (pH 7) at 25 °C and their relative activities were measured periodically based on the esterase activity test (section S1) [48, 51].

4.2.4. CO_2 absorption performance of biocatalytic membranes

The schematic experimental setup for CO_2 absorption in FSMC is illustrated in **Figure 4.2**. Gas-liquid contact area per flat sheet membrane is approximately 0.0041 m^2. The gas streams (flow and composition) were controlled using mass flow controllers. The CO_2 concentration in the outlet gas flow was measured with an IR CO_2 analyzer. A gear pump and a rotameter were used to control and measure the flow rate of the liquid (water in presence of a buffer (Tris; 100 mM, pK_{a2} = 8.07 [7, 19])). The liquid outlet pressure was kept slightly above the gas pressure by using a needle valve. Measurements were performed with fluids (gas and liquid) circulating counter-currently or co-currently. Around 20 - 30 minutes were necessary for the system to reach the steady-state condition. The liquid and gas flow rates (unless otherwise specified) were 26 ml/min and 100 ml/min, respectively, with a volumetric fraction of 15% CO_2 in the inlet gas.

The CO_2 absorption rate (mol/min) was determined as follows:

$$CO_2\ absorption\ rate = Q_{inlet} y_{CO_2,inlet} - Q_{outlet} y_{CO_2,outlet} \quad (4.3)$$

where Q_{inlet} and Q_{outlet} are the inlet and outlet gas molar flow rates (mol/min), respectively and were calculated based on the gas volumetric flow rate (ml/min) and gas concentration (mol/ml). Gas concentrations were calculated via gas pressure and temperature. $y_{CO_2,inlet}$ and $y_{CO_2,outlet}$ are CO_2 mole fractions at the gas inlet and outlet, respectively.

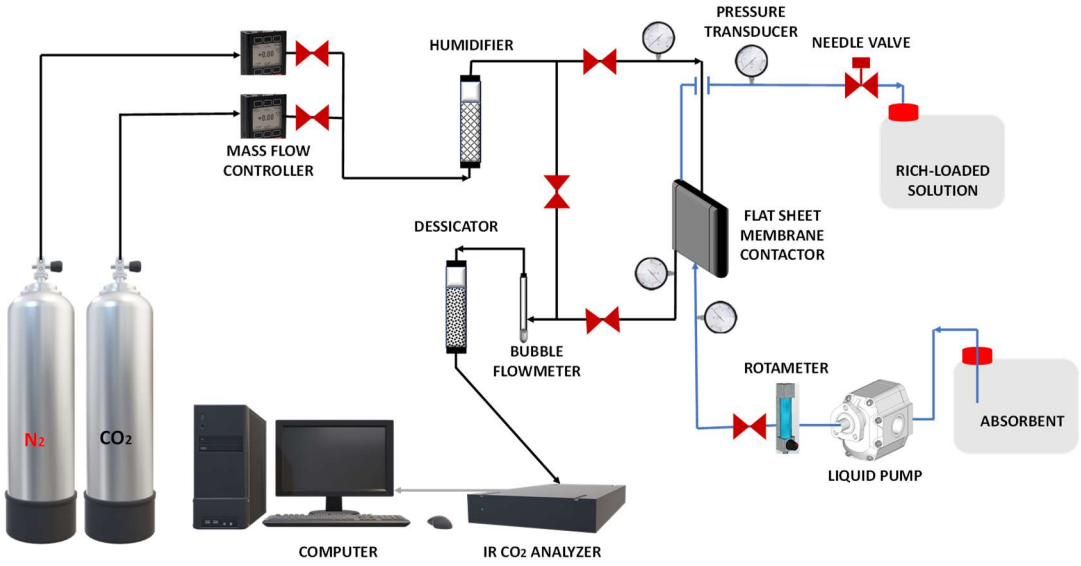

Figure 4.2. FSMC setup.

4.3. Mathematical model of membrane contactor

When CA enzyme is immobilized on the membrane surface and the pores are partially filled with liquid, the enzymatic membrane reactor model involves (i) CO_2 diffusion in the dry membrane zone and (ii) CO_2 diffusion and uncatalyzed CO_2 hydration in the wetted zone. When the enzyme is additionally immobilized inside the pores, the mathematical model involves (i) CO_2 diffusion in the dry zone and (ii) CO_2 diffusion and uncatalyzed/catalyzed CO_2 hydration in the wetted zone (**Figure 4.3**). The mathematical model describes only CO_2 diffusion into the membrane porous structure when the pores are completely filled with gas. In addition, two-dimensional mass transport equations, which includes the enzymatic reaction at the wall, were considered for the liquid phase within the FSMC.

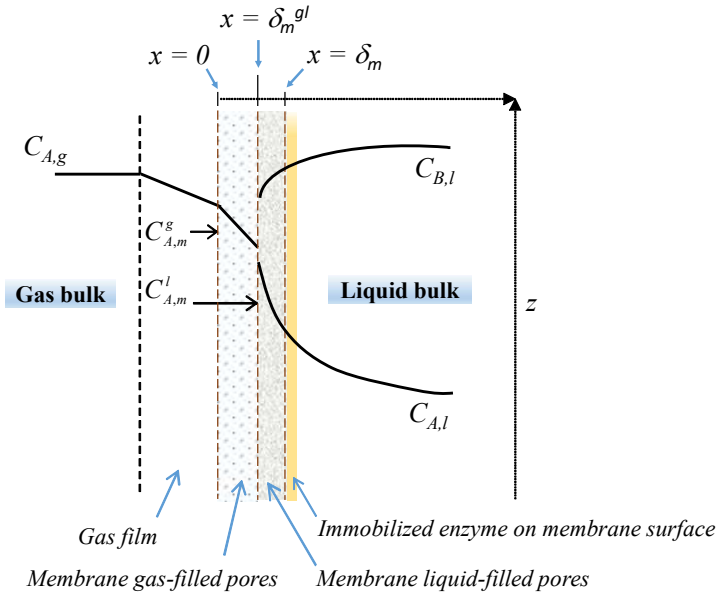

Figure 4.3. Schematic diagram of CO_2 absorption in FSMC (immobilized enzyme on membrane surface and inside the pores) - membrane partially liquid-filled pores.

4.3.1. Enzymatic CO_2 hydration mechanism and kinetics

Enzymatic CO_2 hydration kinetics were described via the pseudo random Quad Quad Iso Ping Pong (prQQIPP) mechanism with one transient complex, rapid solvation in the enzyme binding cavity and competitive inter-molecular proton transfer with respect to buffer (B):

$$CO_2 + ZnOH^-(E) \underset{k_{-1}}{\overset{k_1}{\rightleftharpoons}} ZnHCO_3^-(ES) \tag{4.4}$$

$$H_2O + ZnHCO_3^-(ES) \underset{k_{-2}}{\overset{k_2}{\rightleftharpoons}} HCO_3^- + ZnH_2O(E_W) \tag{4.5}$$

$$E_W \underset{k_{-3}}{\overset{k_3}{\rightleftharpoons}} {}_H E \tag{4.6}$$

$$B + ZnH_2O({}_H E) \underset{k_{-4}}{\overset{k_4}{\rightleftharpoons}} BH^+ + ZnOH^-(E) \tag{4.7}$$

$$HCO_3^- + ZnH_2O({}_H E) \underset{k_{-5}}{\overset{k_5}{\rightleftharpoons}} CO_2 + H_2O + ZnOH^-(E) \tag{4.8}$$

The enzymatic reaction rate corresponding to prQQIPP mechanism is:

$$R^{e}_{CO_2} = \frac{k_h\left(C_{CO_2}C_B - \frac{K_{a2}}{K_{a1}}C_{HCO_3^-}C_{BH^+}\right)\left(1+\frac{C_{HCO_3^-}}{K_{iHCO_3^-,3}}\right)C_{E0}}{\left[\begin{array}{l} K_BC_{CO_2} + K_{CO_2}C_B + \frac{K_B}{2}\frac{K_E}{K_{a1}}C_{HCO_3^-} + 2K_{CO_2}\frac{K_{a2}}{K_E}C_{BH^+} + C_{CO_2}C_B + 2\frac{K_{CO_2}}{K_{HCO_3^-}}\frac{K_{a2}}{K_E}C_{HCO_3^-}C_{BH^+} + \frac{K_B}{K_{iHCO_3^-,1}}C_{CO_2}C_{HCO_3^-} \\ + \frac{K_{CO_2}}{K_{iHCO_3^-,2}}C_BC_{HCO_3^-} + \frac{1}{2}\frac{K_B}{K_{iHCO_3^-,3}}\frac{K_E}{K_{a1}}\left(C_{HCO_3^-}\right)^2 + \frac{K_B}{K_{iHCO_3^-,1}K_{iHCO_3^-,4}}C_{CO_2}\left(C_{HCO_3^-}\right)^2 + \frac{1}{K_{iHCO_3^-,5}}C_{CO_2}C_BC_{HCO_3^-} \end{array}\right]} \tag{4.9}$$

The kinetic parameters were assessed in the conditions of immobilized enzyme in an intensified microreactor [7].

4.3.2. Mechanism and kinetics of the uncatalyzed CO_2 hydration

The kinetics of uncatalyzed CO_2 hydration were expressed via the following mechanism [209]:

$$H_2O + CO_2 \underset{k_{13}}{\overset{k_{31}}{\rightleftharpoons}} H^+ + HCO_3^- \tag{4.10}$$

$$H^+ + HCO_3^- \underset{k_{21}}{\overset{k_{12}}{\rightleftharpoons}} H_2CO_3 \tag{4.11}$$

$$H_2O + CO_2 \underset{k_{23}}{\overset{k_{32}}{\rightleftharpoons}} H_2CO_3 \tag{4.12}$$

The reaction rate is:

$$R^{uc}_{CO_2} = k^{'}_{31}C_{CO_2} - k^{'}_{13}C_{H^+}C_{HCO_3^-} \qquad \text{where } k^{'}_{31} = k_{31} + k_{32} \text{ and } k^{'}_{13} = k_{13} + k_{23}/K_{H_2CO_3} \tag{4.13}$$

The rate constants at 25°C are: $k^{'}_{31} = 0.037\text{s}^{-1}$ and $k^{'}_{13} = 5.5\times10^4\,\text{m}^3/kmol\ s$ [209].

4.3.3. Porous membrane scale model

When CA is attached to the membrane surface and the pores are partially filled with liquid, the membrane scale model expresses (i) the diffusion of CO_2 in the dry membrane zone and (ii) the CO_2 diffusion & uncatalyzed hydration in the wetted zone. The mass balance equations for CO_2 in the membrane dry/wetted zones are given by:

$$D^{eff}_{CO_2,g}\frac{\partial^2 C^{g}_{CO_2,m}}{\partial x^2} = 0 \tag{4.14}$$

$$D^{eff}_{CO_2,\ell}\frac{\partial^2 C^{\ell}_{CO_2,m}}{\partial x^2} - R^{uc}_{CO_2} = 0 \tag{4.15}$$

The matching boundary conditions are ($\delta_m^{g\ell}$ is located inside the membrane):

$$x = 0 \qquad k_g\left(C_{CO_2,g} - C^g_{CO_2,m}\Big|_{x=0}\right) = -D^{eff}_{CO_2,g}\left.\frac{\partial C^g_{CO_2,m}}{\partial x}\right|_{x=0} \tag{4.16}$$

$$x = \delta_m^{g\ell} \qquad D^{eff}_{CO_2,g}\left.\frac{\partial C^g_{CO_2,m}}{\partial x}\right|_{x=\delta_m^{g\ell}} = D^{eff}_{CO_2,\ell}\left.\frac{\partial C^\ell_{CO_2,m}}{\partial x}\right|_{x=\delta_m^{g\ell}} \tag{4.17}$$

$$C^g_{CO_2,m}\Big|_{x=\delta_m^{g\ell}} = C^\ell_{CO_2,m}\Big|_{x=\delta_m^{g\ell}}\frac{1}{m} \tag{4.18}$$

$$x = \delta_m \qquad -D^{eff}_{CO_2,\ell}\left.\frac{\partial C^\ell_{CO_2,m}}{\partial x}\right|_{x=\delta_m} = D_x\left.\frac{\partial C_{CO_2,\ell}}{\partial x}\right|_{x=\delta_m} \tag{4.19}$$

In addition, the steady-state mass balance equations for HCO_3^-, B, and BH^+ in the wetted membrane zone are considered:

$$D^{eff}_{HCO_3^-,\ell}\frac{\partial^2 C^\ell_{HCO_3^-,m}}{\partial x^2} + R^{uc}_{CO_2} = 0 \tag{4.20}$$

$$D^{eff}_{j,\ell}\frac{\partial^2 C^\ell_{j,m}}{\partial x^2} = 0 \qquad \text{where } j=B,\ BH^+ \tag{4.21}$$

The matching boundary conditions reveal the non-volatility at the gas-liquid interface and the equality of molar fluxes in the transverse direction at the limit of the wetted zone of the membrane:

$$x = \delta_m^{g\ell} \qquad D^{eff}_{j,\ell}\left.\frac{\partial C^\ell_{j,m}}{\partial r}\right|_{x=\delta_m^{g\ell}} = 0 \qquad \text{where } j=HCO_3^-,\ B \text{ and } BH^+ \tag{4.22}$$

$$x = \delta_m \qquad D^{eff}_{j,\ell}\left.\frac{\partial C^\ell_{j,m}}{\partial x}\right|_{x=\delta_m} = -D_x\left.\frac{\partial C_{j,\ell}}{\partial x}\right|_{x=\delta_m} \qquad \text{where } j=HCO_3^-,\ B \text{ and } BH^+ \tag{4.23}$$

When the pores are completely filled with gas, the mathematical model only represents the diffusion of CO_2 into the porous structure of the membrane and reduces to Eq. 4.14 with the boundary conditions given in Eqs. 4.24-4.25:

$$x = 0 \qquad k_g\left(C_{CO_2,g} - C^g_{CO_2,m}\Big|_{x=0}\right) = -D^{eff}_{CO_2,g}\left.\frac{\partial C^g_{CO_2,m}}{\partial x}\right|_{x=0} \tag{4.24}$$

$$x = \delta_m \qquad D^{eff}_{CO_2,g} \left.\frac{\partial C^{g}_{CO_2,m}}{\partial x}\right|_{x=\delta_m} = D_x \left.\frac{\partial C_{CO_2,\ell}}{\partial x}\right|_{x=\delta_m} \tag{4.25}$$

When CA is immobilized on the surface of membrane and additionally inside the pores, and the membrane is partially filled with liquid, Eqs. 4.15, 4.20 and 4.21 becomes:

$$D^{eff}_{CO_2,\ell} \frac{\partial^2 C^{\ell}_{CO_2,m}}{\partial x^2} - R^{uc}_{CO_2}\left(C^{\ell}_{j,m}\right) - R^{c}_{CO_2,m}\left(C^{\ell}_{j,m}\right)\frac{1}{\varepsilon_m} = 0 \tag{4.26}$$

$$D^{eff}_{HCO_3^-,\ell} \frac{\partial^2 C^{\ell}_{HCO_3^-,m}}{\partial x^2} + R^{uc}_{CO_2}\left(C^{\ell}_{j,m}\right) + R^{c}_{CO_2,m}\left(C^{\ell}_{j,m}\right)\frac{1}{\varepsilon_m} = 0 \tag{4.27}$$

$$D^{eff}_{B,\ell} \frac{\partial^2 C^{\ell}_{B,m}}{\partial x^2} - R^{c}_{CO_2,m}\left(C^{\ell}_{j,m}\right)\frac{1}{\varepsilon_m} = 0 \tag{4.28}$$

$$D^{eff}_{BH^+,\ell} \frac{\partial^2 C^{\ell}_{BH^+,m}}{\partial x^2} + R^{c}_{CO_2,m}\left(C^{\ell}_{j,m}\right)\frac{1}{\varepsilon_m} = 0 \tag{4.29}$$

4.3.4. Gas–liquid membrane contactor scale model

The higher intensity of liquid turbulence in the vicinity of the membrane and contactor wall associated with the special internal configuration of contactor is responsible for an increased liquid mixing, as well as for an efficient redevelopment of the hydrodynamic boundary layer which subsequently results in the enhancement of mass transfer by convection (this is confirmed by the residence time distribution of the tracer in the membrane contactor which is closer to the ideal plug flow than laminar flow although this behavior is not expected at such low Reynolds numbers – not shown). Thus, a two-dimensional model with axial and radial dispersion and enzymatic reaction at the wall (with CA immobilized on the membrane surface) was generated for the liquid in the HFMC. Steady-state mass balance equations in liquid phase are the following:

$$u_\ell \frac{\partial C_{CO_2,\ell}}{\partial z} = D_{z,\ell} \frac{\partial^2 C_{CO_2,\ell}}{\partial z^2} + D_{x,\ell} \frac{\partial^2 C_{CO_2,\ell}}{\partial x^2} - R^{uc}_{co_2}(C_{j,\ell}) \tag{4.30}$$

$$u_\ell \frac{\partial C_{HCO_3^-,\ell}}{\partial z} = D_{z,\ell} \frac{\partial^2 C_{HCO_3^-,\ell}}{\partial z^2} + D_{x,\ell} \frac{\partial^2 C_{HCO_3^-,\ell}}{\partial x^2} + R^{uc}_{co_2}(C_{j,\ell}) \tag{4.31}$$

$$u_\ell \frac{\partial C_{B,\ell}}{\partial z} = D_{z,\ell} \frac{\partial^2 C_{B,\ell}}{\partial z^2} + D_{x,\ell} \frac{\partial^2 C_{B,\ell}}{\partial x^2} \tag{4.32}$$

$$u_\ell \frac{\partial C_{BH^+,\ell}}{\partial z} = D_{z,\ell} \frac{\partial^2 C_{BH^+,\ell}}{\partial z^2} + D_{x,\ell} \frac{\partial^2 C_{BH^+,\ell}}{\partial x^2} \tag{4.33}$$

The matching boundary conditions are:

$$z = 0 \qquad u_\ell C_{j,\ell}^{in} = u_\ell C_{j,\ell}(0,x) - D_{z,\ell} \frac{\partial C_{j,\ell}}{\partial z}(0,x) \tag{4.34}$$

$$z = L \qquad \frac{\partial C_{j,\ell}}{\partial z}(L,x) = 0 \tag{4.35}$$

$$x = w \qquad \frac{\partial C_{j,\ell}}{\partial r}(z,0) = 0 \tag{4.36}$$

$$x = \delta_m \qquad -D_{x,\ell} \frac{\partial C_{j,\ell}}{\partial x}(z,\delta_m) a_v = R_j^c \left(C_{j,\ell}\Big|_{x=\delta_m} \right) \tag{4.37}$$

CO_2 mass balance equation in gas phase, supposing plug flow, is:

$$\pm \frac{\partial \left(u_g \varepsilon_g C_{CO_2,g} \right)}{\partial z} = D_{CO_2,g}^{eff} \left. \frac{\partial C_{CO_2,m}^g}{\partial x} \right|_{x=0} a_v \tag{4.38}$$

Gas velocity axial gradient was estimated via the gas phase overall mass balance equation:

$$\pm \frac{\partial}{\partial z} \left(u_g \varepsilon_g \frac{P_g}{RT_g} \right) = -k_g \left(C_{CO_2,g} - C_{CO_2,m}^g \Big|_{x=0} \right) a_v \tag{4.39}$$

where the signs "+" and "-" relate, respectively, to the co-current and counter-current flows. The matching boundary conditions are:

a) co-current:

$$z = 0 \qquad C_{CO_2,g}\Big|_{z=0} = C_{CO_2,g}^{in} \qquad u_g\Big|_{z=0} = u_g^{in} \tag{4.40}$$

b) counter-current:

$$z = H \qquad C_{CO_2,g}\Big|_{z=H} = C_{CO_2,g}^{in} \qquad u_g\Big|_{z=H} = u_g^{in} \tag{4.41}$$

4.3.5. Model parameters

The effective diffusion coefficients consider both molecular and Knudsen diffusion processes [228]:

$$\frac{1}{D_j^{eff}} = \frac{\tau}{\varepsilon} \left(\frac{1}{D_j} + \frac{1}{D_{kj}} \right) \tag{4.42}$$

Molecular diffusion coefficients for binary gas systems calculated with Chapman and Enskog equation [229] and Knudsen diffusion coefficient [230] are given by Eqs. 4.43 and 4.44:

$$D_{ij} = 1.858 \times 10^{-3} T^{3/2} \frac{\left[\left(M_i + M_j\right)/M_i M_j\right]^{1/2}}{P\sigma_{ij}^2 \Omega_{ij}} \tag{4.43}$$

$$D_{kj} = \frac{2\bar{r}}{3}\left[\frac{8RT}{\pi M_j}\right]^{0.5} \tag{4.44}$$

Tortuosity factor was evaluated via the correlation of Iversen et al. [231]. Liquid phase molecular diffusion coefficients were evaluated using the Wilke-Chang approach [229]. The gas mass transfer coefficient was calculated with the Eq. (4.45) [232], as recommended by Lin et al. [233]:

$$\frac{k_g d_h}{D_{j,g}} = 0.023\,\mathrm{Re}_g^{0.8}\, Sc_g^{0.33} \tag{4.45}$$

The kinetic parameters were assessed under immobilization conditions in an intensified tubular microreactor [7].

4.4. Results and discussion

4.4.1. Effect of different parameters on enzyme immobilization

4.4.1.1. PDA/PEI ratio

The impact of PDA/PEI ratio on the enzyme immobilization is illustrated in **Figure 4.4a**. At 0/2 ratio, PDA does not exist in the deposition solution. On the other hand, PEI is soluble in water and could not adhere onto the membrane surface efficiently. Thus, the enzymes are immobilized on the membrane surface mainly via an adsorption process [129]. When the PDA content increases (1/2 ratio), a large number of PEI molecules react with PDA and form branched molecules in solution, rather than a coating layer on the membrane surface [52]. Accordingly, the amount of PDA is low and a small part of PEI amount reacts with PDA and is deposited on the membrane surface [52]. In this condition, the enzyme is immobilized on the surface via both adsorption and covalent bonding. The enzyme loading is improved due to the higher amine functionalities on the membrane surface, too. These PDA/PEI ratios (0/2 and 1/2) generate high enzyme activity efficiency because the immobilization via adsorption preserves the enzyme activity more than the covalent bonding method [70]. However, for the

enzymes immobilized by physical adsorption, much lower stability and reusability were reported because the physical interactions between the support and the enzymes are relatively weak, which could potentially lead to CA detachments [45, 48]. Among the other PDA/PEI ratios (2/2, 2/1 and 2/0), the ratio of 2/2 generates higher enzyme loading (54.3%) and enzyme activity efficiency (19.4%). PEI provides large amounts of amine functionalities on the surface. When the mass ratios of PDA/PEI are higher than 2/2, PDA is predominant on the surface and hence, there is a reduction in surface amino groups in the PDA/PEI ratios of 2/1 and 2/0. Thus, the enzyme loading efficiency reduces due to the diminishment of PDA/PEI deposition via Michael addition or Schiff base reaction, and less amino groups are present on the membrane surface [234]. Consequently, the enzyme activity efficiency is attenuated with the enzyme loading reduction. Thus, the PDA/PEI ratio of 2/2 was chosen based on the enzyme loading and activity efficiency.

4.4.1.2. PDA/PEI co-deposition time

FTIR was used to analyze the chemical structure of the pristine and P-PP membranes with deposition times of 3, 5, and 7 h and **Figure 4.5** clearly illustrates the effect of PDA/PEI deposition time on amine functionalities on the membrane surface. Two main absorption peaks at 1576 cm^{-1} and 1653 cm^{-1} appear after co-deposition of PDA/PEI, which are related to the N-H vibration (primary amines) in PDA and PEI and C=N bonds between them. In addition, the broad peak observed between 3000 - 3600 cm^{-1} on the membrane surface is owing to the N-H stretching (secondary amines) and O-H stretching vibrations [129, 137]. With the increase of the deposition time at 7 h, amine functionalities on membrane surface proliferate and consequently, the enzyme loading and enzyme activity efficiency increase (**Figure 4.4b**). The biocatalytic membrane at 7 h deposition time presents the best enzyme activity efficiency and enzyme loading efficiency. However, above 7 h of deposition the enzyme loading and enzyme activity efficiency reduce because the excessive polymerization reactions between PDA and PEI reduce the primary amine groups on membrane surface. In this polymerization process, the primary amine groups of PEI react with PDA via Schiff base reaction and/or Michael addition [133, 134]. Immobilization of CA enzyme on PDA/PEI layer of membrane surface is accomplished by the consumption of primary amine functional groups via covalent bonding. Therefore, the denser primary amine functional groups on the surface provides higher enzyme loading. Also, extensive amounts of PDA/PEI increase steric

hindrance between the enzyme and support and enwrapped the enzyme, thus the enzyme activity efficiency decreases [138].

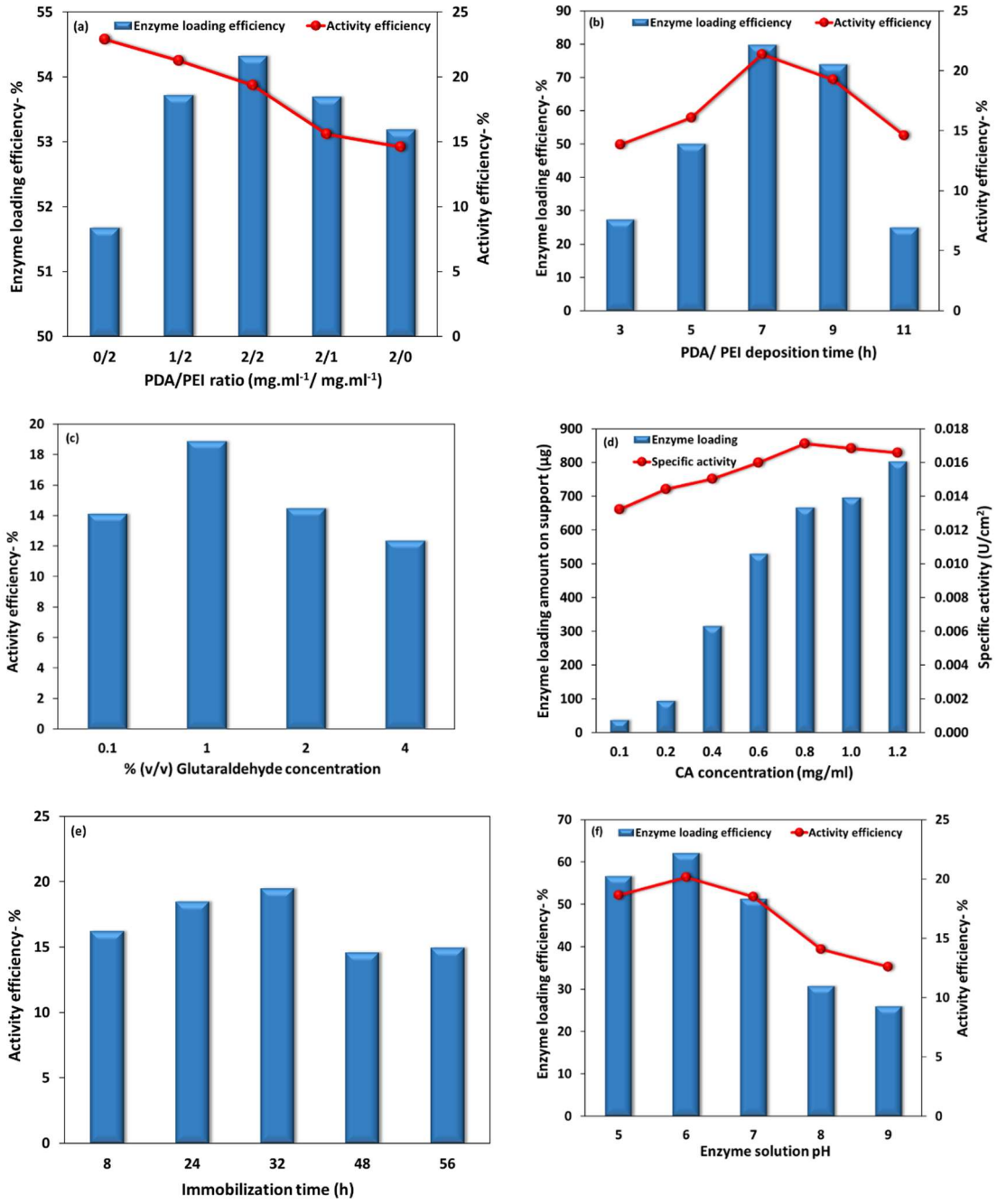

Figure 4.4. Effect of different parameters on enzyme immobilization: (a) PDA/PEI ratio, (b) co-deposition time, (c) glutaraldehyde concentration, (d) CA concentration, (e) CA immobilization time, and (f) enzyme solution pH.

Furthermore, after enzyme immobilization on the membrane surface, the contact angle declines from 130° (pristine membrane) to the values reported in **Figure 4.6** because of the hydrophilic properties of PDA/PEI coated layer. The contact angle of the membranes decreases with increasing the deposition time because the surface hydrophobicity reduces with prolonging the deposition time [52, 234]. At a deposition time of 7 h, the contact angle reaches 76°, at which the highest enzyme loading and enzyme activity efficiency are obtained (**Figure 4.4b**).

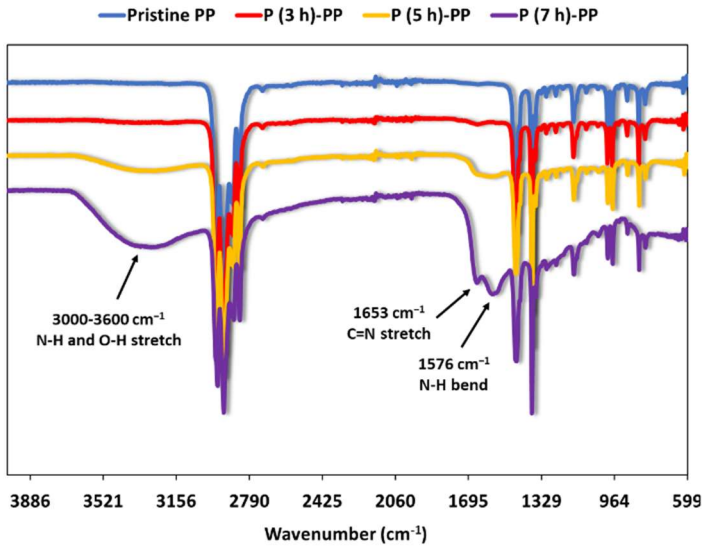

Figure 4.5. FTIR spectra of outer surfaces of pristine PP and P-PP membranes with 3, 5 and 7 h deposition.

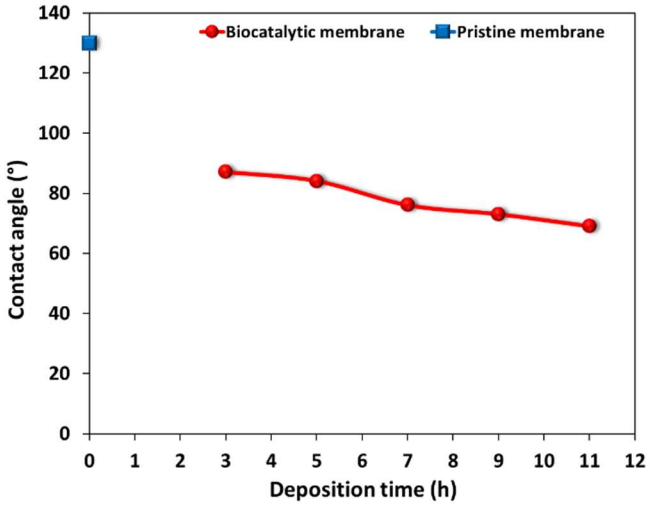

Figure 4.6. Effect of co-deposition time on membrane contact angle.

Table 4.2 indicates that with the increase of deposition time, PDA/PEI loading on the membrane surface gradually increases and after a deposition time of 9 h, no obvious change of deposition weight is observed, the membrane surface reaching a saturation density level [51, 136]. This observation confirms that a full PDA/PEI coverage of the membrane can be achieved in 9 h deposition time.

Table 4.2. PDA/PEI loading and breakthrough pressure of the P-PP membrane for different deposition times.

Membrane	Deposition weight (wt %)	Breakthrough pressure (bar)
Pristine membrane	-	3.24
P (3 h)-PP	0.47	3.31
P (5 h)-PP	1.11	3.72
P (7 h)-PP	1.47	3.52
P (9 h)-PP	2.09	3.24
P (11 h)-PP	2.15	3.25

Li et al. [138] indicated that the surface modification using PDA and PEI narrows the pores of polymeric membranes and alters the surface morphology, as water permeability decreases with membrane modifications. Also, Chew et al. [137] observed that PDA/PEI-coated PVDF membrane has a much narrower pore size distribution with a smaller mean pore size of 0.017 μm in comparison with the pristine membrane with a well-defined distribution and a mean pore size of 0.027 μm. The co-deposition of PDA/PEI covers the outer membrane surface and most of the pores on the outer surface and consequently, a pore size reduction was noticed. Therefore, this modified membrane should be less prone to wetting. Furthermore, coating of polyelectrolyte film on PP membrane reduces the percentage of pore wetting from 4% to 0.5-2.3% based on the numbers of polyelectrolyte layers on the surface, due to the pore obstruction and pore size reduction [70]. Therefore, further investigation was carried out to assess the effect of co-deposition coating time on the breakthrough pressure of both pristine and modified membranes. The pristine membrane has a breakthrough pressure of 3.24 bar. Following the co-deposition, the breakthrough pressure gradually increases due to the membrane pore size reduction [48, 158]. The breakthrough pressure was further reduced after 5 h deposition because of the gradual increase of surface hydrophilicity. The increased

breakthrough pressure mitigates the wetting of membrane pore during the operation process [46].

The immobilization performance is influenced significantly by the nanostructure architecture of the support. **Table 4.3** summarizes the BET surface area, BJH pore diameter, and BJH pore volume for membranes obtained at different deposition times. The PDA/PEI deposition layer provides more nanostructures on the PP membrane surface which generates higher surface area and pore volume. Nevertheless, after 7 h PDA/PEI deposition time, both surface area and pore volume decrease and further deposition time has negligible impact on the subsequent deposited layer structure [158, 213]. These reductions could be explained either by the compression and densification of the deposited layer after 7 h or by the detachment of the large PDA/PEI aggregates. Also, the BJH pore diameter increases to around 87 nm after 7 h deposition time. A larger BJH pore diameter prevents the unwanted inter-molecular interaction between the enzymes and also diminishes mass transfer resistance [212].

Table 4.3. BET surface area, mean BJH pore diameter and pore volume for P-PP membrane at various deposition times.

Membrane	BET surface area (m^2/g)	Mean BJH pore diameter (nm)	BJH pore volume (cm^3/g)
Pristine membrane	27.7	77.8	0.67
P (5 h)-PP	27.8	86.5	0.76
P (7 h)-PP	28.9	87.1	0.81
P (9 h)-PP	28.4	72.8	0.65
P (11 h)-PP	27.9	82.3	0.75

4.4.1.3. Glutaraldehyde concentration

Because glutaraldehyde may or may not improve the enzyme activity efficiency [59, 235], we investigated the effect of GA concentration on enzyme immobilization. The glutaraldehyde bounds the enzymes on the aminated membrane surface through the Michael/Schiff reactions between the aldehydes groups of glutaraldehyde and the amino groups of aminated membrane surface on one hand, and the amine groups of CA enzymes on the other hand [215]. The optimal concentration of glutaraldehyde was investigated by putting the P-PP membranes in 0.2 mg/ml CA solution (pH 7) mixed with 0.1 - 4.0 (v/v)% glutaraldehyde solution. As shown in **Figure 4.4c**, the enzyme activity efficiency improves

with increasing glutaraldehyde concentration from 0.1 to 1.0 (v/v)% and then decreases when the concentration of glutaraldehyde exceeds 1.0%. The glutaraldehyde provides more reactive end groups for enzyme immobilization on the support, but in the case of extensive amount of glutaraldehyde, the excess aldehyde groups of glutaraldehyde would react with the enzyme and change the enzyme conformation. Subsequently, immobilized enzyme activity and enzyme activity efficiency decline for a glutaraldehyde concentration above 1.0 (v/v)%. According to literature, in the presence of high glutaraldehyde concentrations during enzyme immobilization, a part of the aldehyde groups crosslink with the amine groups on aminated membrane, while the remaining groups can further interreact with the ε-amino groups of lysine on the enzyme surface [59, 214, 215].

4.4.1.4. CA concentration and immobilization time

The optimal CA concentration to achieve the best activity of the biocatalytic membrane was examined by immersing the aminated membranes in the CA solution (pH 7) with different enzyme concentrations (0.1-1.2 mg/ml) mixed with 1.0 (v/v)% glutaraldehyde. The CA loading increases with increasing the CA concentration (**Figure 4.4d**). The highest specific activity was obtained at CA concentration of 0.8 mg/ml, when the CA molecules fully bound to the active sites on the support. The membrane surface is overcrowded by further increase of enzyme concentration due to insufficient active sites for enzyme immobilization on the surface and aggravated steric hindrance. As a result, the specific activity decreases [48].

The assessment of the effect of immobilization time (in the range of 8 - 56 h) on the enzyme activity and loading efficiency is illustrated in **Figure 4.4e**. The best enzyme activity efficiency was achieved for an immobilization time of 32 h. However, exceeding this time, the enzyme activity efficiency decreases due to the saturation of all active sites located on the membrane surface. Also, the prolongation of the immobilization process increases the cross-linking by glutaraldehyde, which could alter the enzyme conformation, thus resulting in enzyme activity deterioration.

4.4.1.5. Enzyme solution pH during immobilization

The impact of CA solution pH, varying from 5.0 to 9.0, on enzyme loading and enzyme activity efficiency is shown in **Figure 4.4f**. The highest CA loading and enzyme activity efficiency were obtained at pH 6 because CA has an isoelectric point (IEP) of approximately

6. In these conditions, the electric repulsion between the enzyme molecules would be minimum. The electrostatic repulsive forces reduce the amount of enzyme loading on membrane surface, resulting in the enzyme activity reduction on membrane surface. Also, the enzyme structure is preserved near the IEP point and leads to the high loading and activity on the membrane surface at pH 6 [216]. With the increase of pH over 6, the enzyme loading and enzyme activity efficiency reduce. At pH 5, the enzyme loading efficiency is lower than the one obtained at pH 6, but higher compared to pH 7- 9 [48, 138].

4.4.2. Characterisation of the biocatalytic membrane

FTIR spectra demonstrates the co-deposition of PDA/PEI and enzyme immobilization on the PP membrane surface (**Figure 4.7**). As explained in the sub-section 4.1.2, the peaks at 1576 cm^{-1} and 1653 cm^{-1} correspond to the N-H vibration (primary amines) in PDA and PEI and the C=N bonds between them, and the broad peak at 3000- 3600 cm^{-1} is related to the N-H stretching (secondary amines) and O-H stretching vibrations [129, 137]. FTIR spectrum of the biocatalytic membrane is similar to the one for PDA/PEI deposited membrane with weaker peaks at 1576 cm^{-1} and stronger peak at 3000-3600 cm^{-1}. In fact, the enzyme immobilizes on the aminated surface through covalent bonding with glutaraldehyde, in which the primary amine groups are consumed, resulting in more secondary amine groups.

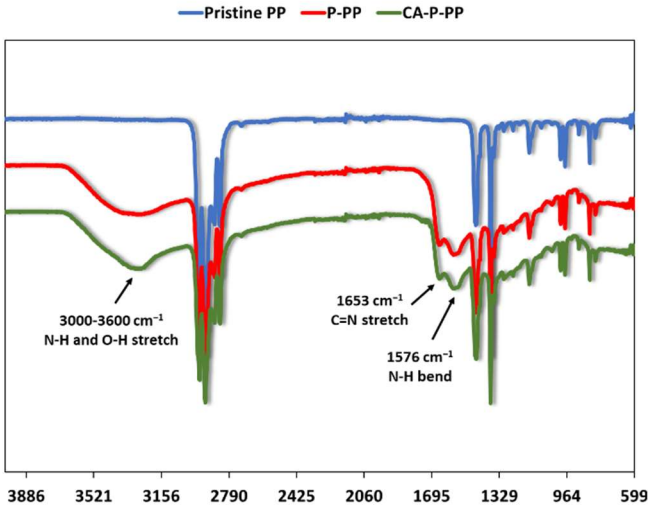

Figure 4.7. FTIR spectra of the outer surfaces of the pristine PP, P-PP and CA-P-PP membranes.

The outer surface and cross-section morphologies of pristine and biocatalytic membranes are illustrated in **Figure 4.8**. The pristine membrane surface is smooth and has abundant

observable pores (**Figures 4.8a1** and **a2**), but after deposition and immobilization, the deposition layer covers thoroughly the membrane surface and the pores become less observable (**Figures 4.8b1** and **b2**). The co-deposition of PDA/PEI on the membrane surface provides a homogeneous and uniform layer on the membrane surface [129] and causes a reduction in pore size which provides additional protection for the biocatalytic membrane against the pore wetting [137] during the absorption process [46]. As expected, the breakthrough pressure increases (from 3.24 bar for the pristine membrane to 3.45 bar for the biocatalytic membrane, for a deposition time of 7 h). This increase is relatively smaller than that corresponding to the co-deposited membrane for the same deposition time (3.52 bar, **Table 3.1**) and could be explained by the hydrophobicity mitigation of the membrane after enzyme immobilization. After the enzyme immobilization, the membrane contact angle slightly decreases because the enzyme fills in the valleys [138].

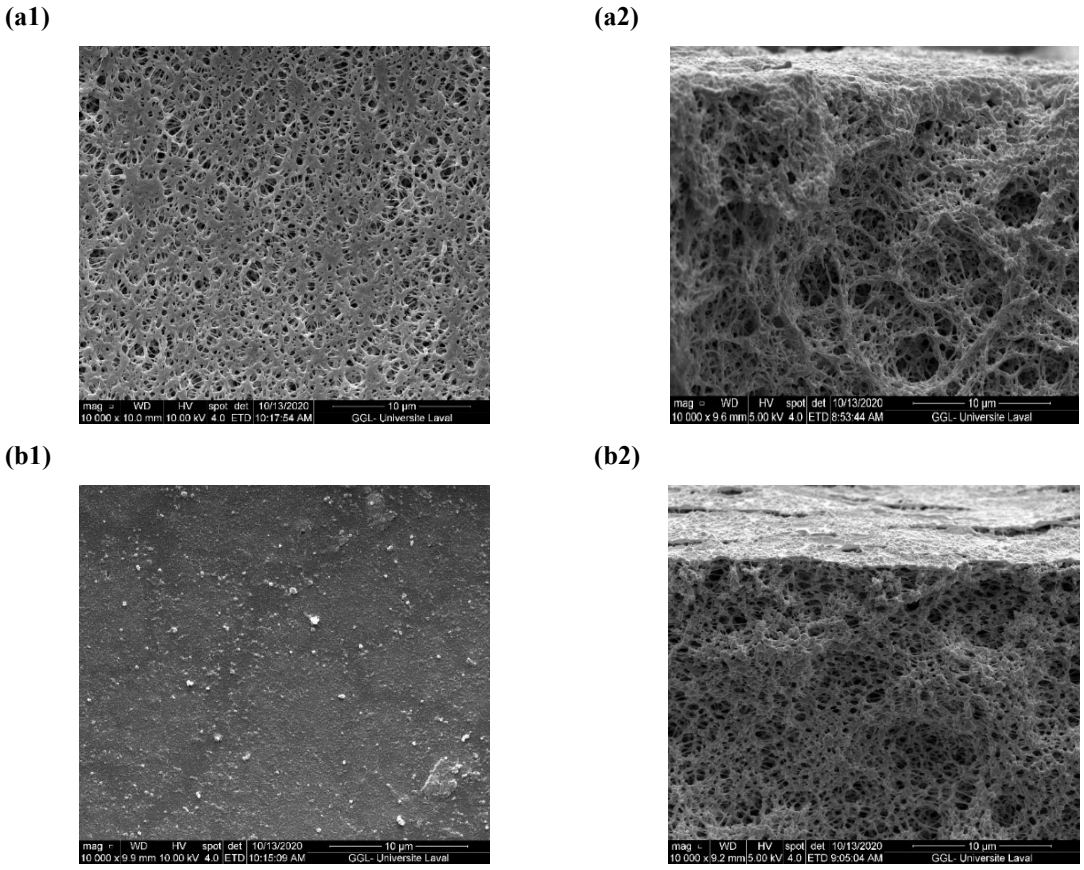

Figure 4.8. Surface SEM images of outer surface morphologies and cross section morphologies of (a1 and a2) the pristine PP and (b1 and b2) CA-P-PP membranes.

Figure 4.8b2 illustrates the thickness of the deposited layer on membrane surface. It is observed that the deposited layer did not penetrate the bulk of the membrane. To further understand if the penetration into the membrane bulk happened or not, EDS analysis was carried out. According to **Figure 4.9 (a** and **b)**, the elemental composition of the inner surface of pristine and biocatalytic membranes are similar, which proves that the coating layer does not penetrate the bulk PP substrate. The presence of Zn in the deposited layer thickness is also observed (**Figure 4.9c**).

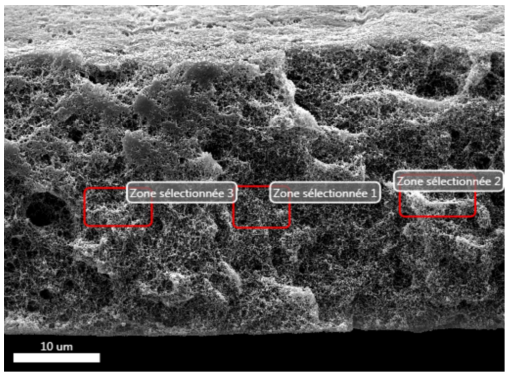

(a)

Element	% Mass
C K	99.87
O K	0.13

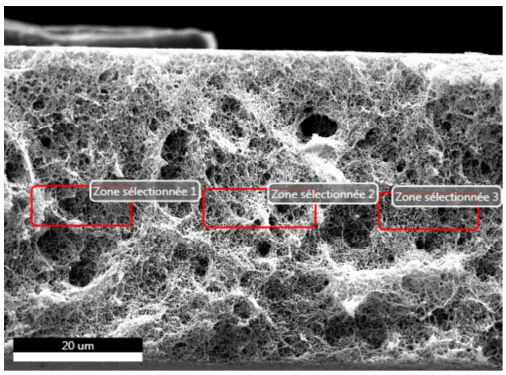

(b)

Element	% Mass
C K	99.47
O K	0.53

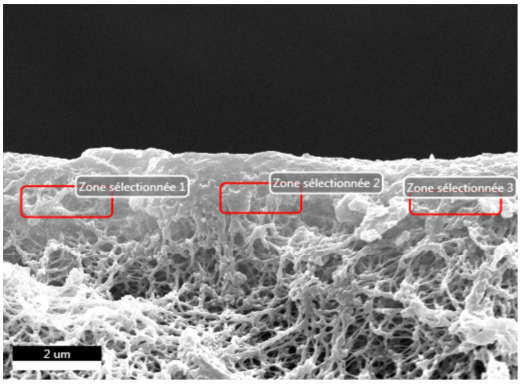

(c)

Element	% Mass
C K	83.08
O K	4.53
Zn K	2.03

Figure 4.9. EDS analysis of inner surfaces of the (a) pristine PP, (b) CA-P-PP membrane and (c) EDS analysis of deposited layer on CA-P-PP membrane.

4.4.3. Stability of immobilized CA

The storage stability of free and immobilized CA was investigated for 40 days. **Figure 4.10** shows that the immobilized CA almost maintains its initial activity for the first 17 days, with only 7% reduction in activity. After 40 days, the immobilized CA still retains 82.3% of its initial activity. By comparison, the free CA loses its initial activity speedily and after 40 days, the relative activity decreases to about 38% of its initial activity. This demonstrates the significant improvement of the storage stability of CA after immobilization. The immobilization through strong covalent bonds avoids enzyme denaturation and preserves its activity, resulting in the enhancement of the CA stability [58].

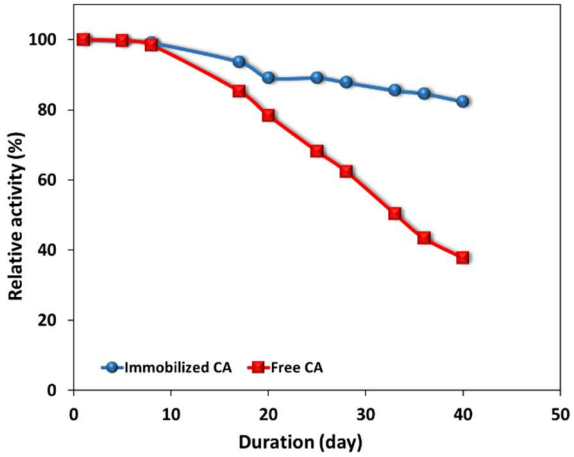

Figure 4.10. Storage stability of immobilized CA.

Table 4.4 presents the literature performance of immobilized CA on different supports. According to these data, TiO_2 coated PVDF membrane has higher CA loading (150 µg/cm^2) than PP membrane used in this work (94.3 µg/cm^2). This might be because of the different glutaraldehyde concentration utilized during the immobilization process: 4% (v/v) glutaraldehyde concentration was used for CA immobilization on TiO_2 coated PVDF membrane, compared to this work (1% (v/v)). Glutaraldehyde can promote the multipoint attachments of enzyme on support [44]. The immobilized CA on TiO_2 coated PVDF membrane has, however, not shown a good storage stability. In terms of the activity efficiency, the highest value reported in the literature was 87.6% with TiO_2 coated nanoparticles which provide a high surface area for enzyme immobilization and, in addition, allow a higher mobility and degree of freedom for immobilized enzyme and reduce the lateral interactions between enzymes. These characteristics help preserve a higher enzyme activity

[44, 57]. The activity efficiency obtained in this work (27.67%) is comparable with the results of Hou et al [48] (28%), Xu et al. [97] (31.5%), and Sun et al. [51] (32%). However, the contact angle of the biocatalytic membranes in Xu et al. [97] and Sun et al. [52] diminishes to about 60° and 40°, respectively, values that are not suitable for membrane contactors.

The calculated k_{cat}/K_m values of free and immobilized CA (with p-NPA hydrolysis, see section 4.2.2.4) were found to be 667.6 M^{-1} s^{-1} and 292.3 M^{-1} s^{-1}, respectively. This expected decrease is possibly due to the structural change and lower mobility of CA on membrane after immobilization.

Table 4.4. Performance of immobilized CA on different supports.

Support	**Pore size (µm)**	**Functional reagent**	**Enzyme loading**	**Activity efficiency (%)**	**Relative activity after 20 days (%)**	**Ref.**
Flat sheet PP	0.1	PDA/PEI and glutaraldehyde	94.3 µg/cm^2	27.67	89.09	Current work
PVDF	0.45	TiO_2 Coating, (3-aminopropyl triethoxy silane (KH550) and glutaraldehyde	150 µg/cm^2	28	60	[**48**]
Hollow fiber PVDF	0.04	PDA/PEI and glutaraldehyde	-	31.5	97	[**97**]
Flat sheet PVDF	0.025	Plasma modification, Silane coupling agents: γ-(2,3-epoxypropoxy) propyl trimethoxy silane (KH560)	-	32	83	[**51**]
Flat sheet PVDF	0.025	Plasma modification, Silane coupling agents: KH550 and glutaraldehyde	-	60	83	[**51**]
Hollow fiber PVDF	0.1	PDA/PEI and glutaraldehyde	-	53	84	[**52**]
TiO_2 coated nanoparticle	-	KH550 and glutaraldehyde	27.4 mg/g support	87.6	72	[**48**]
Porous glass	0.0298	γ-aminopropyl triethoxysilane and glutaraldehyde	32.6 mg/g support	35	85 (at 50 °C)	[**17**]

4.4.4. CO_2 absorption in membrane contactor

The biocatalytic membrane was fabricated using the optimum conditions of immobilization defined above (PDA/PEI 2/2, deposition time 7 h, glutaraldehyde concentration 1.0% (v/v),

enzyme immobilization time 32 h, and enzyme solution pH 6.0), but with an enzyme concentration of 0.2 mg/ml (it should be noted that an initial CA concentration 4 times higher (0.8 mg/ml) used for immobilization only results in 1.18 times increase in the enzyme activity, **Figure 4.4d**). The biocatalytic membrane was integrated into the gas-liquid MC (FSMC) to investigate its ability in the CO_2 absorption process. The CO_2 absorption flux was compared with similar works in the literature, as shown in **Table 4.5**. The biocatalytic membrane prepared in the current work exhibits a CO_2 absorption flux of 0.29×10^{-3} mol/m^2s (with 100 mM Tris concentration in water), which is comparable with other works which use flat sheet or hollow fiber membrane contactors and amine-based absorbents. These results highlight a competitive efficiency of immobilized CA enzyme on polymeric membrane in the CO_2 absorption process in membrane contactors. It is worth mentioning that, while the absorption flux achieved in the current work may be lower than that of some others, the operational conditions (like membrane configuration, CO_2 composition percentage in feed gas, and liquid and gas velocities) must be taken into account in this comparison because they play a determining role in the performance of the absorption process.

4.4.4.1. Impact of buffer type and concentration on the membrane bioreactor performance

Buffers are proton transfer agents in enzymatic CO_2 hydration process and their concentration determines if the intra-molecular or inter-molecular proton-transfer step are the controlling step in the enzymatic reaction. **Figure 4.11** shows that large buffer concentrations increase the absorption rate because the inter-molecular proton transfer step is not rate limiting in this condition [7, 11, 19]. Inter-molecular transfer is rate limiting step in CO_2 hydration process when the buffer concentration is low and leads to the enzymatic reaction rate reduction. Gas solubility in the liquid phase diminishes in the presence of ions. Also, liquid viscosity enhances in the presence of the ions, which decreases the gas diffusivity in the liquid [236]. In addition, enzyme conformation could be altered in the presence of ions in solution and subsequently, the enzyme activity decreases [46, 237]. But in this work, as indicated in **Figure 4.11**, the biocatalytic membranes do not lose their efficiency up to 200 mM Tris concentration.

Table 4.5. Comparison of CO_2 absorption flux in different gas-liquid membrane contactors.

Membrane type	**Membrane material**	**Pore size (nm)**	**Absorbent**	**Liquid velocity (m/s)/ flow rate (ml/min)**	**Feed gas**	**CO_2 absorption flux ($\times 10^{-3}$ mol/m^2.s)**	**Ref.**
Flat sheet	Biocatalytic PP	100	Water and 100 mM buffer	26 ml/min	15% CO_2	0.29	Current work
Flat sheet	Fluorinated TiO_2 PP	200	Water and 100 mM buffer with 200 µg/ml CA immobilized on nanoparticles	300 ml/min	20.4 % CO_2	0.3	[**46**]
Hollow fiber	Fluorinated TiO_2 PP	200	Water and 100 mM buffer with 200 µg/ml CA immobilized on nanoparticles	405 ml/min	20.4 % CO_2	0.15	[**46**]
Hollow fiber	Biocatalytic PVDF	40	Water	0.25 m/s	Pure CO_2	2.3	[**97**]
Flat sheet	Plasma-treated PVDF	190	1 M 2-amino-2-methyl-1-propanol (AMP)	100 ml/min	15% CO_2	0.096	[**233**]
Flat sheet	Coated PVDF-silica	78.23	1 M dimethylamine (DEA)	100 ml/min	Pure CO_2	0.28	[**238**]
Flat sheet	Coated PVDF-silica	78.23	1 M AMP	100 ml/min	Pure CO_2	0.22	[**238**]
Flat sheet	PVDF	-	0.4 M aqueous NaOH	10 ml/min	10% CO_2	0.6	[**239**]
Flat sheet	PTFE	100	23 wt% 2-amino-2-hydroxymethyl-1,3-propanediol (AHPD) and 7 wt% Piperazine (Pz)	20 ml/min	20% CO_2	1.17	[**225**]
Hollow fiber	PTFE	30-80	23 wt% AHPD and 7 wt% Pz	30 ml/min	20% CO_2	0.58	[**240**]
Hollow fiber	PTFE	30-80	23 wt% AHPD	30 ml/min	20% CO_2	0.17	[**240**]

Flat sheet	PTFE	450	Propylene carbonate	-	Pure CO_2	1.0	[**241**]
Flat sheet	PP	360	Propylene carbonate	-	Pure CO_2	0.9	[**241**]

Figure 4.11 also illustrates the impact of buffer type on CO_2 absorption rate in counter-current membrane bioreactor with immobilized CA enzyme on membrane. Tris and N-methylimidazole buffers were used in the experiments. The CO_2 absorption rate increased with the amplification of pK_{a2} of buffer due to the higher CO_2 hydration driving force [11]. pK_{a2} of Tris and N-methylimidazole are 8.07 and 7.19, respectively.

In addition, **Figure 4.11** shows the model simulations when the membrane pores are totally or partially filled with the gas phase. The CO_2 hydration process performance was investigated by artificially forcing enzymatic hydration into the wetted pores assuming that the CA enzyme is also attached inside the surface porous structure of the membrane (not in the bulk of the membrane). A low degree of wetting (1%, as suggested in the sub-section 4.1.2) was considered because the solvents with high surface tension (water, in our case) and P-PP membrane have a low wetting capacity and it is expected that the enzymatic CO_2 hydration process runs eventually under these conditions. Unsurprisingly, with an enzymatic CO_2 hydration process in the wetted membrane porous structure, the performance of the contactor is enhanced especially at higher buffer concentration: the resistance to mass transfer in the wetted pores is overpowered by the enzymatic CO_2 hydration achieved by attaching the CA enzyme inside the membrane pores exposed to wetting [19]. The position of the experimental data in the graph highlights this behavior especially when Tris buffer was used in the experiments.

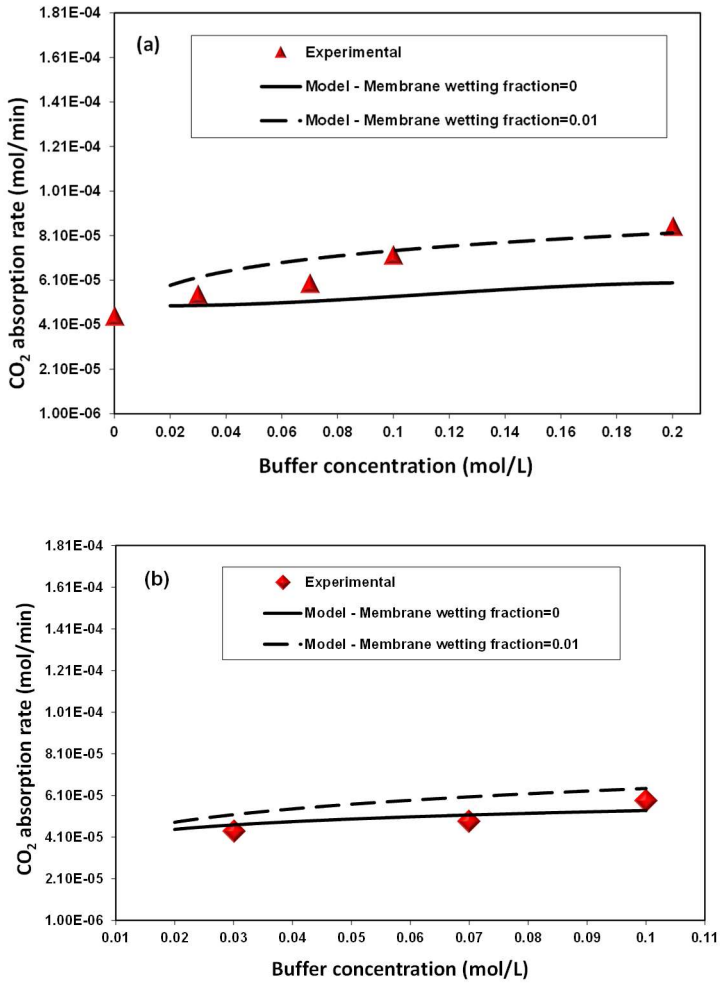

Figure 4.11. Effect of buffer concentration and type on the membrane bioreactor performance (liquid flow rate: 26 ml/min, gas flow rate: 100 ml/min, and counter-current flow): (a) Tris buffer; (b) N-methylimidazole buffer.

4.4.4.2. Impact of liquid flow rate and orientation flow on the membrane bioreactor performance

The effect of liquid flow rate on CO_2 absorption rate in the gas–liquid membrane bioreactor with immobilized CA enzyme is illustrated in **Figure 4.12**. The liquid flow rate enhancement reduces the thickness of liquid boundary layer and thus, mass transfer between the interface and the bulk becomes more efficient and CO_2 absorption rate increases. It should be noted that the enzyme (as a catalyst) only enhances the rate in which the reaction reaches equilibrium [7]. When the liquid flow rate is low, the residence time is long and therefore the uncatalyzed reaction has time to reach or approach the equilibrium and ultimately the contribution of the enzyme to the absorption of CO_2 decreases. Furthermore, the stagnant

liquid film layer formed at low liquid flow rate made the diffusion as the rate limiting step. With the increase of the liquid flow rate, reaction kinetics gradually become the rate limiting mechanism [219]. Also, liquid flow rate enhancement amends the inter-molecular transfer step of the enzyme hydration mechanism due to the enhancement of buffer amount transferred [11].

In addition, the results of CO_2 absorption rate of CO_2-N_2 (15/85 vol%) mixture flowing co- and counter-currently are presented in **Figure 4.12**. The counter-current membrane bioreactor slightly outperforms the co-current membrane bioreactor because of the higher driving force [19, 242].

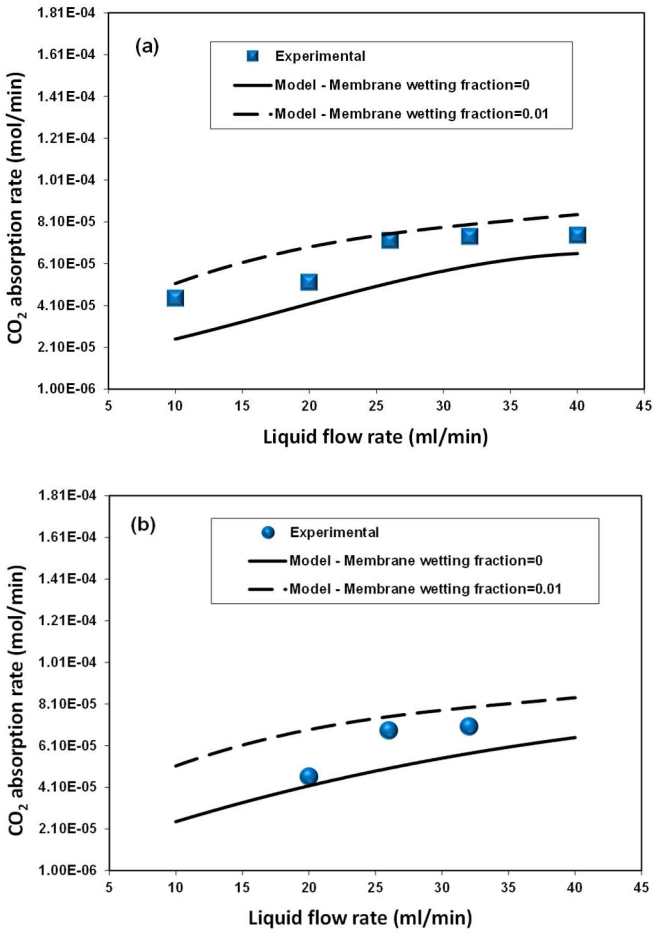

Figure 4.12. Effect of liquid flow rate and orientation flow on the membrane bioreactor performance (gas flow rate: 100 ml/min and 100 mM Tris in water): (a) counter-current flow; (b) co-current flow

Figure 4.12 also illustrates the theoretical CO_2 absorption rate vs. liquid flow rate when the membrane pores are totally or partially filled with gas. The enzymatic CO_2 hydration process in the wetted porous structure overcomes the resistance to mass transfer in this region and consequently the performance of the contactor is amplified, especially at higher liquid flow rates because of the intensification of the mass transfer in the liquid phase. Experimental data emphasizes this comportment especially for large liquid flow rates.

4.4.4.3. Impact of gas flow rate on the membrane bioreactor performance

The impact of gas flow rate on the CO_2 absorption rate is demonstrated in **Figure 4.13**. When the gas flow rate increases from 100 to 300 ml/min at constant water flow rate, the experimental absorption rate grows slightly from 7.2×10^{-5} to 7.9×10^{-5} mol/min. It can be explained that increasing the gas flow rate reduces the boundary layer thickness and enhances the mass transfer through the membrane. This observation is in good agreement with other researcher's works [221-223]. Gas molecules have high diffusivity and thereupon, the impact of gas flow rate on the mass transfer within a MC is not very important [46, 243].

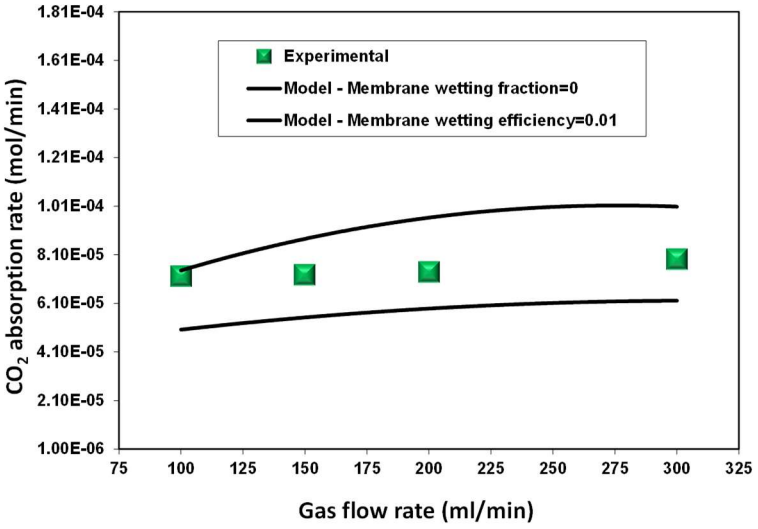

Figure 4.13. Effect of gas flow rate on the membrane bioreactor performance (liquid flow rate: 26 ml/min, counter-current flow, and 100 mM Tris in water).

Figure 4.13 illustrates, also, the theoretical CO_2 absorption rate vs. gas flow rate when the membrane pores are totally or partially filled with gas. As mentioned above, the enzymatic CO_2 hydration process overcomes the resistance to mass transfer in the membrane wetted

pores and, therefore, the performance of the contactor is improved especially at lower gas flow rates because of the higher residence time of the gas phase. Experimental data highlights this behavior especially when small gas flow rates have been used in experimental studies.

4.4.4.4. Impact of liquid temperature on the membrane bioreactor performance

The experimental results show that CO_2 absorption rate diminishes from 7.2×10^{-5} mol/min to 5.8×10^{-5} mol/min with the increase of the liquid temperature from 27 °C to 45 °C and are in agreement with the research done by Hou et al. [46]. The increase of the temperature alters the enzyme conformation and hence, leads to an enzyme activity reduction. Generally, in the membrane bioreactors, the temperature rise is not in favor of increasing the absorption rate. The enzyme used in this work, carbonic anhydrase II widespread in the human body, generates high enzyme activity at 27 °C. However, researchers developed novel CA enzymes which are more thermally stable and potentially could be utilized for the CO_2 hydration under high temperature conditions. For example, a CA enzyme from a thermophilic bacterium (Sulfurihydrogenibium yellowstonense) developed by Migliardini et al. [16] could tolerate a temperature of up to 110 °C.

4.4.4.5. Stability test of membrane bioreactor

To explore the potential of the current membrane bioreactor in industrial applications, the biocatalytic system was operated for several hours to verify the CO_2 absorption rate stability in the condition of counter-current flow, 10 ml/min liquid flow rate, 100 ml/min gas flow rate, and 100 mM Tris in water. As illustrated in **Figure 4.14**, the membrane bioreactor operates effectively with a stable CO_2 absorption rate which is beneficial in industrial applications.

4.5. Conclusion

In summary, the main objective of this work was to investigate the feasibility of using a biocatalytic membrane with immobilized CA in a FSMC to promote CO_2 absorption as a green and environmentally friendly technology.

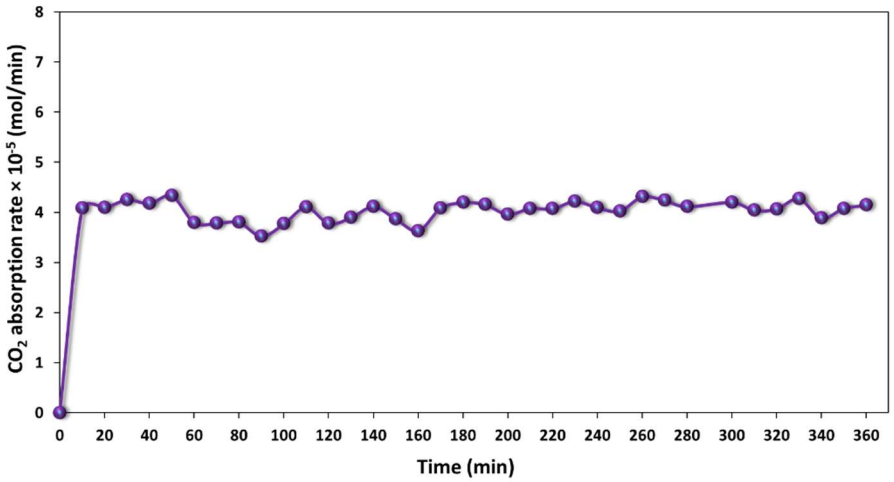

Figure 4.14. Stability test of membrane bioreactor (liquid flow rate: 10 ml/min, gas flow rate: 100 ml/min, counter-current flow, and 100 mM Tris in water).

Biocatalytic membranes were prepared in two steps: co-deposition of PDA/PEI for amine functionalization of the membrane surface and CA immobilization via covalent bonding with glutaraldehyde. Different immobilization conditions were examined to achieve the highest enzyme activity on the membrane surface. The biocatalytic membrane showed good storage stability after 40-day observation. The highest CA activity was achieved at 7 h deposition time, PDA/PEI ratio=2/2, 1.0 (v/v)% glutaraldehyde concentration, 0.8 mg/ml CA solution, 32 h immobilization time, and pH 6.0 in the immobilization process.

The feasibility of biocatalytic membrane utilization in FSMC applications was verified, resulting a CO_2 absorption flux of 0.29 $\times 10^{-3}$ mol/m^2s using 100 mM Tris in water in the absorption process. Moreover, the impact of buffer type and concentration, liquid flow rate, flow orientation and liquid temperature on the flat sheet membrane bioreactor performances was analyzed. The membrane bioreactor operated effectively with a stable absorption rate for several hours, illustrating its potential for industrial applications.

A multiscale model, with a gas-filled or partially liquid-filled membrane porous structure and enzyme attached on the membrane surface and inside the membrane pores, was developed and used to investigate the behaviour of the flat sheet membrane bioreactor. The model showed that the enzymatic CO_2 hydration process in the wetted porous structure overcomes

the resistance to mass transfer in this region, thus amplifying the contactor performance. Experimental data emphasizes this comportment, especially for large liquid flow rates.

This paper clearly reveals that the employment of immobilized CA on membrane surface in gas-liquid membrane contactors is promising and is a competitive candidate for CO_2 capture processes, which is cost effective and environmentally friendly.

The promising results obtained in the previous chapter (chapter 4) confirmed the potential of membrane as an appealing support for CA enzyme immobilization. The feasibility of using the biocatalytic membrane in the flat sheet membrane contactor for CO_2 absorption was also demonstrated. Furthermore, in the chapter 3, we found that the hybrid enzymatic process obtained the promising results with a higher efficiency and lower total required CA enzyme in the packed-bed column bioreactor.

In the following chapter, the CO_2 capture performance in a biocatalytic membrane contactor was intensified, for the first time, by incorporating biocatalytic magnetic nanoparticles (MNPs) dispersed in liquid solution. Detailed analyses were accomplished to investigate impact of different parameters on the CO_2 absorption performance.

Chapter 5: Hybrid enzymatic CO_2 capture process in intensified flat sheet membrane contactors with immobilized carbonic anhydrase

Résumé

Un processus hybride d'absorption enzymatique du CO_2 dans un contacteur à membrane plane intensifiée utilisant l'anhydrase carbonique humaine II (hCA II) immobilisée a été proposé. En plus d'être immobilisée sur la surface de la membrane, l'enzyme a été également immobilisée sur la surface des nanoparticules magnétiques (MNPs) dispersées dans la phase liquide, pour réduire les limitations de transfert de masse et améliorer le processus d'absorption. Ce procédé enzymatique hybride permet d'atteindre des taux d'absorption de CO_2 élevés, même si un composant du système enzymatique, soit la membrane biocatalytique, soit les MNP biocatalytiques, ne fonctionne pas adéquatement. L'amélioration de l'hydratation du CO_2 en présence de MNPs biocatalytiques a été plus significative à des concentrations plus faibles d'enzyme sur la surface de la membrane. La réutilisation des membranes et MNPs biocatalytiques a été démontrée durant 10 cycles d'absorption et le contacteur à membrane intensifié a montré un fonctionnement stable pendant plusieurs heures. Un modèle mathématique multi-échelle (considérant des pores de membrane remplis de gaz ou partiellement remplis de liquide) a été proposé pour explorer le comportement du contacteur à membrane intensifié. Les simulations ont montré que la résistance au transfert de masse dans les zones humides de la membrane est surmontée par l'absorption enzymatique du CO_2 dans ces zones (catalysée par l'enzyme immobilisée dans les pores de la membrane) et réalisable par l'absorption du CO_2 en présence de MNP biocatalytiques.

Abstract

A hybrid enzymatic CO_2 absorption process in an intensified flat sheet membrane contactor with immobilized human carbonic anhydrase II (hCA II) enzyme was proposed. In addition to be immobilized on the membrane surface, extra carbonic anhydrase enzyme was immobilized on the surface of magnetic nanoparticles (MNPs) dispersed in the liquid phase to reduce the mass transfer limitations and enhance the absorption process. This hybrid enzymatic process is beneficial to attain high CO_2 absorption rates, even if a component of the enzymatic system, either the biocatalytic membrane or biocatalytic MNPs, does not operate appropriately. The improvement CO_2 hydration in the presence of biocatalytic MNPs was more significant at lower CA loadings on membrane surface. Reusability of the biocatalytic membranes and biocatalytic MNPs was demonstrated by 10 absorption cycles and the intensified membrane contactor displayed stable operation for several hours. A multiscale mathematical model (under gas-filled or partially liquid-filled membrane pores conditions) was proposed to explore the behaviour of the intensified membrane contactor. Model simulations showed that the resistance to mass transfer in membrane wetted zones is overcame by the CO_2 enzymatic absorption in these zones (catalyzed by enzyme immobilized in membrane pores) and possible by the absorption of CO_2 in the presence of biocatalytic MNPs.

5.1. Introduction

Carbon emissions have been identified as a significant contributor to global warming and climate change in recent decades. Significant effort has gone into creating systems capable of capturing CO_2 before it is discharged into the environment [188]. Carbon capture and storage (CCS) is suggested as one of the main methods for mitigating global CO_2 emissions [187, 244] and post-combustion CO_2 capture has a substantial advantage over other options such as pre-combustion and oxyfuel combustion, since it can be simply adapted to existing plants [245]. The most mature, sufficiently studied and documented technology for post-combustion CO_2 separation is chemical absorption using amine-based solvents [189, 246]. In spite of maturity of amine-based absorption technology, this technology faces several major limitations such as amine degradation, corrosion, high regeneration energy, equilibrium limits, and generation of degradation products [176, 191]. Thus, alternative technologies for CO_2 capture process are highly required. An alternative to overcome these drawbacks of amine-based absorption process is to operate with green benign solvents (water) and biocatalysts to catalyze the CO_2 hydration process [47]. Human carbonic anhydrase II (hCA II or CA for simplicity) enzyme with a high hydration turnover between 10^4 and 10^6 molecules of CO_2 per molecule of CA per second [25, 27] has been shown to facilitate the use of water, catalyzing the CO_2 hydration process [12, 27, 59].

However, poor stability and reusability of free CA have limited its use. A variety of approaches were developed to overcome these limitations, including: sourcing CAs from thermophilic organisms, using protein engineering techniques to create thermo-tolerant CA enzymes [247, 248], and immobilizing the CA enzyme. Immobilization of the enzyme is the most common method to stabilize and improve its life span and reusability. In addition, CA enzyme immobilization assures a continuous enzymatic process and reduces the required enzyme amount, which is significant when using free CA enzyme [38, 249]. Immobilization has been reported on numerous solid supports including polyamide [250], chitosan [251], and alkyl sepharose [39, 252, 253]. The multipoint covalent immobilization (covalent bonding) is a strong and stable technique which requires the interaction of several functional groups of the enzyme with active groups on the support [254].

So far, only a few gas-liquid bioreactors with immobilized CA have been reported for CO_2 hydration such as hollow-fiber membrane contactors [19], random packed-bed columns [11, 12, 159], structured packed-bed columns [13], and integrated vacuum carbonate absorption process (IVCAP) reactors [17]. Membrane contactors have great advantages over other systems: high operational flexibility due to the independent control of gas and liquid flow rates, known interfacial area, modularity and a linear scale-up [240, 255, 256]. Compactness and less energy-consuming are the other significant advantages of membrane contactors [6, 8, 20, 23, 241]. Recently, we proposed ([19] and chapter 4) a novel approach for the biocatalytic CO_2 capture in flat sheet or hollow fiber membrane contactors with immobilizing CA on the membrane surface and inside the membrane pores, near the gas-liquid interface. CO_2 absorption performances were investigated under different conditions via a series of experiments and simulations. The performance of the contactor was ameliorated when the enzymatic CO_2 hydration process also took place in the wetted porous structure, as this enzymatic process overcomes the mass transfer resistance in this region. These works ([19] and chapter 4) displayed a promising concept for the biocatalytic CO_2 capture due to the advanced properties of these low-cost and environment-friendly systems. Yong et al. [70, 73, 182] immobilized CA onto flat sheet and hollow fiber polymer membrane surfaces coated by polyelectrolyte films and mesoporous silica via a layer-by-layer electrostatic adsorption approach for CO_2 hydration in the gas-liquid membrane contactors. These works showed that the rate of CO_2 hydration increased and pore wetting into the membranes reduced compared to the non-biocatalytic reactors. Similarly, a Janus-type hydrophilic/superhydrophobic membrane was developed to immobilize CA on the membrane surface [158] and then was employed in a gas-liquid membrane contactor with improved CO_2 hydration efficiency. However, Janus membranes have a complicated fabrication procedure that limits their wider application [46]. Additionally, a biocatalytic PVDF composite membrane was used in a gas-liquid hollow fiber membrane contactor (HFMC) and CO_2 absorption flux was promoted compared to the non-biocatalytic PVDF membrane [97]. Although membrane contactors with biocatalytic membranes offer a better CO_2 hydration rate, the major constraints are the possibilities of an inadequate gas-liquid mass transfer and the extra mass transfer resistance in the coating structure of the biocatalytic membranes. At large immobilized CA enzyme loading on the membrane surface, biocatalytic membrane contactors do not fully utilize the

high hydration turnover of CA enzyme because the enzymatic process is severely limited by the diffusion [48]. As a result, the hydration of CO_2 remains in the same range or even decreases at large CA loadings [32, 46, 97, 249]. A maximum impact on the CO_2 hydration kinetics is obtained when the enzyme is located closer to the gas-liquid interface in the liquid phase [157]. Therefore, it is preferably to take advantage of immobilized CA enzyme on nanoparticle surfaces dispersed in the liquid phase [46, 157-159].

Among several nanoparticles that can be used as support for the immobilization of enzymes, magnetic nanoparticles (MNPs) have been extensively developed and received widespread attention. MNPs have many advantages such as high specific surface area, efficient enzyme loading, facile and inexpensive separation from the reaction medium by applying an external magnetic field, low toxicity, and low mass-transfer limitations in solution [133, 184, 196, 197, 257]. Several reactive functional groups such as amine, hydroxyl, carboxyl, and epoxy were employed to activate the MNPs surfaces for enzyme immobilization [54, 58, 71, 84, 96, 184, 196, 258]. Previously, CA was immobilized on amine-functionalized silica coated MNPs and on carboxyl-functionalized MNPs [91, 199]. In different studies, MNPs surfaces were activated by carbodiimide for covalent CA enzyme immobilization [198]. In chapter 4, pristine membranes were amine-functionalized by co-deposition of polydopamine (PDA)/polyethyleneimine (PEI) and then CA enzyme was covalently immobilized via glutaraldehyde, which resulted in biocatalytic membranes with high CA enzyme loading and activity. These functionalization and immobilization approaches have the advantages of a being simple and offer an excellent adhesion capacity, abundant functional active groups, and good biocompatibility and biodegradability [124, 126-128, 130-133, 185, 196, 200-202, 259, 260]. Their application to the synthesis of biocatalytic MNPs would then be highly relevant.

In the present work, an enhanced hybrid enzymatic process in a flat sheet membrane contactor (FSMC) using CA immobilized on the surface of both membranes and MNPs dispersed in the liquid phase (water with buffer (B) solution) is proposed. CA enzymes were covalently immobilized on the modified surfaces of membrane and MNPs (amine-functionalized by PDA/PEI layers) via glutaraldehyde. The two components of the system, CA-membranes and CA-MNPs, can operate independently and amplify each other to achieve greater CO_2 conversion. The performance of CO_2 absorption process in the biocatalytic

FSMC in the presence of additional CA immobilized on MNPs surface (named intensified membrane contactor) was studied and the impact of the membrane quantity, buffer type, buffer concentration, and operational parameters on the CO_2 absorption performance were evaluated. Furthermore, the stability of the CO_2 absorption and reusability of the immobilized CA in intensified membrane contactor were assessed. This is the first study investigating this intensified system with immobilized CA enzyme. This research aims to illustrate that this innovative hybrid enzymatic process in membrane contactors, which is a low-cost, green, and environmentally friendly technology, could be a very attractive alternative for CO_2 capture processes.

5.2. Experimental

5.2.1. Materials and chemicals

Table 5.1 presents the characteristics of polypropylene **(**PP) flat sheet membranes and modules. Membranes were supplied by Membrana (North Carolina, USA). The production and purification of HCA II enzyme (molecular weight: 29.200 kDa) was carried out in our biotechnology laboratory. The glutaraldehyde (25 wt% solution in water) and PEI (MW = 600 Da; ≥ 99%) were purchased from Thermo Fischer Scientific. Dopamine hydrochloride (≥ 98%, CAS no. 62-31-7) and Bradford reagent were supplied from Sigma-Aldrich and Bio Basic, respectively. For MNPs synthesis, ferric chloride hexahydrate ($FeCl_3 \cdot 6H_2O$, 99.4%, MP Biomedicals LLC), ferrous chloride tetrahydrate ($FeCl_2 \cdot 4H_2O$, 99.0%−103.0%, Avantor Performance Materials, Inc.), and ammonium hydroxide (NH_4OH, 28%−30%) were utilized. Tris, 2-amino-2-methyl-1,3-propanediol (AMPD; ≥ 99%) and *N*-methylimidazole (≥ 99%) were supplied from Bio Basic, Laboratoire MAT, and Alfa Aesar, respectively. The CO_2 and N_2 gases of commercial grade were supplied from Praxair, Canada with a minimum purity of 99.9%.

Table 5.1. Flat sheet membrane and module specifications.

Parameters	PP membrane	Module/1 membrane
Thickness (µm)	100	-
Pore diameter (µm)	0.1	-
Porosity	0.8	-
Length (m)	-	0.059
Width (m)	-	0.070
Gas-liquid contact area (m^2)	-	0.0041

5.2.2. Biocatalytic membrane preparation

Figure 5.1 illustrates the schematic biocatalytic membranes preparation. CA immobilization on the membrane surface followed the same immobilization procedure described in chapter 2. Briefly, amine functionalization on the membranes surface was carried out by co-deposition of PDA/PEI (2/2 $mg.ml^{-1}/mg.ml^{-1}$ ratio and co-deposition time of 7 h) and then the CA enzyme was covalently immobilized on the amine-functionalized membranes surface with glutaraldehyde (glutaraldehyde concentration: 1% (v/v), immobilization time: 32 h and initial CA concentration: 0.04-0.25 mg/ml).

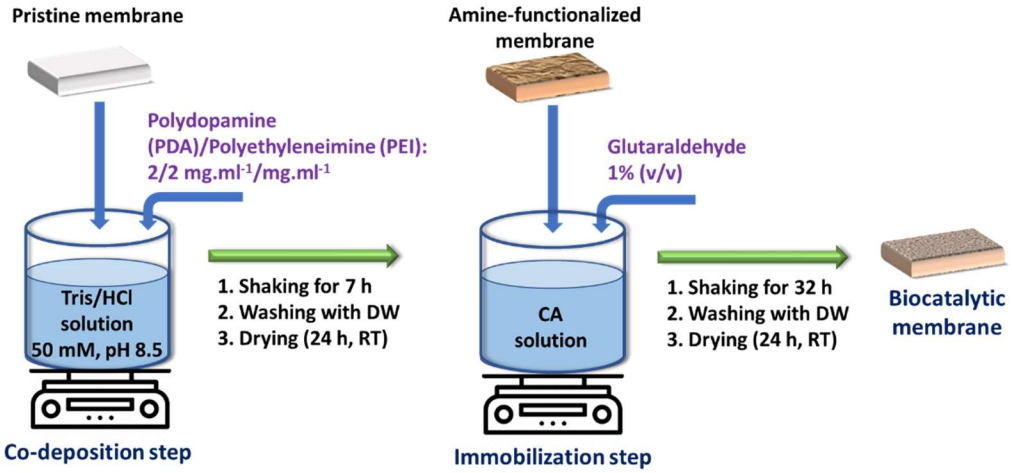

Figure 5.1. Illustration of the biocatalytic membranes preparation.

5.2.3. Biocatalytic MNPs preparation

The schematic illustration of biocatalytic MNPs preparation is depicted in **Figure 5.2**. First, MNPs (Fe_3O_4 nanoparticles) were synthesized via a co-precipitation method in basic solution

[184]. Second, MNPs surface was amine-functionalized by co-deposition of PDA/PEI (2 mg/ml dopamine and 2 mg/ml PEI for a 24 h co-deposition time). The resultant MNPs were separated and collected with a magnet and subsequently washed with distillated water several times and then, CA enzyme was immobilized on the modified MNPs surface with glutaraldehyde through covalent bondings (glutaraldehyde concentration: 2.0 % (v/v), immobilization time 24 h). The biocatalytic MNPs were collected with a magnet and subsequently rinsed with distillated water several times to remove the remaining glutaraldehyde.

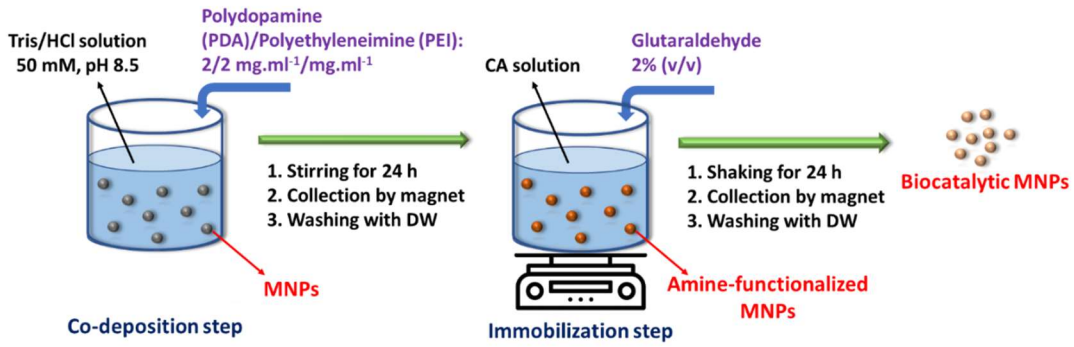

Figure 5.2. Biocatalytic MNPs preparation.

5.2.4. Quantification of immobilized enzyme loading

The immobilized CA enzyme loading on the surface of membranes or MNPs was determined by subtracting the protein amount of the final enzyme solution and washing solution from the protein amount of initial enzyme solution, measured by the Bradford method (Chapter 2).

5.2.5. Characterization tests

The contact angle of water on the membranes was measured by an optical contact angle analyzer (OCA 15 Plus) based on the sessile drop method. The breakthrough pressure of the membranes using water was measured based on the Laplace-Young equation, using the breakthrough pressure setup [178]. A Scanning Electron Microscope (SEM; Inspect F50 from FEI) was used to evaluate the surface morphology of the membranes and Transmission Electron Microscopy (TEM) (JEOL JEM 1230 electron microscope with an accelerating voltage of 80 kV) was employed to study the morphologies of MNPs.

5.2.6. CO_2 absorption performance of the intensified membrane contactor

The schematic experimental setup of CO_2 absorption in the intensified FSMC is illustrated in **Figure 5.3**. A detailed description of this experimental setup can be found in chapter 2. FSMC was operated counter-currently and the absorbent was distillated water in presence of 100 mM Tris buffer (pH: 9.5, CO_2 diffusion coefficient: 1.91×10^{-5} cm^2/s at atmospheric pressure and 25 °C, viscosity: 0.0091 poise at 25 °C) with or without dispersed biocatalytic MNPs. Gas-liquid contact area per flat sheet membrane is approximately 0.0041 m^2. All experiments in this work were performed at 298 K with FSMC containing one membrane. The CO_2 absorption rate (mol/min) was determined with the following equation:

$$CO_2\ absorption\ rate = Q_{inlet}y_{CO_2,inlet} - Q_{outlet}y_{CO_2,outlet} \quad (5.1)$$

where Q_{inlet}, Q_{outlet}, $y_{CO_2,inlet}$ and $y_{CO_2,outlet}$ are the inlet gas molar flow rate (mol/min), outlet gas molar flow rate (mol/min), CO_2 mole fraction at the gas inlet and CO_2 mole fraction at the gas outlet, respectively.

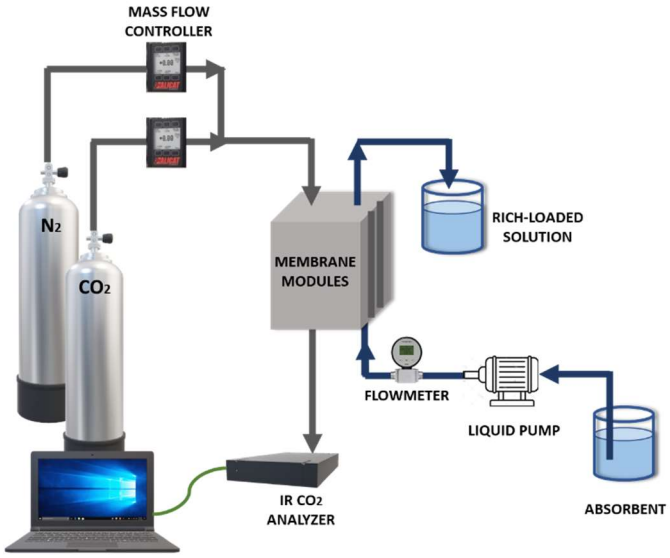

Figure 5.3. FSMC setup.

5.2.7. Reusability of the intensified membrane contactor

The immobilized CA reusability in the intensified membrane contactor was determined by measuring the CO_2 absorption rate for 10 absorption cycles. Upon the completion of each

cycle, the biocatalytic MNPs were collected by a magnet, washed with distillated water and then, were re-suspended in a fresh liquid absorbent for the next cycle.

5.3. Mathematical model of the membrane contactor

The mathematical model was developed for an intensified membrane contactor with CA enzyme immobilized on the membrane surface, inside the membrane pores partially filled with liquid and on the surface of micro-particles dispersed in the liquid phase.

5.3.1. Gas–liquid membrane contactor scale model

Mass balance equations in the liquid phase were generated via a 2D model with axial and transverse dispersion and enzymatic reaction at the membrane/micro-particles surface (CA immobilized on the membrane/micro-particles surface):

$$u_\ell \frac{\partial C_{CO_2,\ell}}{\partial z} = D_{z,\ell} \frac{\partial^2 C_{CO_2,\ell}}{\partial z^2} + D_{x,\ell} \frac{\partial^2 C_{CO_2,\ell}}{\partial x^2} - R^{uc}_{co_2}(C_{j,\ell}) - R^{mp}_{co_2}(C_{j,\ell}, C_{E,mp}) \tag{5.2}$$

$$u_\ell \frac{\partial C_{HCO_3^-,\ell}}{\partial z} = D_{z,\ell} \frac{\partial^2 C_{HCO_3^-,\ell}}{\partial z^2} + D_{x,\ell} \frac{\partial^2 C_{HCO_3^-,\ell}}{\partial x^2} + R^{uc}_{co_2}(C_{j,\ell}) + R^{mp}_{co_2}(C_{j,\ell}, C_{E,mp}) \tag{5.3}$$

$$u_\ell \frac{\partial C_{B,\ell}}{\partial z} = D_{z,\ell} \frac{\partial^2 C_{B,\ell}}{\partial z^2} + D_{x,\ell} \frac{\partial^2 C_{B,\ell}}{\partial x^2} - R^{mp}_{co_2}(C_{j,\ell}, C_{E,mp}) \tag{5.4}$$

$$u_\ell \frac{\partial C_{BH^+,\ell}}{\partial z} = D_{z,\ell} \frac{\partial^2 C_{BH^+,\ell}}{\partial z^2} + D_{x,\ell} \frac{\partial^2 C_{BH^+,\ell}}{\partial x^2} + R^{mp}_{co_2}(C_{j,\ell}, C_{E,mp}) \tag{5.5}$$

The greater intensity of liquid turbulence, related to the special internal arrangement of the membrane contactor, generates an intensified flow regime (confirmed via the experimental study of residence time distribution) with a substantial enhancement of liquid mixing and convective mass transfer in the laminar flow. The flattening of the laminar parabolic velocity profile generates an elevated transversal and axial backmixing of the liquid.

The matching boundary conditions for Eqs. (5.2-5.5) are:

$$z = 0 \qquad u_\ell C^{in}_{j,\ell} = u_\ell C_{j,\ell}(0,x) - D_{z,\ell} \frac{\partial C_{j,\ell}}{\partial z}(0,x) \tag{5.6}$$

$$z = L \qquad \frac{\partial C_{j,\ell}}{\partial z}(L,x) = 0 \tag{5.7}$$

$$x = w \qquad \frac{\partial C_{j,\ell}}{\partial r}(z,0) = 0 \tag{5.8}$$

$$x = \delta_m \qquad -D_{x,\ell}\frac{\partial C_{j,\ell}}{\partial x}\left(z,\delta_m\right)a_v = R_j^c\left(C_{j,\ell}\Big|_{x=\delta_m}\right) \tag{5.9}$$

Species balance equation for micro-particles with immobilized enzyme (the dispersion coefficients of the micro-particles were supposed to be similar to those of the dissolved species) is:

$$u_\ell \frac{\partial C_{E,mp}}{\partial z} = D_{z,\ell}\frac{\partial^2 C_{E,mp}}{\partial z^2} + D_{x,\ell}\frac{\partial^2 C_{E,mp}}{\partial x^2} \tag{5.10}$$

The mass balance equation for CO_2 in gas phase, for counter-current plug flow, is:

$$-\frac{\partial\left(u_g \varepsilon_g C_{CO_2,g}\right)}{\partial z} = D_{CO_2,g}^{eff}\left.\frac{\partial C_{CO_2,m}^g}{\partial x}\right|_{x=0} a_v \tag{5.11}$$

Gas velocity axial gradient was evaluated via the overall mass balance equation of the gas phase:

$$-\frac{\partial}{\partial z}\left(u_g \varepsilon_g \frac{P_g}{RT_g}\right) = -k_g\left(C_{CO_2,g} - C_{CO_2,m}^g\Big|_{x=0}\right)a_v \tag{5.12}$$

The matching boundary conditions are:

$$z = H \qquad C_{CO_2,g}\Big|_{z=H} = C_{CO_2,g}^{in} \qquad u_g\Big|_{z=H} = u_g^{in} \tag{5.13}$$

5.3.2. Porous membrane scale model

When the enzyme is attached on the membrane surface and the membrane pores are partly wetted, the membrane scale model describes (i) the diffusion of CO_2 in the dry membrane region and (ii) the diffusion of CO_2 and uncatalyzed CO_2 absorption in the wetted membrane region. When CA enzyme is additionally immobilized inside the pores, the membrane scale model describes (i) the diffusion of CO_2 in the dry membrane and (ii) the diffusion of CO_2 and catalyzed/uncatalyzed CO_2 absorption in the wetted membrane (**Figure 5.4**). The membrane scale model describes only CO_2 diffusion when the membrane pores contain the gas phase.

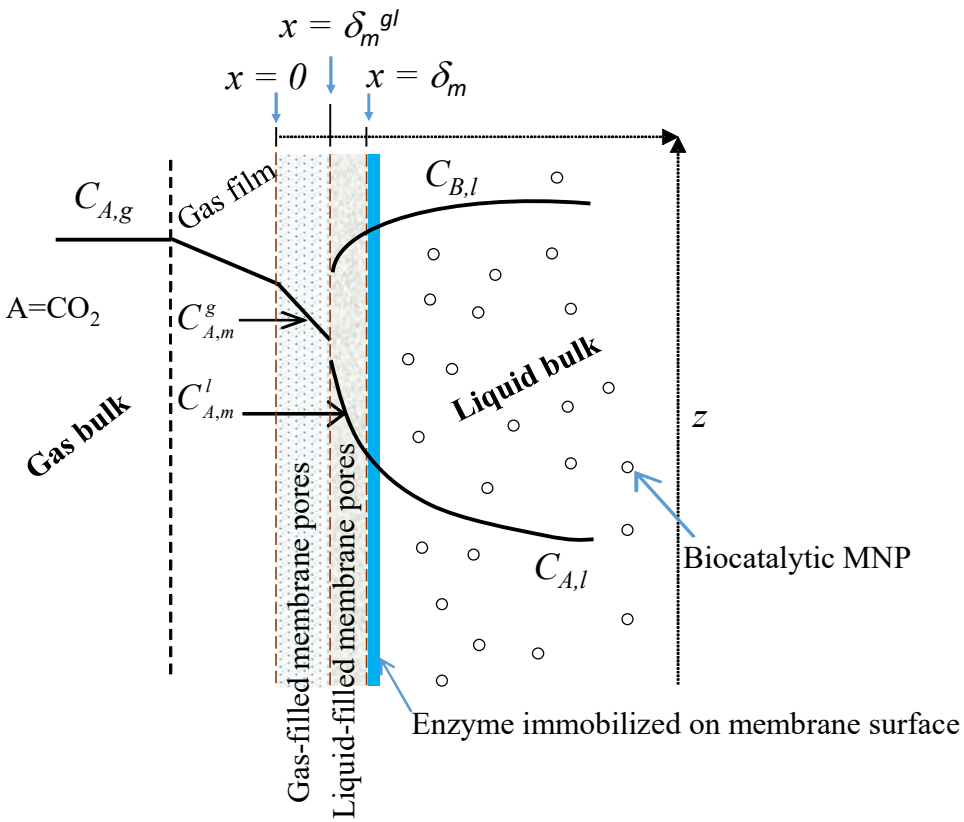

Figure 5.4. Schematic diagram of CO_2 absorption in FSMC (immobilized enzyme on membrane surface and inside the pores) - membrane partially liquid-filled pores

CA attached on the membrane surface - membrane pores partially wetted

Mass balance equations for CO_2 in the membrane dry/wetted regions and the matching boundary conditions are ($\delta_m^{g\ell}$ is positioned inside the membrane):

$$D^{eff}_{CO_2,g}\frac{\partial^2 C^g_{CO_2,m}}{\partial x^2}=0 \tag{5.14}$$

$$D^{eff}_{CO_2,\ell}\frac{\partial^2 C^\ell_{CO_2,m}}{\partial x^2}-R^{uc}_{CO_2}=0 \tag{5.15}$$

$$x=0 \qquad k_g\left(C_{CO_2,g}-C^g_{CO_2,m}\Big|_{x=0}\right)=-D^{eff}_{CO_2,g}\frac{\partial C^g_{CO_2,m}}{\partial x}\Bigg|_{x=0} \tag{5.16}$$

$$x=\delta_m^{g\ell} \qquad D^{eff}_{CO_2,g}\frac{\partial C^g_{CO_2,m}}{\partial x}\Bigg|_{x=\delta_m^{g\ell}}=D^{eff}_{CO_2,\ell}\frac{\partial C^\ell_{CO_2,m}}{\partial x}\Bigg|_{x=\delta_m^{g\ell}} \tag{5.17}$$

$$C^{g}_{CO_2,m}\Big|_{x=\delta_m^{g\ell}} = C^{\ell}_{CO_2,m}\Big|_{x=\delta_m^{g\ell}} \frac{1}{m} \tag{5.18}$$

$$x=\delta_m \qquad -D^{eff}_{CO_2,\ell}\frac{\partial C^{\ell}_{CO_2,m}}{\partial x}\bigg|_{x=\delta_m} = D_x \frac{\partial C_{CO_2,\ell}}{\partial x}\bigg|_{x=\delta_m} \tag{5.19}$$

Additionally, the mass balance equations for HCO_3^-, B, and BH^+ in the wetted membrane and the matching boundary conditions (which describe the non-volatility at the gas-liquid interface and the equality of molar fluxes at the limit of the wetted membrane area) are considered:

$$D^{eff}_{HCO_3^-,\ell}\frac{\partial^2 C^{\ell}_{HCO_3^-,m}}{\partial x^2} + R^{uc}_{CO_2} = 0 \tag{5.20}$$

$$D^{eff}_{j,\ell}\frac{\partial^2 C^{\ell}_{j,m}}{\partial x^2} = 0 \qquad \text{where } j=B,\ BH^+ \tag{5.21}$$

$$x=\delta_m^{g\ell} \qquad D^{eff}_{j,\ell}\frac{\partial C^{\ell}_{j,m}}{\partial r}\bigg|_{x=\delta_m^{g\ell}} = 0 \qquad \text{where } j=HCO_3^-,\ B \text{ and } BH^+ \tag{5.22}$$

$$x=\delta_m \qquad D^{eff}_{j,\ell}\frac{\partial C^{\ell}_{j,m}}{\partial x}\bigg|_{x=\delta_m} = -D_x \frac{\partial C_{j,\ell}}{\partial x}\bigg|_{x=\delta_m} \qquad \text{where } j=HCO_3^-,\ B \text{ and } BH^+ \tag{5.23}$$

When the porous structure is filled with gas, the membrane scale model only characterizes the diffusion of CO_2 in membrane: Eq. 5.14 with the boundary conditions 5.24-5.25:

$$x=0 \qquad k_g\left(C_{CO_2,g} - C^{g}_{CO_2,m}\Big|_{x=0}\right) = -D^{eff}_{CO_2,g}\frac{\partial C^{g}_{CO_2,m}}{\partial x}\bigg|_{x=0} \tag{5.24}$$

$$x=\delta_m \qquad D^{eff}_{CO_2,g}\frac{\partial C^{g}_{CO_2,m}}{\partial x}\bigg|_{x=\delta_m} = D_x \frac{\partial C_{CO_2,\ell}}{\partial x}\bigg|_{x=\delta_m} \tag{5.25}$$

CA immobilized on the membrane pores/surface - membrane pores partially wetted

When CA is attached on the membrane surface and inside the membrane porous structure, and the pores are partially wetted, Eqs. 5.15, 5.20 and 5.21 becomes:

$$D^{eff}_{CO_2,\ell}\frac{\partial^2 C^{\ell}_{CO_2,m}}{\partial x^2} - R^{uc}_{CO_2}\left(C^{\ell}_{j,m}\right) - R^{c}_{CO_2,m}\left(C^{\ell}_{j,m}\right)\frac{1}{\varepsilon_m} = 0 \tag{5.26}$$

$$D_{HCO_3^-,\ell}^{eff}\frac{\partial^2 C_{HCO_3^-,m}^{\ell}}{\partial x^2}+R_{CO_2}^{uc}\left(C_{j,m}^{\ell}\right)+R_{CO_2,m}^{c}\left(C_{j,m}^{\ell}\right)\frac{1}{\varepsilon_m}=0 \tag{5.27}$$

$$D_{B,\ell}^{eff}\frac{\partial^2 C_{B,m}^{\ell}}{\partial x^2}-R_{CO_2,m}^{c}\left(C_{j,m}^{\ell}\right)\frac{1}{\varepsilon_m}=0 \tag{5.28}$$

$$D_{BH^+,\ell}^{eff}\frac{\partial^2 C_{BH^+,m}^{\ell}}{\partial x^2}+R_{CO_2,m}^{c}\left(C_{j,m}^{\ell}\right)\frac{1}{\varepsilon_m}=0 \tag{5.29}$$

The corresponding boundary conditions are given by Eqs. 5.17-5.19, 5.22, 5.23.

5.3.3. Kinetics of CO_2 hydration

Quad Quad Iso Ping Pong mechanism with a transitory complex, rapid solvation in the enzyme binding cavity and competitive inter-molecular proton transfer with respect to buffer was used to describe the catalyzed (by human carbonic anhydrase II) CO_2 hydration [208]:

$$CO_2+ZnOH^-(E)\underset{k_{-1}}{\overset{k_1}{\rightleftarrows}}ZnHCO_3^-(ES) \tag{5.30}$$

$$H_2O+ZnHCO_3^-(ES)\underset{k_{-2}}{\overset{k_2}{\rightleftarrows}}HCO_3^-+ZnH_2O(E_W) \tag{5.31}$$

$$E_W\underset{k_{-3}}{\overset{k_3}{\rightleftarrows}}{}_H E \quad \text{(enzyme isomerization)} \tag{5.32}$$

$$B+ZnH_2O({}_H E)\underset{k_{-4}}{\overset{k_4}{\rightleftarrows}}BH^++ZnOH^-(E) \tag{5.33}$$

$$HCO_3^-+ZnH_2O({}_H E)\underset{k_{-5}}{\overset{k_5}{\rightleftarrows}}CO_2+H_2O+ZnOH^-(E) \tag{5.34}$$

The enzymatic reaction rate in the presence of solution-phase hCA II enzyme is [208]:

$$R_{CO_2}^{c}=\frac{k_h\left(C_{CO_2}C_B-\frac{K_{a2}}{K_{a1}}C_{HCO_3^-}C_{BH^+}\right)\left(1+\frac{C_{HCO_3^-}}{K_{iHCO_3^-,3}}\right)C_{E0}}{\left[\begin{array}{l}K_BC_{CO_2}+K_{CO_2}C_B+\frac{K_B}{2}\frac{K_E}{K_{a1}}C_{HCO_3^-}+2K_{CO_2}\frac{K_{a2}}{K_E}C_{BH^+}+C_{CO_2}C_B+2\frac{K_{CO_2}}{K_{HCO_3^-}}\frac{K_{a2}}{K_E}C_{HCO_3^-}C_{BH^+}+\frac{K_B}{K_{iHCO_3^-,1}}C_{CO_2}C_{HCO_3^-}\\+\frac{K_{CO_2}}{K_{iHCO_3^-,2}}C_BC_{HCO_3^-}+\frac{1}{2}\frac{K_B}{K_{iHCO_3^-,3}}\frac{K_E}{K_{a1}}\left(C_{HCO_3^-}\right)^2+\frac{K_B}{K_{iHCO_3^-,1}K_{iHCO_3^-,4}}C_{CO_2}\left(C_{HCO_3^-}\right)^2+\frac{1}{K_{iHCO_3^-,5}}C_{CO_2}C_BC_{HCO_3^-}\end{array}\right]} \tag{5.35}$$

The kinetic parameters were amended by Hanna et al. [7] in the case of CO_2 hydration with immobilized enzyme. Hydration/dehydration rate constants (k_h and k_d), bicarbonate inhibition

constants ($K_{iHCO_3^-,j}$) and binding constants (K_B, K_{CO_2} and $K_{HCO_3^-}$) are defined in Larachi [208] and Hanna et al. [7].

Uncatalyzed CO_2 hydration was described with Ho and Sturtevant [209] mechanism:

$$H_2O + CO_2 \underset{k_{13}}{\overset{k_{31}}{\rightleftharpoons}} H^+ + HCO_3^- \tag{5.36}$$

$$H^+ + HCO_3^- \underset{k_{21}}{\overset{k_{12}}{\rightleftharpoons}} H_2CO_3 \tag{5.37}$$

$$H_2O + CO_2 \underset{k_{23}}{\overset{k_{32}}{\rightleftharpoons}} H_2CO_3 \tag{5.38}$$

The uncatalyzed CO_2 hydration reaction rate is:

$$R_{CO_2}^{uncat}\Big|_{\ell} = k_{31}^{'} C_{CO_2} - k_{13}^{'} C_{H^+} C_{HCO_3^-} \quad \text{where } k_{31}^{'} = k_{31} + k_{32};\ k_{13}^{'} = k_{13} + k_{23} / K_{H_2CO_3} \tag{5.39}$$

The rate constants are (25°C): $k_{31}^{'} = 0.037 \text{s}^{-1}$; $k_{13}^{'} = 5.5 \times 10^4 \text{m}^3 / kmol_l\, s$ [209].

5.4. Results and discussion

5.4.1. Characterisation tests of biocatalytic membranes and biocatalytic MNPs

Figure 5.5 shows the SEM images of outer surface morphologies of the pristine PP membranes and biocatalytic membranes. The virgin PP membranes had smooth and plentiful pores, as presented in **Figures 5.5**a. After co-deposition of PDA/PEI on the membranes surface, a homogeneous layer with less observable pores was formed on the surface (**Figure 5.5**b) [129]. This layer reduced the pore size of membranes (from 0.23 to 0.084 μm), so that the breakthrough pressure of biocatalytic membrane (immobilized enzyme loading of 0.042 mg/cm^2) with water enhanced from 3.2 bar (for virgin PP membrane) to 3.5 bar. This enhancement of breakthrough pressure is favorable for pore wetting reduction within the membranes during the absorption process [46, 137]. The pore narrowing by the coating layer, which could be regarded as a "fouling layer" [138], could increase the membrane resistance during the absorption process. However, the contact angle of water on biocatalytic membranes declined from 131° (for virgin PP membranes) to 78°, as displayed in **Figure 5.6.** This diminution of contact angle is consistent with the hydrophilic properties of PDA/PEI coating layer on the surface of biocatalytic membranes [52, 234] and to the filling of the surface valleys by immobilized enzymes [138]. Therefore, on one side, the pore size

reduction of biocatalytic membrane enhances the breakthrough pressure and on the other side, the membrane surface hydrophilicity decreases the breakthrough pressure, which is consistent with the small increase of the breakthrough pressure after enzyme immobilization.

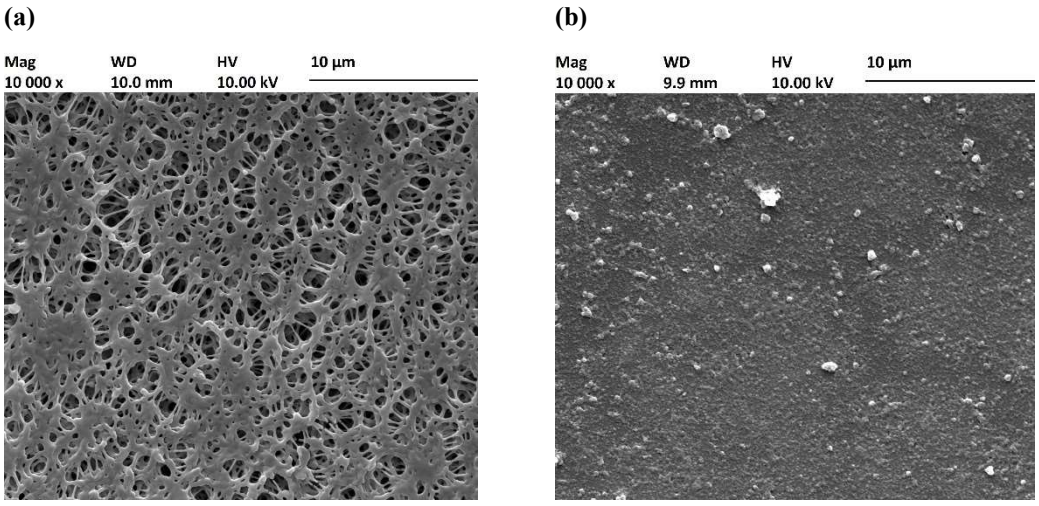

Figure 5.5. SEM images of outer surface morphologies of (a) pristine PP membrane, and (b) biocatalytic membrane.

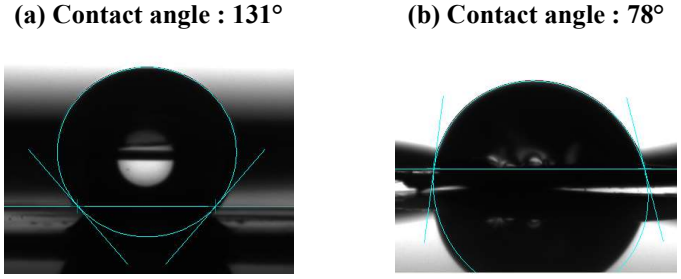

Figure 5.6. Contact angle display for: (a) the virgin membrane, and (b) the biocatalytic membrane.

TEM images of bare MNPs and the biocatalytic MNPs are illustrated in **Figure 5.7**. After CA enzyme immobilization, particle size of MNPs increased from 10.6 to 19.4 nm due to the addition of deposition layers and immobilized CA enzymes[58].

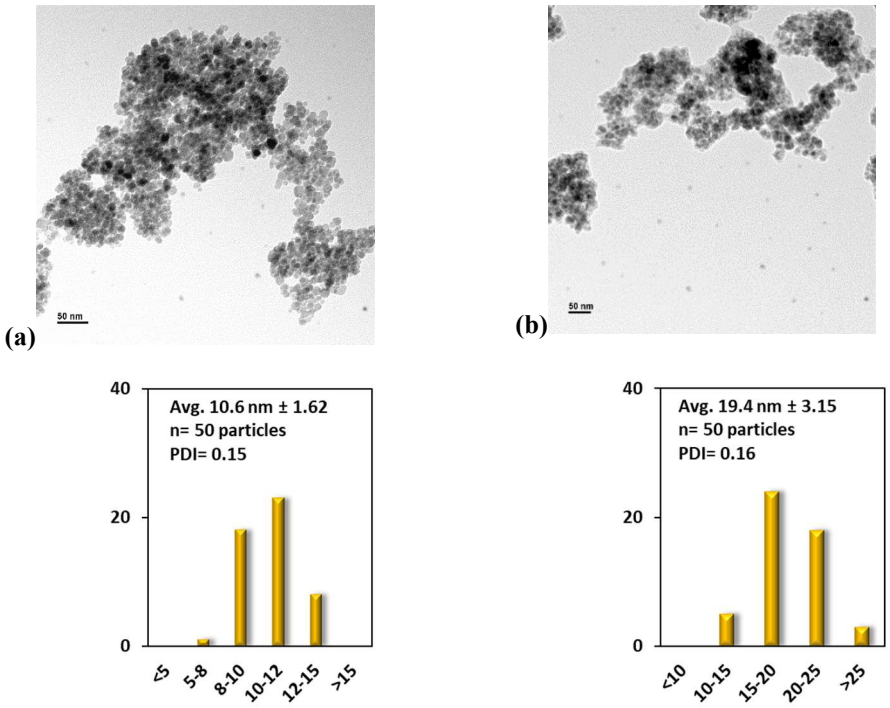

Figure 5.7. TEM images of (a) MNPs and (b) biocatalytic MNPs, (PDI: Polydispersion index).

5.4.2. CO_2 absorption performance of the intensified membrane contactor

Biocatalytic membranes with different immobilized CA enzyme loading were developed and then integrated into the gas-liquid membrane contactor operated with a 34 ml/min liquid flow rate, a 100 ml/min gas flow rate, a 100 mM Tris buffer solution, 15% inlet gas CO_2 concentration and counter-current flow. The impact of CA enzyme concentration in FSMC bioreactor (CA enzyme immobilized on the membranes surface) on bioreactor performance is illustrated in **Figure 5.8**. As shown in this figure, the enhancement of CA concentration in bioreactor (in the range: 6.49- 65.44 mg/$L_{reactor}$) ameliorated the CO_2 hydration rate [87, 89, 123]. It should be noted that the increase of CA enzyme concentration over 19.49 mg/$L_{reactor}$ up to 65.44 mg/$L_{reactor}$ (337% increase in total CA enzyme concentration) only led to a marginal boost of the CO_2 absorption rate in the bioreactor by about 3%. Such an observation illustrates that at large CA enzyme loading on the membrane surface, the CO_2 hydration process is limited by high internal/external diffusional limitations. High diffusional limitations reduce the mass transfer coefficient and avoid taking full advantage of the CA enzyme's high turnover number. Similar observations can be found in other works using large CA enzyme loading on the membrane surfaces [46, 97, 249].

In addition, **Figure 5.8** illustrates the theoretical CO_2 hydration process performance when the membrane pores are partly wetted by the liquid phase. The enzymatic hydration in wetted pores was artificially enforced assuming that CA enzyme is also immobilized in the surface pores of the membrane (as suggested in sub-section 4.1). The figure shows the ability of the model to capture the impact of the enzyme loading on the bioreactor performance when a low membrane wetting was considered. Thus, the resistance to mass transfer in the membrane wetted zones is overcame by the enzymatic hydration catalyzed by the enzyme attached in this membrane zone (as suggested in the sub-section 4.1). Also, it is possible that the CO_2 absorption process catalyzed by the biocatalytic MNPs may help to overcome the resistance to mass transfer in the wetted membrane. The model underestimates the experimental data regarding the absorption rate of CO_2 vs. CA enzyme loading when the porous structure of the membrane is considered to be completely gas-filled (not shown).

Figure 5.8 shows a reduction of CO_2 absorption rate from 6.97 $\times 10^{-5}$ mol/min to 5.3 $\times 10^{-5}$ mol/min when CA enzyme loading in FSMC bioreactor decreases from 34.81 mg/$L_{reactor}$ to 6.49 mg/$L_{reactor}$.

However, as shown in **Figure 5.9**, this 32% reduction of the CO_2 absorption rate was approximately compensated with the addition of a CA enzyme loading of 5.39 mg/$L_{reactor}$ in the FSMC bioreactor via biocatalytic MNPs. This extra amount of CA enzyme provided by biocatalytic MNPs represents only an 83% increase (instead of 5.4 times) in total CA enzyme loading in FSMC bioreactor, considering an enzyme loading of 6.49 mg/$L_{reactor}$ on membrane surface. Also, an additional CA enzyme loading of 2.5 mg/$L_{reactor}$ provided by the immobilization of the enzyme on the MNPs surface, which represented only a 38% elevation in total enzyme concentration (as regards the same level of 6.49 mg/$L_{reactor}$), generates an increase of CO_2 absorption rate of 21% (6.38 $\times 10^{-5}$ mol/min, **Figure 5.9**).

CA enzyme immobilization on MNPs surface promotes the CO_2 hydration process in intensified membrane bioreactor [160, 184] because the biocatalytic MNPs dispersed in the liquid phase operate as a free solution-phase CA enzyme in the liquid phase, increasing the CO_2 absorption rate significantly. Consequently, with this hybrid enzymatic process, CO_2 absorption rate in FSMC bioreactor is considerably promoted, while total required amount of CA enzyme in bioreactor is reduced. **Figure 5.9** further illustrates that even with a little

amount of CA enzyme immobilized on MNPs, membrane contactor with bare membrane and biocatalytic MNPs operates efficiently.

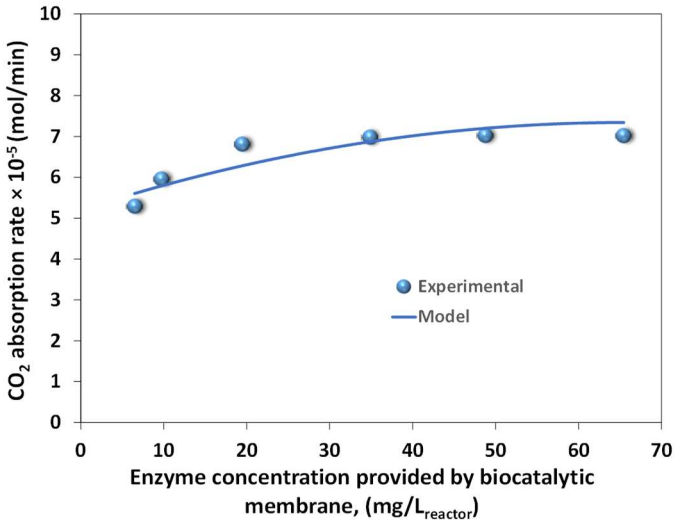

Figure 5.8. Impact of enzyme loading (provided by biocatalytic membranes) on FSMC performance (100 mM Tris buffer, inlet gas CO_2 concentration: 15%, liquid flow rate: 34 ml/min (Re_L = 31.6), gas flow rate: 100 ml/min (Re_G = 6), and counter-current flow).

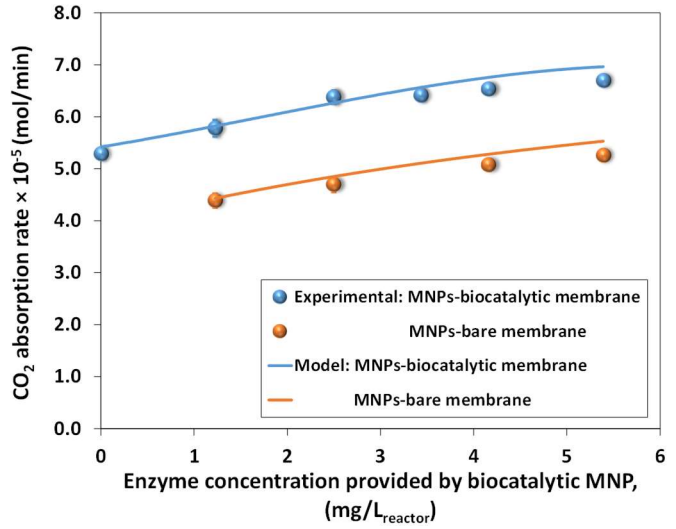

Figure 5.9. Impact of enzyme loading (provided by biocatalytic MNPs) on intensified membrane contactor performance (enzyme loading immobilized on membrane surface = 6.49 mg/Lreactor (MNPs-biocatalytic membrane) or 0 mg/Lreactor (MNPs-bare membrane), 100 mM Tris buffer, inlet gas CO_2 concentration: 15%, liquid flow rate: 34 ml/min (ReL = 31.6), gas flow rate: 100 ml/min (ReG = 6), and counter-current flow).

Besides, this hybrid enzymatic process is beneficial to attain high CO_2 absorption rates, even if a component of the enzymatic system, either the biocatalytic membrane or biocatalytic MNPs, does not work appropriately. In the following sections, CO_2 hydration rate of the intensified membrane contactor (FSMC-MNP, CA enzyme immobilized on membrane and MNPs surface) is compared to the FSMC bioreactor (CA enzyme immobilized on membrane surface) under various operating circumstances.

5.4.2.1. Impact of buffer concentration and type on intensified membrane contactor performance

Buffer type and concentration would impose a significant effect on the overall efficiency of the membrane contactor. In terms of the buffer concentration, higher concentration values effectively promote the CO_2 hydration reaction in counter-current membrane bioreactors (FSMC and FSMC-MNP, **Figure 5.10**) due to the larger inter-molecular proton transfer [11, 19, 152]. When the buffer concentration is low, inter-molecular transfer is a rate-limiting step in the CO_2 hydration process, resulting in a drop in the rate of the enzymatic reaction. CO_2 hydration process increases remarkably in the intensified membrane contactor with the CA enzyme on the membrane and MNPs surfaces, especially at greater buffer concentrations.

Different buffers with distinct pK_{a2} constants (*N*-methylimidazole, Tris and AMPD with pK_{a2} constants of 7.19, 8.07, 8.83, repectively) were employed to assess the performance of CO_2 hydration process in membrane bioreactors: FSMC and FSMC-MNP. **Figure 5.11** shows higher CO_2 absorption rates in both biocatalytic systems at larger pK_{a2} constant of buffer [11], providing the greater driving force of the CO_2 hydration process and improving the mass transfer coefficient on the liquid side [11, 196]. The CO_2 hydration process is greatly accelerated by intensified membrane contactor with the CA enzyme immobilized on both the membrane and MNPs surfaces.

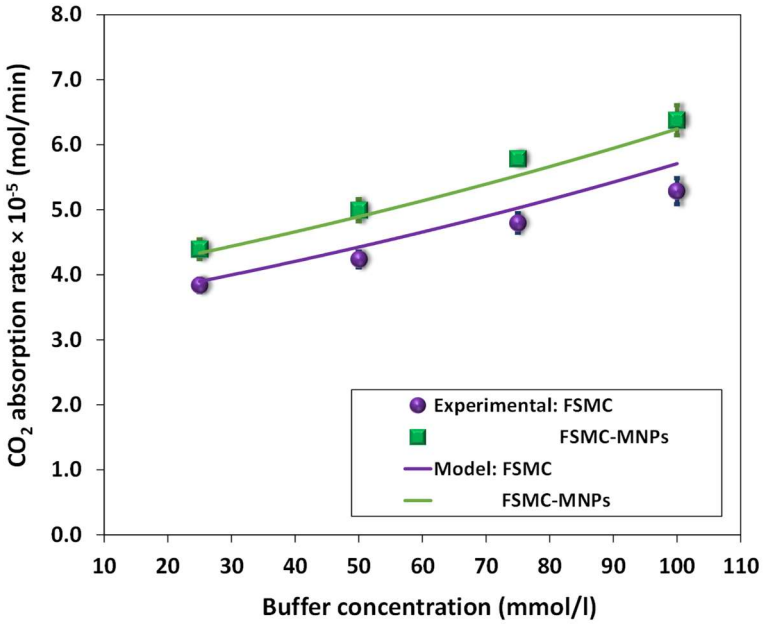

Figure 5.10. Impact of buffer concentration on intensified membrane contactor performance (enzyme loading immobilized on membrane surface = 6.49 mg/$L_{reactor}$, enzyme loading immobilized on MNPs surface = 2.5 mg/$L_{reactor}$, Tris buffer, inlet gas CO_2 concentration: 15%, liquid flow rate: 34 ml/min (Re_L = 31.6), gas flow rate: 100 ml/min (Re_G = 6), and counter-current flow).

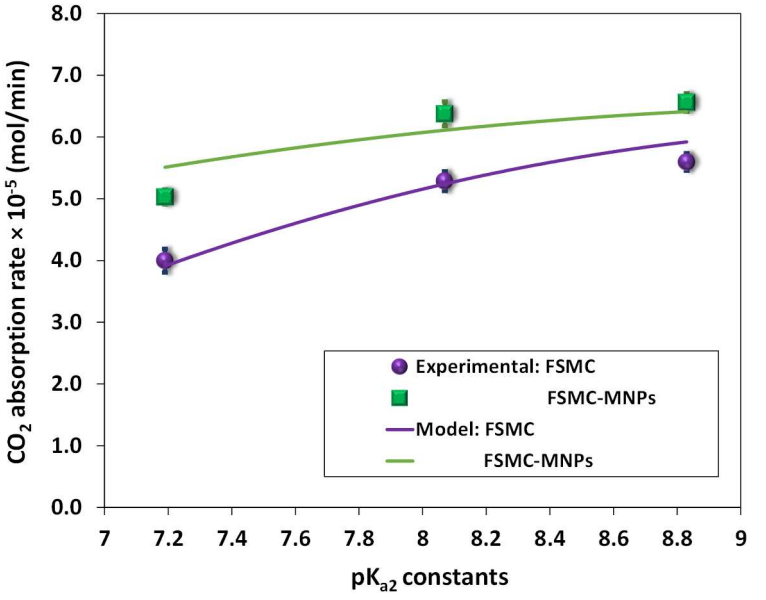

Figure 5.11. Impact of buffer type on intensified membrane contactor performance (enzyme loading immobilized on membrane surface = 6.49 mg/$L_{reactor}$, enzyme loading immobilized on MNPs surface = 2.5 mg/$L_{reactor}$, 100 mM buffer, inlet gas CO_2 concentration: 15%, liquid flow rate: 34 ml/min (Re_L = 31.6), gas flow rate: 100 ml/min (Re_G = 6), and counter-current flow).

With the enzymatic CO_2 hydration in the wetted membrane zone (1% membrane wetting), the model is capable to estimate the impact of buffer concentration and type on the bioreactor performances (**Figures 5.10 and 5.11**). This means that the resistance to mass transfer in the membrane wetted structure is overcame by the hydration of CO_2 (with the condition that CA enzyme is also immobilized in this membrane area). Impact of operational parameters on intensified membrane contactor performance

5.4.2.2. Impact of operational parameters on intensified membrane contactor performance

Figure 5.12 presents the CO_2 absorption rate of the counter-current immobilized enzyme-based membrane contactors under different absorbent flow rates. As shown in **Figure 5.12**, for both biocatalytic membrane contactors, the CO_2 absorption rate increases when the absorbent flow rate enhances from 15 to 34 ml/min. These results indicate that the great resistance is found in the liquid phase, where the CO_2 absorption occurs. This could be attributed to the decrease in thickness of liquid boundary layer at high flow rates which increases mass transfer coefficients [219, 261, 262]. Therefore, an increase in absorbent flow rate allows a sufficient amount of absorbent to flow through the gas-liquid boundary, enhancing the CO_2 absorption rate [263], particularly in the membrane bioreactor with immobilized CA enzyme on the membrane and MNPs surfaces. Furthermore, at a higher liquid flow rate, the intermolecular transfer step of enzymatic CO_2 hydration process enhances due to the higher transfer of the buffer, elevating the CO_2 hydration performance [11].

Moreover, in order to evaluate the impact of gas phase flow rate on the absorption process in the biocatalytic membrane contactors, CO_2 absorption rate was measured at different gas flow rates from 100 to 200 ml/min. **Figure 5.13** displayes that for both immobilized enzymatic systems, there is a slight growth in the rate of CO_2 absorption because of the small amplitude of gas flow rate. Gas-liquid mass transfer enhances with the increase of gas flow rate due to the decrease in the thickness of stagnant diffusion layer [262, 264]. However, the absorption rate is only slightly influenced by the gas phase flow rates because of the minor mass transfer resistance in the gas phase [242].

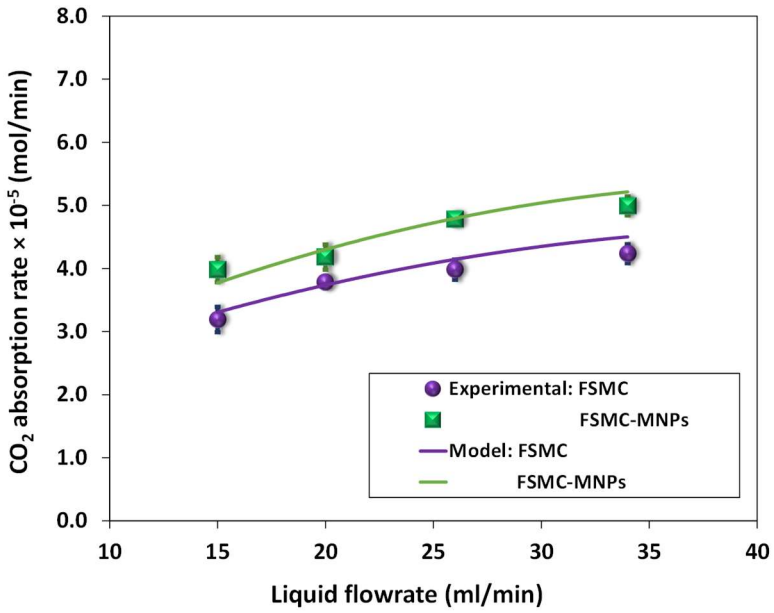

Figure 5.12. Impact of liquid flow rate (Re_L = 13.9 to 31.6) on intensified membrane contactor performance (enzyme loading immobilized on membrane surface = 6.49 mg/$L_{reactor}$, enzyme loading immobilized on MNPs surface = 2.5 mg/$L_{reactor}$, 50 mM Tris buffer, inlet gas CO_2 concentration: 15%, gas flow rate: 100 ml/min (Re_G = 6), and counter-current flow).

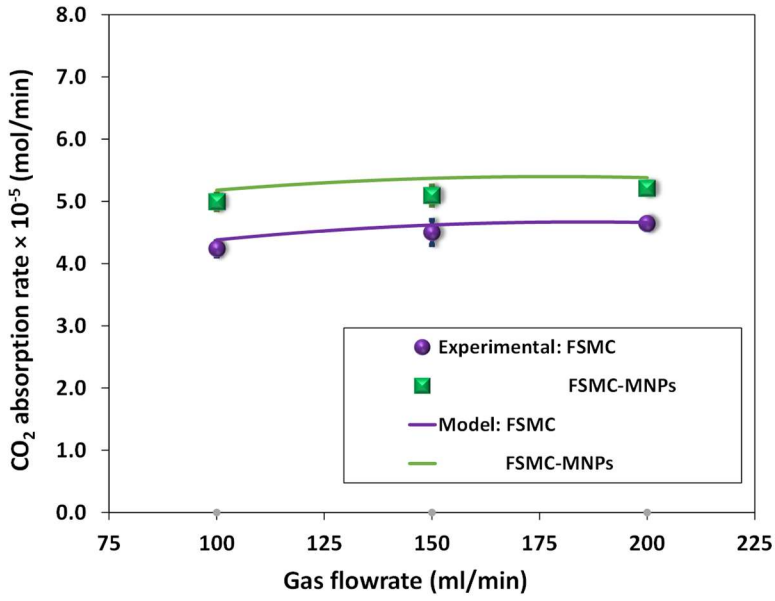

Figure 5.13. Impact of gas flow rate (Re_G = 6 to 12) on intensified membrane contactor performance (enzyme loading immobilized on membrane surface = 6.49 mg/$L_{reactor}$, enzyme loading immobilized on MNPs surface = 2.5 mg/$L_{reactor}$, 100 mM Tris buffer, inlet gas CO_2 percentage: 15%, liquid flow rate: 34 ml/min (Re_L = 31.6), and counter-current flow).

The model underestimates the experimental data regarding the absorption rate of CO_2 relative to the absorbent/gas flow rate when the porous structure of the membrane is considered to be completely gas-filled (not shown). However, with the enzymatic CO_2 hydration in the wetted membrane zone (1% membrane wetting), the model is in very good agreement with experimental data for the two biocatalytic membrane contactors (**Figures 5.12 and 5.13**). This means that the resistance to mass transfer in this region is overcame by the hydration of CO_2 in the wetted porous structure (with the condition that CA enzyme is also immobilized in this membrane zone). In addition, it is possible that CO_2 absorption generated by biocatalytic MNPs may help to overcome the resistance to mass transfer in the wetted membrane.

CO_2 absorption rate in the membrane contactors with CA enzyme immobilized on only membrane surface and CA enzyme immobilized on both membrane and MNPs surfaces was determined with 10, 15 and 20% inlet CO_2 concentration, as depicted in **Figure 5.14**. Due to the greater driving force in the gas phase, CO_2 absorption rate promotes with increase of inlet CO_2 concentration [153].

Figure 5.12, **5.13** and **5.14** demonstrates the improvement of the CO_2 absorption process in intensified membrane contator with CA enzyme immobilized on membrane and MNPs surfaces, highlighting the compelling characteristics of the proposed hybrid enymatic process for green CO_2 capture.

5.4.3. Stability and reusability of intensified membrane contactor

The intensified membrane contactor was operated for several hours to investigate the stability of CO_2 absorption rate. A very stable CO_2 absorption rate (no sign of declining) was attained in the current intensified membrane contactor with 34 ml/min liquid flow rate, 100 ml/min gas flow rate, 50 mM Tris buffer in water, 15% inlet gas CO_2 percentage and counter-current flow, as illustrated in **Figure 5.15**.

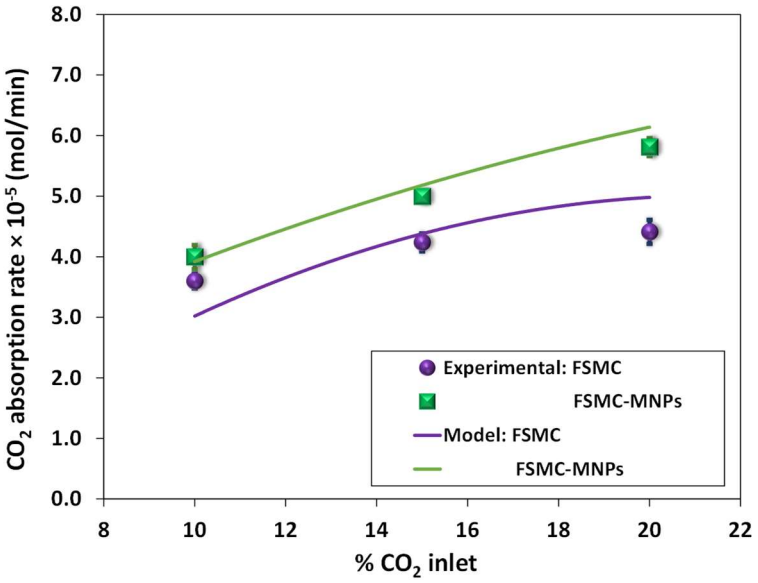

Figure 5.14. Impact of inlet gas CO_2 concentration on intensified membrane contactor performance (enzyme loading immobilized on membrane surface = 6.49 mg/$L_{reactor}$, enzyme loading immobilized on MNPs surface = 2.5 mg/$L_{reactor}$, 100 mM Tris buffer, liquid flow rate: 34 ml/min (Re_L = 31.6), gas flow rate: 100 ml/min (Re_G = 6), and counter-current flow).

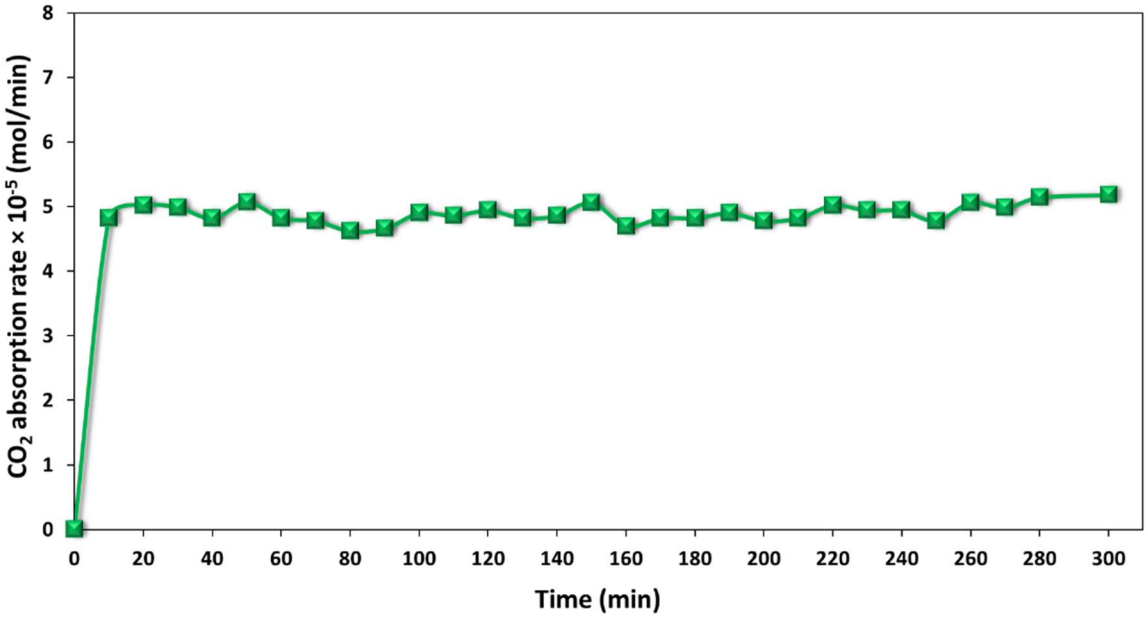

Figure 5.15. Stability test of intensified membrane contactor (enzyme loading immobilized on membrane surface = 6.49 mg/$L_{reactor}$, enzyme loading immobilized on MNPs surface = 2.5 mg/$L_{reactor}$, 50 mM Tris buffer, inlet gas CO_2 percentage: 15%, liquid flow rate: 34 ml/min (Re_L = 31.6), gas flow rate: 100 ml/min (Re_G = 6), and counter-current flow).

The reuse of enzymes immobilized on membrane surfaces and MNPs during CO_2 hydration tests was evaluated in the intensified membrane contactor. In this work, 10 cycles of CO_2 hydration were conducted and according to **Figure 5.16**, the enzymes immobilized on the membrane and MNPs surfaces presents an excellent reusability, preserving the original CO_2 hydration activity even after 10 cycles of reuse. The result is in good agreement with other studies of the literature [46].

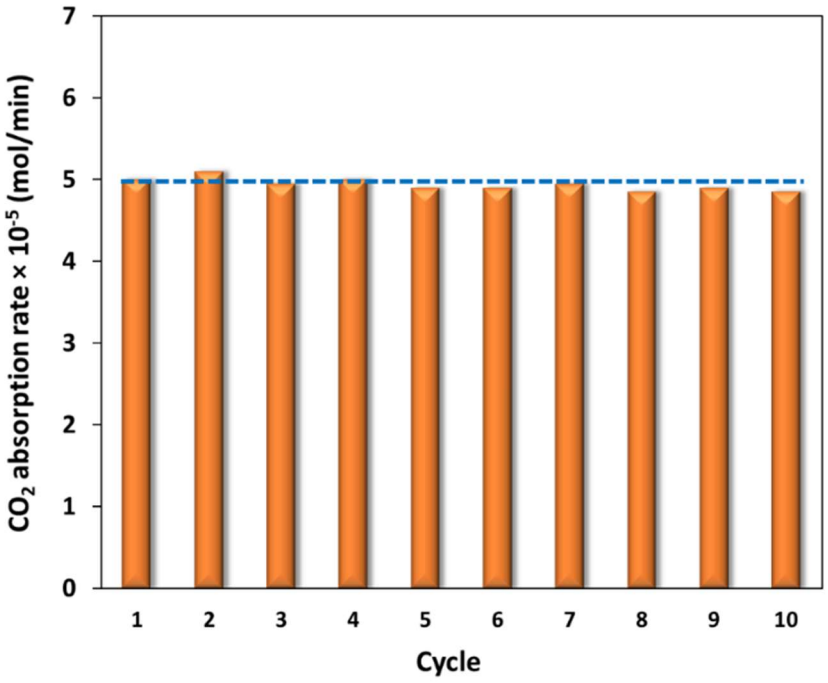

Figure 5.16. Reusability of the enzyme in intensified membrane contactor (enzyme loading immobilized on membrane surface = 6.49 mg/$L_{reactor}$, enzyme loading immobilized on MNPs surface = 2.5 mg/$L_{reactor}$, 50 mM Tris buffer, inlet gas CO_2 percentage: 15%, liquid flow rate: 34 ml/min (Re_L = 31.6), gas flow rate: 100 ml/min (Re_G = 6), and counter-current flow).

5.4.4. CO_2 absorption performance of intensified membrane contactor compared to the performance of other membrane contactors

CO_2 absorption performance of different membrane contactors is summarized in **Table 5.2** (few works have used CA enzyme in gas-liquid membrane contactors [46, 97, 265]). Compared to FSMC using CA immobilized on the membrane surface and inside the pores (enzyme loading = 48.8 mg/$L_{reactor}$), the intensified membrane contactor of the present work

exhibits a similar CO_2 absorption performance, with an overall mass transfer coefficient of 4.4 $\times 10^{-5}$ m/s, but using a much lower CA enzyme loading (12.0 mg/$L_{reactor}$). Xu et al. [97] immobilized the CA enzyme on the surface of PVDF membrane at a loading of 210 mg/L in a hollow fiber membrane contactor and obtained a overall mass transfer coefficient of 6.12 $\times 10^{-5}$ m/s at high liquid velocity (0.25 m/s, much greater than the present work - 0.002 m/s). The rate of CO_2 absorption increases significantly in the systems working at high liquid velocity, as in the case of Xu et al. [97], due to the boost of mass transfer coefficients [219, 261, 262]. The overall mass transfer coefficient obtained in the work of Xu et al. [97] was higher than ours due to more favorable conditions. The operational conditions such as gas velocity (not mentioned) must be considered in the comparison because of the high impact on the performance of the absorption process. The overall mass transfer coefficient obtained in present work is higher than the one obtained in a flat sheet membrane contactor operating with 200 mg/L CA immobilized on nanoparticles dispersed in liquid phase [46]. Also, the liquid flow rate and CA enzyme loading were respectively 10 and 20 times higher than ours.

It should be noted that the intensified membrane contactor of the present work attains a larger overall mass transfer coefficient than some membrane contactors using 1 M 2-amino-2-methyl-1-propanol (AMP), 5 wt% MEA, 1 M dimethylamine or 0.5 M aqueous NaOH (**Table 5.2**) [238, 239, 266, 267]. Furthermore, the performance of intensified membrane contactor of this work is at the same level with the performance of some PVDF and PP membrane contactors using 2 M diethanolamine (DEA) [173, 221].

The intensified membrane contactor shows a competitive CO_2 absorption compared to traditional membrane contactors using amine-based absorbents or aqueous NaOH. Moreover, our work focused on capturing a dilute CO_2 feed (10-20%), which makes capture more difficult [25], but the amount of CO_2 absorption rate was outstanding compared to the studies that used pure CO_2 as feed gas. The present work clearly reveals that a high-efficient CO_2 capture is obtained in an intensified membrane contactor using immobilized CA enzyme on membrane and MNPs surfaces, which decreases the total amount of CA enzyme required in the reactor while maximizing the employment of enzyme's high turnover number.

Table 5.2. CO_2 absorption comparison in various membrane contactors.

Membrane material/ type*	**Modification layer on membrane**	**Absorbent**	**Feed gas**	**Liquid velocity (m/s)/ flow rate (ml/min)**	**Overall mass transfer coefficient ($\times 10^{-5}$ m/s)**	**Ref.**
PP/FS	PDA/PEI/CA (6.49 mg/$L_{reactor}$ CA enzyme)	Water and 100 mM buffer with 5.4 mg/$L_{reactor}$ CA immobilized on MNPs	15% CO_2	34 ml/min (Re_L = 31.6)	4.40	Current work
PP/FS	PDA/PEI/CA (48.8 mg/$L_{reactor}$ CA enzyme)	Water and 100 mM buffer	15% CO_2	32 ml/min	4.89	Chapter 4
PVDF/HF	PDA/PEI/CA (210 mg/L CA loading conc.)	Water	Pure CO_2	0.25 m/s	6.12	[97]
PP/FS	Fluorinated TiO_2	Water and 100 mM buffer with 200 mg/L CA immobilized on TiO_2 nanoparticles	20% CO_2	300 ml/min	3.67	[46]
PP/PVDF/FS	-	30% MDEA with 10 g/L CA	15% CO_2	NA**	0.86	[265]
PVDF/FS	Silica coating	1 M dimethylamine	Pure CO_2	100 ml/min	0.69	[238]
PVDF/FS	Silica coating	1 M 2-amino-2-methyl-1-propanol (AMP)	Pure CO_2	100 ml/min	0.54	[238]
PVDF/FS	Plasma treatment	1 M AMP	15% CO_2	100 ml/min	1.63	[266]

PP/HF	-	5 wt% MEA	12.5 % CO_2	50 ml/min	1.0	[267]
PP/HF	-	2 M DEA	20% CO_2	0.12 m/s	3.67	[173]
PP/HF	-	2 M DEA	20% CO_2	0.15 m/s	3.67	[221]
PVDF/FS	-	0.5 M aqueous NaOH	10% CO_2	10 ml/min	0.37	[239]
PP/HF	-	Silica nanofluid in water	15% CO_2	267 ml/min	0.69	[268]
Polyetherimide (PEI)/HF	Silicon rubber coating	Water	Pure CO_2	0.02 m/s	0.49	[269]
PEI/HF	Heat treated at 80 °C	Water	Pure CO_2	0.1 m/s	0.44	[270]
PVDF/HF	-	Water	Pure CO_2	0.25 m/s	0.49	[271]
PTFE/FS	-	23 wt% 2-amino-2-hydroxymethyl-1,3-propanediol (AHPD) and 7 wt% Piperazine (Pz)	20% CO_2	20 ml/min	14.31	[225]

*** FS: Flat Sheet, and HF: Hollow Fiber**

**** NA: Not available**

5.5. Conclusion

Membrane contactors with CA enzyme immobilized on the membrane surface exhibit insufficient mass transfer (high diffusional limitation) to fully exploit the enzyme's high turnover frequency. The dispersion of biocatalytic MNPs in the liquid phase effectively enhances the CO_2 hydration process because CA enzyme attached on MNPs works as a free solution-phase enzyme in the liquid phase and catalyzes immediately the CO_2 hydration

reaction. Thus, a novel hybrid enzymatic process was proposed in this work with CA enzyme immobilized on both membrane and MNPs surfaces in a gas-liquid flat sheet membrane contactor. The promotion of CO_2 hydration process via addition of biocatalytic MNPs was more important in the membrane contactors with lower loadings of CA enzyme on membrane surface (reduced total CA enzyme loading in membrane bioreactor). The hybrid enzymatic process is beneficial to attain high CO_2 absorption rates, even if a component of the enzymatic system, either the biocatalytic membrane or biocatalytic MNPs, does not operate appropriately.

A gentle boost of CA enzyme loading on biocatalytic MNPs considerably improved the CO_2 absorption process in intensified FSMC-MNP bioreactor, outperforming the FSMC bioreactor with CA enzyme immobilized only on membrane surface. The feasibility of utilizing such a biocatalytic system for practical application was demonstrated by exposing the contactor to a range of different experimental circumstances. Finally, the performance of CO_2 absorption process in the intensified membrane contactor was ameliorated at larger buffer concentration, higher pKa_2 values, and enhancement of liquid flow rate, gas flow rate and CO_2 inlet concentration. Note that the intensified membrane contactor displayed a stable CO_2 hydration rate for several hours. Furthermore, high CO_2 absorption rate even after 10 cycles was attained with the intensified membrane contactor which depicted the excellent reusability of immobilized CA.

The multiscale mathematical model (developed under gas-filled or partially liquid-filled membrane pores conditions), proposed to explore the behaviour of the membrane bioreactors, underestimated the experimental data when the porous structure of the membrane is considered to be completely gas-filled. However, with the enzymatic CO_2 hydration in the wetted membrane zone (1% membrane wetting), the model was in very good agreement with experimental data for the two biocatalytic membrane contactors. This means that the resistance to mass transfer in this region was overcame by the absorption of CO_2 in the wetted porous structure (when CA enzyme is immobilized in this membrane zone) and possible by the absorption of CO_2 in the presence of biocatalytic MNPs.

This is the first study about the performance of membrane contactors with immobilized hCA II enzyme on the membrane surface, improved by the incorporation of an additional hCA II

enzyme via immobilization on MNPs surface in the liquid absorbent. This novel intensified biocatalytic membrane contactor expands the degree of utilization of the CA enzyme's high hydration turnover and has significant potential for green capture of CO_2.

General conclusions and future outlook

1. General conclusions

Considering the growing interest for the enzymatic CO_2 capture technologies using CA II (CA) enzyme, the present thesis dealt with the development of efficient biocatalytic materials with immobilized CA enzyme for green CO_2 capture. The developed materials were completely characterized by different techniques, including XRD, SEM, FTIR, TEM, nitrogen adsorption-desorption, contact angle and breakthrough pressure measurements. Additionally, the developed materials were integrated in CO_2 absorption bioreactors (packed-bed column and flat sheet membrane contactors) and their impact on CO_2 absorption performance was evaluated. The influence of various parameters such as buffer type and concentration, liquid and gas flow rates, flow orientation, liquid temperature, and inlet CO_2 concentration on the bioreactors performance was thoroughly analyzed.

The summary of this thesis is outlined as follows:

(1) An improved CA immobilization technique was developed in this work using two steps: co-deposition and covalent bonding. The co-deposition of PDA/PEI with amino functional groups was first employed for amine-functionalization of the support surfaces. The enzyme was then immobilized covalently on the aminated surfaces using glutaraldehyde. The proposed immobilization approach is appealing because of its simplicity, abundant amine functionalities of PEI, and great adhesion capacity of PDA on surface during surface functionalization process, as well as the stability and reusability of immobilized enzyme via covalent bonding.

(2) An enhanced CO_2 absorption rate was attained in packed-bed column reactors via an innovative hybrid enzymatic process where CA was immobilized on the packing and MNPs dispersed in the liquid phase. The packing and MNPs surface were amine-functionalized by co-deposition of PDA/PEI and then, CA was immobilized on the modified surface via glutaraldehyde. The immobilized CA on packing and MNPs showed remarkable stability (preserved 84.7% of initial activity) and the CO_2 hydration process improved greatly because the enzyme immobilized on MNPs acts as a free solution-phase enzyme.

(3) Co-deposition of PDA/PEI approach was employed for amine functionalization of the membrane surface and CA was then immobilized with glutaraldehyde on the modified membrane surface to develop a biocatalytic membrane. Optimum conditions of immobilization process were thoroughly investigated (deposition time: 7 h, PDA/PEI ratio: 2/2, glutaraldehyde concentration: 1.0 (v/v)%, CA concentration: 0.2 mg/ml, immobilization time: 32 h, and pH of enzyme solution: 6.0) to obtain the highest immobilized enzyme activity of biocatalytic membrane. The biocatalytic membrane showed good storage stability (immobilized CA preserved 82.3% of its original activity after 40 days) and a high CO_2 absorption flux of 0.29×10^{-3} mol/m^{2}s was obtained in a flat sheet membrane contactor. The enzymatic CO_2 hydration process in the partially wetted porous structure overcame the resistance to mass transfer in this region, resulting in improved contactor performance.

(4) The performance of the CO_2 hydration process was further improved in an intensified biocatalytic membrane contactor by incorporating additional CA immobilized on MNPs, which act as a free solution-phase enzyme. This improvement was more significant for lower CA loading on membrane surface (enzyme loading immobilized on membrane surface: 6.49 mg/$L_{reactor}$), resulting in a less total amount of enzyme in the membrane bioreactor (12.0 mg/$L_{reactor}$). Furthermore, good stability and high reusability of immobilized CA for CO_2 hydration rate were achieved. The findings illustrated that enzymatic CO_2 absorption rate in the wetted porous structure of membrane (1% membrane wetting) and in the presence of biocatalytic MNPs overcame the mass transfer resistance.

Overall, the results of this thesis confirmed that the employment of immobilized CA enzyme for CO_2 absorption in bioreactors (packed-bed column and flat sheet membrane contactor) are promising and competitive candidates for green capture processes. Enzyme-based CO_2 capture processes open new avenues for making CO_2 capture systems more cost-effective and allowing for further commercialization of technologies that decrease CO_2 emissions and contribute to climate change reduction. The investigated processes meet the requirements of green technology because (i) CA enzyme is non-toxic and biodegradable, (ii) the absorbent is water (iii), and the process operates at atmospheric pressure and ambient temperature.

2. Future outlooks

The fundamental aspects related to enzyme immobilization and enzymatic CO_2 capture technologies that could be carried out in further research have been addressed in the following:

- Designing effective immobilization techniques to maintain enzyme activity and stability in long-time applications has a lot of potential to investigate. It would be of interest to create new cost-effective immobilization techniques and improve the immobilization process design, since this subject plays an important role in the widespread use of biomimetic CCS.
- Another critical element that should be investigated further is the development of low-cost and high-efficient immobilization support materials. The most attractive support materials are with characteristics including high mechanical and chemical stability, inexpensive, easy and moderate production conditions, strong affinity for the substrate, minimal mass transfer resistance, and preserver of the enzyme structure.
- Membrane contactors offer high efficiency in CO_2 absorption rate and have a small footprint, reducing total costs significantly. However, only a few works have been so far focused on the development of enzymatic membrane contactors, stimulating future studies.
- More emphasis should be paid to the long-term stability of CO_2 absorption rates in CO_2 capture technologies to assess the potential of such systems in industrial applications.
- Integration of enzymatic CO_2 capture technologies with in-situ bicarbonate removal processes to enhance the efficiency is another interesting area of research.
- Further studies should also focus on techno-economic evaluations, especially for CA immobilized systems.

References

[1] IEA, World energy outlook 2016, Paris, France: OECD/IEA, (2016).

[2] International energy agency, Global energy & CO_2 status report, (2021).

[3] T. Wilberforce, A. Olabi, E.T. Sayed, K. Elsaid, M.A. Abdelkareem, Progress in carbon capture technologies, Sci. Total Environ., 761 (2020) 143203.

[4] T. Sharma, S. Sharma, H. Kamyab, A. Kumar, Energizing the CO_2 utilization by chemo-enzymatic approaches and potentiality of carbonic anhydrases: a review, J. Clean. Prod., 247 (2020) 119138.

[5] M.M. Abu-Khader, Recent progress in CO_2 capture/sequestration: a review, Energ Sources A, 28 (2006) 1261-1279.

[6] P. Luis, T. Van Gerven, B. Van der Bruggen, Recent developments in membrane-based technologies for CO_2 capture, Prog. Energy Combust. Sci., 38 (2012) 419-448.

[7] J. Hanna, I. Iliuta, F. Larachi, M.C. Iliuta, Enzymatic CO_2 capture by immobilized hCA II in an intensified microreactor—kinetic study of the catalytic hydration, Int. J. Greenh. Gas Control., 15 (2013) 78-85.

[8] S. Zhao, P.H. Feron, L. Deng, E. Favre, E. Chabanon, S. Yan, J. Hou, V. Chen, H. Qi, Status and progress of membrane contactors in post-combustion carbon capture: a state-of-the-art review of new developments, J. Membr. Sci., 511 (2016) 180-206.

[9] A. Raza, R. Gholami, R. Rezaee, V. Rasouli, M. Rabiei, Significant aspects of carbon capture and storage–A review, Petroleum, 5 (2019) 335-340.

[10] D.Y. Leung, G. Caramanna, M.M. Maroto-Valer, An overview of current status of carbon dioxide capture and storage technologies, Renew. Sust. Energ. Rev., 39 (2014) 426-443.

[11] I. Iliuta, M.C. Iliuta, Enzymatic CO_2 capture in countercurrent packed-bed column reactors with high performance random packings, Int. J. Greenh. Gas Control., 63 (2017) 462-474.

[12] R. Blais, P. Rogers, Process and apparatus for the treatment of carbon dioxide with carbonic anhydrase, US6524843B1, 2003.

[13] I. Iliuta, F. Larachi, Enzyme-mediated CO_2 capture in oscillating structured packed-bed columns-hydrodynamics and process performance for offshore applications, Ocean Eng., 144 (2017) 157-174.

[14] C. Parent, F. Dutil, Triphasic bioreactor and process for gas effluent treatment,

US7176017B2, 2007.
[15] S. Fradette, Process and apparatus using a spray absorber bioreactor for the biocatalytic treatment of gases, WO2004056455A1, 2004.
[16] F. Migliardini, V. De Luca, V. Carginale, M. Rossi, P. Corbo, C.T. Supuran, C. Capasso, Biomimetic CO_2 capture using a highly thermostable bacterial α-carbonic anhydrase immobilized on a polyurethane foam, J. Enzyme Inhib. Med. Chem., 29 (2014) 146-150.
[17] S. Zhang, Z. Zhang, Y. Lu, M. Rostam-Abadi, A. Jones, Activity and stability of immobilized carbonic anhydrase for promoting CO_2 absorption into a carbonate solution for post-combustion CO_2 capture, Bioresour. Technol., 102 (2011) 10194-10201.
[18] R. Cowan, J.J. Ge, Y.J. Qin, M. McGregor, M. Trachtenberg, CO_2 capture by means of an enzyme‐based reactor, Ann. NY Acad. Sci., 984 (2003) 453-469.
[19] I. Iliuta, M.C. Iliuta, Investigation of CO_2 removal by immobilized carbonic anhydrase enzyme in a hollow‐fiber membrane bioreactor, AIChE J., 63 (2017) 2996-3007.
[20] S. He, X. Jiang, S. Li, F. Ran, J. Long, L. Shao, Intermediate thermal manipulation of polymers of intrinsic microporous (PIMs) membranes for gas separations, AIChE J., 66 (2020) e16543.
[21] M.C. Trachtenberg, Enzyme systems for gas processing, US6143556A, 2000.
[22] L.A. Neves, C. Afonso, I.M. Coelhoso, J.G. Crespo, Integrated CO_2 capture and enzymatic bioconversion in supported ionic liquid membranes, Sep. Purif. Technol., 97 (2012) 34-41.
[23] F. Bougie, Sterically hindered amine based absorbents and application for CO_2 capture in membrane contactors, Ph.D Thesis, Université Laval, Quebec, 2014.
[24] A. Mansourizadeh, A. Ismail, Hollow fiber gas–liquid membrane contactors for acid gas capture: a review, J. Hazard. Mater., 171 (2009) 38-53.
[25] J.K. Yong, G.W. Stevens, F. Caruso, S.E. Kentish, The use of carbonic anhydrase to accelerate carbon dioxide capture processes, J. Chem. Technol. Biotechnol., 90 (2015) 3-10.
[26] S. Lindskog, Structure and mechanism of carbonic anhydrase, Pharmacol. Ther., 74 (1997) 1-20.
[27] C.K. Savile, J.J. Lalonde, Biotechnology for the acceleration of carbon dioxide capture and sequestration, Curr. Opin. Biotechnol., 22 (2011) 818-823.
[28] S.K. Bhatia, R.K. Bhatia, J.-M. Jeon, G. Kumar, Y.-H. Yang, Carbon dioxide capture

and bioenergy production using biological system–a review, Renew. Sust. Energ. Rev., 110 (2019) 143-158.
[29] G.P. Miscione, M. Stenta, D. Spinelli, E. Anders, A. Bottoni, New computational evidence for the catalytic mechanism of carbonic anhydrase, Theor. Chem. Acc., 118 (2007) 193-201.
[30] B.K. Kanth, J. Lee, S.P. Pack, Carbonic anhydrase: Its biocatalytic mechanisms and functional properties for efficient CO_2 capture process development, Eng. Life Sci., 13 (2013) 422-431.
[31] J. Hanna, Capture enzymatique du dioxyde de carbone par l'HCA II immobilisee: etude cinetique de l`hydration catalytique, Mémoire, Department de genie chnimique, Facultes des sciences et genie, Universite Laval, Quebec, 2012.
[32] I. Iliuta, F. Larachi, New scrubber concept for catalytic CO_2 hydration by immobilized carbonic anhydrase II and in-situ inhibitor removal in three-phase monolith slurry reactor, Sep. Purif. Technol., 86 (2012) 199-214.
[33] L. Bao, M.C. Trachtenberg, Facilitated transport of CO_2 across a liquid membrane: comparing enzyme, amine, and alkaline, J. Membr. Sci., 280 (2006) 330-334.
[34] Z. Wu, Y. Nan, Y. Zhao, X. Wang, S. Huang, J. Shi, Immobilization of carbonic anhydrase for facilitated CO_2 capture and separation, Chin. J. Chem. Eng., 28 (2020) 2817-2831.
[35] R.A. Sheldon, S. van Pelt, Enzyme immobilisation in biocatalysis: why, what and how, Chem. Soc. Rev., 42 (2013) 6223-6235.
[36] A. Basso, S. Serban, Industrial applications of immobilized enzymes—a review, Mol. Cat., 479 (2019) 110607.
[37] J. Shi, Y. Jiang, Z. Jiang, X. Wang, X. Wang, S. Zhang, P. Han, C. Yang, Enzymatic conversion of carbon dioxide, Chem. Soc. Rev., 44 (2015) 5981-6000.
[38] I. Iliuta, M.C. Iliuta, F. Larachi, Catalytic CO_2 hydration by immobilized and free human carbonic anhydrase II in a laminar flow microreactor–model and simulations, Sep. Purif. Technol., 107 (2013) 61-69.
[39] N.R. Mohamad, N.H.C. Marzuki, N.A. Buang, F. Huyop, R.A. Wahab, An overview of technologies for immobilization of enzymes and surface analysis techniques for immobilized enzymes, Biotechnol. Biotechnol. Equip., 29 (2015) 205-220.

[40] J.-M. Park, M. Kim, H.J. Lee, A. Jang, J. Min, Y.-H. Kim, Enhancing the production of Rhodobacter sphaeroides-derived physiologically active substances using carbonic anhydrase-immobilized electrospun nanofibers, Biomacromolecules, 13 (2012) 3780-3786.
[41] X. Fei, S. Chen, D. Liu, C. Huang, Y. Zhang, Comparison of amino and epoxy functionalized SBA-15 used for carbonic anhydrase immobilization, J. Biosci. Bioeng., 122 (2016) 314-321.
[42] W.C. Floyd III, S.E. Baker, C.A. Valdez, J.K. Stolaroff, J.P. Bearinger, J.H. Satcher Jr, R.D. Aines, Evaluation of a carbonic anhydrase mimic for industrial carbon capture, Environ. Sci. Technol., 47 (2013) 10049-10055.
[43] F. Secundo, Conformational changes of enzymes upon immobilisation, Chem. Soc. Rev., 42 (2013) 6250-6261.
[44] J. Hou, G. Dong, Y. Ye, V. Chen, Laccase immobilization on titania nanoparticles and titania-functionalized membranes, J. Membr. Sci., 452 (2014) 229-240.
[45] M. Vinoba, D.H. Kim, K.S. Lim, S.K. Jeong, S.W. Lee, M. Alagar, Biomimetic sequestration of CO_2 and reformation to $CaCO_3$ using bovine carbonic anhydrase immobilized on SBA-15, Energy Fuels, 25 (2010) 438-445.
[46] J. Hou, M.Y. Zulkifli, M. Mohammad, Y. Zhang, A. Razmjou, V. Chen, Biocatalytic gas-liquid membrane contactors for CO_2 hydration with immobilized carbonic anhydrase, J. Membr. Sci., 520 (2016) 303-313.
[47] M. Russo, G. Olivieri, A. Marzocchella, P. Salatino, P. Caramuscio, C. Cavaleiro, Post-combustion carbon capture mediated by carbonic anhydrase, Sep. Purif. Technol., 107 (2013) 331-339.
[48] J. Hou, G. Dong, B. Xiao, C. Malassigne, V. Chen, Preparation of titania based biocatalytic nanoparticles and membranes for CO_2 conversion, J. Mater. Chem. A, 3 (2015) 3332-3342.
[49] S. Wanjari, C. Prabhu, R. Yadav, T. Satyanarayana, N. Labhsetwar, S. Rayalu, Immobilization of carbonic anhydrase on chitosan beads for enhanced carbonation reaction, Process Biochem., 46 (2011) 1010-1018.
[50] M. Oviya, V. Sukumaran, S.S. Giri, Immobilization and characterization of carbonic anhydrase purified from E. coli MO1 and its influence on CO_2 sequestration, World J. Microbiol. Biotechnol., 29 (2013) 1813-1820.

[51] J. Sun, L. Wei, Y. Wang, Z. Zhao, W. Liu, Immobilization of carbonic anhydrase on polyvinylidene fluoride membranes, Biotechnol. Appl. Biochem., 65 (2018) 362-371.
[52] J. Sun, C. Wang, Y. Wang, S. Ji, W. Liu, Immobilization of carbonic anhydrase on polyethylenimine/dopamine codeposited membranes, J. Appl. Polym. Sci., 136 (2019) 47784.
[53] E. Ozdemir, Biomimetic CO_2 sequestration: 1. immobilization of carbonic anhydrase within polyurethane foam, Energy Fuels, 23 (2009) 5725-5730.
[54] K. Maeshima, M. Yoshimoto, Preparation and characterization of carbonic anhydrase-conjugated liposomes for catalytic synthesis of calcium carbonate particles, Enzyme Microb. Technol., 105 (2017) 9-17.
[55] J.D. Badjić, N.M. Kostić, Effects of encapsulation in sol− gel silica glass on esterase activity, conformational stability, and unfolding of bovine carbonic anhydrase II, Chem. Mater., 11 (1999) 3671-3679.
[56] M. Vinoba, K.S. Lim, S.H. Lee, S.K. Jeong, M. Alagar, Immobilization of human carbonic anhydrase on gold nanoparticles assembled onto amine/thiol-functionalized mesoporous SBA-15 for biomimetic sequestration of CO_2, Langmuir, 27 (2011) 6227-6234.
[57] H. Jia, G. Zhu, P. Wang, Catalytic behaviors of enzymes attached to nanoparticles: the effect of particle mobility, Biotechnol. Bioeng., 84 (2003) 406-414.
[58] G. Jing, F. Pan, B. Lv, Z. Zhou, Immobilization of carbonic anhydrase on epoxy-functionalized magnetic polymer microspheres for CO_2 capture, Process Biochem., 50 (2015) 2234-2241.
[59] A.H.A. Al-Dhrub, S. Sahin, I. Ozmen, E. Tunca, M. Bulbul, Immobilization and characterization of human carbonic anhydrase I on amine functionalized magnetic nanoparticles, Process Biochem., 57 (2017) 95-104.
[60] R. Yadav, M. Joshi, S. Wanjari, C. Prabhu, S. Kotwal, T. Satyanarayanan, S. Rayalu, Immobilization of carbonic anhydrase on chitosan stabilized Iron nanoparticles for the carbonation reaction, Water Air Soil Pollut., 223 (2012) 5345-5356.
[61] M. Vinoba, M. Bhagiyalakshmi, S.K. Jeong, Y.I. Yoon, S.C. Nam, Capture and sequestration of CO_2 by human carbonic anhydrase covalently immobilized onto amine-functionalized SBA-15, J. Phys. Chem. C, 115 (2011) 20209-20216.
[62] M. Vinoba, M. Bhagiyalakshmi, S.K. Jeong, Y.I. Yoon, S.C. Nam, Carbonic anhydrase conjugated to nanosilver immobilized onto mesoporous SBA-15 for sequestration of CO_2, J.

Mol. Catal., B Enzym., 75 (2012) 60-67.
[63] M. Hartmann, X. Kostrov, Immobilization of enzymes on porous silicas–benefits and challenges, Chem. Soc. Rev., 42 (2013) 6277-6289.
[64] M. Yoshimoto, P. Walde, Immobilized carbonic anhydrase: preparation, characteristics and biotechnological applications, World J. Microbiol. Biotechnol., 34 (2018) 151.
[65] J.M. Guisan, Immobilization of enzymes and cells, Springer, 2006.
[66] S. Ren, R. Chen, Z. Wu, S. Su, J. Hou, Y. Yuan, Enzymatic characteristics of immobilized carbonic anhydrase and its applications in CO_2 conversion, Colloids Surf. B, (2021) 111779.
[67] R.R. Yadav, K. Krishnamurthi, S.N. Mudliar, S.S. Devi, P.K. Naoghare, A. Bafana, T. Chakrabarti, Carbonic anhydrase mediated carbon dioxide sequestration: Promises, challenges and future prospects, J. Basic Microbiol., 54 (2014) 472-481.
[68] D.-M. Liu, J. Chen, Y.-P. Shi, Advances on methods and easy separated support materials for enzymes immobilization, Trends Analyt. Chem., (2018).
[69] K.A. Joshi, J. Tang, R. Haddon, J. Wang, W. Chen, A. Mulchandani, A disposable biosensor for organophosphorus nerve agents based on carbon nanotubes modified thick film strip electrode, Electroanalysis, 17 (2005) 54-58.
[70] J.K. Yong, G.W. Stevens, F. Caruso, S.E. Kentish, In situ layer-by-layer assembled carbonic anhydrase-coated hollow fiber membrane contactor for rapid CO_2 absorption, J. Membr. Sci., 514 (2016) 556-565.
[71] H.H. Nguyen, M. Kim, An overview of techniques in enzyme immobilization, Appl. Sci. Converg. Technol., 26 (2017) 157-163.
[72] U. Hanefeld, L. Gardossi, E. Magner, Understanding enzyme immobilisation, Chem. Soc. Rev., 38 (2009) 453-468.
[73] J.K. Yong, J. Cui, K.L. Cho, G.W. Stevens, F. Caruso, S.E. Kentish, Surface engineering of polypropylene membranes with carbonic anhydrase-loaded mesoporous silica nanoparticles for improved carbon dioxide hydration, Langmuir, 31 (2015) 6211-6219.
[74] W. Zhao, J.J. Xu, H.Y. Chen, Electrochemical biosensors based on layer‐by‐layer assemblies, Electroanalysis, 18 (2006) 1737-1748.
[75] M. Shaolin, Bioelectrochemical response of the polyaniline galactose oxidase electrode, J. Electroanal. Chem., 370 (1994) 135-139.
[76] R.R. Yadav, S.N. Mudliar, A.Y. Shekh, A.B. Fulke, S.S. Devi, K. Krishnamurthi, A.

Juwarkar, T. Chakrabarti, Immobilization of carbonic anhydrase in alginate and its influence on transformation of CO_2 to calcite, Process Biochem., 47 (2012) 585-590.
[77] R. Sheldon, Cross-linked enzyme aggregates (CLEAs): stable and recyclable biocatalysts, Biochem. Soc. Trans., 35 (2007) 1583-1587.
[78] E. Górecka, M. Jastrzębska, Immobilization techniques and biopolymer carriers, Food Sci. Biotechnol., 75 (2011) 65-86.
[79] C. Prabhu, A. Valechha, S. Wanjari, N. Labhsetwar, S. Kotwal, T. Satyanarayanan, S. Rayalu, Carbon composite beads for immobilization of carbonic anhydrase, J. Mol. Catal. B Enzym., 71 (2011) 71-78.
[80] A. Subramanian, S.J. Kennel, P.I. Oden, K.B. Jacobson, J. Woodward, M.J. Doktycz, Comparison of techniques for enzyme immobilization on silicon supports, Enzyme Microb. Technol., 24 (1999) 26-34.
[81] S. Peirce, M.E. Russo, V. De Luca, C. Capasso, M. Rossi, G. Olivieri, P. Salatino, A. Marzocchella, Immobilization of carbonic anhydrase for biomimetic CO_2 capture in a slurry absorber as cross-linked enzyme aggregates (CLEA), in: Chemical Engineering Transactions, Italian Association of Chemical Engineering-AIDIC, 2015, 259-264.
[82] S. Peirce, M.E. Russo, R. Isticato, R.F. Lafuente, P. Salatino, A. Marzocchella, Structure and activity of magnetic cross-linked enzyme aggregates of bovine carbonic anhydrase as promoters of enzymatic CO_2 capture, Biochem. Eng. J., 127 (2017) 188-195.
[83] S. Peirce, M. Russo, R. Perfetto, C. Capasso, M. Rossi, R. Fernandez-Lafuente, P. Salatino, A. Marzocchella, Kinetic characterization of carbonic anhydrase immobilized on magnetic nanoparticles as biocatalyst for CO_2 capture, Biochem. Eng. J., 138 (2018) 1-11.
[84] D.-M. Liu, J. Chen, Y.-P. Shi, An online immobilized α-glucosidase microreactor for enzyme kinetics and inhibition assays, RSC Adv., 5 (2015) 56841-56847.
[85] J. Zdarta, A. Meyer, T. Jesionowski, M. Pinelo, A general overview of support materials for enzyme immobilization: characteristics, properties, practical utility, Catalysts, 8 (2018) 92.
[86] P. Shao, H. Chen, Q. Ying, S. Zhang, Structure–activity relationship of carbonic anhydrase enzyme immobilized on various silica-based mesoporous molecular sieves for CO_2 absorption into a potassium carbonate solution, Energy Fuels, 34 (2020) 2089-2096.
[87] S. Zhang, H. Lu, Y. Lu, Enhanced stability and chemical resistance of a new nanoscale

biocatalyst for accelerating CO_2 absorption into a carbonate solution, Environ. Sci. Technol., 47 (2013) 13882-13888.
[88] M. Vinoba, M. Bhagiyalakshmi, S.K. Jeong, Y.I. Yoon, S.C. Nam, Immobilization of carbonic anhydrase on spherical SBA-15 for hydration and sequestration of CO_2, Colloids Surf. B, 90 (2012) 91-96.
[89] S. Zhang, Y. Lu, X. Ye, Catalytic behavior of carbonic anhydrase enzyme immobilized onto nonporous silica nanoparticles for enhancing CO_2 absorption into a carbonate solution, Int. J. Greenh. Gas Control., 13 (2013) 17-25.
[90] H. Lim, D. Kim, I. Hwang, Sequestration of CO_2 into $CaCO_3$ using carbonic anhydrase immobilization on functionalized aluminum oxide, Appl. Biochem. Microbiol., 55 (2019) 375-379.
[91] M. Vinoba, M. Bhagiyalakshmi, S.K. Jeong, S.C. Nam, Y. Yoon, Carbonic anhydrase immobilized on encapsulated magnetic nanoparticles for CO_2 sequestration, Chem. Eur. J., 18 (2012) 12028-12034.
[92] K.M. Woo, I. Lee, S.-G. Hong, S. An, J. Lee, E. Oh, J. Kim, Crosslinked chitosan coating on magnetic mesoporous silica with pre-adsorbed carbonic anhydrase for carbon dioxide conversion, Chem. Eng. J., 276 (2015) 232-239.
[93] H.S. Kim, S.-G. Hong, K.M. Woo, V. Teijeiro Seijas, S. Kim, J. Lee, J. Kim, Precipitation-based nanoscale enzyme reactor with improved loading, stability, and mass transfer for enzymatic CO_2 conversion and utilization, ACS Catal., 8 (2018) 6526-6536.
[94] S. Faridi, H. Bose, T. Satyanarayana, Utility of immobilized recombinant carbonic anhydrase of Bacillus halodurans TSLV1 on the surface of modified iron magnetic nanoparticles in carbon sequestration, Energy Fuels, 31 (2017) 3002-3009.
[95] W. Xu, Z. Wang, G. Chen, Z. Fu, G. Jiang, J. Chen, J. Wu, Z. Liu, Accelerating CO_2 absorption in aqueous amine solutions at high temperature with carbonic anhydrase in magnetic nanogels, Catal. Lett., 148 (2018) 1827-1833.
[96] G. Merle, S. Fradette, E. Madore, J.E. Barralet, Electropolymerized carbonic anhydrase immobilization for carbon dioxide capture, Langmuir, 30 (2014) 6915-6919.
[97] Y. Xu, Y. Lin, N.G.P. Chew, C. Malde, R. Wang, Biocatalytic PVDF composite hollow fiber membranes for CO_2 removal in gas-liquid membrane contactor, J. Membr. Sci., 572 (2019) 532-544.

[98] B. Kanbar, E. Ozdemir, Thermal stability of carbonic anhydrase immobilized within polyurethane foam, Biotechnol. Prog., 26 (2010) 1474-1480.
[99] Y.-T. Zhang, T.-T. Zhi, L. Zhang, H. Huang, H.-L. Chen, Immobilization of carbonic anhydrase by embedding and covalent coupling into nanocomposite hydrogel containing hydrotalcite, Polymer, 50 (2009) 5693-5700.
[100] S.-H. Jun, J. Yang, H. Jeon, H.S. Kim, S.P. Pack, E. Jin, J. Kim, Stabilized and immobilized carbonic anhydrase on electrospun nanofibers for enzymatic CO_2 conversion and utilization in expedited microalgal growth, Environ. Sci. Technol., 54 (2020) 1223-1231.
[101] R. Yadav, S. Wanjari, C. Prabhu, V. Kumar, N. Labhsetwar, T. Satyanarayanan, S. Kotwal, S. Rayalu, Immobilized carbonic anhydrase for the biomimetic carbonation reaction, Energy Fuels, 24 (2010) 6198-6207.
[102] V. Asadi, R. Kardanpour, S. Tangestaninejad, M. Moghadam, V. Mirkhani, I. Mohammadpoor-Baltork, Novel bovine carbonic anhydrase encapsulated in a metal–organic framework: a new platform for biomimetic sequestration of CO_2, RSC Adv., 9 (2019) 28460-28469.
[103] S. Ren, Y. Feng, H. Wen, C. Li, B. Sun, J. Cui, S. Jia, Immobilized carbonic anhydrase on mesoporous cruciate flower-like metal organic framework for promoting CO_2 sequestration, Int. J. Biol. Macromol., 117 (2018) 189-198.
[104] S. Ren, C. Li, Z. Tan, Y. Hou, S. Jia, J. Cui, Carbonic anhydrase@ZIF-8 hydrogel composite membrane with improved recycling and stability for efficient CO_2 capture, J. Agric. Food Chem., 67 (2019) 3372-3379.
[105] S. Zhang, M. Du, P. Shao, L. Wang, J. Ye, J. Chen, J. Chen, Carbonic anhydrase enzyme-MOFs composite with a superior catalytic performance to promote CO_2 absorption into tertiary amine solution, Environ. Sci. Technol., 52 (2018) 12708-12716.
[106] M. Jiao, J. He, S. Sun, F. Vriesekoop, Q. Yuan, Y. Liu, H. Liang, Fast immobilization of human carbonic anhydrase II on Ni-Based metal-organic framework nanorods with high catalytic performance, Catalysts, 10 (2020) 401.
[107] A. Kołodziejczak‐Radzimska, J. Zdarta, T. Jesionowski, Physicochemical and catalytic properties of acylase I from aspergillus melleus immobilized on amino‐and carbonyl‐grafted stöber silica, Biotechnol. Prog., 34 (2018) 767-777.
[108] T. Jesionowski, A. Krysztafkiewicz, Preparation of the hydrophilic/hydrophobic silica

particles, Colloid Surf. A-Physicochem. Eng. Asp, 207 (2002) 49-58.
[109] P. Zucca, E. Sanjust, Inorganic materials as supports for covalent enzyme immobilization: methods and mechanisms, Molecules, 19 (2014) 14139-14194.
[110] A. Crumbliss, K. McLachlan, J. O'Daly, R. Henkens, Preparation and activity of carbonic anhydrase immobilized on porous silica beads and graphite rods, Biotechnol. Bioeng., 31 (1988) 796-801.
[111] S. Wanjari, C. Prabhu, T. Satyanarayana, A. Vinu, S. Rayalu, Immobilization of carbonic anhydrase on mesoporous aluminosilicate for carbonation reaction, Microporous Mesoporous Mater., 160 (2012) 151-158.
[112] D. Vallés, S. Furtado, C. Villadóniga, A.M.B. Cantera, Adsorption onto alumina and stabilization of cysteine proteinases from crude extract of Solanum granuloso-leprosum fruits, Process Biochem, 46 (2011) 592-598.
[113] M. Cao, Z. Li, J. Wang, W. Ge, T. Yue, R. Li, V.L. Colvin, W.Y. William, Food related applications of magnetic iron oxide nanoparticles: enzyme immobilization, protein purification, and food analysis, Trends Food Sci Technol, 27 (2012) 47-56.
[114] A.S. Drozdov, O.E. Shapovalova, V. Ivanovski, D. Avnir, V.V. Vinogradov, Entrapment of enzymes within sol–gel-derived magnetite, Chem. Mater., 28 (2016) 2248-2253.
[115] H. Bose, T. Satyanarayana, Microbial carbonic anhydrases in biomimetic carbon sequestration for mitigating global warming: prospects and perspectives, Front. Microbiol., 8 (2017) 1615.
[116] F.B.-O. Daoud, S. Kaddour, T. Sadoun, Adsorption of cellulase Aspergillus niger on a commercial activated carbon: kinetics and equilibrium studies, Colloids Surf B Biointerfaces, 75 (2010) 93-99.
[117] X. Chen, Y. Wang, P. Wang, Peptide-induced affinity binding of carbonic anhydrase to carbon nanotubes, Langmuir, 31 (2015) 397-403.
[118] Y. Fang, X.-J. Huang, P.-C. Chen, Z.-K. Xu, Polymer materials for enzyme immobilization and their application in bioreactors, BMB Rep., 44 (2011) 87-95.
[119] D. Hetemi, J. Pinson, Surface functionalisation of polymers, Chem. Soc. Rev., 46 (2017) 5701-5713.
[120] J.L. Kaar, H.-I. Oh, A.J. Russell, W.J. Federspiel, Towards improved artificial lungs through biocatalysis, Biomaterials, 28 (2007) 3131-3139.

[121] J. Kimmel, D. Arazawa, S.-H. Ye, V. Shankarraman, W. Wagner, W. Federspiel, Carbonic anhydrase immobilized on hollow fiber membranes using glutaraldehyde activated chitosan for artificial lung applications, J. Mater. Sci. Mater. Med., 24 (2013) 2611-2621.
[122] D. Arazawa, J. Kimmel, M. Finn, W. Federspiel, Acidic sweep gas with carbonic anhydrase coated hollow fiber membranes synergistically accelerates CO_2 removal from blood, Acta Biomater., 25 (2015) 143-149.
[123] D.T. Arazawa, H.-I. Oh, S.-H. Ye, C.A. Johnson Jr, J.R. Woolley, W.R. Wagner, W.J. Federspiel, Immobilized carbonic anhydrase on hollow fiber membranes accelerates CO_2 removal from blood, J. Membr. Sci., 403 (2012) 25-31.
[124] K. Ariga, J.P. Hill, Q. Ji, Layer-by-layer assembly as a versatile bottom-up nanofabrication technique for exploratory research and realistic application, Phys. Chem. Chem. Phys., 9 (2007) 2319-2340.
[125] W. Hu, S. Lu, Y. Ma, P. Ren, X. Ma, N. Zhou, T. Zhang, Z. Ji, Poly (dopamine)-inspired surface functionalization of polypropylene tissue mesh for prevention of intra-peritoneal adhesion formation, J. Mater. Chem. B, 5 (2017) 575-585.
[126] H. Lee, S.M. Dellatore, W.M. Miller, P.B. Messersmith, Mussel-inspired surface chemistry for multifunctional coatings, Science, 318 (2007) 426-430.
[127] G. Zhang, Y. Li, A. Gao, Q. Zhang, J. Cui, S. Zhao, X. Zhan, Y. Yan, Bio-inspired underwater superoleophobic PVDF membranes for highly-efficient simultaneous removal of insoluble emulsified oils and soluble anionic dyes, Chem. Eng. J., 369 (2019) 576-587.
[128] J. Fan, J. Luo, X. Chen, Y. Wan, Polydopamine meets porous membrane: a versatile platform for facile preparation of membrane adsorbers, J. Chromatogr. A, 1448 (2016) 121-126.
[129] Y. Lv, H.-C. Yang, H.-Q. Liang, L.-S. Wan, Z.-K. Xu, Nanofiltration membranes via co-deposition of polydopamine/polyethylenimine followed by cross-linking, J. Membr. Sci., 476 (2015) 50-58.
[130] J. Jiang, L. Zhu, L. Zhu, B. Zhu, Y. Xu, Surface characteristics of a self-polymerized dopamine coating deposited on hydrophobic polymer films, Langmuir, 27 (2011) 14180-14187.
[131] P. Salazar, M. Martín, J. González-Mora, Polydopamine-modified surfaces in biosensor applications, in: A. Méndez-Vilas, A. Solano (Eds.), Polymer science: research advances,

practical applications and educational aspects, Formatex Research Center, 2016, 385-396.
[132] W.-Z. Qiu, H.-C. Yang, Z.-K. Xu, Dopamine-assisted co-deposition: an emerging and promising strategy for surface modification, Adv. Colloid Interface Sci., 256 (2018) 111-125.
[133] Y. Wang, Y. Zhang, C. Hou, M. Liu, Mussel-inspired synthesis of magnetic polydopamine–chitosan nanoparticles as biosorbent for dyes and metals removal, J. Taiwan Inst. Chem. Eng., 61 (2016) 292-298.
[134] L.C. Capozzi, F.M. Mehmood, M. Giagnorio, A. Tiraferri, M. Cerruti, M. Sangermano, Ultrafiltration membranes functionalized with polydopamine with enhanced contaminant removal by adsorption, Macromol. Mater. Eng., 302 (2017) 1600481.
[135] X. Cao, J. Luo, J.M. Woodley, Y. Wan, Mussel-inspired co-deposition to enhance bisphenol A removal in a bifacial enzymatic membrane reactor, Chem. Eng. J., 336 (2018) 315-324.
[136] X. Li, C. Liu, W. Yin, T.H. Chong, R. Wang, Design and development of layer-by-layer based low-pressure antifouling nanofiltration membrane used for water reclamation, J. Membr. Sci., 584 (2019) 309-323.
[137] N.G.P. Chew, S. Zhao, C. Malde, R. Wang, Superoleophobic surface modification for robust membrane distillation performance, J. Membr. Sci., 541 (2017) 162-173.
[138] S. Li, J. Luo, Y. Wan, Regenerable biocatalytic nanofiltration membrane for aquatic micropollutants removal, J. Membr. Sci., 549 (2018) 120-128.
[139] P. Maksym, M. Tarnacka, A. Dzienia, K. Matuszek, A. Chrobok, K. Kaminski, M. Paluch, Enhanced polymerization rate and conductivity of ionic liquid-based epoxy resin, Macromolecules, 50 (2017) 3262-3272.
[140] H. Wen, L. Zhang, Y. Du, Z. Wang, Y. Jiang, H. Bian, J. Cui, S. Jia, Bimetal based inorganic-carbonic anhydrase hybrid hydrogel membrane for CO_2 capture, J. CO_2 Util., 39 (2020) 101171.
[141] B. Krajewska, Application of chitin-and chitosan-based materials for enzyme immobilizations: a review, Enzyme Microb. Technol., 35 (2004) 126-139.
[142] K. Kurita, Controlled functionalization of the polysaccharide chitin, Prog. Polym. Sci., 26 (2001) 1921-1971.
[143] C. Prabhu, S. Wanjari, S. Gawande, S. Das, N. Labhsetwar, S. Kotwal, A.K. Puri, T. Satyanarayana, S. Rayalu, Immobilization of carbonic anhydrase enriched microorganism on

biopolymer based materials, J. Mol. Catal., B Enzym., 60 (2009) 13-21.
[144] F.A. Simsek-Ege, G.M. Bond, J. Stringer, Matrix molecular weight cut-off for encapsulation of carbonic anhydrase in polyelectrolyte beads, J. Biomater. Sci. Polym. Ed., 13 (2002) 1175-1187.
[145] H. Furukawa, K.E. Cordova, M. O'Keeffe, O.M. Yaghi, The chemistry and applications of metal-organic frameworks, Science, 341 (2013) 1230444.
[146] M. Giménez-Marqués, T. Hidalgo, C. Serre, P. Horcajada, Nanostructured metal–organic frameworks and their bio-related applications, Coord. Chem. Rev., 307 (2016) 342-360.
[147] K. Liang, R. Ricco, C.M. Doherty, M.J. Styles, S. Bell, N. Kirby, S. Mudie, D. Haylock, A.J. Hill, C.J. Doonan, Biomimetic mineralization of metal-organic frameworks as protective coatings for biomacromolecules, Nat. Commun., 6 (2015) 1-8.
[148] Y. Zhang, H. Wang, J. Liu, J. Hou, Y. Zhang, Enzyme-embedded metal–organic framework membranes on polymeric substrates for efficient CO_2 capture, J. Mater. Chem., 5 (2017) 19954-19962.
[149] A. Gabelman, S.-T. Hwang, Hollow fiber membrane contactors, J. Membr. Sci., 159 (1999) 61-106.
[150] S. Bhattacharya, A. Nayak, M. Schiavone, S. K. Bhattacharya, Solubilization and concentration of carbon dioxide: novel spray reactors with immobilized carbonic anhydrase, Biotechnol. Bioeng., 86 (2004) 37-46.
[151] S. Bhattacharya, M. Schiavone, S. Chakrabarti, S.K. Bhattacharya, CO_2 hydration by immobilized carbonic anhydrase, Biotechnol. Appl. Biochem., 38 (2003) 111-117.
[152] F. Larachi, O. Lacroix, B.P. Grandjean, CO_2 hydration by immobilized carbonic anhydrase in Robinson–Mahoney and packed-bed scrubbers—role of mass transfer and inhibitor removal, Chem. Eng. Sci., 73 (2012) 99-115.
[153] J. Li, X. Zhou, L. Zhang, H. Di, H. Wu, L. Yang, Investigation on the immobilization of carbonic anhydrase and the catalytic absorption of carbon dioxide, Energ Fuel, 31 (2017) 778-784.
[154] T.L. Bucholz, M.K. Hulvey, J.P. Reardon, B.M. Rambo, D.C. Pulvirenti, L.E. Weber, A. Zaks, Development of an organosilica coating containing carbonic anhydrase for applications in CO_2 capture, in: Novel Materials for Carbon Dioxide Mitigation Technology,

Elsevier, 2015, 117-147.
[155] M. Leimbrink, T. Limberg, A.-K. Kunze, M. Skiborowski, Different strategies for accelerated CO_2 absorption in packed columns by application of the biocatalyst carbonic anhydrase, Energy Procedia, 114 (2017) 781-794.
[156] E. Madore, S. Fradette, J. Lawson, Activity replenishment and in situ activation for enzymatic CO_2 capture packed reactor, US20150104782A1, 2015.
[157] S. Fradette, J. Gingras, N. Voyer, J. Carley, G.R. Kelly, O. Ceperkovic, Process for CO_2 capture using micro-particles comprising biocatalysts, EP2461894A1, 2014.
[158] J. Hou, C. Ji, G. Dong, B. Xiao, Y. Ye, V. Chen, Biocatalytic Janus membranes for CO_2 removal utilizing carbonic anhydrase, J. Mater. Chem. A, 3 (2015) 17032-17041.
[159] I. Iliuta, M.C. Iliuta, Enhanced enzyme-based CO_2 capture in countercurrent packed-bed column reactors, Sep. Purif. Technol., 248 (2020) 116908.
[160] M. Leimbrink, K.G. Nikoleit, R. Spitzer, S. Salmon, T. Bucholz, A. Górak, M. Skiborowski, Enzymatic reactive absorption of CO_2 in MDEA by means of an innovative biocatalyst delivery system, Chem. Eng. J., 334 (2018) 1195-1205.
[161] O. Lacroix, F. Larachi, Scrubber designs for enzyme-mediated capture of CO_2, Recent Pat. Eng., 1 (2008) 93-105.
[162] M.E. Russo, P. Bareschino, G. Olivieri, R. Chirone, P. Salatino, A. Marzocchella, Modeling of slurry staged bubble column for biomimetic CO_2 capture, Int. J. Greenh. Gas Control., 47 (2016) 200-209.
[163] M. Trachtenberg, J. Ge, R. Cowan, Y. Qin, M. McGregor, CO_2 capture by means of an enzyme-based reactor, Biochemistry, 28 (2003) 7913-7918.
[164] S. Duan, T. Kai, S.-i. Nakao, Effect of carbonic anhydrase on CO_2 separation performance of thin poly (amidoamine) dendrimer/poly (ethylene glycol) hybrid membranes, Membranes,, 9 (2019) 167.
[165] M.C. Trachtenberg, R.M. Cowan, D.A. Smith, D.A. Horazak, M.D. Jensen, J.D. Laumb, A.P. Vucelic, H. Chen, L. Wang, X. Wu, Membrane-based, enzyme-facilitated, efficient carbon dioxide capture, Energy Procedia, 1 (2009) 353-360.
[166] L.-H. Cheng, L. Zhang, H.-L. Chen, C.-J. Gao, Hollow fiber contained hydrogel-CA membrane contactor for carbon dioxide removal from the enclosed spaces, J. Membr. Sci., 324 (2008) 33-43.

[167] Y.-T. Zhang, L. Zhang, H.-L. Chen, H.-M. Zhang, Selective separation of low concentration CO_2 using hydrogel immobilized CA enzyme based hollow fiber membrane reactors, Chem. Eng. Sci., 65 (2010) 3199-3207.
[168] Y. Fu, Y.-B. Jiang, D. Dunphy, H. Xiong, E. Coker, S.S. Chou, H. Zhang, J.M. Vanegas, J.G. Croissant, J.L. Cecchi, Ultra-thin enzymatic liquid membrane for CO_2 separation and capture, Nat. Commun., 9 (2018) 1-12.
[169] M.Y.M. Abdelrahim, C.F. Martins, L.A. Neves, C. Capasso, C.T. Supuran, I.M. Coelhoso, J.G. Crespo, M. Barboiu, Supported ionic liquid membranes immobilized with carbonic anhydrases for CO_2 transport at high temperatures, J. Membr. Sci., 528 (2017) 225-230.
[170] A. Bednár, N. Nemestóthy, P. Bakonyi, L. Fülöp, G. Zhen, X. Lu, T. Kobayashi, G. Kumar, K. Xu, K. Bélafi-Bakó, Enzymatically-boosted ionic liquid gas separation membranes using carbonic anhydrase of biomass origin, Chem. Eng. J., 303 (2016) 621-626.
[171] N. Nemestóthy, P. Bakonyi, Z. Németh, K. Bélafi-Bakó, Evaluation of pectin-reinforced supported liquid membranes containing carbonic anhydrase: The role of ionic liquid on enzyme stability and CO_2 separation performance, J. CO_2 Util., 24 (2018) 59-63.
[172] Z. Cui, D. deMontigny, Part 7: a review of CO_2 capture using hollow fiber membrane contactors, Carbon Manag., 4 (2013) 69-89.
[173] R. Wang, H. Zhang, P. Feron, D. Liang, Influence of membrane wetting on CO_2 capture in microporous hollow fiber membrane contactors, Sep. Purif. Technol., 46 (2005) 33-40.
[174] P. Kumar, J. Hogendoorn, P. Feron, G. Versteeg, New absorption liquids for the removal of CO_2 from dilute gas streams using membrane contactors, Chem. Eng. J., 57 (2002) 1639-1651.
[175] S. Boributh, S. Assabumrungrat, N. Laosiripojana, R. Jiraratananon, A modeling study on the effects of membrane characteristics and operating parameters on physical absorption of CO_2 by hollow fiber membrane contactor, J. Membr. Sci., 380 (2011) 21-33.
[176] J.-L. Li, B.-H. Chen, Review of CO_2 absorption using chemical solvents in hollow fiber membrane contactors, Sep. Purif. Technol., 41 (2005) 109-122.
[177] S. Mosadegh-Sedghi, D. Rodrigue, J. Brisson, M.C. Iliuta, Wetting phenomenon in membrane contactors–causes and prevention, J. Membr. Sci., 452 (2014) 332-353.
[178] F. Bougie, M.C. Iliuta, Analysis of laplace–young equation parameters and their

influence on efficient CO_2 capture in membrane contactors, Sep. Purif. Technol., 118 (2013) 806-815.
[179] I. Sreedhar, T. Nahar, A. Venugopal, B. Srinivas, Carbon capture by absorption–path covered and ahead, Renew. Sust. Energ Rev., 76 (2017) 1080-1107.
[180] M. Leimbrink, K. Neumann, K. Kupitz, A. Górak, M. Skiborowski, Enzyme accelerated carbon capture in different contacting equipment-a comparative study, Energy Procedia, 114 (2017) 795-812.
[181] A. Babin, F. Bougie, D. Rodrigue, M.C. Iliuta, A closer look on the development and commercialization of membrane contactors for mass transfer and separation processes, Sep. Purif. Technol., 227 (2019) 115679.
[182] J.K. Yong, G.W. Stevens, F. Caruso, S.E. Kentish, The resilience of carbonic anhydrase enzyme for membrane-based carbon capture applications, Int. J. Greenh. Gas Control., 62 (2017) 122-129.
[183] H.C. Yang, J. Hou, V. Chen, Z.K. Xu, Janus membranes: exploring duality for advanced separation, Angew. Chem. Int., 55 (2016) 13398-13407.
[184] A. Bahrami, T. Vincent, A. Garnier, F. Larachi, J. Boukouvalas, M.C. Iliuta, Noncovalent immobilization of optimized bacterial cytochrome P450 BM3 on functionalized magnetic nanoparticles, Ind. Eng. Chem. Res., 56 (2017) 10981-10989.
[185] Z. Wang, J. Guo, J. Ma, L. Shao, Highly regenerable alkali-resistant magnetic nanoparticles inspired by mussels for rapid selective dye removal offer high-efficiency environmental remediation, J. Mater. Chem. A, 3 (2015) 19960-19968.
[186] J.W. Niemantsverdriet, Spectroscopy in catalysis: an introduction, John Wiley & Sons, 2007.
[187] Y.-J. Lin, T.-H. Pan, D.S.-H. Wong, S.-S. Jang, Y.-W. Chi, C.-H. Yeh, Plantwide control of CO_2 capture by absorption and stripping using monoethanolamine solution, Ind. Eng. Chem. Res., 50 (2011) 1338-1345.
[188] K. Salvinder, H. Zabiri, S.A. Taqvi, M. Ramasamy, F. Isa, N. Rozali, H. Suleman, A. Maulud, A. Shariff, An overview on control strategies for CO_2 capture using absorption/stripping system, Chem. Eng. Res. Des., 147 (2019) 319-337.
[189] S. Liu, H. Ling, H. Gao, P. Tontiwachwuthikul, Z. Liang, H. Zhang, Kinetics and new brønsted correlations study of CO_2 absorption into primary and secondary alkanolamine with

and without steric-hindrance, Sep. Purif. Technol., 233 (2020) 115998.
[190] Z. Liang, R. Idem, P. Tontiwachwuthikul, F. Yu, H. Liu, W. Rongwong, Experimental study on the solvent regeneration of a CO_2 - loaded MEA solution using single and hybrid solid acid catalysts, AIChE J., 62 (2016) 753-765.
[191] B. Feng, M. Du, T.J. Dennis, K. Anthony, M.J. Perumal, Reduction of energy requirement of CO_2 desorption by adding acid into CO_2-loaded solvent, Energy Fuels, 24 (2010) 213-219.
[192] I.R. Soosaiprakasam, A. Veawab, Corrosion and polarization behavior of carbon steel in MEA-based CO_2 capture process, Int. J. Greenh. Gas. Con., 2 (2008) 553-562.
[193] S. Ren, S. Jiang, X. Yan, R. Chen, H. Cui, Challenges and opportunities: porous supports in carbonic anhydrase immobilization, J. CO_2 Util., 42 (2020) 101305.
[194] S. Zhang, Y. Lu, Kinetic performance of CO_2 absorption into a potassium carbonate solution promoted with the enzyme carbonic anhydrase: comparison with a monoethanolamine solution, Chem. Eng. J., 279 (2015) 335-343.
[195] A. Crumbliss, S. Perine, J. Stonehuerner, K. Tubergen, J. Zhao, R. Henkens, J. O'Daly, Colloidal gold as a biocompatible immobilization matrix suitable for the fabrication of enzyme electrodes by electrodeposition, Biotechnol. Bioeng., 40 (1992) 483-490.
[196] W. Tang, C. Chen, W. Sun, P. Wang, D. Wei, Low-cost mussel inspired poly (Catechol/Polyamine) modified magnetic nanoparticles as a versatile platform for enhanced activity of immobilized enzyme, Int. J. Biol. Macromol., 128 (2019) 814-824.
[197] C. Luo, Z. Tian, B. Yang, L. Zhang, S. Yan, Manganese dioxide/iron oxide/acid oxidized multi-walled carbon nanotube magnetic nanocomposite for enhanced hexavalent chromium removal, Chem. Eng. J., 234 (2013) 256-265.
[198] R. Perfetto, S. Del Prete, D. Vullo, G. Sansone, C.M. Barone, M. Rossi, C.T. Supuran, C. Capasso, Production and covalent immobilisation of the recombinant bacterial carbonic anhydrase (SspCA) onto magnetic nanoparticles, J. Enzyme Inhib. Med. Chem., 32 (2017) 759-766.
[199] B. Lv, Z. Yang, F. Pan, Z. Zhou, G. Jing, Immobilization of carbonic anhydrase on carboxyl-functionalized ferroferric oxide for CO_2 capture, Int. J. Biol. Macromol., 79 (2015) 719-725.
[200] J. Shi, X. Wang, S. Zhang, L. Tang, Z. Jiang, Enzyme-conjugated ZIF-8 particles as

efficient and stable Pickering interfacial biocatalysts for biphasic biocatalysis, J Mater Chem B, 4 (2016) 2654-2661.
[201] C.-Y. Chien, W.-B. Tsai, Poly (dopamine)-assisted immobilization of Arg-Gly-Asp peptides, hydroxyapatite, and bone morphogenic protein-2 on titanium to improve the osteogenesis of bone marrow stem cells, ACS Appl Mater Interfaces., 5 (2013) 6975-6983.
[202] Y. Liu, K. Ai, L. Lu, Polydopamine and its derivative materials: synthesis and promising applications in energy, environmental, and biomedical fields, Chem. Rev., 114 (2014) 5057-5115.
[203] I. Iliuta, B. Grandjean, S. Piché, F. Larachi, Two-fluid model for counter-current dumped packing-containing columns, Chem. Eng. Sci., 58 (2003) 1373-1380.
[204] A. Attou, G. Ferschneider, A two-fluid hydrodynamic model for the transition between trickle and pulse flow in a cocurrent gas–liquid packed-bed reactor, Chem. Eng. Sci., 55 (2000) 491-511.
[205] R. Rajagopalan, C. Tien, Trajectory analysis of deep‐bed filtration with the sphere‐in‐cell porous media model, AIChE J. , 22 (1976) 523-533.
[206] C. Tien, R.M. Turian, H. Pendse, Simulation of the dynamic behavior of deep bed filters, AIChE J. , 25 (1979) 385-395.
[207] K. Lappalainen, M. Manninen, V. Alopaeus, CFD modeling of radial spreading of flow in trickle-bed reactors due to mechanical and capillary dispersion, Chem. Eng. Sci., 64 (2009) 207-218.
[208] F. Larachi, Kinetic model for the reversible hydration of carbon dioxide catalyzed by human carbonic anhydrase II, Ind. Eng. Chem. Res., 49 (2010) 9095-9104.
[209] C. Ho, J.M. Sturtevant, The kinetics of the hydration of carbon dioxide at 25 C, J. Biol. Chem, 238 (1963) 3499-3501.
[210] M. Ma, Y. Zhang, W. Yu, H.-y. Shen, H.-q. Zhang, N. Gu, Preparation and characterization of magnetite nanoparticles coated by amino silane, Colloids Surf. A, 212 (2003) 219-226.
[211] K. Can, M. Ozmen, M. Ersoz, Immobilization of albumin on aminosilane modified superparamagnetic magnetite nanoparticles and its characterization, Colloids Surf. B Biointerfaces 71 (2009) 154-159.
[212] J. Hou, G. Dong, Y. Ye, V. Chen, Enzymatic degradation of bisphenol-A with

immobilized laccase on TiO_2 sol–gel coated PVDF membrane, J. Membr. Sci., 469 (2014) 19-30.
[213] W. Zhong, J. Hou, H.-C. Yang, V. Chen, Superhydrophobic membranes via facile bio-inspired mineralization for vacuum membrane distillation, J. Membr. Sci., 540 (2017) 98-107.
[214] D.-S. Jiang, S.-Y. Long, J. Huang, H.-Y. Xiao, J.-Y. Zhou, Immobilization of pycnoporus sanguineus laccase on magnetic chitosan microspheres, Biochem. Eng. J., 25 (2005) 15-23.
[215] T.N. Nwagu, B. Okolo, H. Aoyagi, S. Yoshida, Improved yield and stability of amylase by multipoint covalent binding on polyglutaraldehyde activated chitosan beads: Activation of denatured enzyme molecules by calcium ions, Process Biochem., 48 (2013) 1031-1038.
[216] M. van der Veen, W. Norde, M.C. Stuart, Electrostatic interactions in protein adsorption probed by comparing lysozyme and succinylated lysozyme, Colloid. Surf. B, 35 (2004) 33-40.
[217] L. Wang, Y. Shi, S. Chen, W. Wang, M. Tian, N. Ning, L. Zhang, Highly efficient mussel-like inspired modification of aramid fibers by UV-accelerated catechol/polyamine deposition followed chemical grafting for high-performance polymer composites, Chem. Eng. J., 314 (2017) 583-593.
[218] M. Vinoba, D.H. Kim, K.S. Lim, S.K. Jeong, S.W. Lee, M. Alagar, Biomimetic sequestration of CO_2 and reformation to $CaCO_3$ using bovine carbonic anhydrase immobilized on SBA-15, Energ Fuel, 25 (2011) 438-445.
[219] M. Mavroudi, S. Kaldis, G. Sakellaropoulos, A study of mass transfer resistance in membrane gas–liquid contacting processes, J. Membr. Sci., 272 (2006) 103-115.
[220] X. Luo, M. Wang, J. Lee, J. Hendry, Dynamic modelling based on surface renewal theory, model validation and process analysis of rotating packed bed absorber for carbon capture, Appl. Energy, 301 (2021) 117462.
[221] H.-Y. Zhang, R. Wang, D.T. Liang, J.H. Tay, Modeling and experimental study of CO_2 absorption in a hollow fiber membrane contactor, J. Membr. Sci., 279 (2006) 301-310.
[222] S.-p. Yan, M.-X. Fang, W.-F. Zhang, S.-Y. Wang, Z.-K. Xu, Z.-Y. Luo, K.-F. Cen, Experimental study on the separation of CO_2 from flue gas using hollow fiber membrane contactors without wetting, Fuel Process. Technol., 88 (2007) 501-511.

[223] H.J. Lee, E. Magnone, J.H. Park, Preparation, characterization and laboratory-scale application of modified hydrophobic aluminum oxide hollow fiber membrane for CO_2 capture using H_2O as low-cost absorbent, J. Membr. Sci., 494 (2015) 143-153.
[224] Y. Zhang, X. Cheng, X. Jiang, J.J. Urban, C.H. Lau, S. Liu, L. Shao, Robust natural nanocomposites realizing unprecedented ultrafast precise molecular separations, Mater. Today, 36 (2020) 40-47.
[225] F. Bougie, I. Iliuta, M.C. Iliuta, Flat sheet membrane contactor (FSMC) for CO_2 separation using aqueous amine solutions, Chem. Eng. Sci., 123 (2015) 255-264.
[226] R.W. Baker, Membrane technology and applications, John Wiley & Sons, 2012.
[227] S. Paul, A.K. Ghoshal, B. Mandal, Theoretical studies on separation of CO_2 by single and blended aqueous alkanolamine solvents in flat sheet membrane contactor (FSMC), Chem. Eng. J., 144 (2008) 352-360.
[228] G. Van den Berg, C. Smolders, Diffusional phenomena in membrane separation processes, J. Membr. Sci., 73 (1992) 103-118.
[229] R.C. Reid, J.M. Prausnitz, B.E. Poling, The properties of gases and liquids, McGraw-Hill, New York, 1987.
[230] R.E. Treybal, Mass-transfer operations, 2d ed., McGraw-Hill, New York,, 1967.
[231] S.B. Iversen, V.K. Bhatia, K. Dam-Johansen, G. Jonsson, Characterization of microporous membranes for use in membrane contactors, J. Membr. Sci., 130 (1997) 205-217.
[232] E.R. Gilliland, T.K. Sherwood, Diffusion of vapors into air streams, Ind. Eng. Chem., 26 (1934) 516-523.
[233] S.H. Lin, K.L. Tung, H.W. Chang, K.R. Lee, Influence of fluorocarbon flat-membrane hydrophobicity on carbon dioxide recovery, Chemosphere, 75 (2009) 1410-1416.
[234] F. Zhang, C. Tuck, R. Hague, Y. He, E. Saleh, Y. Li, C. Sturgess, R. Wildman, Inkjet printing of polyimide insulators for the 3D printing of dielectric materials for microelectronic applications, J. Appl. Polym. Sci., 133 (2016) 43361.
[235] C. Garcia-Galan, J.C. dos Santos, O. Barbosa, R. Torres, E.B. Pereira, V.C. Corberan, L.R. Gonçalves, R. Fernandez-Lafuente, Tuning of lecitase features via solid-phase chemical modification: effect of the immobilization protocol, Process Biochem., 49 (2014) 604-616.
[236] S. Atchariyawut, R. Jiraratananon, R. Wang, Separation of CO_2 from CH_4 by using

gas–liquid membrane contacting process, J. Membr. Sci., 304 (2007) 163-172.
[237] H. Zhao, Effect of ions and other compatible solutes on enzyme activity, and its implication for biocatalysis using ionic liquids, J. Mol. Catal. B Enzym., 37 (2005) 16-25.
[238] A. Rosli, N. Shoparwe, A. Ahmad, S. Low, J. Lim, Dynamic modelling and experimental validation of CO_2 removal using hydrophobic membrane contactor with different types of absorbent, Sep. Purif. Technol., 219 (2019) 230-240.
[239] N. Ghasem, M. Al-Marzouqi, Modeling and experimental study of carbon dioxide absorption in a flat sheet membrane contactor, J. Membr. Sci. Res., 3 (2017) 57-63.
[240] F. Bougie, I. Iliuta, M.C. Iliuta, Absorption of CO_2 by AHPD–Pz aqueous blend in PTFE hollow fiber membrane contactors, Sep. Purif. Technol., 138 (2014) 84-91.
[241] V. Dindore, D.W.F. Brilman, F. Geuzebroek, G. Versteeg, Membrane–solvent selection for CO_2 removal using membrane gas–liquid contactors, Sep. Purif. Technol., 40 (2004) 133-145.
[242] I. Iliuta, F. Bougie, M.C. Iliuta, CO_2 removal by single and mixed amines in a hollow‐fiber membrane module—investigation of contactor performance, AIChE J., 61 (2015) 955-971.
[243] W. Rongwong, C. Fan, Z. Liang, Z. Rui, R.O. Idem, P. Tontiwachwuthikul, Investigation of the effects of operating parameters on the local mass transfer coefficient and membrane wetting in a membrane gas absorption process, J. Membr. Sci., 490 (2015) 236-246.
[244] B. Metz, O. Davidson, H. De Coninck, M. Loos, L. Meyer, IPCC special report on carbon dioxide capture and storage, Cambridge: Cambridge University Press, 2005.
[245] M. Lucquiaud, J. Gibbins, Effective retrofitting of post-combustion CO_2 capture to coal-fired power plants and insensitivity of CO_2 abatement costs to base plant efficiency, Int. J. Greenh. Gas Control., 5 (2011) 427-438.
[246] A. Chikukwa, N. Enaasen, H.M. Kvamsdal, M. Hillestad, Dynamic modeling of post-combustion CO_2 capture using amines–a review, Energy Procedia, 23 (2012) 82-91.
[247] L.M. Newman, L. Clark, C. Ching, S. Zimmerman, Carbonic anhydrase polypeptides and uses thereof, WO10081007, 2010.
[248] R. Daigle, M. Desrochers, Carbonic anhydrase having increased stability under high temperature conditions, US7521217, 2009.

[249] B.M. Rambo, T.L. Bucholz, D.C. Powell, L.E. Weber, A.J. Linder, C.M. Duesing, A. Zaks, Polysilicate-polysilicone enzyme immobilization materials, US8895280B2, 2014.
[250] A. Belzil, C. Parent, Methods of chemical immobilization of an enzyme on a solid support, Biochem. Cell Biol., 83 (2005) 70-77.
[251] A. Sharma, A. Bhattacharya, A. Shrivastava, Biomimetic CO_2 sequestration using purified carbonic anhydrase from indigenous bacterial strains immobilized on biopolymeric materials, Enzyme Microb. Technol., 48 (2011) 416-426.
[252] F. Azari, M. Nemat‐Gorgani, Reversible denaturation of carbonic anhydrase provides a method for its adsorptive immobilization, Biotechnol. Bioeng., 62 (1999) 193-199.
[253] C. Mateo, J.M. Palomo, G. Fernandez-Lorente, J.M. Guisan, R. Fernandez-Lafuente, Improvement of enzyme activity, stability and selectivity via immobilization techniques, Enzym. Microb. Technol., 40 (2007) 1451-1463.
[254] D.S. Rodrigues, A.A. Mendes, W.S. Adriano, L.R. Gonçalves, R.L. Giordano, Multipoint covalent immobilization of microbial lipase on chitosan and agarose activated by different methods, J. Mol. Catal. B Enzym., 51 (2008) 100-109.
[255] T. Van Gerven, A. Stankiewicz, Structure, energy, synergy, time- the fundamentals of process intensification, Ind. Eng. Chem. Res., 48 (2009) 2465-2474.
[256] Y. Xu, K. Goh, R. Wang, T.-H. Bae, A review on polymer-based membranes for gas-liquid membrane contacting processes: Current challenges and future direction, Sep. Purif. Technol., (2019) 115791.
[257] Y. Ren, J.G. Rivera, L. He, H. Kulkarni, D.-K. Lee, P.B. Messersmith, Facile, high efficiency immobilization of lipase enzyme on magnetic iron oxide nanoparticles via a biomimetic coating, BMC Biotechnol., 11 (2011) 1-8.
[258] E.P. Cipolatti, A. Valerio, R.O. Henriques, D.E. Moritz, J.L. Ninow, D.M. Freire, E.A. Manoel, R. Fernandez-Lafuente, D. de Oliveira, Nanomaterials for biocatalyst immobilization–state of the art and future trends, RSC Adv., 6 (2016) 104675-104692.
[259] C. Lee, S.-Y. Lee, Mussel-inspired bolaamphiphile sticky self-assemblies for the preparation of magnetic nanoparticles, Colloids Surf. B, 127 (2015) 89-95.
[260] J. Gao, Y. Jiang, J. Lu, Z. Han, J. Deng, Y. Chen, Dopamine-functionalized mesoporous onion-like silica as a new matrix for immobilization of lipase Candida sp. 99-125, Sci. Rep., 7 (2017) 1-9.

[261] A. Alavinasab, T. Kaghazchi, M.T. Ravanchi, K. Shabani, Modeling of carbon dioxide absorption in a gas/liquid membrane contactor, Desalin Water Treat., 29 (2011) 336-342.
[262] A.A. Ghoreyshi, Amine based CO_2 absorption in membrane contactor using polyvinyl pyrrolidone-modified polysulfone flat sheet membrane: experimental study and mass transfer resistance analysis, Int. J. Eng., 29 (2016) 1489-1498.
[263] Y. Lin, Y. Xu, C.H. Loh, R. Wang, Development of robust fluorinated TiO_2/PVDF composite hollow fiber membrane for CO_2 capture in gas-liquid membrane contactor, Appl. Surf. Sci., 436 (2018) 670-681.
[264] Y. Lv, X. Yu, S.-T. Tu, J. Yan, E. Dahlquist, Wetting of polypropylene hollow fiber membrane contactors, J. Membr. Sci., 362 (2010) 444-452.
[265] T.-J. Kim, A. Lang, A. Chikukwa, E. Sheridan, P.I. Dahl, M. Leimbrink, M. Skiborowski, J. Roubroeks, Enzyme carbonic anhydrase accelerated CO_2 absorption in membrane contactor, Energy Procedia, 114 (2017) 17-24.
[266] S.-H. Lin, K.-L. Tung, H.-W. Chang, K.-R. Lee, Influence of fluorocarbon flat-membrane hydrophobicity on carbon dioxide recovery, Chemosphere, 75 (2009) 1410-1416.
[267] X. Yu, L. An, J. Yang, S.-T. Tu, J. Yan, CO_2 capture using a superhydrophobic ceramic membrane contactor, J. Membr. Sci., 496 (2015) 1-12.
[268] A. Golkhar, P. Keshavarz, D. Mowla, Investigation of CO_2 removal by silica and CNT nanofluids in microporous hollow fiber membrane contactors, J. Membr. Sci., 433 (2013) 17-24.
[269] S. Hashemifard, A. Ismail, T. Matsuura, M.R. DashtArzhandi, Performance of silicon rubber coated polyetherimide hollow fibers for CO_2 removal via a membrane contactor, RSC Adv., 5 (2015) 48442-48455.
[270] H. Ahmadi, S. Hashemifard, A. Ismail, A research on CO_2 removal via hollow fiber membrane contactor: the effect of heat treatment, Chem. Eng. Res. Des., 120 (2017) 218-230.
[271] R. Naim, A. Ismail, Effect of fiber packing density on physical CO_2 absorption performance in gas–liquid membrane contactor, Sep. Purif. Technol., 115 (2013) 152-157.